Sand/waste rubber mixtures : A micromechanical analysis

Pravin Ravindra Badarayani

▶ **To cite this version:**

Pravin Ravindra Badarayani. Sand/waste rubber mixtures : A micromechanical analysis. Mechanics of materials [physics.class-ph]. École centrale de Nantes, 2019. English. NNT : 2019ECDN0045 . tel-02479748

HAL Id: tel-02479748
https://theses.hal.science/tel-02479748

Submitted on 14 Feb 2020

THESE DE DOCTORAT DE

L'ÉCOLE CENTRALE DE NANTES
COMUE UNIVERSITE BRETAGNE LOIRE

ECOLE DOCTORALE N° 602
Sciences pour l'Ingénieur
Spécialité : *Mécanique des solides, des matériaux, des structures et des surfaces*

Par

Pravin BADARAYANI

Sand/waste rubber mixtures: A micromechanical analysis

Thèse soutenue à Nantes, le 20 Novembre 2019
Unité de recherche : Institut français des sciences et technologies des transports,
de l'aménagement et des réseaux (IFSTTAR)
Laboratoire Granulats et procédés d'élaboration des matériaux (GPEM)

Rapporteurs avant soutenance :

Luc OGER   Directeur de Recherche, CNRS, Université de Rennes, France.
Matthew EVANS   Associate Professor, Oregon State University, USA.

Composition du Jury :

Président :   Giulio SCIARRA   Professeur des Universités, Ecole Centrale de Nantes, France.
Examinateurs :   Vanessa MAGNANIMO   Associate Professor, University of Twente, Netherlands.
                   Andrea DIAMBRA   Senior Lecturer, University of Bristol, UK.
                   Luc OGER   Directeur de Recherche, CNRS, Université de Rennes, France.
                   Matthew EVANS   Associate Professor, Oregon State University, USA.

Directeur de thèse :   Patrick RICHARD   Directeur de Recherche, IFSTTAR Nantes, France.
Co-directeur de thèse: Bogdan CAZACLIU   Directeur de Recherche, IFSTTAR Nantes, France.
Encadrant de thèse: Riccardo ARTONI   Chargé de Recherche, IFSTTAR Nantes, France.

RÉSUMÉ

Les déchets issus de caoutchouc (pneus usagés) sont produits en grand nombre par nos industries et par notre mode de vie. Afin de réduire leur impact sur l'environnement et de s'inscrire dans une logique d'économie circulaire, il est envisageable de recycler ces déchets dans des matériaux granulaires dans le but d'obtenir des composites aux propriétés notables. L'objectif de ce projet est d'étudier si l'ajout de grains de caoutchouc dans les sols à base de sable améliore les propriétés des matériaux ainsi obtenus. Les applications visées sont les infrastructures telles que les murs de soutènement, les ponts routiers et ferroviaires et leurs piliers ou encore les tunnels et les ponceaux. Par rapport à des sols « classiques » nous nous attendons à ce que ces mélanges aient des propriétés remarquables telles que : une compressibilité élevée, une faible densité, un coefficient de frottement élevé et un bon drainage. Ce projet porte ainsi sur l'étude des composites caoutchouc-sable et en particulier sur la relation entre la qualité du mélange obtenu et les propriétés mécaniques.

Le premier chapitre de la thèse présente l'état de l'art. Cela implique les travaux effectués jusqu'à présent sur l'étude des mélanges sable-caoutchouc. Par ailleurs, il présente la littérature spécifique concernant les différentes méthodes expérimentales et numériques utilisées dans cette étude. Il insiste également sur l'importance d'étudier l'effet du mélange sable-caoutchouc en regard des performances mécaniques souhaitées.

Le deuxième chapitre, quant à lui, présente des expériences caractérisant le mélange du sable et du caoutchouc. Elles ont été effectuées en trois étapes. 1) Tout d'abord, le mélange de grains de sable et de caoutchouc a été réalisé en utilisant différents rapports de taille et de fraction volumique de caoutchouc. 2) Ensuite la ségrégation des deux espèces de gains a été testée sous différentes conditions, par exemple lorsque le mélange est soumis à des vibrations reproduisant le transport routier. 3) Enfin nous avons analysé ces échantillons produits en les solidifiant puis en les coupant en tranches afin de caractériser l'évolution spatiale du mélange et la ségrégation entre le sable et le caoutchouc. Après analyse, il a été observé que la ségrégation existait dans les mélanges même en l'absence de sollicitations extérieures. Les grains de caoutchouc montrent en effet une forte tendance à former des « clusters ». Finalement, il a été montré qu'un ajout d'eau pendant la phase de mélange des grains de sable et de caoutchouc a conduisait à une diminution de la ségrégation.

La caractérisation de nos mélanges sable/caoutchouc a montré la présence de ségrégation. Dans le but de quantifier l'effet de cette dernière sur les propriétés mécaniques de nos mélanges,

des tests mécaniques classiques à l'œdomètre ont été réalisés à l'université de Bristol, UK en collaboration avec le Prof. Erdin Ibraim. Les paramètres étudiés sont : la fraction volumique de caoutchouc, la compacité du mélange ainsi que différents rapports de taille entre grains de sable et de caoutchouc. Globalement, il a été observé que l'homogénéité du mélange lors de la préparation de l'échantillon pour les tests était importante. En d'autres termes, l'arrangement des grains de sable et de caoutchouc dans le mélange a une forte influence sur la réponse mécanique du mélange sous compression. Afin d'aller plus loin, des expériences ont également été menées en préparant des mélanges avec différentes répartitions géométriques de sable et de caoutchouc. Elles ont montré une le fort effet de l'arrangement des grains pour des fractions volumiques de caoutchouc inférieures jusqu'à 20%. Cet effet diminue avec l'augmentation de la fraction volumique de caoutchouc jusqu'à devenir peu significatif lorsque cette dernière atteint à 50%.

Les expériences présentées au chapitre 3 ont montré une forte influence de l'arrangement initial des grains de sable et de caoutchouc. Malheureusement cette étude est restée à l'échelle macroscopique i.e. celle du mélange. Afin de mieux cerner le comportement à l'échelle du grain, des simulations de type éléments discrets (DEM) ont été réalisées et sont présentés au sein du quatrième chapitre. Avec l'aide de la DEM, il a notamment été possible de caractériser les différentes propriétés au niveau granulaire en distinguant les espèces (sable ou caoutchouc) ou le type de contact (sable-sable ; sable-caoutchouc et caoutchouc-caoutchouc). Nos résultats numériques sont en accord avec les expériences présentées au chapitre 3. Notamment, l'effet de l'arrangement des grains n'est visible que pour des faibles fractions volumiques. Une analyse locale des forces entre grains nous permet de mieux cerner l'effet du mélange sur les propriétés mécaniques.

Les résultats présentés dans quatrième chapitre ont été obtenus en supposant des petites déformations des grains de caoutchouc, la DEM n'étant valable que lorsque ces dernières sont négligeables. Afin d'aller plus loin, nous avons développé un nouveau modèle dans lequel les volumes des chevauchements entre grains (inhérents à la méthode DEM utilisée) sont redistribués aux grains de caoutchouc impliqués, tout en respectant leur caractère incompressible. Les résultats préliminaires obtenus à l'aide de ce modèle sont présentés dans chapitre 5. En particulier, l'apport de l'aspect déformable sur la réponse mécanique est quantifié.

Enfin, nous présentons les conclusions et les perspectives de ce travail. Nous rappelons en particulier que les mélanges sable-caoutchouc ont une tendance naturelle à la ségrégation, tendance qui peut être amoindrie par l'ajout d'eau. L'importance de cette ségrégation sur les propriétés mécaniques n'est pas forcément cruciale, notamment à forte fraction volumique de caoutchouc. Nous avons également montré que des outils numériques pouvaient être utilisés à bon escient pour comprendre les mécanismes à l'échelle du grain.

TABLE OF CONTENTS

LIST OF FIGURES

LIST OF TABLES

GENERAL INTRODUCTION

Problem statement and context

The volume of scrap tires is increasing at an alarming rate throughout the world. It is a frequent sight that the used tires are stockpiled on the landfill sites. This has caused an increasing interest in the use of recycled rubber (in powder or shredded form) from waste tires in combination with other materials such as cement, soil, asphalt, etc. for geotechnical applications [Irfan et al., 2018, Farhan et al., 2016, Elchalakani et al., 2016]. An advantage of using rubber as an additive is its properties viz. lightweight, elasticity, good damping capacity, etc. which makes it an interesting choice for such applications. In this respect, a lot of work has been done and is in progress to test the viability of mixing the recycled rubber chips with soil. The sand-rubber mixture can be an interesting solution for geotechnical applications such as the backfill of the retaining structures, highway embankments and reinforced soil structures [Lee et al., 1999, Bosscher et al., 1997, Garga and O'shaughnessy, 2000, Poh and Broms, 1995]. The dynamic properties of these mixtures allow their use in a damping system e.g. machine foundations or railroad track beds as well to reduce the vibrations since rubber has a high damping capacity [Feng and Sutter, 2000]. The sand-rubber mixtures also have excellent drainage capabilities and hence useful in filtration applications [Valdes and Evans, 2008].

For such geotechnical applications, the quality of mixing between sand and rubber can be quite important and it still remains to be well understood. A few cases could be imagined wherein rubber can accumulate completely on one side; thus causing the mixture to segregate and hence may cause a failure at the given application use. For the same reason, the practical use of such mixtures needs the development of numerical analyses. One of the ways to achieve this can be using the homogenization approaches based on 'rule of mixtures'. However, sand-rubber mixture is not like a regular composite and hence the 'rule of mixtures' no more remains valid due to a contrasting difference between their stiffness [Pindera et al., 2009]. Sand and rubber are materials which have a significant difference between their mechanical properties. Hence, their mixing still remains a complex issue to be addressed.
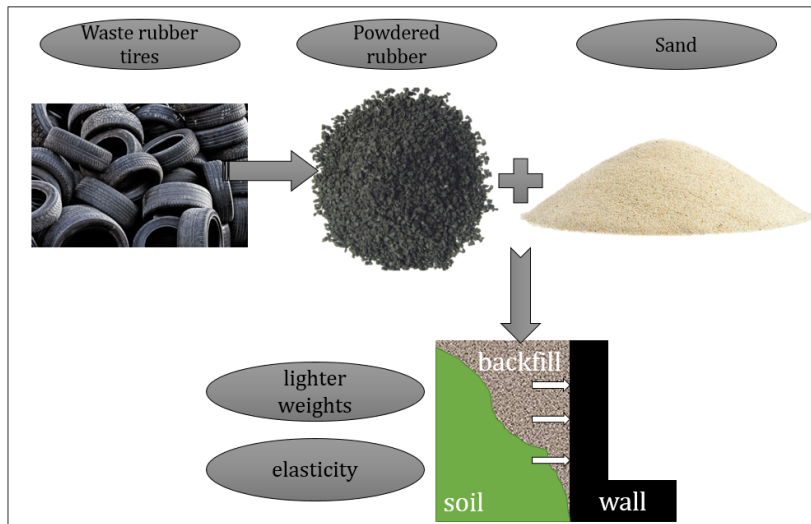
FIGURE A. Figure explaining the context where sand-rubber mixture is used.

Objectives of the thesis

The thesis concerns with the analysis of the effect of the mixing quality on the mechanical behavior of sand-rubber mixtures. The mixing of heterogeneous granular materials such as sand and rubber is quite complex to understand. For the same purpose, the problem has been addressed using both experimental as well as numerical simulation tools.

There exist several conventional geotechnical testing methods to characterize the mechanical behavior of soil, sand, or even sand-rubber mixtures. One such conventional testing method *viz.* oedometric compression has been implemented in the experimental analysis of sand-rubber mixtures. The results obtained in these experiments motivated to characterize the mixing phenomena for these mixtures.

In real-time conditions, it is not easy to achieve perfectly homogeneous mixture and at the same time it is also difficult to realize an imperfect sand-rubber mixture. For the same reason, numerical simulations using the Discrete Element Method (DEM) have been employed to better understand the effect of mixing on the behavior of the sand-rubber mixtures. An oedometric compression model was implemented in these numerical simulations.

In order to emphasize the characterization of mixing, the segregation between sand and rubber has been studied. Effort has been made to replicate certain real time possible sources of segregation; *viz.* mixing process, transportation of sand-rubber mixtures in trucks/lorries. Since, in real time condtions, the transportation will cause vibrations, the same has been characterized experimentally to investigate the segregation between sand and rubber.

FIGURE B. Logo of IFSTTAR and University of Bristol.

Thesis collaborators

The host institute for this thesis was French Institute of science and technology for transport, development and networks (IFSTTAR); which is a public research organization. The aggregates and materials processing (GPEM) Laboratory of IFSTTAR focuses on a multidisciplinary research revolving around 4 main topics *viz.* Aggregates, Rheology, Processes and Recycling. This thesis is a part of the project theme: Alternative Materials for buildings and infrastructures of the GPEM Laboratory. Further, the project functions in collaboration with Dr. Erdin IBRAIM of University of Bristol.

Thesis chapter outline

This thesis manuscript is divided into following chapters:

Chapter 1: Bibliographical study: State of the Art

Chapter 2: Analysis of mixing and segregation between sand and rubber

Chapter 3: Oedometer testing of sand-rubber mixtures: Experimental analysis

Chapter 4: Oedometer testing of sand-rubber mixtures: Numerical analysis using Discrete Element Method (DEM) simulations

Chapter 5: Introduction to a new deformable particles model using DEM

INTRODUCTION: STATE OF THE ART

Summary

This chapter explains the need to act on the problem of the used waste tires. It puts forward the different potential methodologies investigated till now and being investigated for recycling and reusing this waste rubber.

Further, an introduction concerning sand-rubber mixtures, their potential applications, means of testing their mechanical properties (experimentally as well as numerically) has been detailed out.

The chapter ends with explaining the mixing phenomena and segregation between granular materials such as sand and rubber.

Contents

1.1   Waste tire recycling: need and methodologies

The volume of waste caused by the used tires is increasing at an alarming rate day by day. It is a frequent sight that the used tires are stockpiled on the landfill sites. This is leading to grave environmental problems and hence it is of utmost importance to take action on this problem on a global scale. If we consider the statistics, then in France alone, the amount of waste tires reported was around 350,000 metric tons in 2017 (equivalent to 46 million passenger car tires) according to Aliapur Collection Report, (2017). This number is definitely high in developing countries especially those with high population, *e.g.* India. In most of the developing countries, such a high amount of waste is just burnt off to get rid of it. However, such measures in turn cause environmental problems of pollution.

Research is continuously in progress to find sustainable solutions for minimizing the tire waste. It is quite important to understand that one solution will not be sufficient to minimize this waste due to its enormous quantity and hence multiple solutions are necessary to be implemented. The use of such waste tires has become quite common in some thermochemical methodologies of recycling as well such as tire pyrolysis, incineration, etc. [Choi et al., 2014, Williams and Brindle, 2003, Huang and Tang, 2009]. Another interesting application for these used waste tires has been in the electric arc furnaces for the production of steel [Zaharia et al., 2009]. Such combustion of waste tires has been proved to be clean and non-polluting. The used waste rubber tires also find interesting use in applications such as roadways wherein they are used as modified asphalt [Heitzman, 1992, Cao, 2007]. Such rubber-asphalt mixtures have found to have improved resistance to deformation at high temperatures as well as to cracking at low temperatures.

Table 1.1 precisely describes the different possible pathways which have been studied or are being studied for the treatment of waste rubber [Fang et al., 2001].

Using powdered rubber or shredded rubber is one of the most adopted waste rubber recycling method. The main reasons for this; to name a few include:

(i) Reduced consumption of facilities and energy since processes such as desulfurizing, cleaning, drying, leaching and refining (included in the production of regenerated rubber) are reduced.

(ii) Decreased product cost by combining powdered rubber with raw rubber.

(iii) Production of powdered rubber has no harmful environmental effect such as pollution.

(iv) Better mechanical behavior, due to which it has wide prospects of applications.

Rubber, in general, has interesting properties *viz.* lightweight, elasticity, good damping capacity, etc. Consequently, the use of powdered rubber mixed with materials such as cement, asphalt or even soil is particularly interesting for civil and geotechnical engineering applications.

No.	Approach	Application
1.	Recycling energy as fuel	One solution is reclaiming energy through direct burning. This method is simple but it will cause air pollution. The other is to make fuel, that is, waste rubber is blended with other burnable discard for making rubbish solid fuel which is used in cement revolving tubular kiln instead of coal, moreover, it can be used in generating electricity. This method can obtain another material, charcoal black. It can be used as activated charcoal black after activating.
2.	Thermal Decomposition	Making use of the products of thermal decomposition of waste rubber, such as: coal gas, oil and charcoal black and so on. But the cost of facilities and operation is quite high.
3.	Modification	Tires renew, making man-made fish shelter, conservation materials, lifebuoy and cleaning of leaking oil [Rajalingam et al., 1993]. These materials consume a little energy and make the best use of waste rubber, so it is a valuable recycling approach.
4.	Modification asphalt	Roadway material.
5.	Regenerated rubber	Making regenerative rubber through desulfurization of waste rubber, and the cost of cryo-regenerating rubber products will decrease, if regenerative rubber is blended with fresh rubber.
6.	Powdered rubber	The main recycling approach of waste rubber is to make PR (powdered rubber) or FRP (fine rubber powder). In general, cryogenic crushing is the main process for FRP. The temperature in the process is lower than the glass transition temperature (T_g) of the polymer in rubber. For example: the temperature of the blends of NR (natural rubber) and SBR (styrene-butadiene rubber) is under -90 to -67°C at least, usually, the freezing agent is liquid nitrogen.

Table 1.1: Table showing the different approaches for recycling waste rubber tires [Fang et al., 2001]

1.1.1 Use of powdered waste rubber for civil/geotechnical engineering applications

Powdered waste rubber as described before, can be mixed with materials such as cement, soil, asphalt and such mixtures have been found to have enhanced properties. [Farhan et al., 2016] have reported that the addition of rubber in rubberized cement aggregate mixtures improved the properties of the mixture such as energy absorption capacity, toughness and unconfined compressive strength. Similar studies concerning the effect of addition of rubber on the behavior of rubberized-cement mixtures have been reported by [Balaha et al., 2007,

3

Eiras et al., 2014, Najim and Hall, 2012]. The motivation behind all these studies has been to investigate the possible sustainable use of waste rubber for applications such as pavements, highway sound walls, exterior wall materials, etc. especially since such mixtures have shown improved dynamic and vibration damping properties.

Similarly, powdered rubber and asphalt mixtures have been studied [Liang and Lee, 1996, Shu and Huang, 2014, Irfan et al., 2018] for applications such as pavements since addition of rubber has proved to minimize the pavement degradation due to deformation and thus improve its service life.

The use of rubber along with soil/sand has also been under investigation since a long time. Such sand-rubber mixtures have been investigated with an aim to use them in applications such as backfill of the retaining walls, railway track beds, highway embankments, etc. to name a few. The next section, section 1.2 gives a detailed account of the sand-rubber mixtures, which is the interest of this thesis.

1.2 Sand-rubber mixtures: an overview

Sand or soil is one of the most conventional materials used in the geotechnical/ civil engineering applications. Due to an increased number of the waste rubber tires at the landfill sites throughout the world, there has been an increasing interest to quantify the use of these waste rubber tires in combination with sand to form an unconventional mixture for certain geotechnical applications. The advantage firstly lies in the re-utilization of waste rubber tires, thus contributing towards the circular economy of such materials. Secondly, rubber has properties of particular interest for geotechnical applications such as good damping capacity, lightweight, elasticity and especially, the sand-rubber mixtures have been found to have interesting properties for certain applications which will be discussed further.

Sand-rubber mixtures are particularly interesting option for the backfill of retaining walls or embankments. Lee et al. [1999] have reported that the strength of such mixtures is adequate enough for such applications. Moreover, the sand-rubber mixtures are lightweight than the regular sandy gravel backfill. The design and analysis of the behavior of such rubber reinforced walls as well as embankments has been conducted by Youwai and Bergado [2004], Bosscher et al. [1997]. These works detail out the benefits of using the waste rubber tire chips for such applications. Moreover, they provide certain procedures to be followed while designing such structures using the waste tire rubber in support with certain laboratory tests conducted for analyzing the mechanical properties of such sand-rubber mixtures. The works of Garga and O'shaughnessy [2000], Poh and Broms [1995] also suggest the use of such waste rubber tires for retaining walls and slope stabilization. These works further analyze the construction and behavior of such structures using the waste rubber tires.

Rubber has a good vibration damping capacity. For the same reason, it has been a research interest to study the behavior of sand-rubber mixtures for applications such as soil foundations.

Thus a lot of research is still under progress to use such sand-rubber mixtures for applications such as seismic isolations. Such applications employ a shallow, resilient layer of sand-rubber mixtures beneath a structural foundation which is called as Geotechnical Seismic Isolation (GSI). A lot of works clearly suggest that the use of waste rubber for such applications seems to be quite promising. To name a few, Kaneko et al. [2012], Xiong et al. [2014], Brunet et al. [2016], have conducted laboratory analysis as well as numerical analysis to investigate the potential of such mixtures. Pamukcu and Akbulut [2006] also show the effectiveness of rubber in improving the vibration attenuation of earthen structures when mixed with sand up to certain percentage volume fractions of inclusion.

Moreover, some recent applications include the use of waste rubber in the foundation of soil for applications such as playgrounds. Rubber being elastic in nature, absorbs the downward forces exerted on the players' feet *e.g.* football players, athletes, etc. and provide a return energy, thus reducing the stress on the feet of the athletes and consequently reducing the injuries.

The applications stated above clearly quantify the potential use of sand-rubber mixtures. However, it is quite important for any application, especially in geotechnical engineering to test the mechanical behavior of the material before its actual implementation. This will be discussed further in detail in section 1.3.

1.3 Laboratory testing of sand-rubber mixtures

1.3.1 Sand-rubber mixture fabrication methodologies

An important first step in any laboratory testing method is the test specimen/sample preparation. Especially, the preparation phase gains much more importance if the sample to be tested is a mixture of two or three different constituents. For sand-rubber mixtures, this is one of the most critical steps in the testing. Sand and rubber are granular materials with differing properties from each other. Hence, to achieve a pathologically unbiased mixture is the key to testing the sand-rubber mixture in a better way.

There are different methods for laboratory preparation of sand-rubber mixtures. These mixtures were prepared by Youwai and Bergado [2003] using a method called undercompaction suggested by Ladd [1978]. Five layers of sand-rubber mixtures, each having 40mm height were achieved using 7.5% water content. The lower layers were compacted to a small degree with an aim to compensate for the additional compaction of the top layers. Similar method was used by Fu et al. [2014] to prepare sand-rubber mixtures in six layers having a height of 20mm each by using 10% water content for triaxial samples and 3% to 10% moisture for oedometer samples. Kawata et al. [2007] and Hazarika et al. [2012] used 10% moisture content to prepare sand-rubber mixtures in five layers, each with a height of 20mm. Further, Rao and Dutta [2006] used soaked sand and rubber particles to achieve three layers of the mixture, 66mm thickness each and followed by compaction with a rubber tamper inside a triaxial mold.

Sand and rubber mixtures were also prepared in dry conditions. Lee et al. [2010] used a spoon to deposit the sand-rubber mixtures and then compacted using a steel rod tamper in an oedometer cell. Sand rubber samples were prepared and deposited in three layers by Mashiri et al. [2015], Ghazavi and Sakhi [2005]. A scoop was used instead of funnel in their case due to the tire chip sizes and each layer was carefully compacted. In the case of Promputthangkoon [2009], eight layers of sand-rubber mixture, 25mm thickness each were deposited using dry deposition method but without any compaction. In order to minimize segregation, the funnel was raised slowly and zero deposition height was maintained; however no uniformity assessment was done.

A segregation controlled technique developed by trial and error method was used by Ngo and Valdes [2007] and Valdes and Evans [2008]. In this case, sand-rubber mixtures were mixed in a semicircular bowl and poured up and down along the length of a crease paper until a homogeneous mixtures was attained. The homogeneous mixture was then deposited in the cylindrical mold by using a funnel. The homogeneity was evaluated by visual inspection in a horizontal plane level.

In conclusion, although the uniformity of sand-rubber mixtures is quite important, there has been no specific, qualitative and quantitative assessment of this phenomenon. The quality (uniformity or homogeneity) assessment has been only limited to visual inspection in both laboratory as well as field applications. This is a major objective of this study and will be detailed out in the later sections.

1.3.2 Review of different laboratory testing methods for sand-rubber mixtures

The geotechnical testing methods to characterize the mechanical behavior of the sand-rubber mixtures varies with the application. Various conventional laboratory testing methods are used to quantify the mechanical properties of sand-rubber mixtures. Some of the most common laboratory testing methods include triaxial test, direct simple shear test, oedometer test, resonant column test, piezoceramic bender element test, ring shear test, etc.

The choice of the testing method to be used depends on the intended application use of the sand-rubber mixtures. Since with the varying application, the sand-rubber mixtures are subjected to varied strain levels and hence their behavior differs. In general, for geomaterials used in different geotechnical applications the strain level ranges from less than 0.001% to 20% (see Fig.1.1) [Atkinson, 2000, Lee et al., 2014]. The range of strains less than 0.01% is covered by dynamic loadings; consolidation (oedometer test) produces 0.1-2%, and all strength and penetration tests are described by large strains (1% 20%). The differing behavior of the granular materials under different strains shows the different internal deformation mechanisms.

1. Behavior under small strain is a constant fabric response, highlighted in inter-particle contact, packing arrangement, elastic stiffness of the materials and the state of stress
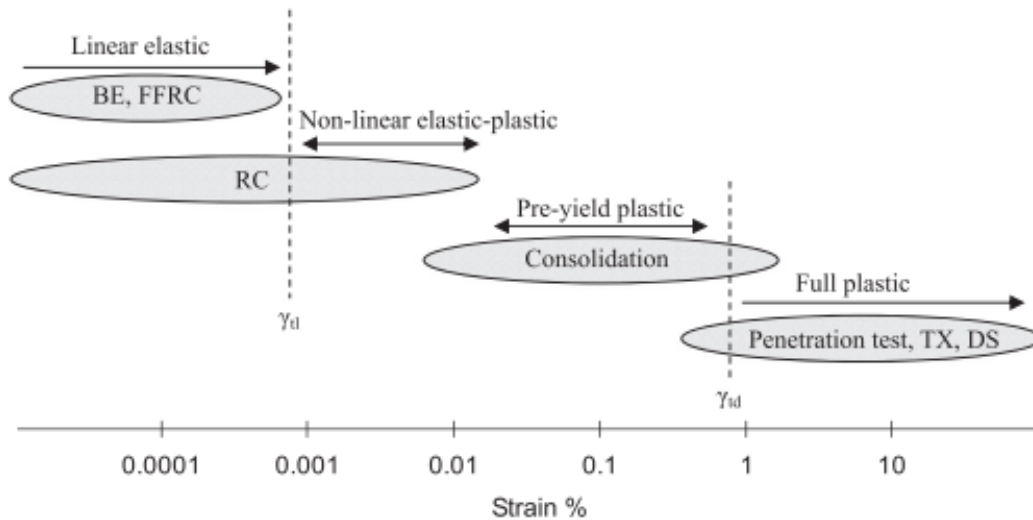
FIGURE 1.1. Figure showing the characteristics of soil behavior with typical tests [Lee et al., 2014, Atkinson, 2000]. BE is bender element; FFRC is free-free resonant column test; TX is triaxial test, DS is direct shear test, γ_{tl} is the linear elastic threshold strain; γ_{td} is the degradation threshold strain

[Mindlin, 1949]. The maximum stiffness and linear elastic behavior of materials is observed in this regime. The linear elastic threshold strain, γ_{tl} separates this from the nonlinear elastic regime where the start of fabric changes can be observed.

2. With the increasing strains, non-linear behavior starts and minor fabric changes can be observed. However, the strains due to a complete cycle of loading, unloading and reloading are still fully recoverable in the nonlinear elastic zone. Irrecoverable strains can be seen in the pre-yield plastic regime.

3. The increasing strain causes a destruction of the soil fabric leading to irrecoverable plastic shear deformation. The degradation threshold strain, γ_{td} separates the intermediate and large strain regimes [Vucetic, 1994].

The sand-rubber mixtures undergo different behavioral characteristics with the increasing strain for different volume fractions of the individual constituents, since rubber being elastic, ductile and having high damping capacity [Zornberg et al., 2004, Feng and Sutter, 2000, Yang et al., 2002]. Thus, laboratory testing helps to investigate the important properties of sand-rubber mixtures such as their shear behavior, axial strain capacity, compressibility behavior, etc. This section highlights the importance of laboratory tests for sand-rubber mixtures by reporting some laboratory studies conducted till now.

A lot of research exists in relation to the laboratory testing of sand-rubber mixtures especially to account for its shear strength and behavior under shear. The behavior of sand-rubber mixtures under shear was first studied by Ahmed [1993] by performing triaxial tests. Different parameters such as influence of size and ratio of rubber chips, sample preparation, confining

pressures,etc. were studied and reported. It was mainly the amount of rubber chips and the confining pressure responsible for the shear behavior of such mixtures. Edil and Bosscher [1994] investigated and concluded similarly, that the shear behavior of sand improved with the addition of rubber. Foose et al. [1996] also investigated and concluded that the normal stress and the volume of rubber chips added to sand were some of the factors affecting the shear strength of such mixtures. In both the above studies mentioned, large shear box tests were performed for analyzing the shear behavior. Zornberg et al. [2004] performed triaxial tests and used the rubber tire chips of specific lengths and widths and varying thicknesses. It was reported that the largest shear strength increment was achieved at a low confining pressure for 35% (by volume) of rubber content in the mixture. Similarly, Rao and Dutta [2006] observed that the highest shear strength improvement occured at 20% rubber content and at low confining pressure. This was also reported on the basis of laboratory triaxial tests. Whereas, Ghazavi and Sakhi [2005] performed direct shear tests on 3 different sand-rubber mixing ratios (by volume) and concluded that the shear behavior depended on the normal stress, volume of rubber content, width of rubber chips and aspect ratio (length to width ratio). On the other hand, Neaz Sheikh et al. [2012] performed similar analyses of sand-rubber mixtures using triaxial tests and observed a decrease in the shear strength of the mixtures with the increasing rubber content. However, it was reported that it also depended on the relative size ratios between sand and rubber and hence was not entirely conclusive.

Similar to shear behavior, compressibility is one of the most important parameters for geotechnical applications where both stability and serviceability are of extreme importance. It was reported by Ahmed [1993] that the percentage addition of chips to sand significantly affected the compression response of such mixtures, however the compaction effort had a very low effect on the deformation response of snad-rubber mixtures. Edil and Bosscher [1994], Bosscher et al. [1997] reported that the tire chips-sand mixtures exhibited an initial plastic compression under load, which was related to the void ratio of the mixtures. At a particular load and a reduced void ratio level, it behaved like an elastic material. Moreover, it was also reported by Bosscher et al. [1997] that the smaller chips and larger shreds had similar response.

Thus, a significant research suggests that the laboratory tests are useful and needed in order to test the viability of sand-rubber mixtures for the geotechnical applications. It is quite evident that a good number of studies exist in terms of shear strength and shear behavior investigation for sand-rubber mixtures. However, there have been limited studies in terms of compressibility behavior. As mentioned before as well, it is quite important to study the behavior of sand-rubber mixtures under compression for geotechnical applications. In this thesis, the compression studies were conducted on sand-rubber mixtures by implementing conventional laboratory method called oedometer test. Section 1.4 details the methodology of oedometer tests.

1.4 Conventional laboratory oedometer test

1.4.1 What is an oedometer test?
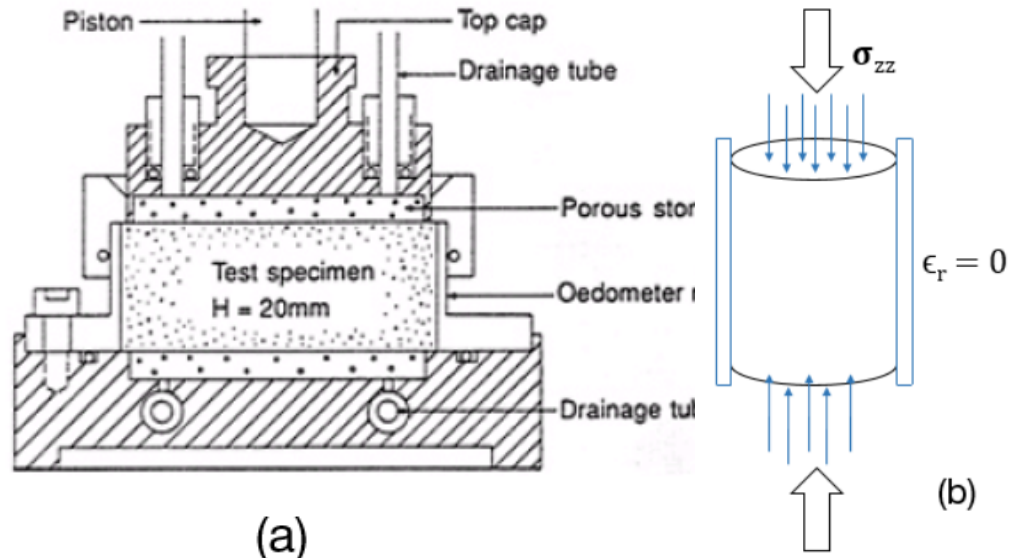
FIGURE 1.2. Figure showing (a) the schematic of oedometer cell for a typical test specimen of 20mm height [Sandbækken et al., 1986] and (b) stresses acting on the test specimen in an oedometer cell.

An oedometer test is a conventional laboratory test used in soil mechanics and for geotechnical investigations which measures the consolidation properties and compressibility behavior of the test material. Fig. 1.2(a) shows the schematic of a typical oedometer test setup. It consists of a cylindrical test specimen, typically with a cross-sectional area of 20, 35 or 50 cm^2 and a typical height of 20 mm. The specimen is enclosed in a stainless steel ring. The top cap and the base plate are usually provided with porous stones and are connected with two drainage tubes. In the oedometer test, stress is applied to the test specimen along the vertical axis while the strain in horizontal directions is prevented (Fig. 1.2(b)). A cylindrical test sample, usually with a thickness/diameter ratio nearly equal to 1/3, is confined in a metallic ring and loaded with a vertical axial pressure. Due to the rigidity of the metallic ring, the radial strain, $\epsilon_r = 0$. However, the axial strain, $\epsilon_a \neq 0$. Thus, $\epsilon_a = \epsilon_v$, where ϵ_v is volumetric strain.

1.4.2 Methodology

As mentioned before, the oedometer test is the conventional test for measuring the consolidation and compression behavior of soil or soil with inclusion mixtures *e.g.* sand-rubber mixtures. According to Karl von Terzaghi, consolidation is "any process which involves a decrease in water content of saturated soil without the replacement of water by air". In a more general way, it is the process of volume change of soils in response to the applied pressure over a long period

of time. On the other hand, compression denotes the changes in volume due to the change in applied load, however without reference to the time scale.

Usually, the oedometer test is performed under saturated conditions, *i.e.* the entire oedometer assembly sits in an open cell of water. The initial pressure applied depends on the specimen being tested and then a sequence of pressures is applied, with each one usually being double the previous pressure. For a consolidation test, each pressure is usually maintained for 24h. At
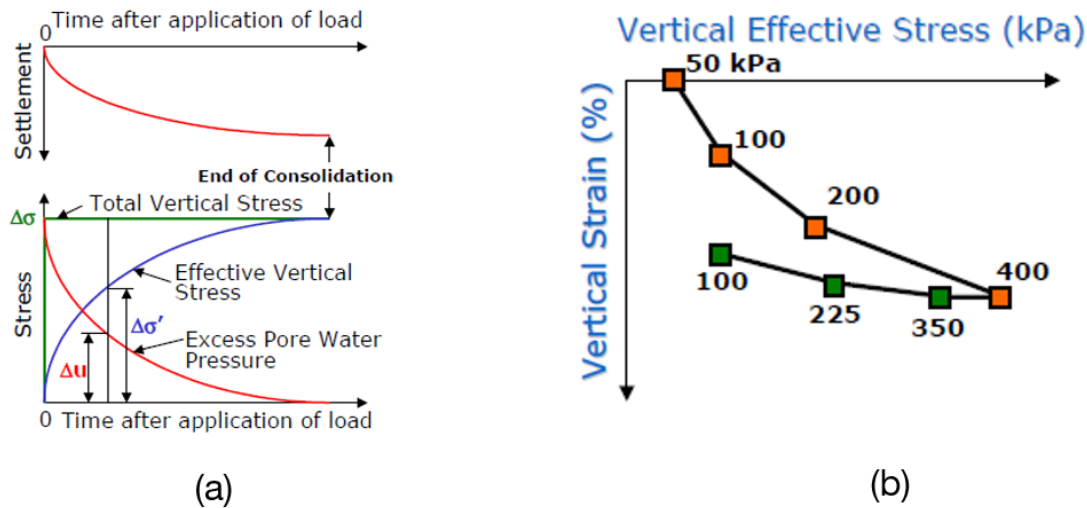
FIGURE 1.3. Figure showing (a) the settlement of the test specimen with time and (b) typical representation of oedometer test result in the form of vertical stress against the vertical strain.

the end of the load increment, when the excess pore water pressure has completely dissipated, vertical stress is equal to the applied pressure. The pore water begins to flow out of the voids due to the stress applied. This causes a decrease in the pore water pressure and thus increase in the effective vertical stress and hence, the soil sample settles (Fig. 1.3 (a)). The oedometer test result is typically represented in the form of vertical effective stress against the vertical strain (Fig. 1.3 (b)). The increment for the vertical strain, $\Delta \epsilon_v$ is given by, $\Delta \epsilon_v = \Delta h / h_0$, where, Δh is the settlement for the load increment (*i.e.* change in sample height) and h_0 is the initial height of the sample/ test specimen. Since the settlement of the specimen is only due to change in the void ratio, the vertical strain, $\Delta \epsilon_v$ can be expressed in terms of the void ratio of the sample at the different stages of loading (Fig. 1.4(a)). Hence,

$$\Delta \epsilon_v = \frac{\Delta h}{h_0} = \frac{\Delta e}{1 + e_0}, \tag{1.1}$$

where, Δe is the change in void ratio due to loading and e_0 is the initial void ratio.

A typical consolidation test result, is thus presented by plotting void ratio at the end of each load increment against the corresponding effective stress. The effective vertical stress can also be plotted on a logarithmic scale. A typical test consists of two major test phases *viz.* loading
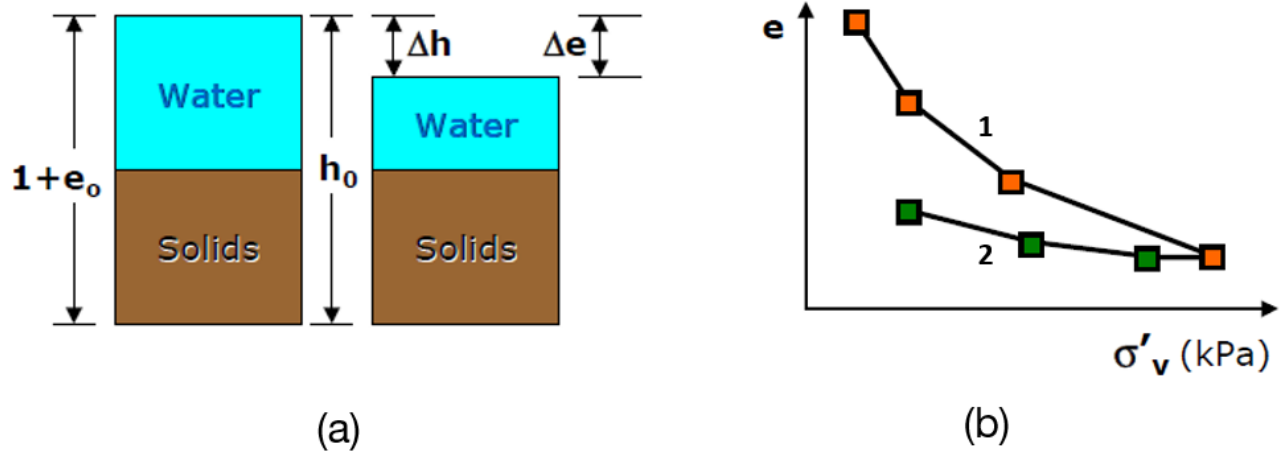
FIGURE 1.4. Figure showing the typical oedometer test result representation with e denoting void ratio and σ'_v denoting effective vertical stress. In the figure, 1 represents loading phase and 2 denotes the unloading phase.

and unloading (Fig. 1.4(b)). Loading phase is the phase of compression or stress application and unloading phase is the one in which the test specimen is subsequently unloaded of the applied stress. During the unloading phase, the soils have a tendency to expand or swell due to the removal of the load applied. The initial void ratio, e_0 will depend on the material as well as the history of the material.

One of the difficulties in oedometer test is the control of side friction. The shear stresses develop along the cylindrical surface of the test specimen as the vertical strains occur. This presence of side friction disturbs the 1-D state of the strain and prevents some axial force from not reaching the bottom portions of specimen. For the same reason, the thickness to diameter ratio is kept as practically low as possible (usually 1:3).

The test specimens can have varying packing volume fractions *i.e.* in other words, the void ratio can be different in different test specimens depending on the material being tested and also the preparation of the material, grain size and shape, etc. In general, depending on the range of void ratios, they are classified as dense and loose packings. Thus, loose soils have higher void ratio owing to more voids throughout the packing as compared to dense soils. Following are a few interesting parameters which can be measured from the oedometer test to quantify the mechanical response of the test specimen.

Confined modulus (M)

The oedometer test is performed on soil or soil-like materials (*i.e.* soil with inclusions such as sand-rubber mixtures). Since such materials are not perfectly elastic, it is important to define the 1-D stiffness in incremental terms, *i.e.* incremental vertical effective stress, $\Delta\sigma'_v$ and incremental vertical strain, $\Delta\epsilon_v$. The ratio of the incremental effective stress to the incremental

strain is called as confined stiffness or confined modulus and denoted by M or E_0, given by,

$$M = \frac{\Delta\sigma'_v}{\Delta\epsilon_v}.$$ (1.2)

M is not constant. As the compression load increases, the test specimen becomes denser since the voids decrease. Due to this, the stiffness of the sample increases. Thus, it can be said that the confined stiffness or confined modulus, M is dependent on the applied pressure and typically it is given by,

$$M = m\sigma_{ref}\left(\frac{\sigma'_v}{\sigma_{ref}}\right)^\alpha,$$ (1.3)

where, σ'_v is the effective vertical stress, σ_{ref} is the reference pressure of 100 kPa, m and α are material parameters.

Compression and swelling indices

When the e-σ'_v curve is plotted on a log scale, the curve becomes almost linear. The slope of the loading curve gives a value called as compression index, denoted as C_c. It is dimensionless and given by,

$$C_c = -\frac{\Delta e}{\Delta(log\sigma'_v)}.$$ (1.4)

The negative sign is used since the void ratio decreases with the increasing stress. Similarly, the swelling index is the slope of the unloading curve and is denoted as C_s. These two parameters give information concerning the compression and expansion behavior of the test specimen. In general, $C_s << C_c$.

The above sections, section 1.4.1 and section 1.4.2 detail the concept of the oedometer test, its methodology and the parameters measured using this test. The next section will give a brief account about the existing research studies concerning the oedometer tests performed for testing sand-rubber mixtures.

1.4.3 Oedometer testing of sand-rubber mixtures: an overview

The laboratory testing of sand-rubber mixtures has been a research interest since quite a long time in order to better understand the mechanical behavior of such mixtures for geotechnical applications. Since oedometer tests give information concerning the consolidation behavior, compressibility and expansion characteristics as well as the time dependent behavior of the material being tested, several studies have been done in order to investigate these mechanical characteristics for sand-rubber mixtures.

Lee et al. [2007] have studied the small and large strain response of sand-rubber mixtures using the oedometer cell with bender elements. The bender elements were installed at the top and bottom plates to capture the shear wave propagation velocity. The mixture was found to have a transitional behavior between sand-like to rubber-like depending on the confinement. Moreover, they concluded that the deformation modulus at small, medium and large strain

does not vary linearly with the volume fraction. It was also reported that the soft particles affect the formation of force chains and act as a supporting element to prevent the buckling of these chains.

Lee et al. [2009] also performed similar experiments and report a similar response of sand-rubber mixtures. They also reported that the small particles in the mixture are dominantly responsible for the change in the porosity of the mixture. Kim and Santamarina [2008] performed similar oedometer tests with bender elements on sand-rubber mixtures with different rubber volume fractions and large rubber chips ($D_s/D_r \approx 10$; D_s: diameter of sand grains, D_r: diameter of rubber grains). They observed that the mixtures behave between sand-like and rubber-like depending on the volume fraction. Further, they reported that the segregation between sand and rubber and the particle interactions depend not only on the rubber volume fraction but also on the size ratio between sand and rubber, which hence affects their macroscopic response. Promputthangkoon and Hyde [2007] performed oedometer tests on sand-rubber mixtures using Leighton Buzzard sand and tire chips. The compressibility of the mixtures was studied. It was reported that 20% rubber volume fraction was the safety threshold for use of such mixtures in geotechnical applications. Beyond this value, such mixtures cannot be tolerated from the design point of view. The use of sand-rubber mixtures for filtration applications was investigated by Valdes and Evans [2008] using oedometer tests and numerical simulations. They reported that the deformation response depended on the material composition and type of loading. Further, high residual strains were observed after unloading due to the particle interlocking effects and the sidewall friction caused by rigid boundaries. Oedometer tests were conducted on low plastic and high plastic clayey soils mixed with rubber tire chips by Trouzine et al. [2012]. The compressibility and swelling behavior of the mixtures was reported. It was observed that the addition of rubber improved the compressibility of mixtures and reduced the swelling characteristics. Lee et al. [2014] report the observations from resonant column tests, oedometer tests and direct shear tests in order to verify the effect of strain level on the sand-rubber mixture behavior. They reported that rubber plays different role in the mixture at different strain levels. For small strain, it increases the co-ordination number and controls plasticity, for intermediate strain it prevents the buckling of force chains and for high strain level, it showed a contractive behavior (see Fig.1.5).

Fu et al. [2014] used completely decomposed granite (CDG) mixed randomly with rubber in an oedometer cell to study the compressive characteristics of the mixture. It was observed that the rubber addition improved the compressive strength of the mixtures, however a large proportion of rubber was needed in order to observe a significant effect. Further, Fu et al. [2017] report that a critical state framework can be applied to sand-rubber mixtures. For this purpose, they report the results of the oedometer tests using two sands *viz*. Leighton Buzzard sand and completely decomposed granite (CDG) mixed with rubber granules. It was observed that type of sand affected the stress strain behavior as well as the small strain stiffness behavior of the mixtures. The oedometer compression tests were also conducted on mixtures of Chlef sand and

Strain level	Small strain	Intermediate strain	Large strain
Sand-like	sf > 0.2	sf ≥ 0.8	sf > 0.8
Transition	sf ≤ 0.2	0.4 ≤ sf ≤ 0.6	sf ≤ 0.8
Rubber-like		sf ≤ 0.2	
Role of rubber particle			
	Increase coordination number	Prevent buckling of force chain	Leads a contractive behavior
	High elasticity and low stiffness	Secondary particle	
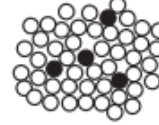
White and black circles denote sand and rubber particles, respectively.

FIGURE 1.5. Figure showing the strain level transition and changing role of rubber particles with the strain level. sf is sand fraction [Lee et al., 2014]

recycled rubber granules by Benessalah et al. [2019] to investigate compressive characteristics of the mixture. It was reported that the compression index and swelling index increased with the increase in rubber volume fraction whereas the compressibility of the mixtures was found to decrease. Energy dissipation and deformation of sand-rubber mixtures was investigated by Fonseca et al. [2019] using 1-D oedometer compression experiments. Particle-scale properties were studied by using a mini oedometer placed inside an X-ray scanner and performing 3D image analysis. They have reported that the energy dissipation is dominated by the sliding of the contacts at the start of loading phase. However, with the progression of the test, rubber particles fill the voids and then the dissipation depends on the rubber content and hence on the deformation of the rubber particles.

While these studies clearly indicate the interest in laboratory testing of sand-rubber mixtures under oedometric compression, they are not exhaustive. Consequently, it is of extreme interest to further investigate the mechanical response of sand-rubber mixtures. The same has been pursued in this study and will be presented and explained in detail subsequently in the later chapters.

Along with the laboratory testing, the study of the behavior of sand-rubber mixtures using numerical tools is extremely important. The main reason for this being the inability to capture microscopic properties of the mixtures during the laboratory tests. With the numerical simulations, it is possible to study the micro scale properties of such mixtures, *e.g.* number of contacts between the grains, contact particle forces, force networks, etc. to name a few. These properties can then be linked to understand the macroscopic behavior of sand-rubber mixtures. Section 1.5 will give a brief account concerning the analysis of sand-rubber mixtures using numerical simulations, specifically using the Discrete Element Method (DEM).

1.5 Discrete Element Method (DEM) for sand-rubber mixtures

In general, granular materials can be modeled using a continuum approach or a discrete approach. The difference between the continuum and the discrete modeling approach has been shown schematically in Fig. 1.6. In the continuum approach, the constitutive behavior of granular materials is described by constitutive laws generally represented in the form of differential equations relating mechanical variables (e.g. stress and strain). However, such modeling approach assumes that the substance being studied is continuous and completely fills the space it occupies, thus ignoring the individual particle behavior. The resulting equations are then solved numerically *e.g.* using Finite Element Method.
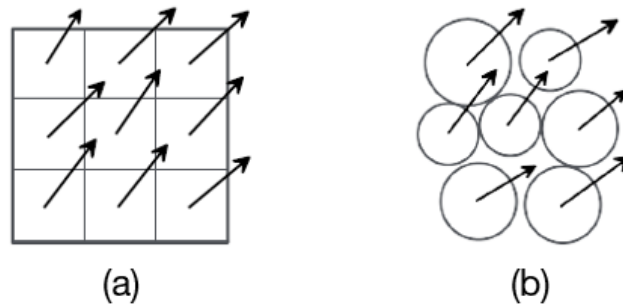
FIGURE 1.6. Figure showing (a) continuum modeling approach and (b) discrete modeling approach

On the other hand, the discrete approaches model each single particle as a distinct entity and represent the granular material as an assembly of particles. The macroscopic behavior thus depends on the individual particle interactions. Hence, the discrete approach is good for granular systems such as sand-rubber mixtures Since the phenomena occurring at the length scale of the particle diameter can be investigated and the bulk behavior of the particles be simulated.

One of the issues in using continuum approaches for granular materials is the proper formulation of constitutive behavior. The appropriate stress-strain laws are often complicated. Moreover, granular systems are highly dependent on the particle scale behavior. Hence, discrete approach offers a more realistic modeling of such materials, although simple forces are used in DEM to reproduce the grain-grain interactions. Moreover, the grain shape is often oversimplified.

1.5.1 Discrete Element Method: Principle and Methodology

The Discrete Element Method (DEM), also called as Distinct Element Method was first developed by Cundall and Strack [1979]. The DEM can be identified as an approach extremely

suitable for modeling the bulk behavior of materials. The simulations of discontinuous media provide a better understanding and often help in reducing the physical experiments. It is possible to calculate the forces acting on the particles by using suitable contact detection algorithms and contact models in DEM. The accelerations, velocities and positions of the particles can then be calculated by integrating the Newton's equations of motion.

Any given particle in a granular flow can have two types of motion: translational and rotational. During its movement, the particle can interact with the neighboring particles or the surrounding fluid or even the walls and due to these interactions, momentum and energy exchanges occur. The particle movement is not only affected by the neighboring particle and nearby fluid but also by the waves propagated due to other particle and fluid interactions far away from it. Analytically, it is extremely complex to realize this phenomena. However, in DEM approach, it can be overcome by choosing the numerical time-step lower than a critical value so that in a single time step the disturbance cannot reach beyond the neighboring particle and fluid [Cundall and Strack, 1979]. The typical value of time step in DEM depends on the particle size, stiffness of the particles and the contact model used.

Hence, at all times the resultant forces acting on the particle can be calculated only from its interactions with the contacting particles and fluid in case of a coarse media. In case of a fine system, it is important to consider even the non-contact forces such as electrostatic forces and van der Waals. Based on this, the governing equations for translational and rotational motion of particle, i with mass, m_i and moment of inertia, I_i is given by,

$$m_i \frac{dv_i}{dt} = \sum_j F_{ij}^c + \sum_k F_{ik}^{nc} + F_i^f + F_i^g, \tag{1.5}$$

$$I_i \frac{d\omega_i}{dt} = \sum_j M_{ij}, \tag{1.6}$$

where, v_i and ω_i are translational and angular velocities of particle i respectively, F_{ij}^c and M_{ij} are contact force and torque acting on particle i by particle j or walls, F_{ik}^{nc} is the non-contact force acting on particle i by particle k or other sources. F_i^f is particle-fluid interaction force on particle i and F_i^g is the gravitational force [Zhu et al., 2007]. Different contact force models exist in order to calculate these forces and torques. Once the forces are known, it is possible to determine the subsequent particle accelerations and velocities. The accelerations obtained using the force models are numerically integrated over the time-step to obtain the subsequent particle velocities and positions. The schematic for the same can bee seen in Fig. 1.7.

$$x(t + \Delta t) = x(t) + v(t)\Delta t, \tag{1.7}$$

$$v(t + \Delta t) = v(t) + a(t)\Delta t, \tag{1.8}$$

where, $v(t)$ is the velocity, $x(t)$ is the position and $a(t)$ is the acceleration of the particle at a given time t, and Δt is the time step.

The rotational velocities and particle orientations are updated in a similar way. Different types
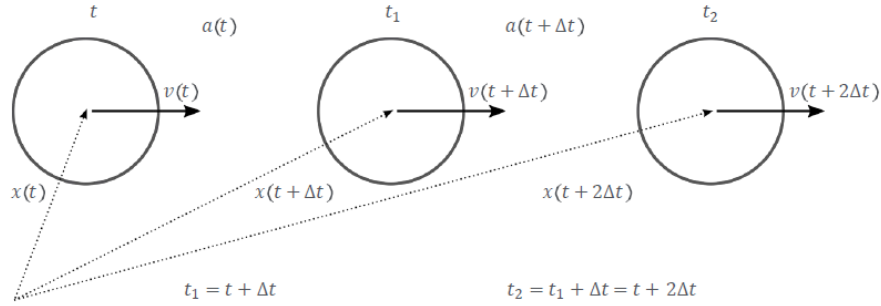
FIGURE 1.7. Schematic showing the calculation of particle position in terms of acceleration and velocity for a single element in DEM

of contact force models exist in DEM in order to model the normal and tangential forces due to the particle collisions. These contact models are based on the theories of contact mechanics and they are capable of modeling both elastic as well as plastic collisions for both non-cohesive and cohesive materials. For other forces as well such as the gravity forces, electrostatics, Van der Waals, etc., models exist which can be used in the simulations.

1.5.2 Types of DEM models

1. **Hard Sphere Molecular Dynamics or Event-driven model**

   In the hard sphere model, the particles are assumed to be perfectly rigid and they follow undisturbed motions until a collision occurs. The particles being rigid, the collisions are instantaneous and the interaction forces are assumed to be impulsive. Hence, an event driven simulation method is used to model it. In this method, the sequence of events are discretized using a variable time step which corresponds to the time till the next collision occurs. Thus, the particles follow an undisturbed motion as mentioned before until an event *i.e.* a collision occurs. In this approach, the forces between the particles are not considered explicitly. Such hard sphere collisions although artificial can be valid in certain circumstances where multi particle contacts are rare. Hence, such a model is not useful for dense particle systems and especially not for sand-rubber mixtures, due to the presence of soft rubber particles.

2. **Contact Dynamics model**

   The non-smooth contact dynamics or in short Contact Dynamics (CD) method was developed by Jean Jacques Moreau in the year 1984. It can be used for many applications however, this method is particularly found useful in case of quasi-static packings and dense granular flows. The method consists of a formulation of unilateral contact, Coulomb friction and shock laws. An implicit algorithm such as the Non-Linear Gauss Seidel algorithm is used to manage it [Dubois et al., 2018]. The main difference between Molecular Dynamics method (described below) and Contact Dynamics is the time step. In case of

17

the Contact Dynamics method, the time step considered is quite large. This time-step is system dependent, *e.g.* in case of a shear event, it decreases with the shear rate. Unlike the Molecular Dynamics method, here the effect of small time scale is included in every contact interaction through a non-smooth approach and the interest lies more in understanding the large time scale effect and large displacements. Such a method can be useful to better understand mechanical systems such as masonry structures wherein there exist frictional contact interactions. However, again such a method cannot be applied for studying granular systems such as sand-rubber mixtures since the grains are assumed to be perfectly rigid.

3. **Soft Sphere Molecular Dynamics model**

The soft sphere approach is another approach of the Molecular Dynamics method, wherein the particles are rigid as well. However, this approach considers small overlaps between the contacting particles in order to accommodate for particle elasticity. It was first developed by Cundall and Strack [1979]. Such a method is useful to model granular systems wherein the particles have difference in the elasticity. Thus, using the small overlap approach as shown in Fig. 1.8, the difference in the particle elasticities can be incorporated and can help to mimic the real behavior of such systems to a considerable extent. Such a method is hence useful for studying the behavior of granular systems
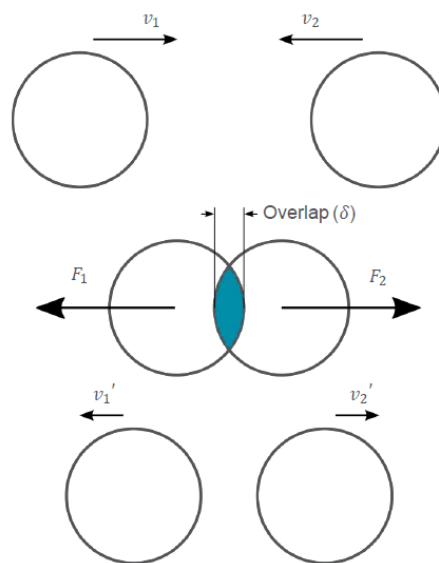
FIGURE 1.8. Figure showing the overlap between the contacting particles which are used to calculate the magnitudes of the forces acting on the particles for soft sphere approach

such as sand-rubber mixtures, wherein rubber particles are deformable. Hence, a small overlap between the contacting particles can help to replicate the small deformations of rubber particles in such systems.

Further, there are even models which implement combined Finite Element and Discrete

Element (FEM-DEM) method in order to accommodate for larger deformations of rubber particles [Indraratna et al., 2019]. But such models can be computationally demanding. Another method can be imagined wherein the volume of overlap is redistributed to the rubber particles. Then, in such a case, higher deformation of rubber particles can be studied as compared to the conventional soft sphere approach. Such a method is the first of its kind and will be discussed in the last chapter of this manuscript.

1.5.3 Numerical analysis of sand-rubber mixtures using DEM: State of the art

As mentioned before, the DEM analysis may help to investigate the micro-scale properties of sand-rubber mixtures, *i.e.* properties at the contacts of the particles, which is difficult to realize using the laboratory tests. Hence, it has been a subject of interest and there exist a few numerical studies on sand-rubber mixtures.

Valdes and Evans [2008] investigated the behavior of sand-rubber mixtures under isotropic as well as 1-D compression, mainly for strains smaller than 20% and specifically with an aim to use the sand-rubber mixtures for filtration applications. They have reported that with the increasing sand content, residual strains decrease, however the compressibility of the mixtures reduces. Further, Evans and Valdes [2011] studied the 1-D compression of sand-rubber mixtures using DEM to understand the force percolation, load bearing and void ratio evolution. They conducted the studies on different mixing fractions and particle sizes. They have reported that the force percolation depends on the mixing fraction and particle size ratio. Moreover, highly stiff particles are the major force carriers in the network. They conclude that the mixing fraction and size ratio are the major factors involved in the mixtures design affecting the mechanical response of these mixtures.

Eidgahee and Hosseininia [2013] report the results of bi-axial tests on sand-rubber mixtures simulated using DEM. They conclude that with an increasing rubber fraction, the shear strength decreases and compressibility of the mixtures increases. Moreover, lateral strain ratio was also found to decrease with the increasing rubber fraction; thus encouraging the use of such mixtures for applications such as the backfills of retaining walls. The numerical simulations performed by Lee et al. [2014] under oedometric compression report the effect of rubber content on the behavior of sand-rubber mixtures. They have reported an interesting observation that sand-rubber mixtures show a transitional behavior from sand-like to rubber-like depending on the rubber content and the strain level.

Perez et al. [2016] studied the behavior of sand-rubber mixtures under triaxial compression using DEM. They report the effect of rubber to sand particle size ratio and rubber content on the micro-mechanical properties of the mixtures. They have explained the effect of rubber content and size ratio with the help of a phase diagram, shown in Fig. 1.9. The dependence of the mixture behavior on the sand-rubber type of contacts in the mixtures with the increasing
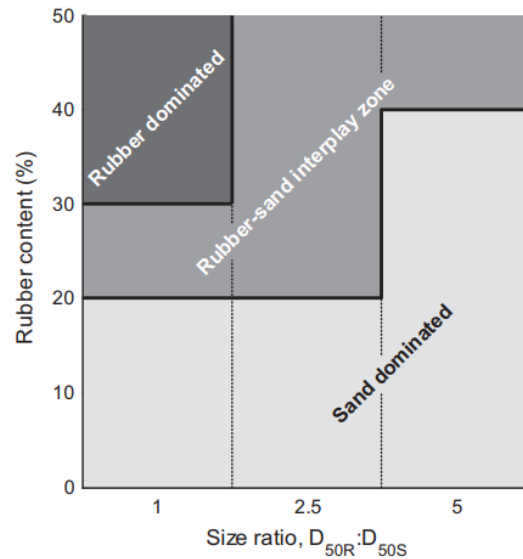
FIGURE 1.9. Phase diagram to explain the effect of rubber content and size ratio on the behavior of sand-rubber mixtures [Perez et al., 2016].

rubber content has been clearly pointed out in Fig. 1.9. Instability and small strain behavior of sand-rubber mixtures has been investigated by Lopera Perez et al. [2017a] and Lopera Perez et al. [2017b] respectively, by performing DEM simulations of triaxial monotonic compression tests. Different parameters such as coordination number, fabric tensor and normal contact force anisotropy has been studied. The effect and contribution of each type of contact, *i.e.* sand-sand, sand-rubber and rubber-rubber has been studied. A similar observation, *i.e.* mixture behavior lying in between sand-dominated and rubber-dominated was reported. Liquefaction characteristics of sand-rubber mixtures was studied by Lopera Perez and Kwok [2016] by performing DEM simulations on sand-rubber mixtures under shear. It has been reported that with the increasing rubber content, the mixtures became less susceptible to liquefaction. Further, micro-mechanical analysis from shearing stage to critical stage was studied by Perez et al. [2017] by performing a series of triaxial tests on sand-rubber mixtures using DEM simulations. The effect of particle size ratio and rubber content was studied. It was reported that with the increase in the rubber size, the shear strength of the mixtures reduced. In general, the contribution of sand-rubber contacts and the rubber size were the main parameters affecting the overall strength.

Platzer et al. [2018] have reported a minimal model by studying the isotropic loading of sand-rubber mixtures. It has been hypothesized that with the increase in loading, rubber particles deform and hence volume of voids reduces which is then filled by rubber particles. In short, it has been reported that rubber particles play two different roles, *i.e.* participating in load bearing network and acting like an inert void portion. Asadi et al. [2018] have reported the results of DEM simulations performed on sand-rubber mixtures under triaxial compression. It was observed that the strength and stiffness of the mixtures reduced with the increasing rubber content. Moreover, 40% rubber content has been reported to be the boundary line between

sand-like and rubber-like mixture behavior.

Although as mentioned before, several good number of studies exist for sand-rubber mixtures using DEM analysis, still there are very few studies which concentrate on the DEM analysis under oedometric compression and also on the effect of microstructure on the macroscopic response of the sand-rubber mixtures. Hence, there is always an interest to investigate the mechanical response of sand-rubber mixtures using DEM. For the same reason, DEM analysis has been done in this study and will be discussed in detail in a later chapter of this manuscript.

1.6 Is mixing quality important for sand-rubber mixtures?

Both, the laboratory studies and numerical studies mentioned in the previous sections describe the effect of rubber content, rubber particle size, initial void ratio, etc. on the mechanical response of sand-rubber mixtures. A few laboratory studies clearly point out the importance of homogeneity of mixtures during their fabrication. However, the majority of the studies done till now investigate the homogeneity of mixtures only by visual inspection. However, the homogeneity or uniformity of mixtures has a high importance, especially because sand and rubber are heterogeneous constituents. Hence, their perfect mixing is not straightforward.

All the studies point out that the major load bearing force network consists of maximum number of sand-sand type of contacts, thus indicating the importance of sand particles as force carriers. Consider Fig. 1.10 which shows a typical force carrying chain. Obviously, high
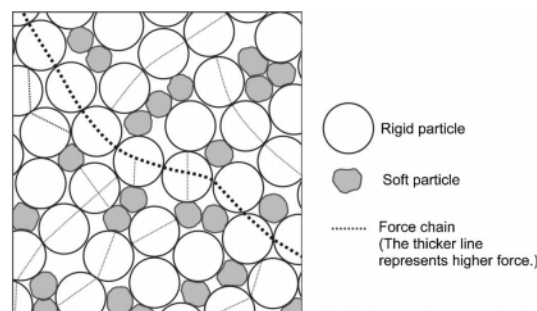
FIGURE 1.10. Figure showing the typical photo-elastic result interpreting the force chains. High load carrying chains do not involve soft particles but still rubber prevents buckling of these force chains [Lee et al., 2007].

load carrying chain is always formed by the stiffer particles, hence in this case by the sand particles. However, this supposition is valid on the basis of the mixture uniformity. It can be imagined that a sand-rubber mixture is formed with alternate layers of sand and rubber having equal layer-size. In such a case, the force chains are forced to include even the soft particles in the high load carrying network. This, in turn will affect the deformability of the sand-rubber mixtures. Hence, such a mixture will deform at a lower stress than a similar mixture with a

better homogeneity. Moreover, even if more rubber particles are not involved in the high load bearing networks, still a non-homogeneous distribution of rubber particles might not provide a similar stability to the major force carrying chains throughout the packing.

Consider a real time application of backfill of a retaining wall reinforced using shredded waste tires. If there is a huge accumulation of rubber in a certain section of the backfill, then there is a huge potential of failure of the wall in this particular section due to different reasons. A localized excessive deformation may occur as compared to the other sections. Moreover, sand-rubber mixtures show a time-dependent mechanical response [Ngo and Valdes, 2007, AbdelRazek et al., 2018], especially with an increasing rubber content. Hence, such a huge accumulation of rubber will cause a greater settlement and thus the failure of the entire structure.

Similar mechanical problems can be imagined in case of other geotechnical applications of sand-rubber mixtures. Additionally, the conventional laboratory testing is the most chosen pathway to explain the potential of sand-rubber mixtures, however the effect of non-homogeneity can be expected to be higher at the laboratory scale. Hence, it is interesting to quantify the effect of mixture quality in case of sand-rubber mixtures. However, mixing goes hand-in-hand with the segregation phenomena.

Segregation is a popular research interest in the domain of granular materials Ottino and Khakhar [2000]. In the case of heterogeneous granular materials such as sand and rubber, it is challenging and interesting to study the segregation phenomena. At the laboratory scale, the segregation phenomena can occur during the mixing of sand and rubber particles. However, in real-time conditions, certain situations can be imagined where segregation can be observed; *e.g.* on-site mixing of sand and rubber particles, transportation of mixed sand and rubber by lorries/ trucks to use it for a certain application, pouring of sand-rubber mixtures from the lorries at the application site, etc. Hence, quantifying segregation is equally important in order to completely understand the effect of mixing quality for sand-rubber mixtures.

The main objective of this study is to analyze and quantify the quality of mixing for sand-rubber mixtures and in turn quantify the segregation at a laboratory scale to better understand its occurrence by replicating certain real-time conditions mentioned before.

1.7 Organization of the thesis

In this chapter of the thesis, a brief introduction to the importance of waste rubber tire recycling, use of powdered rubber and the increasing research interest concerning sand-rubber mixtures has been presented. Further, a literature review concerning the experimental and numerical analysis of sand-rubber mixtures was also presented.

Chapter 2 of this thesis presents the segregation analysis conducted at the laboratory-scale by performing vertical tap experiments using a vibrating shaker. The segregation has been studied using image analysis techniques and these results will be presented in this Chapter.

Chapter 3 of this thesis will present the laboratory-scale oedometer test results conducted on sand-rubber mixtures. It will detail out the effect of initial void ratio, rubber content, size fraction on the mechanical response of sand-rubber mixtures. In the end, an idea concerning the analysis and quantification of mixing quality will be presented in this Chapter.

In Chapter 4 of the thesis, results of the numerical simulations using Discrete Element Method (DEM) will be presented. The response of sand-rubber mixtures under oedometer compression has been quantified in this Chapter using DEM. The mixing phenomena has been analyzed in detail and the results of the same will be presented. Further, the micro-mechanical parameters such as contact forces, force distributions, force orientations have been studied and will be detailed out in order to support and validate the results presented in the previous Chapter.

Chapter 5 of this study, will present in brief the results for a new numerical model using DEM which can allow for the consideration of larger overlaps and hence higher deformation of rubber particles than the conventional soft sphere model.

This thesis is the starting point for a new research subject in GPEM laboratory. Although sand-rubber mixtures have been under extensive research throughout the world, it is a wide domain and there are still a lot of things to be unravelled in this particular domain. An effort has been made in this thesis to address the question of mixing quality in sand-rubber mixtures via different techniques. Thus, the reader will be able to see that the subjects addressed and the tools used in this thesis are quite diverse, thus requiring a constant learning and development of new experimental and numerical techniques and methods.

SEGREGATION ANALYSIS USING VERTICAL TAP EXPERIMENTS

Summary

This chapter aims to address the problem of segregation in sand-rubber mixtures. Since sand and rubber particles have different densities, hence it is quite expected to observe segregation in such mixtures. Moreover, size difference, rubber volume fraction, conditions at the point of application as well affect the mixture quality. An effort has been made to analyze the segregation due to vertical taps at the laboratory scale, which on a real time scale can be related to conditions such as transport of sand-rubber mixtures in lorries or trucks. Further, Digital Image Processing techniques have been used in order to better understand and analyze the segregation observed under the aforementioned conditions.

Contents

2.1 Introduction

The main objective of this study is to analyze the effect of mixing quality on the mechanical response of sand-rubber mixtures. Sand and rubber being the constituents with extremely different density, it is interesting to study the segregation behavior of such type of mixtures. Analyzing the segregation between sand and rubber can help to better understand the variation of the mixture quality and further its effect on the mechanical response of sand-rubber mixtures. Whenever mixing between particulate materials is involved, segregation is ought to occur. It is the type of segregation which varies depending upon the mixing conditions. When a system of particulate materials with different properties is mixed, then the particles with the same properties show a tendency to collect together. Consequently, such systems show that the particles unmix upon handling. The different particle properties which can cause segregation include [Williams, 1976]:

1. Difference in particle size

2. Difference in particle density

3. Particle shape difference

4. Difference in particle resilience

Obtaining a good mixture quality in a system consisting of particles with different properties is quite challenging. However, it can be important from an industrial point of view. A simple schematic shown in Fig. 2.1 explains the different types of mixtures. Consequently, a perfect
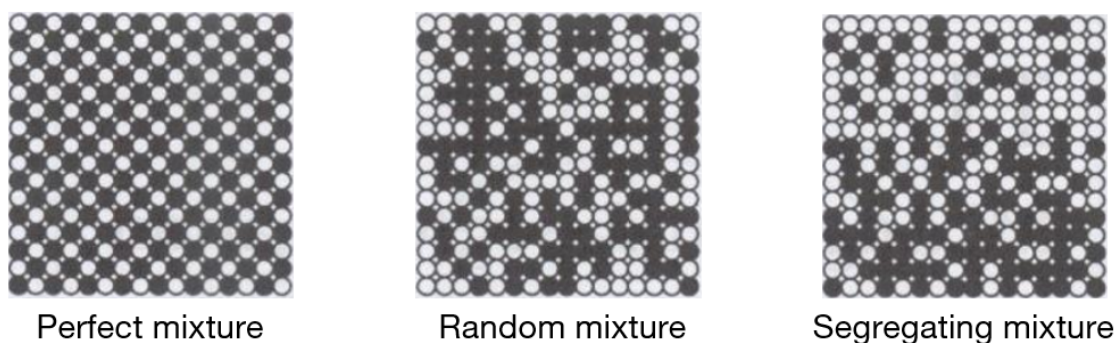
FIGURE 2.1. Schematic showing the basic mixture types.

mixture will have the same proportions of any type of particle at any position in the mixture as the proportions present in the whole mixture. On the other hand, a random mixture is the one in which the probability of finding a particular type of particle is the same at all positions in the mixture and it is equal to the proportion of that type of particle in the whole mixture. Further, segregated mixture is an unmixed mixture which has reached this state due to the aforementioned difference in the properties of the constituent particles. Even if the particles

have been mixed, due to their different properties they tend to segregate during handling and hence it makes important to understand segregation due to the difference in the particle properties.

The first work reported on segregation was by Donald and Roseman [1962], who performed the experiment of mixing particles of different sizes and densities in a rotating horizontal drum. In general, the commonly known segregation mechanisms include trajectory segregation, fine particles percolation, and the rise of coarse particles on vibration [Kudrolli, 2004]. However, all these mechanisms are attributed to the segregation due to size difference between the particles of the system. Some other works have also been reported which detail out the segregation due to mechanisms such as rolling, sieving, soil crushing, etc. [Kuerbis and Vaid, 1988, Ottino and Khakhar, 2000, Lőrincz et al., 2005, Watabe et al., 2014].

Particularly, in case of sand and rubber mixtures, material segregation can occur during the preparation, *i.e.* mixing, compaction, pouring or even transportation phases. Since sand-rubber mixtures have interesting applications in geotechnics, such segregation can lead to heterogeneity and thus cause instability problems such as liquefaction [Yoshimine and Koike, 2005]. Sand and rubber differ clearly in terms of density and hence it is the major factor responsible for segregation in such mixtures. Moreover, there are differences in the surface roughness as well as the particle elasticity. A distribution analysis for the laboratory fabrication of sand-rubber mixtures was done by Rouhanifar and Ibraim [2015] using a 3D X-ray CT testing. It was reported that the dry deposition, compaction and vibration of samples showed segregation with a higher concentration of rubber particles at the tops of the sample. The most recent work on the study of segregation in sand-rubber mixtures has been reported by Wang et al. [2018]. They have performed a comparative study of the experiments and Discrete Element Method (DEM) to verify the segregation of sand-rubber mixtures forming a heap. Thus, they have performed experiments and numerical simulations involving pouring of sand-rubber mixtures through a hopper to form a heap and then studying the heap formed using the Digital Image Analysis techniques. They have concluded that the segregation in such mixtures is highly driven by the density difference. Other parameters such as surface roughness, material stiffness, etc. almost had a negligible impact.

In this study, an effort has been made to investigate the segregation in sand-rubber mixtures for two real-time conditions, *viz.* mixing and transportation of sand-rubber mixtures. The idea was to mix the sand-rubber mixtures and then simulate experimentally a condition similar to the transportation of such mixtures on roads using lorries/trucks. Digital Image Analysis techniques have then been used to quantify the segregation observed under both these conditions. This Chapter will report the methodology, experimental setup and the observations during these experiments in detail.

2.2 Experimental Method

As mentioned before, the objective of the experiments was to verify the segregation in sand-rubber mixtures after mixing and after subjecting to vibrations of specific frequency to replicate the real-time transportation process of these mixtures. The sand used for the experiments was white quartz sand and the rubber used was recycled tire rubber. The sand chosen was white quartz since it was convenient (due to its color) to perform the segregation analysis using the Digital Image Analysis techniques. Both the sand and rubber were sieved between the same particle size distribution of 0.8mm-4mm. The experimental procedure consisted of 4 major steps:

1. Mixing of measured mass of sand and rubber

2. Vibration of mixed sand and rubber using a vibrating shaker

3. Solidification of sample using a binder

4. Capturing images of solidified samples

All these stages will be detailed out in the following sections. Three important parameters which were studied during the experiments were: sand/rubber grain size ratio, rubber volume fraction and moisture content. In particular,

(a) 3 sand/rubber (S/R) size ratios were studied: S/R=0.63 (sand: 1.25-1.6mm, rubber: 2-2.5mm), S/R= 1(sand: 2-2.5mm, rubber: 2-2.5mm) and S/R= 1.98 (sand: 2.5-3.15mm, rubber: 1.25-1.6mm)

(b) 2 rubber volume fractions were studied: 25% and 50%

(c) 2 moisture conditions, *viz.* without moisture and with moisture were studied.

An important point to be noted is that all these processes have been carried out at the laboratory scale.

2.2.1 Sand-rubber mixing process

Before starting the mixing process, it was important to consider the type of mixer to be used in order to mix the soft (rubber) and rigid (sand) grains. Apart from this, these mixed samples were also to be subjected to vertical vibrations on a vibrating shaker and to be used for solidifying the entire sample using a binder for further analysis. Thus, choosing an appropriate mixing bowl/ mixing container as well as the type of mixer was an important first step. It was possible to use some laboratory mixer such as a planetary mixer. However, the mixing bowl of such a mixer is quite big to be used for vibration tests. Secondly, if the mixed samples were to be poured into another container, then segregation could occur during pouring as well. Moreover,

due to the metal blades in such mixers, the rubber particles may get cut. For this purpose, mixing blades were fabricated using a polymer material called PLA (Polylactic acid), in a laboratory 3D printer (ULTIMAKER 2+). Further, a cylindrical metal container of 110 mm in height and 108mm in diameter was chosen as the mixing container. The mixing blades were designed by taking into account the dimensions of this container. Given that the container was also to be used for further purpose of vibration experiments and solidification using a binder, a height/diameter aspect ratio of 0.6 was chosen for fixing the top height of the material and consequently calculating the required mass of sand and rubber. In order to achieve mixing till the bottom depth of the container, 4 vertically equally spaced mixing blades were mounted on a shaft. This shaft with the mixing blades was mounted on a commonly used laboratory agitator (see Fig. 2.2). It can be seen that each of the mixing blade is arranged perpendicular to the other in order to ensure uniform mixing. For the measurement of masses of sand and rubber to
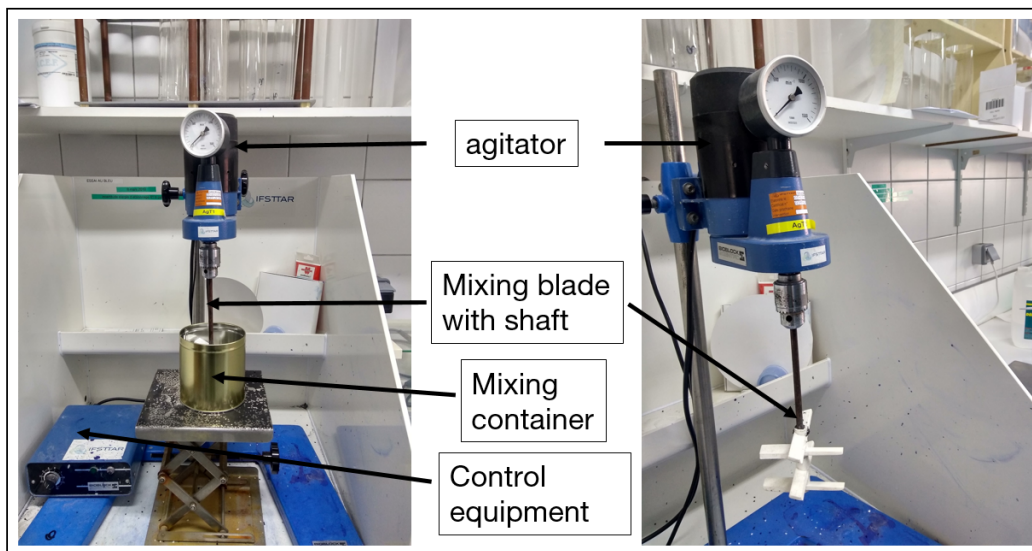
FIGURE 2.2. Experimental setup for mixing sand and rubber.

be used, the bulk density of sand was considered as $\rho_{bulk_{sand}}$ = 1500 kg/m^3 and for rubber as $\rho_{bulk_{rubber}}$ = 600 kg/m^3. Considering a height/diameter aspect ratio of 0.6 as mentioned earlier, masses of sand and rubber required for the given volume of the metal container were calculated accordingly. Moreover, the masses also varied with the variation in the rubber volume fraction. The mixing process started with measuring the required mass of sand and rubber in glass beaker and pouring it using a small hopper into the mixing container fixed with the mixing blades. In case of mixing process with cohesion (with moisture), measured quantity of water was added to the mixture poured in the container. Further, using the control equipment, the rotational speed of the shaft could be adjusted. In order to have uniform mixing and also not allow the lighter rubber particles to fly due to high rotational speed, the speed was fixed as 250 rpm (revolutions per minute) and the sample was mixed for 1 minute. After the mixing process, the container was lowered using the adjusting platform and moved carefully to the

vibrating shaker equipment. The mixing quality had to be analyzed as well and it constituted as a basis to quantify the segregation (if any) due to the vibrating shaker. Hence, for such cases the mixed sample container was carefully lowered down and directly the solidification process using the binder (explained in further sections) was implemented.

2.2.2 Tests using the vibrating shaker

The sand-rubber mixture container was transferred carefully to the vibrating shaker in order to perform tests for segregation under vibration. The objective behind subjecting the sand-rubber mixture to vertical vibrations was to replicate the process of transport of such mixtures in trucks/ lorries on roadways. It was impossible to replicate it to a real time scale, and hence the vibrating shaker was found to be the best choice. An advantage of the vibrating shaker was the possibility of its control using an external signal control and acquisition system. This allowed to test and modify different control parameters such as frequency of vibrations, intensity of the vibrations, number of vibrations/ time, etc. Fig. 2.3 shows the the experimental setup for
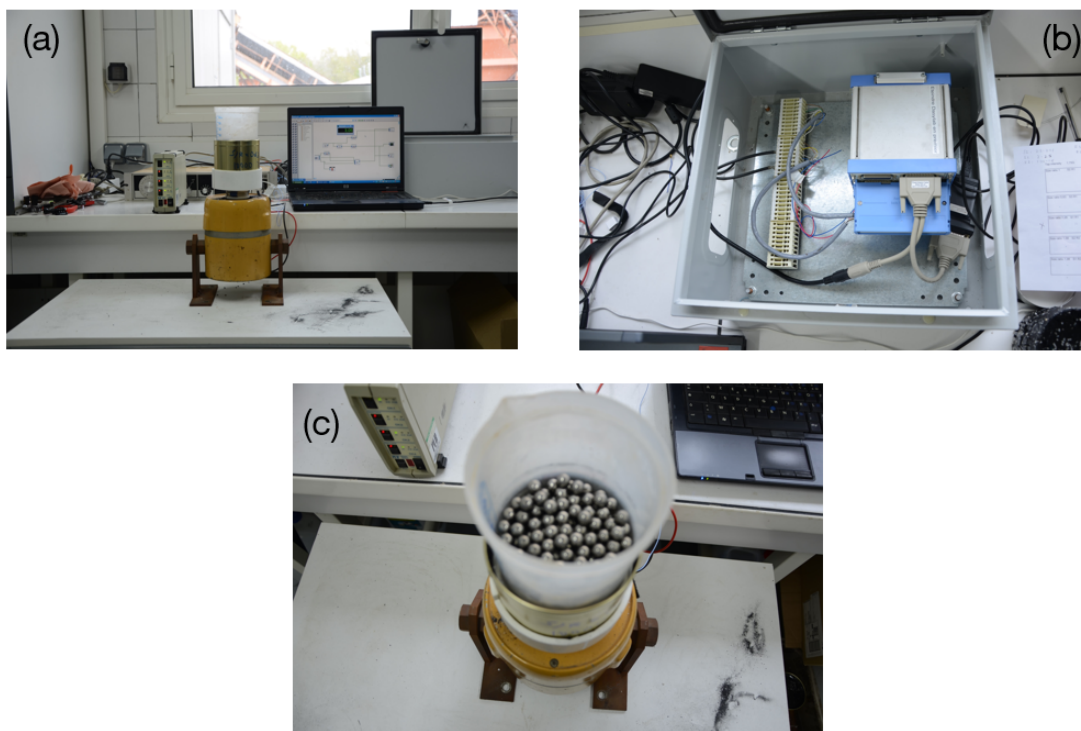
FIGURE 2.3. Experimental setup showing (a) vibrating shaker with the sand-rubber mixture container on top and with all the control equipment, (b) signal control and acquisition system, (c) counter-mass containing steel beads used during the experiments.

the vibration tests. In Fig. 2.3(a), the vibrating shaker with the sand-rubber mixture container mounted on top can be seen connected with the external signal control and acquisition system. The signal control and data acquisition were performed using the InstruNet control system

(see Fig. 2.3(b)) and the software DasyLab.

The sand-rubber mixture container was placed on the top of a holding arrangement connected to the vibrating shaker (LDS V406). In order to replicate the real-time condition of transportation of sand-rubber mixtures, the method adopted by Ribiere et al. [2005] was found to be coherent. Consequently, the vertical tap/ vertical displacement was created in the vibrating shaker by using the signal control system comprising of Instrunet (iNet 410) and DasyLab software. Each vertical tap was created by selecting an entire period of sine wave at a constant frequency $f =$ 30Hz and the mixture container was shaken at intervals of $\Delta t = 1$s. As explained by Ribiere et al. [2005], the resulting overall motion of the entire system is much more complex. For a better understanding, an example of a signal monitored by the accelerometer has been presented in Fig. 2.4. As seen in Fig. 2.4, shown by the red circle, the system initially undergoes
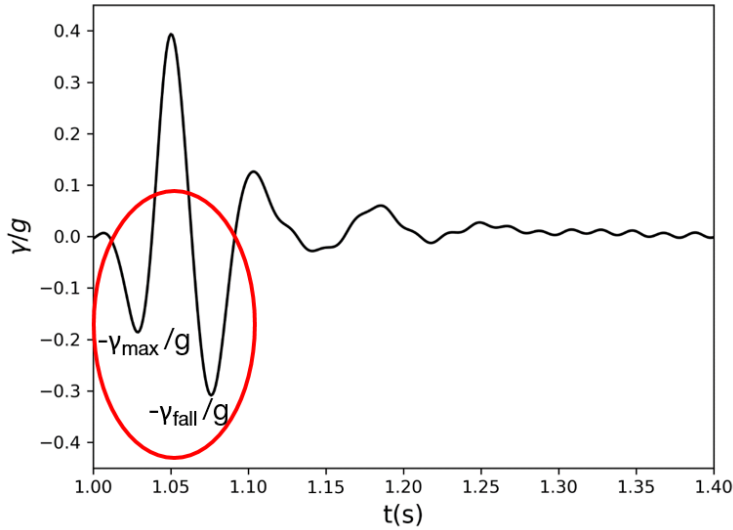
FIGURE 2.4. Example of a signal monitored by the accelerometer.

a positive acceleration followed by a negative peak equal to $-\gamma_{max}$. Further it again undergoes a rise shown by a positive acceleration and then the fall of the mixture to the bottom of the container has been represented by $-\gamma_{fall}$. Thus, the acceleration created by the fall, $-\gamma_{fall}$ can be different from the first acceleration peak, $-\gamma_{max}$. For this study, only the first acceleration peak was of interest. The most important parameter was the intensity (Γ) of the vertical tap, defined by $\Gamma = \gamma_{max}/g$, where g is the acceleration due to gravity.

The choice of the vertical tap intensity (Γ) was important considering that the objective was to observe and investigate the segregation between sand and rubber. Thus, the tap intensity chosen had to be enough to achieve segregation. Moreover, it was not be high enough wherein the segregation observed would be including the effect of the shape of the mixture container, since that would render useless the entire aim of the replication of transport process. For this purpose, tests were conducted for different vertical tap intensities wherein the top free surface of the mixture container was analyzed using the images captured with a high speed

camera. A simple contrast level analysis differentiating the black and white contrasts, helped to verify the segregation at the different tap intensities. As shown in Fig. 2.5, for each of the
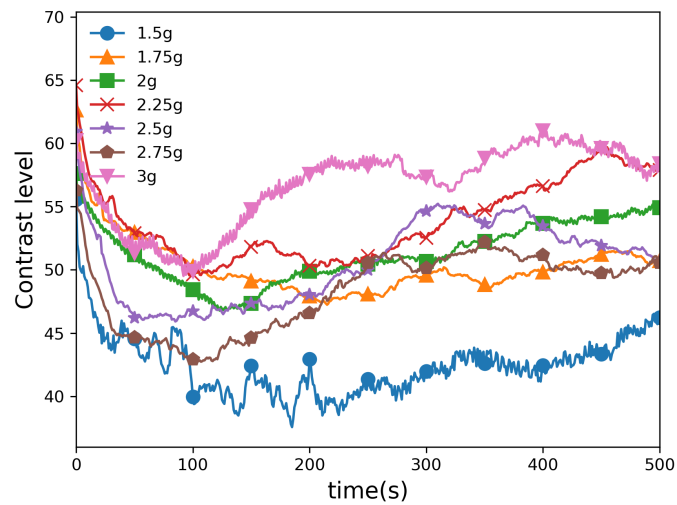
FIGURE 2.5. Contrast level of the free surface of mixture container observed for different vertical tap intensities (tap intensities indicated are in the form of γ_{max}).

tap intensities, the contrast level goes on decreasing, thus indicating that the number of black particles, *i.e.* rubber grains goes on increasing with the time. However, slowly the contrast level can be seen to rise, indicating that the particles at the bottom start to come up and the mixture undergoes remixing (convection effect). However, this remixing is strongly dependent on the size and shape of the container used. It can be probably attributed to the small system size and therefore, it had to be avoided in this study. For this purpose, a technique suggested by Philippe [2002] was used, wherein a mass equivalent to the mass of sand-rubber mixture was placed on the top of the container. This counter-mass placed on the free surface of the mixture container during the vertical taps has been in shown in Fig. 2.3(c). This technique was observed to be extremely effective in avoiding the effect of the shape of the container. Further, the intensity of the vertical taps chosen for the tests was $\gamma_{max} = 3g$, since the earliest onset of segregation was observed for this intensity (see Fig. 2.5). Different sequences of vertical taps ranging from 10^2 to 10^4 were performed which will be explained in detail in the further sections.

2.2.3 Solidification of the sand-rubber mixture sample using a binder

The sand-rubber mixture sample was to be analyzed for segregation after the mixing process as well as after being subjected to the vertical taps using the vibrating shaker. One would think that the contrast level analysis (see Fig. 2.5) could be the simplest way of analyzing it. However, this analysis allowed only to study the segregation at the surface of the sample (the

mixture container used being metal) and moreover, the vertical taps were performed with the counter-mass, thus the surface no more being visible.

For this purpose, the solidification technique used by Dal Grande et al. [2008] was found to be effective. A commercial gel for candles by Candelis was used as the binder material. The mass of gel used was equal to the mass of sand-rubber mixture in the container. The binder gel was solid enough to be cut and placed on the mixture sample in the container. So, the gel was cut and placed on top of the mixture after the mixing and the vertical tap process (see Fig. 2.6). This was another reason chosen for the height/diameter aspect ratio to be 0.6 for the experiments, to allow enough space to accommodate the gel. Such a container with the mixture
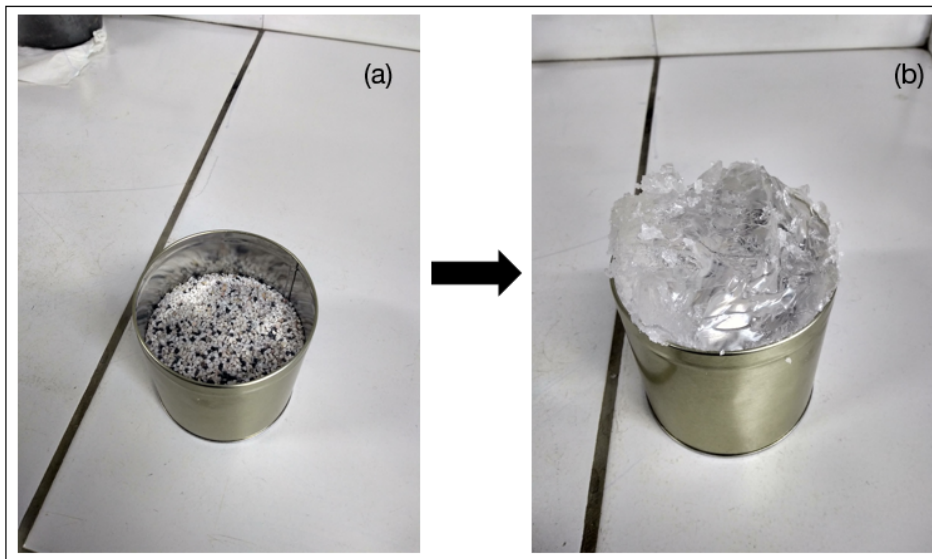
FIGURE 2.6. Sand-rubber mixture sample (a) without gel and (b) after placing cut gel on the top.

sample and gel was then placed in the oven at 80°C for 6h in order to allow the gel to melt and uniformly impregnate the container. The gel melting temperature was about 75°C. Further, in order to avoid the entrapment of air bubbles in the mixture container, several small holes (diameter 0.5mm) were drilled at the bottom of the container before filling the container with the sample. After 6h, it was ensured that the excess gel was coming out through all the holes at the bottom of the mixture container, thus confirming the completion of the melting of the gel. The mixture containers were then removed from the oven and allowed to cool down and solidify at the room temperature for over 12h. One of the most critical steps in this process was ensuring that the gel had wetted the entire mixture in the container, thus not leaving any dry zones which would lead to the loss of structural integrity in the container and lead to hollow spaces during the slicing operation (see Fig. 2.7). For this purpose, several initial tests were conducted wherein the mass of the binder gel used, temperature of the oven and time for which the samples were kept in the oven were varied. The parameters mentioned above and the process described were found to be effective in obtaining good quality solidified samples.
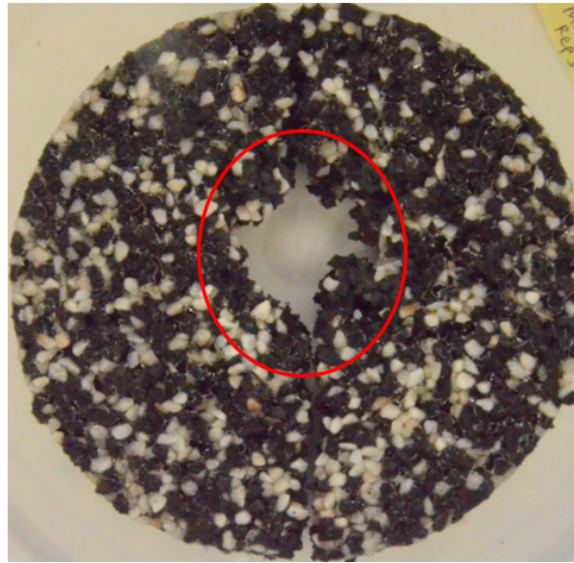
FIGURE 2.7. Partially solidified slice leading to dry zone of particles (shown by red circle) which escaped during slicing.

2.2.4 Capturing images of solidified samples
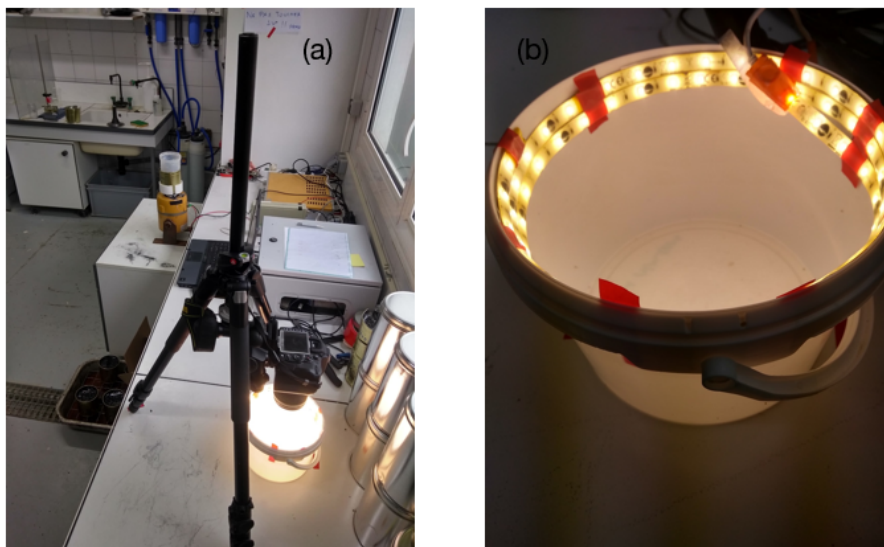
FIGURE 2.8. Setup used for capturing images: (a) Entire setup with the digital camera and the container for placing the slices, (b) White container with the LED lights for placing the sample slices to capture images.

After ensuring that the sand-rubber samples with the gel in the container were completely solidified, the mixture containers were cut with a knife and opened in order to remove the sample. Now, it was possible to cut the sample into slices in order to study the segregation inside the mixture. An important step was the decision concerning horizontal or vertical slice cuts and the number of slices. It was important in order to avoid a biased approach in quantifying the segregation inside the mixture. Hence, several slicing tests were done and no vertical profile for

segregation was observed. Moreover, the number of slices was quite important as well in order to obtain maximum possible information to better quantify the segregation and at the same time, not to disturb the structure while slicing. Thus, it was decided to have 5 horizontal slices of the entire solidified mixture sample. The slices were cut very carefully in order to minimize the loss of grains during the process.

The slices of the solidified samples were then placed inside the white container with LED lights (see Fig. 2.8) and images were captured using the digital camera. For every slice, there were two surfaces of which the images were taken, *i.e.* bottom surface and top surface of the slice. Images of all such slices were taken and then they were used further for analyzing the segregation in the mixture.

When the images of the slices were captured, some tiny portions of the gel were observed on the surface of the slice. Since they would cause a problem during the digital image analysis, it was best to minimize such portions of gel as much as possible. For this purpose, after the slices were cut, a heat gun was used to gently allow the small portions of the gel to melt and settle down. Then, the images of the slices were captured using the process described above.

Thus, the experimental process was followed in the way described above and images of the samples were obtained which were then analyzed. The analysis and the results have been explained in the further sections.

2.3   Digital Image Analysis framework

The Digital Image Analysis or Digital Image Processing is the method of converting an image into digital form and then analyzing such digital image to extract the underlying information. The image analysis has been performed in this study by using a Python script. Some sample images of the slices of mixtures for sand/rubber (S/R) size ratio 1 have been shown in Fig. 2.9. If the images shown in Fig. 2.9 are observed closely, it can be seen that the after-treatment of the cut slices with the heat gun has helped to melt the pieces of gel, however it causes a glare effect which may alter the segregation analysis. Hence, it was one of the important points during the analysis. Moreover, the varying grain sizes was another important point since it may cause such glare spots to vary.

The image analysis framework applied in this study consists of the following steps:

1. The images captured were cropped around the size yielding an image size of nearly 3000 pixels x 3000 pixels (slight differences were observed due to the difference in the vertical height setting of the tripod used for capturing the images).

2. Any image is represented by the number of pixels. Each pixel is a combination of primary colors. Usually, a standard digital image uses red (R), green (G) and blue (B) channels which can be easily perceived by human eyes. Thus, the information extracted from the image is in the form of three intensity matrices, each corresponding to one of the R, G
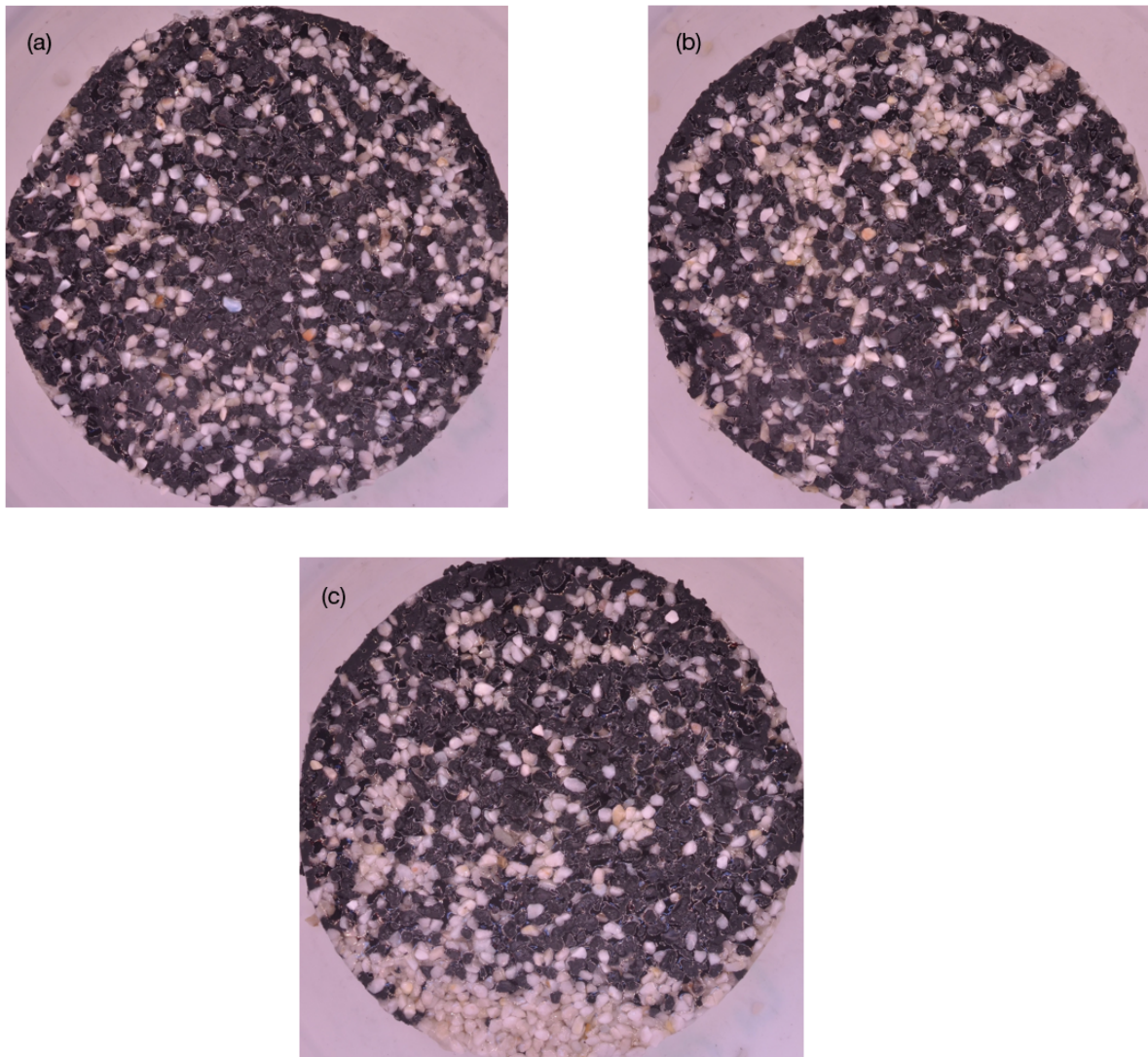
FIGURE 2.9. Sample images of sand-rubber mixture for size ratio 1: (a) after 100 vertical taps, (b) after 1000 vertical taps and (c) after 10000 vertical taps.

and B channels. The process of the image analysis started by reading these images in the RGB format, then they were converted to a grayscale format in order to have 1 intensity matrix instead of 3. In this case, it is easier since there is a clear distinction between black and white grains (sand and rubber). However, in much complex cases, the grayscale analysis might be complicated.

3. Further, a median filtering was applied to the images to minimize the glare spots produced and also to remove other noise in the images.

4. An image thresholding technique was applied in order to achieve a basic image segmentation. The mean threshold filter was used in this case (refer Filters Module in scikit-image using Python). This method simply calculates the mean of all the grayscale values of the image and replaces it with a black pixel if the image intensity, $I_{i,j}$ is less than some fixed

constant value or by a white pixel if the image intensity is greater than this constant value. Here, i and j represent the two gray channels of the intensity matrix for the grayscale image. Such an image thresholding helped to obtain a binary image of black and white pixels.

5. Since the background of the images (part outside the slices in Fig. 2.9) also has an attributed threshold value, it was important that this background was substituted with some value other than the black and white pixels to avoid its inclusion in the segregation quantification. Consequently it was done and the background was substituted with values other than 0 (white) and 1 (black).

6. Further, all the lines of the images were read and the lengths of the contiguous strips of white and black pixels over the horizontal rows as well as the vertical columns were measured for all the 5 slices of each sample, *i.e.* for 10 images and a histogram for the average of these lengths over all the slices was calculated. This histogram of the average lengths represented the basic quantification of segregation since it showed the lengths of the black and white pixel strips for a given image.

7. With the help of the histogram, different statistical parameters such as the mean and the variance could be plotted to better quantify and understand the segregation in the mixtures.

The parameters which varied in this framework were the parameters of which the effect on the sand-rubber mixture was to be studied, *i.e.* sand/rubber (S/R) size ratio, rubber volume fraction, effect of cohesion (moisture) and effect of the number of taps/ sequences of taps (10^2 to 10^4). The same have been discussed in the further sections.

2.3.1 Choice for the median filter kernel size

As pointed out previously, in the Section 2.3, a median filtering technique had to be applied to the images in order to remove the noise in the images as well as the glare spots due to the molten parts of gel. The median filtering is a non-linear filtering technique which analyzes the image pixel by pixel and replaces it with the median values of the consecutive neighboring pixels throughout the image. The kernel size used for the filtering is an important parameter. The kernel size is basically a filter aperture. Thus the pixels of the image smaller than the aperture size will be filtered out.

Consequently, different kernel sizes (N) varying between 1 and 100 were applied on the images of the slices and some of them have been shown in Fig. 2.10. For simplicity, only one face (same face) for each slice has been shown for every value of the kernel size and the images have been shown for the slices of sand-rubber mixtures after 10000 vertical taps. An optimum value of the kernel size had to be chosen because the important information was to be captured and at the same time the small noise and glare spots had to be removed. As can be seen in Fig. 2.10,
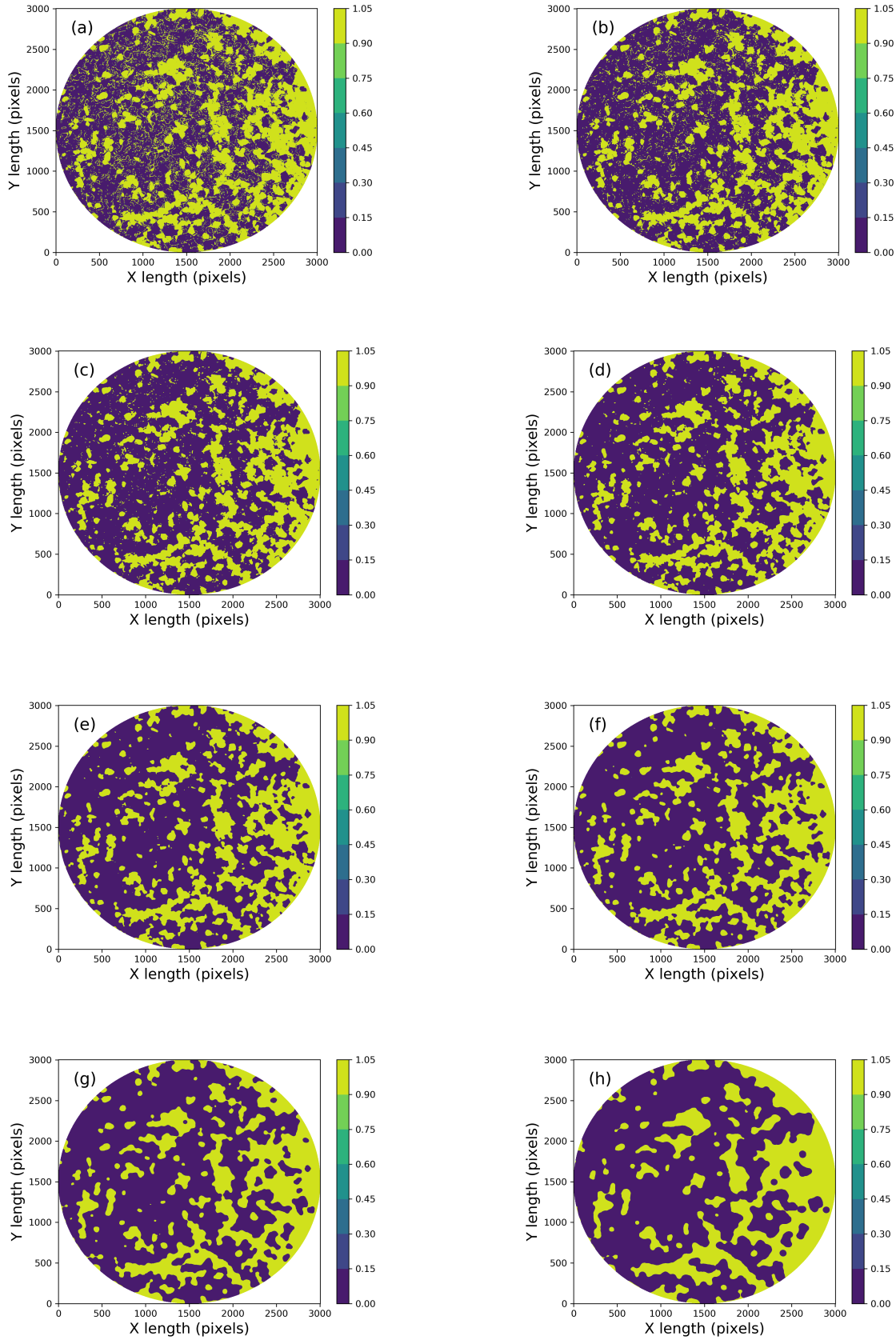
FIGURE 2.10. Masked slices of sand-rubber mixture for size ratio 1 with different kernel sizes (N) of median filtering: (a) N=1, (b) N=6, (c) N=11, (d) N=16, (e) N=21, (f) N=31, (g) N=51 and (h) N=81.

with the increasing kernel size, the small noisy lines present due to the molten gel can be seen to be decreasing. However, from the kernel size, $N= 21$ (see Fig. 2.10(e)), care should be taken to not lose the information. If the N value becomes greater than the particle size, then the filter leads to a smoothing out of the particles causing a loss of information. A huge difference can be observed between the images for the increasing kernel sizes (see Fig. 2.10(e) to (h)). A huge loss in the information of the grains can be seen between $N= 21$, $N= 51$ and $N = 81$. Apart from just analyzing the masked images, it was important to analyze the statistics over these slices. The plots for the same have been shown in Fig. 2.11. As explained before, the histogram for the
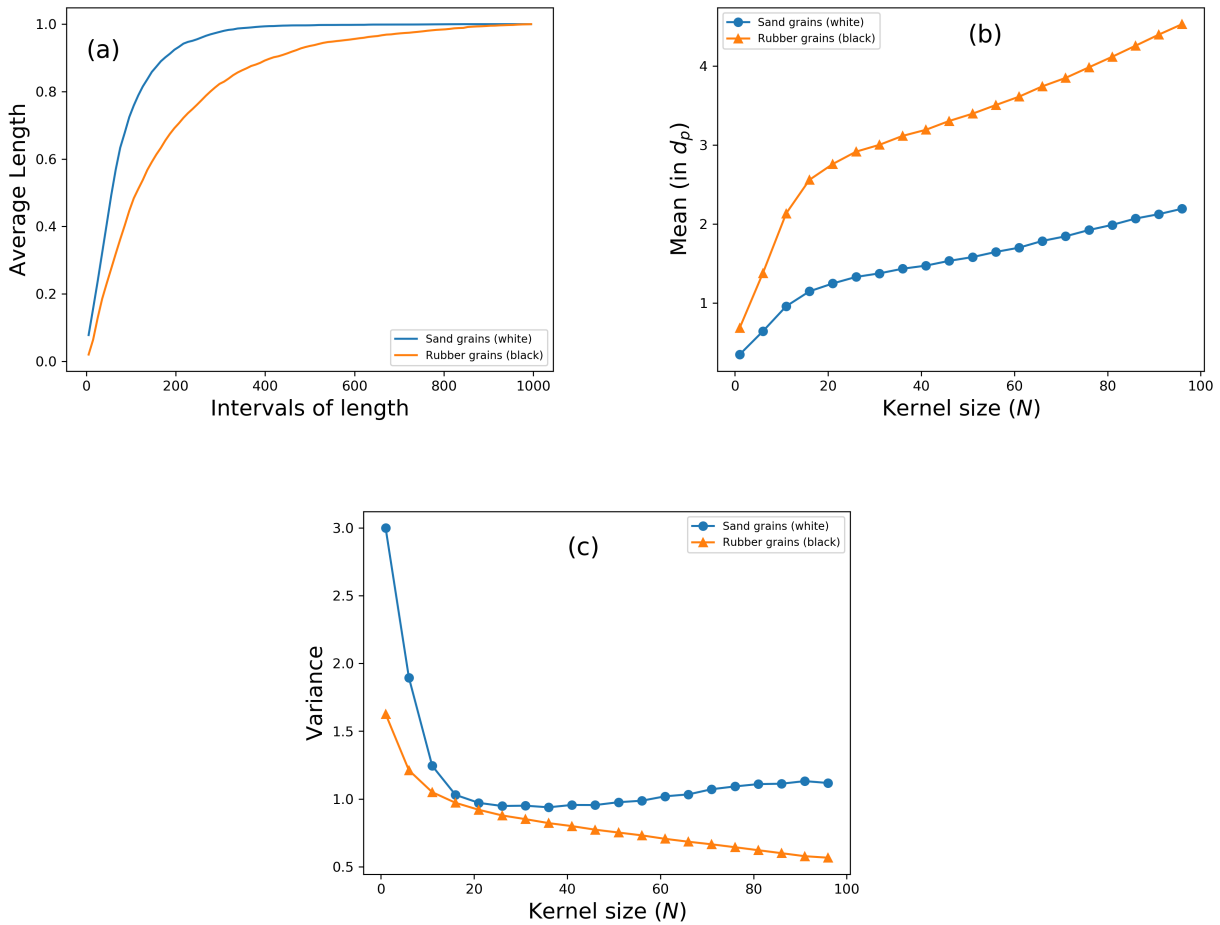
FIGURE 2.11. Statistical data measured over all the slices for sand-rubber mixture for size ratio 1 and 10000 vertical taps with different kernel sizes (N) of median filtering: (a) An example histogram for the lengths of black and white pixels over all slices for N=21, (b) Mean of the length distribution for black and white pixels over all the slices and (c) Variance of the length distribution for black and white pixels over all the slices.

lengths of contiguous white and black pixels over all the slices was constructed and then these statistical values have been calculated from such a histogram. All the information from the images is in the form of pixels. In order to better correlate the information with the real size of

the slices used for the images, a scaling factor had to be used. For this purpose, the data was converted from pixel to mm by multiplying all the statistical values with the scaling factor of $((108/3000)/ d_p)$. Here, d_p denotes the mean particle diameter for both sand and rubber grains, 3000 is the size of the slices in pixels and 108 is the size of the slices in mm. The parameter d_p was also important since the tests have also been performed to verify the effect of size ratio on the segregation behavior. Fig. 2.11(a) shows an example histogram for kernel size, $N= 21$. For all the tests, such a histogram gave an initial idea concerning the segregation between the sand and rubber particles. As shown in Fig. 2.11(a), the span of the histogram can be clearly seen to be different for the black and white pixels, thus indicating a segregation between the sand and rubber grains. In order to better understand it, the span of the histogram has been characterized with the help of two descriptors, *i.e.* mean and variance. The mean, m and the variance, V have been calculated respectively using the following formulae:

$$m = \frac{\Sigma(LB1)}{\Sigma(L)},$$ (2.1)

where, L = average length and $B1$ = number of intervals/bins in the histogram

$$V = \frac{\Sigma(L(B1-m)^2)/\Sigma(L)}{(m)^2}.$$ (2.2)

Fig. 2.11(b) shows the mean of this histogram for S/R= 1, rubber volume fraction of 50% and for the images of slices obtained after 10000 vertical taps. From the masked slices, it can be seen that with the increasing kernel size N (above $N = 21$), the important pixel data also is lost. If it is related to the plot in Fig. 2.11(b), then it can be seen that the value for the mean increases continuously, however the rate of increase beyond $N=21$ is low as compared to the values of N up to 21. However, the plot for the variance of the histogram (see Fig. 2.11(c))helps to better understand the choice for the kernel size. The variance gives an idea as to how the values deviate from the mean of the data. Thus, it can be clearly seen in Fig. 2.11(b) that the variance values nearly remain constant for the white pixels for values beyond $N= 21$, thus suggesting their low dependence on the kernel size. However, for the black pixels, *i.e.* those corresponding to rubber grains, it goes on decreasing with the increasing N even beyond $N= 21$. When studied along with the respective images of the slices, it can be seen that the increasing kernel size leads to loss of certain important pixels leading to the results observed.

Another important parameter studied was the effect of kernel size on the varying sand/rubber (S/R) size ratio. The plots for the statistical values, *i.e.* mean and variance with the varying kernel size have been shown in Fig. 2.12 for S/R=0.63 and S/R=1.98. Initially, it was expected that the kernel size N should be varied with the varying size ratio. However, after studying the data shown in Fig. 2.12, a similar variation was observed as in the case of S/R=1. As explained before, the parameter d_p has taken into account the mean particle size as well. Of course, the similar variation is only from the point of view of the kernel size and does not signify the quantitative comparison between different S/R.
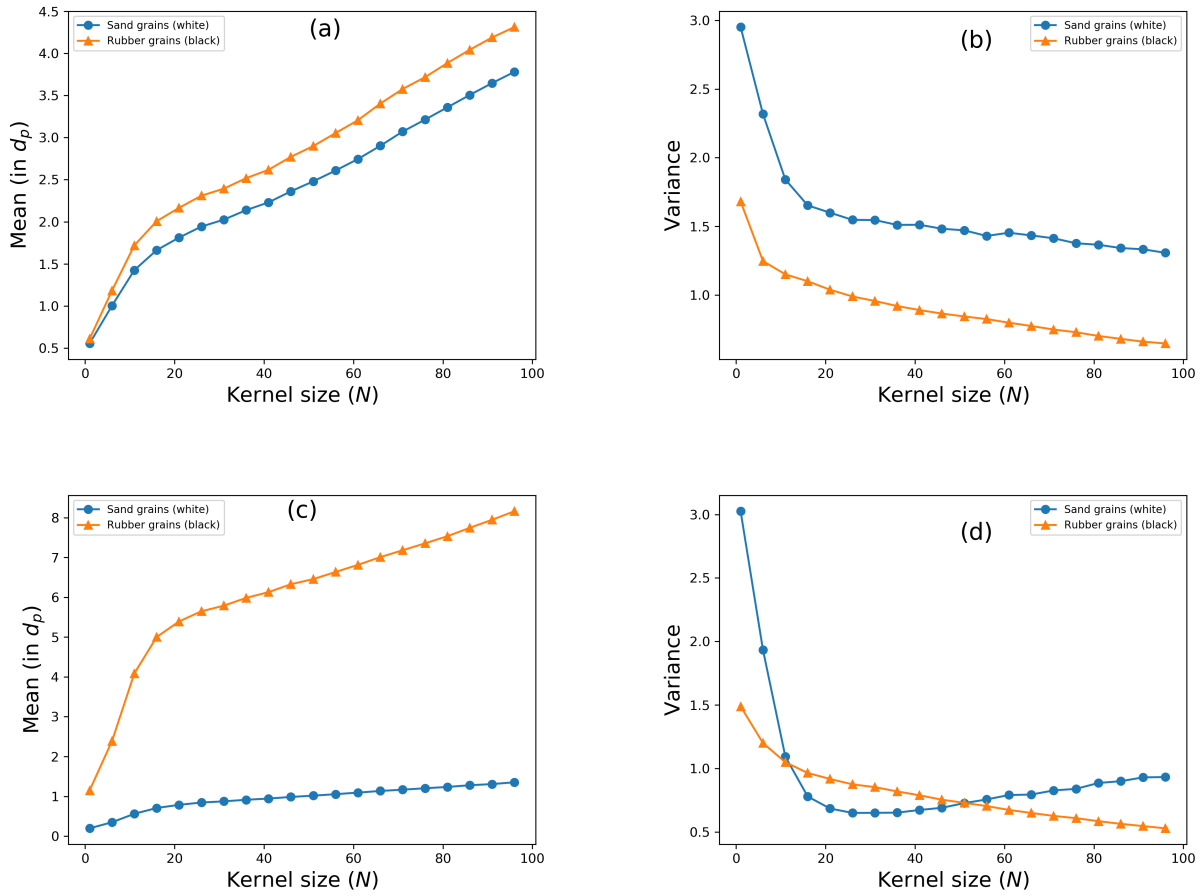
FIGURE 2.12. Statistical data measured over all the slices for sand-rubber mixture after 10000 vertical taps with different kernel sizes (N) of median filtering: (a) Mean of the lengths for black and white pixels for S/R=0.63, (b) Variance of the lengths for black and white pixels for S/R=0.63, (c) Mean of the lengths for black and white pixels for S/R=1.98 and (d) Variance of the lengths for black and white pixels for S/R=1.98.

Thus, after considering both the statistical data and the images of the slices, as well as the statistical data for the differing S/R, an optimum value of the kernel size for the analysis of all the sand-rubber mixture samples was fixed to be N= 21. The main reason for this being the mean values observed. For any mean particle size d_p, *i.e.* irrespective of the size ratio, the value of N= 21 is smaller than the mean of the histogram. This confirms that there will be no loss of information by using N= 21, since the filter aperture is small enough, but at the same time, the noise can be seen to be reduced (see Fig. 2.10(e)).

2.3.2 Effect of number of vertical tap sequences

Two of the most important parameters in the vibrating shaker experiments were the intensity of vertical taps and the number of vertical tap sequences. Given that the objective of the

experiments was to study the segregation for sand-rubber mixtures, tests were performed for the number of vertical tap sequences as well, similar to those conducted for different tap intensities. For this purpose, sand/rubber (S/R) size ratio of 1 and rubber volume fraction of 50% was chosen. Fig. 2.13 shows the images of one slice for each of the samples, *i.e.* for sand-rubber
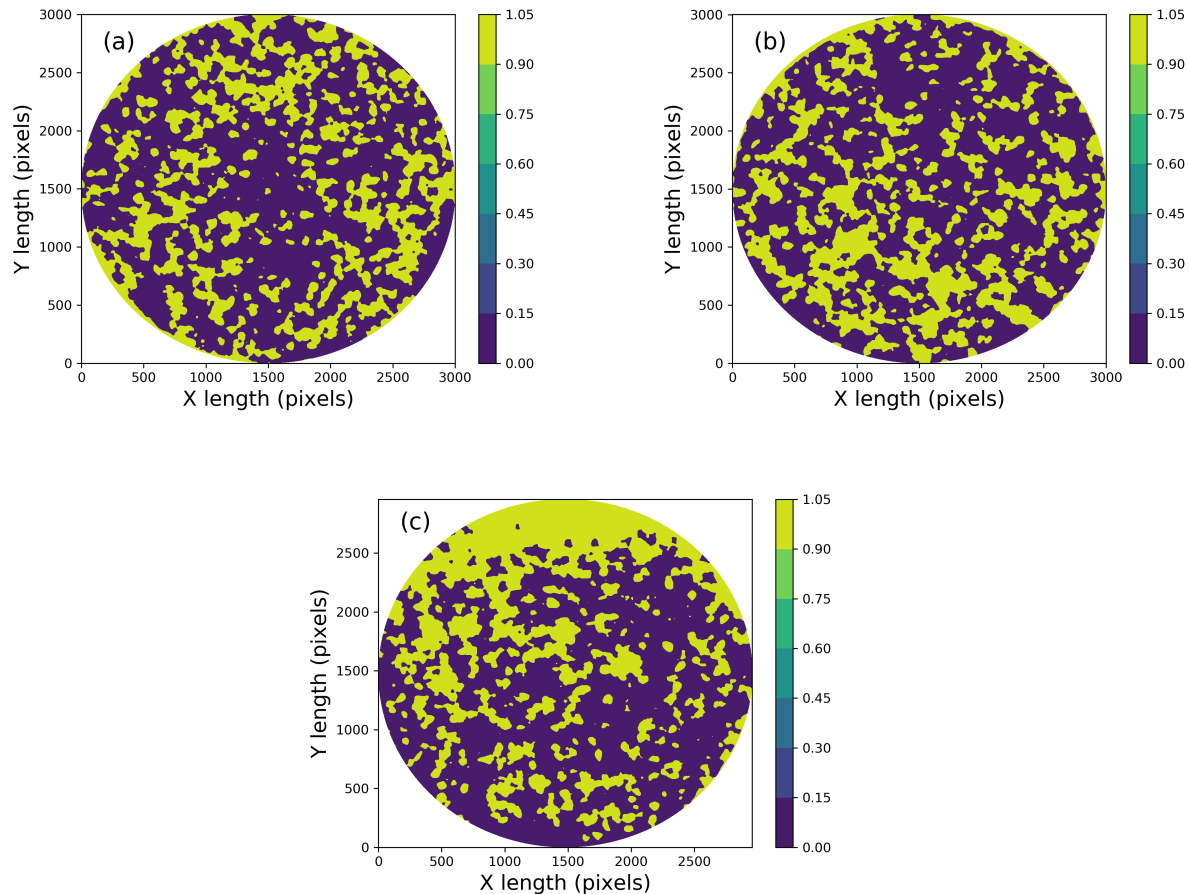
FIGURE 2.13. Masked slices of sand-rubber mixture for size ratio 1 and 50% rubber volume fraction for: (a) 100 vertical tap sequences, (b) 1000 vertical tap sequences and (c) 10000 vertical tap sequences.

mixture after 100 taps, 1000 taps and 10000 taps. From the images of the slices, it can be seen that the segregation between sand and rubber grains is clear in the case of 10000 vertical taps, whereas for 100 taps, the sample looks like a mixed one and the same is true in the case of 1000 taps. Although for 1000 taps, a larger number of clusters of sand grains can be seen as compared to the case of 100 taps. For this purpose, to better quantify the segregation, it was decided to test all the samples for 10000 vertical taps on the vibrating shaker.

As mentioned before in Section 2.2.3, if air is entrapped in the sample during the solidification using a gel binder, then the final sample obtained consists of dry zones which lead to the loss of structural integrity. A similar observation, *i.e.* a large void of air was noted if the samples are solidified immediately after the mixing process (in spite of drilled holes at the bottom of the mixture container). Hence, the slices of samples which could be used after mixing and the slices
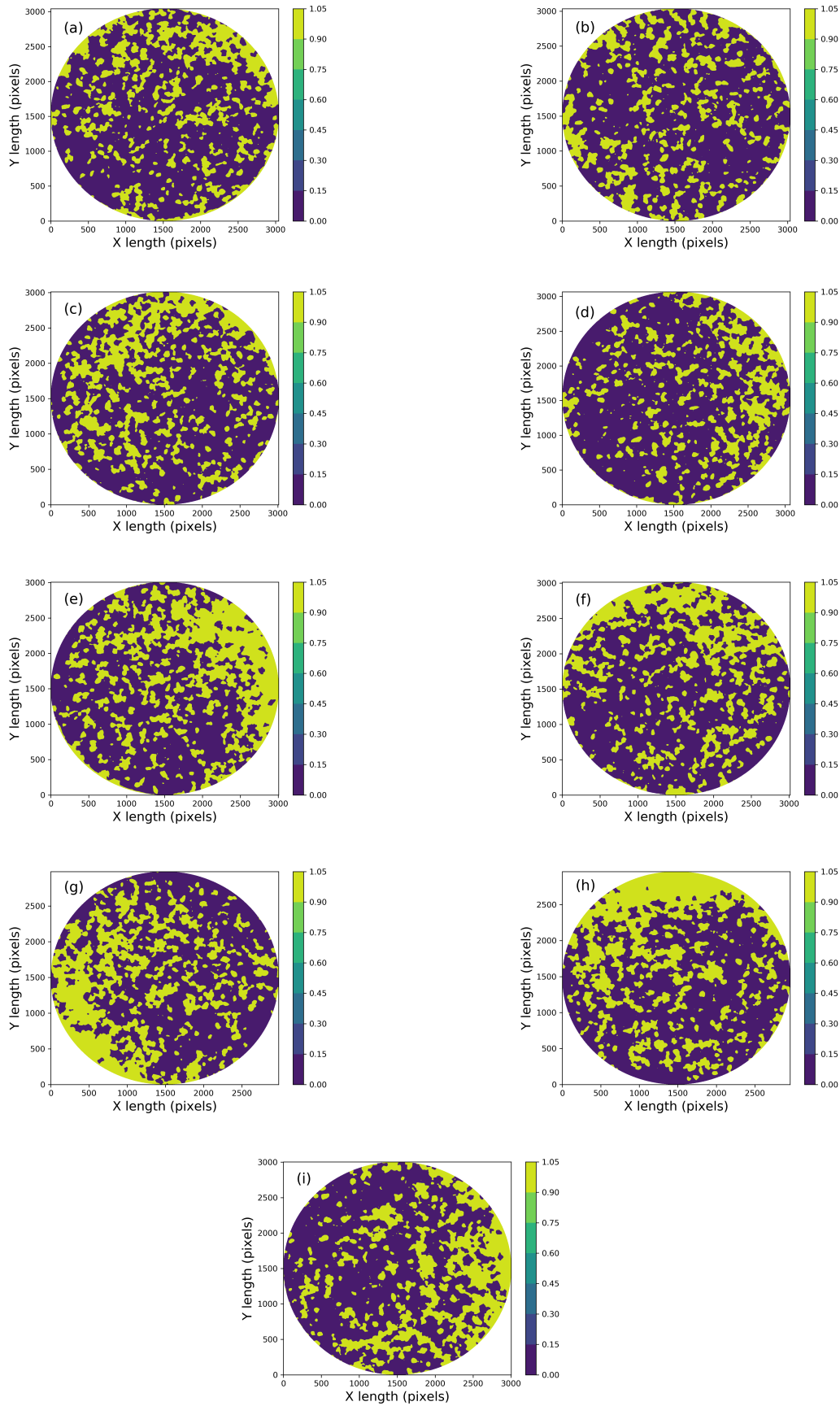
FIGURE 2.14. All masked slices of sand-rubber mixture for size ratio 1, rubber volume fraction 50% and 10000 vertical taps: (slices from bottom to topmost of the mixture sample): (a) slice1 (face1), (b) slice1 (face2), (c) slice2 (face1), (d) slice2 (face2), (e) slice3 (face1), (f) slice3 (face2), (g) slice4 (face1), (h) slice4 (face2) and (i) slice5 (face1).

43

of samples after 100 vertical taps were compared. The difference observed between the two was negligible. For this purpose, the samples were subjected to 100 vertical taps after mixing process and then solidified. Thus, the results which will be discussed in the further sections (different size ratios, rubber volume fractions and moisture content) will be presented for the case of mixing (with 100 vertical taps) and the samples subjected to 10000 vertical taps. For all
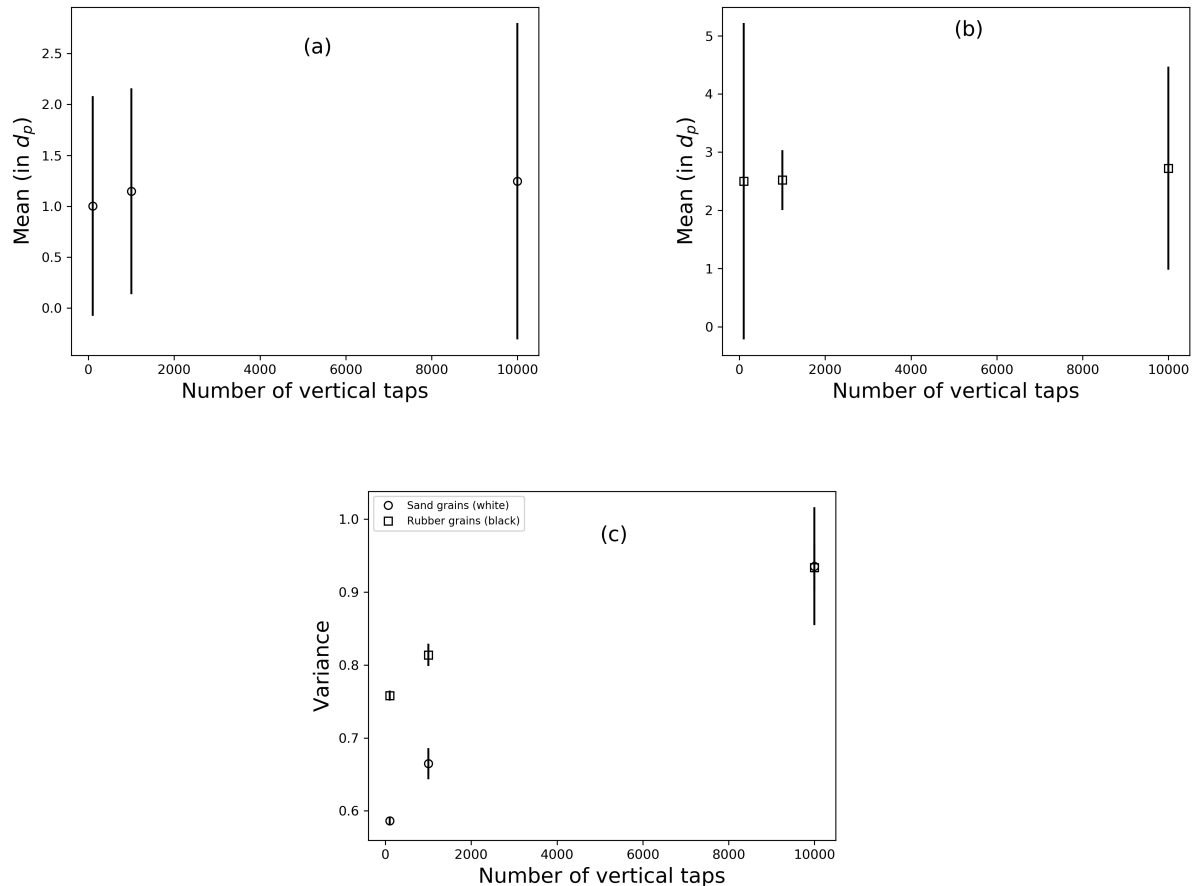
FIGURE 2.15. The statistical data over all the slices of sand-rubber mixture samples of S/R=1 and 50% rubber volume fraction after 100, 1000 and 10000 vertical taps: (a) Mean of the lengths for white pixel series, (b) Mean of the lengths for black pixel series and (c) Variance of the lengths for white and black pixel series.

the discussions done till now, only one slice for each type of sample have been shown. However, as mentioned before in Section 2.2.4, 5 slices for every test sample were used for the Image Analysis. Thus, it means that in total images of 10 faces (2 faces for each slice) were captured. Since during the solidification process, a little extra gel binder was used, there is excess gel binder on the top face of the uppermost slice. The post-treatment of heat gun could be used to melt it, however there was a possibility that it would cause some grain loss and loss of the integrity of the slice. Hence, it was decided not to use this face of the uppermost slice for the analysis. Thus, in total for every sample, images of 9 slice faces were captured.

Depending on the discussions presented before, it could be argued that the segregation is

observed only near the top or in the specific regions of the sample. However, this was not the case observed and for this purpose images for all the slices of sand-rubber mixture of S/R=1, 50% rubber volume fraction and subjected to 10000 vertical taps have been shown in Fig. 2.14. The images presented here are in the order from bottom-most slice to the topmost slice over the height of the mixture. So it can be clearly seen that the segregation between sand and rubber is observed over the entire height of the packing. Moreover, these images reiterate that there is no specific vertical profile for segregation observed over the height of the packing, and thus validating the choice of cutting and studying horizontal slices.

As usual the statistics were performed over all the slices of the packings (S/R=1, 50% rubber volume fraction) for samples subjected to 100, 1000 and 10000 vertical taps. The mean and the variance of the lengths of the white and black pixels have been shown in Fig. 2.15. The plots have been presented with error bars. 3 repetitions of all the process for every sample were performed and the images of the same were analyzed with an aim to check the repeatability effect of the process. With the increase in the number of vertical taps, the error bars can be seen to be bigger (especially in the case of variance), thus suggesting a higher difference in the segregation observed with every repetition for higher sequences of vertical taps.

If the mean of the lengths is observed (see Fig. 2.15(a) and (b)), then it can be observed that there is a huge difference between the mean values for sand and rubber grains, even for the mixing case (100 vertical taps). This indicates that the segregation between sand and rubber is present even during mixing. However, the evolution of the mean values is not significant with the increase in the number of taps. On the other hand, a significant difference can be observed for the variance values (see Fig. 2.15(c)). The variance over the lengths has a huge difference between sand (white pixels) and rubber (black pixels) for the case of 100 vertical taps, suggesting that the rubber particles have a tendency to form clusters and segregate even during mixing. It is also possible that there are certain weakly segregated rubber zones, but not strong enough as compared to sand particles. Further, the increasing variance value with the increasing number of taps, especially difference between the value for 1000 and 10000 taps signifies that the span of the histogram increases with the increasing number of taps. This in fact is a proof of the existence of segregation in the sand-rubber mixtures.

This although does not shed any light on the pattern of segregation, still delivers an important information that both sand and rubber grains equally segregate throughout the packing height of the mixture. Thus, there may be some rubber grain-dominant zones as well as sand grain-dominant zones for the entire mixture. This, in turn justifies the choice concerning 10000 vertical tap sequences for quantifying segregation for all the sand-rubber mixture samples. The further sections will present the different parameters, *i.e.* S/R size ratio, rubber volume fraction and moisture content varied during the experiments. However, as explained before, it is important to remember that after mixing the samples were subjected to 100 vertical taps, hence all the results will be presented at 100 vertical taps (mixing case) and 10000 vertical taps for quantifying the segregation observed.

2.4   Effect of sand/rubber size ratio

As mentioned in the beginning (see Section 2.2), 3 different sand/rubber (S/R) size ratio mixture samples were prepared and analyzed with an objective to quantify the effect of size ratio on the segregation characteristics. Moreover, 3 repetitions for each *i.e.* mixing and vertical tap tests were conducted. One sample slice for both mixing and vertical tap condition for all the size ratios has been shown in Fig. 2.16. For simplicity, the mixing and vertical tap sample slices have been shown side by side for each of the size ratios. It has been pointed out in the images of the samples (see Fig. 2.14) shown in the previous Section 2.3.2, that there are sand-dominant zones near the uppermost slices and rubber-dominant zones for the bottom slices. This is valid in the case of all the size ratios. However, it can be imagined that for S/R = 1.98, rubber-dominant zones are highly observed since the rubber grains are smaller in size than the sand grains (see Fig. 2.16(e) and (f)). For all the three size ratios, important point to be noted is a visible change in the mixture arrangement due to the vertical taps pointing towards the segregation induced due to the taps. The statistical descriptors for the histogram of the length of white and black pixels, *i.e.* mean and variance were calculated and have been shown in Fig. 2.17. Again as in the previous case (results shown in Section 2.3.2), the error bars are higher in the case of vertical tap experiments showing a huge variation of segregation with every repetition. Moreover, the deviations observed are higher for S/R=0.63 and S/R=1.98. But, clearly for a given S/R size ratio, with the increasing number of vertical tap sequences, the mean and variance values increase. However, the mean values do not show a significant difference between the cases of mixing and vertical taps. But, the mean value for rubber is higher than for the sand, indicating the tendency of rubber to segregate more by forming clusters than the sand particles. However, the variance seems to be a better defining descriptor due to a clear difference between the mixing and vertical tap cases for each size ratio. The variance values show a significant rise in the case of sand particles after the vertical taps, thus indicating that with the increasing vertical taps, the sand particles show increasing tendency towards segregation by formation of clusters. (see also Fig. 2.16).

The variance for S/R size ratio= 1 has close values for both sand and rubber grains, showing that both the sand and rubber equally contribute to the segregation phenomena throughout the mixture. Whereas, for S/R= 0.63, the variance for rubber is lower compared to sand when the values for mixing and vertical taps are compared, suggesting that the sand grains are much dominant in segregation than the rubber grains. For the case of S/R= 1.98, it is exactly the opposite as compared to S/R= 0.63, *i.e.* rubber grains are more dominant in segregation than sand grains.

One reason which could explain this phenomena is the particle size. For the initial condition, *i.e.* after mixing, in a given space, for lower S/R size ratio (0.63), there will be higher number of sand grains than the rubber grains due to a smaller particle size. Whereas, it can be imagined to be exactly opposite for S/R size ratio of 1.98. Further, in case of vertical tap experiments,
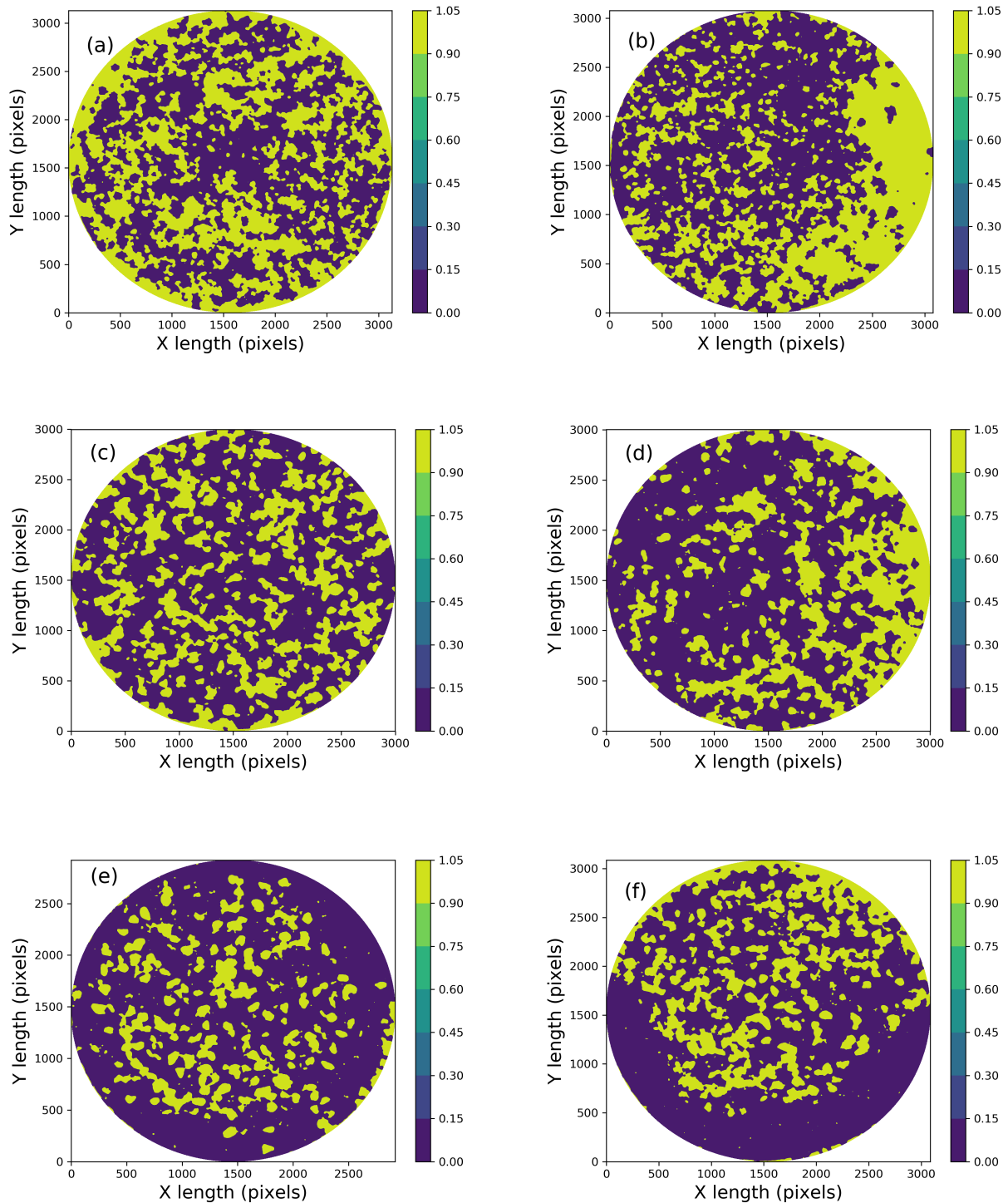
FIGURE 2.16. Masked slices of sand-rubber mixture for size ratio 0.63, 1 and 1.98: (a) after mixing for S/R= 0.63, (b) after vertical taps for S/R=0.63 , (c) after mixing for S/R= 1, (d) after vertical taps for S/R= 1, (e) after mixing for S/R= 1.98, and (f) after vertical taps for S/R= 1.98.
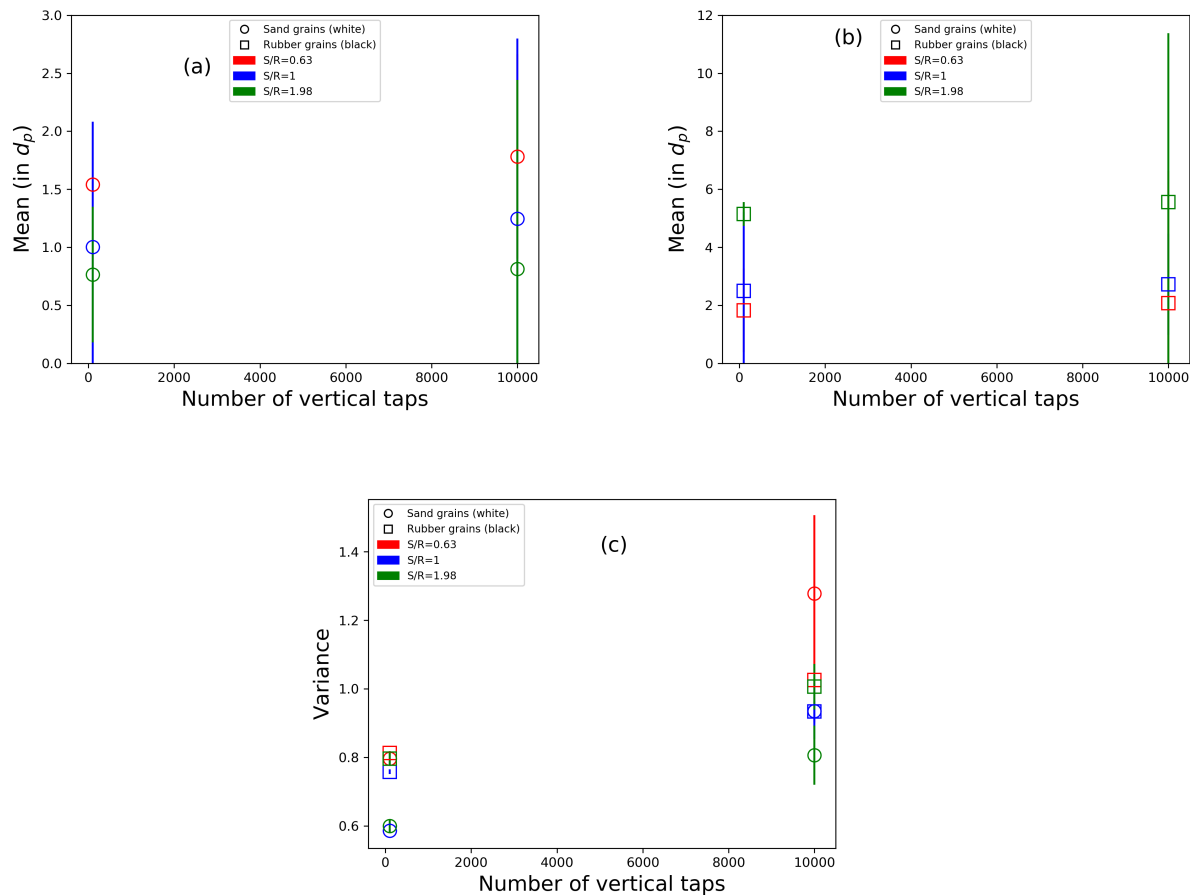
FIGURE 2.17. The statistical data over all the slices of sand-rubber mixture samples of S/R= 0.63,1 and 1.98 and 50% rubber volume fraction after mixing and after 10000 vertical taps: (a) Mean of the lengths for white pixel series, (b) Mean of the lengths for black pixel series and (c) Variance of the lengths for white and black pixel series.

with every tap, the packing takes off from the bottom of the mixture container and then settles down. Moreover, since the packing takes off from the bottom and is subjected to kind of a jump, there is even dilation of the packing which occurs leading to the formation of new voids (although in this case due to the use of counter-mass, the dilation is expected to be very low). Thus, with every take off, there is a possibility for particle rearrangement. So, for lower S/R, *i.e.* 0.63, the particle size of sand being smaller than rubber, with every take-off from the bottom, sand particles show a tendency of forming clusters higher than that of rubber particles and in the case of S/R= 1.98, it is the rubber grains which show the same tendency.

There is a clear effect of the size ratio on the segregation behavior of sand-rubber mixtures, from the results presented above.

48

2.5 Effect of rubber fraction
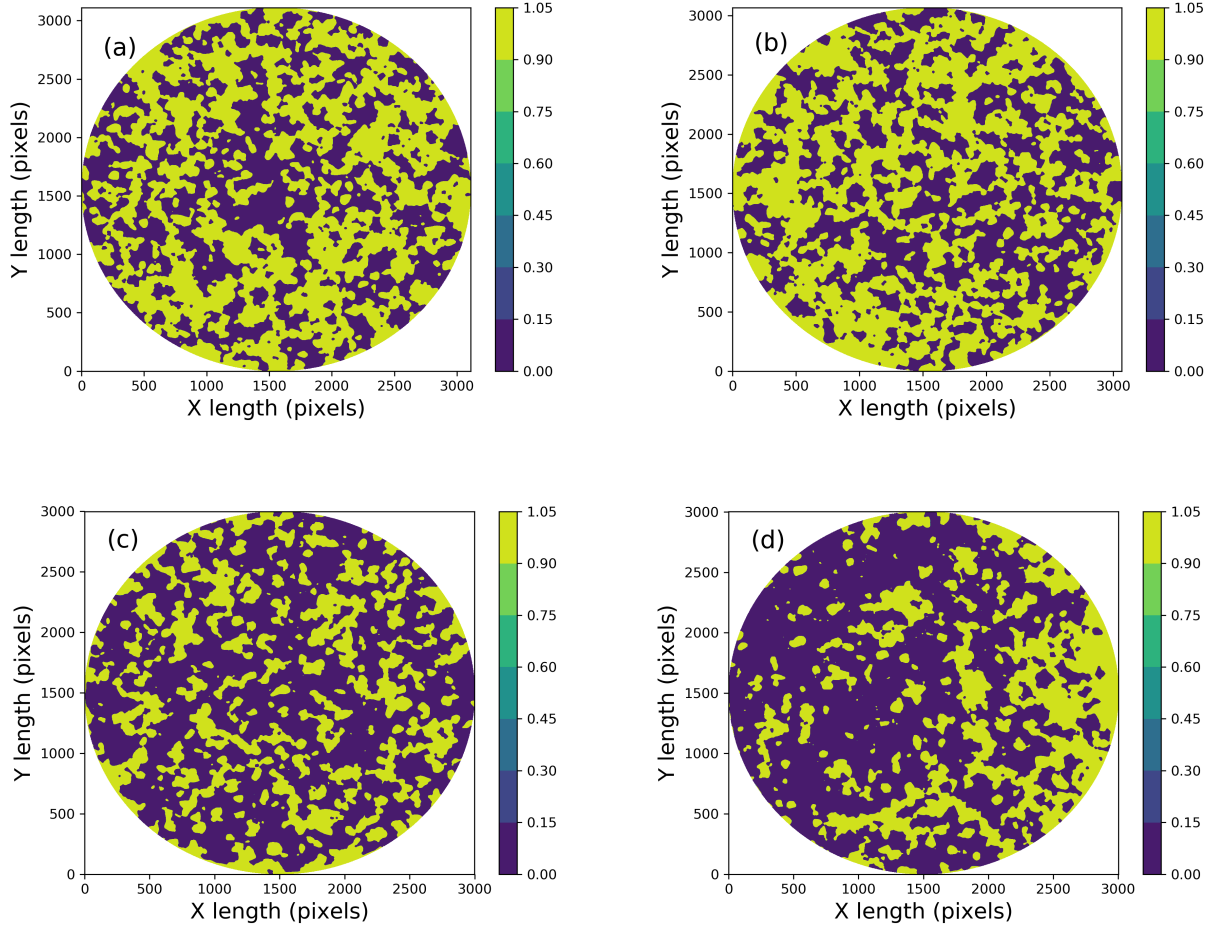
FIGURE 2.18. Masked slices of sand-rubber mixture for rubber fraction of 25% and 50% by volume: (a) after mixing for X_R=25%, (b) after vertical taps for X_R=25% , (c) after mixing for X_R=50%, and (d) after vertical taps for X_R=50%.

Rubber fraction can play an important role in the segregation characteristics of the sand-rubber mixtures, since the densities are very different for the two constituents. Tests were performed on the mixture samples with 2 different rubber fractions, *viz.* 25% and 50% (by volume). Initially, an effort was made to prepare and test the samples for 10% rubber fraction as well, however such samples were found to be very hard to cut after solidification and the slice cutting process also caused a huge loss of grains. Hence, only 25% and 50% rubber fractions have been discussed here.

The sample slices for mixing and vertical tap cases for 25% and 50% rubber fraction have been shown in Fig. 2.18. Clearly, the difference between the mixing and vertical tap case for lower rubber fraction is lower than in the case of higher rubber fraction. If the mean values are observed for both the mixing and vertical tap cases for sand and rubber grains (see Fig. 2.19(a)

49

and (b)), then a clear difference in the magnitude of the values for sand and rubber grains can be seen. Thus, for both the rubber fractions, rubber grains have a higher tendency to from clusters and segregate. However, the difference in the mean values for mixing and vertical taps increases with the increasing rubber fraction. Although, this increase is not significant. On the other hand, a difference between the variance values for both sand and rubber grains for mixing and vertical tap cases can be seen in Fig. 2.19(c). The evolution of variance values is
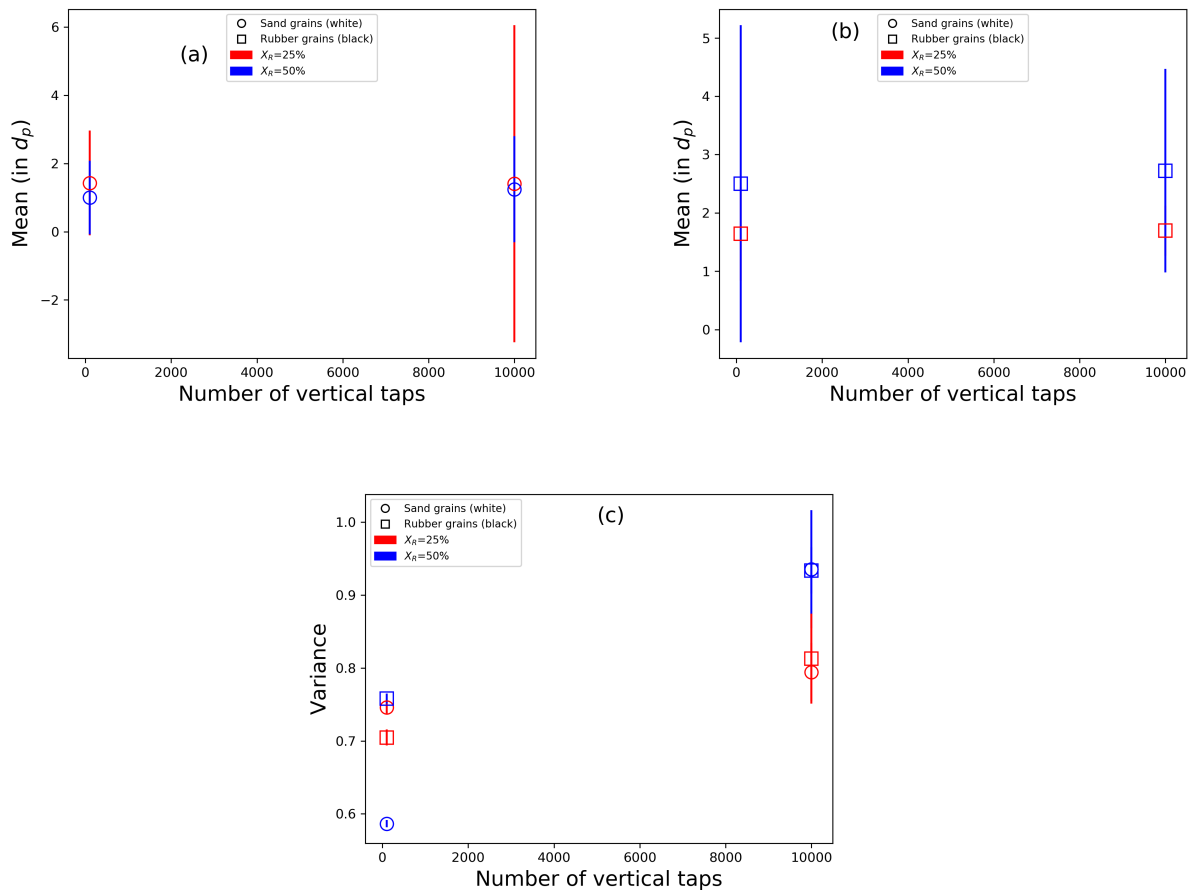
FIGURE 2.19. The statistical data over all the slices of sand-rubber mixture samples of 25% and 50% rubber fraction after mixing and after 10000 vertical taps: (a) Mean of the lengths for white pixel series, (b) Mean of the lengths for black pixel series and (c) Variance of the lengths for white and black pixel series.

higher for $x_R = 50\%$ than in the case of $x_R = 25\%$. This clear difference in the variance value between mixing and vertical tap cases suggests that the segregation effect is lower in lower rubber fractions and it increases with the increasing rubber fraction. An obvious reason for this is the notable difference in the mass values of rubber and sand for a given rubber fraction. For lower rubber fraction, $i.e.$ for 25% (by volume), the equivalent mass of sand is much higher than that of rubber. Further, the number of rubber particles can also be imagined to be very low as compared to the sand particles. On the other hand, this changes totally for $X_R = 50\%$, and thus a visible effect on the segregation characteristics can be observed.

2.6 Effect of water addition
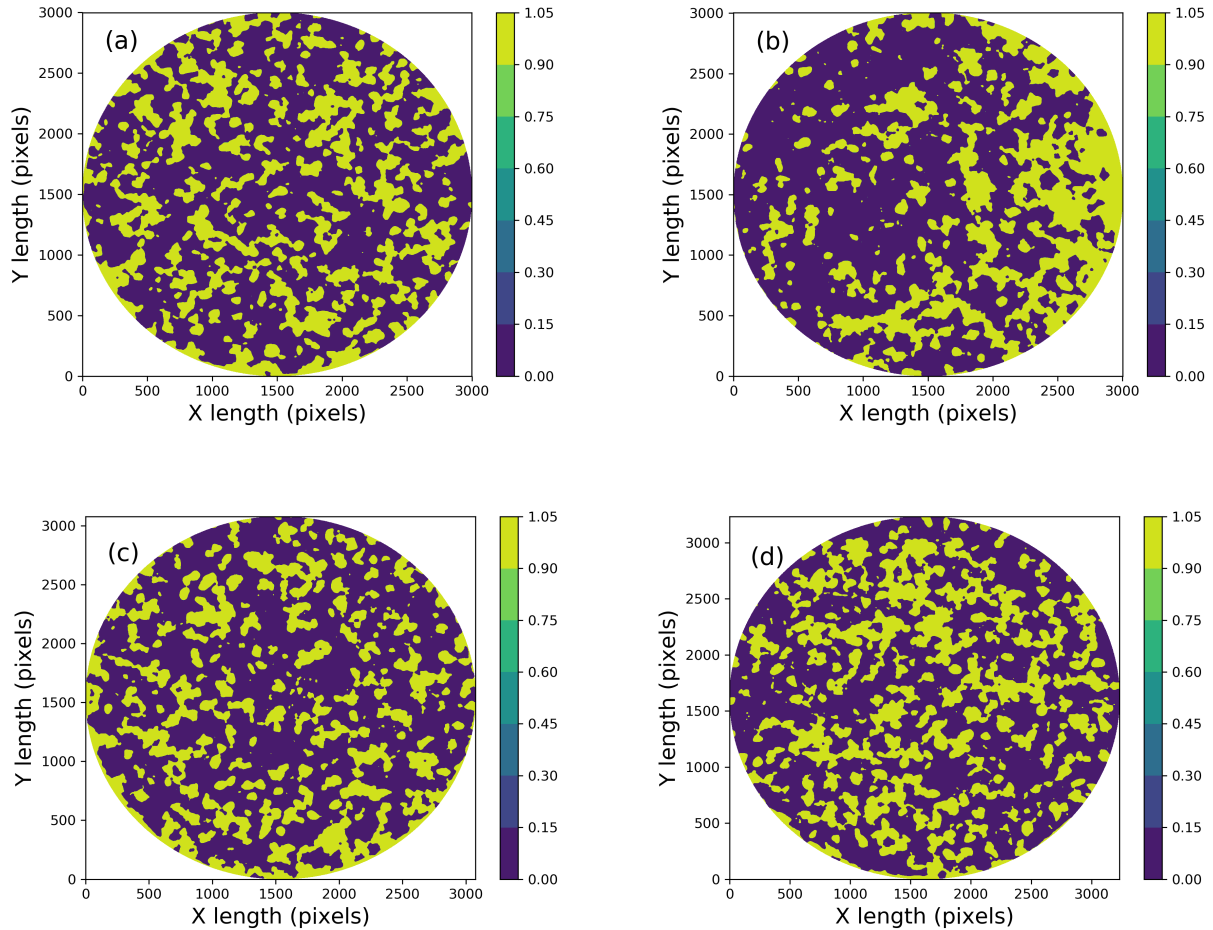
FIGURE 2.20. Masked slices of sand-rubber mixture without and with moisture content: (a) after mixing without moisture, (b) after vertical taps without moisture, (c) after mixing with moisture, and (d) after vertical taps with moisture.

Addition of a small amount of liquid (*e.g.* oil, water) increases the cohesion between the granular materials causing to decrease their flowability and thus reduces the segregation [Mosby et al., 1996, Tang and Puri, 2004]. Since, the sand-rubber mixtures under study are found to segregate, it was interesting to study the effect of addition of water to such mixtures during the mixing process. However, an important point was the amount of water to be used. Thus, the objective was to wet the particles enough in order to create liquid bridges between them, thus reducing their flowability during the mixing and vertical tap experiments. But, at the same time, it was important to not add so much water as would lead to a flowing liquid throughout the mixture. To decide this, the most important parameter was the particle size of sand and rubber grains being used. The particles of sand and rubber used in the experiments were considerably coarse (2mm - 2.5mm). In case of coarse sand particles (mean particle size

> 1mm), it has been pointed out that the addition of up to 5% (by weight) of the wetting liquid such as water leads to a decrease in the effective friction between the particles which is related to the lubrication of interparticle contacts due to the wetting liquid [Artoni et al., 2019]. Consequently, tests for mixing and vertical taps were performed by adding 4% water of the total weight of the mixture used. The other parameters fixed were S/R size ratio= 1 and rubber fraction $X_R = 50\%$. Water was added during the mixing process itself and then the samples were subjected to vertical taps. Similar to the previous tests, 3 repetitions for each condition ,*i.e.* mixing and vertical taps were performed.
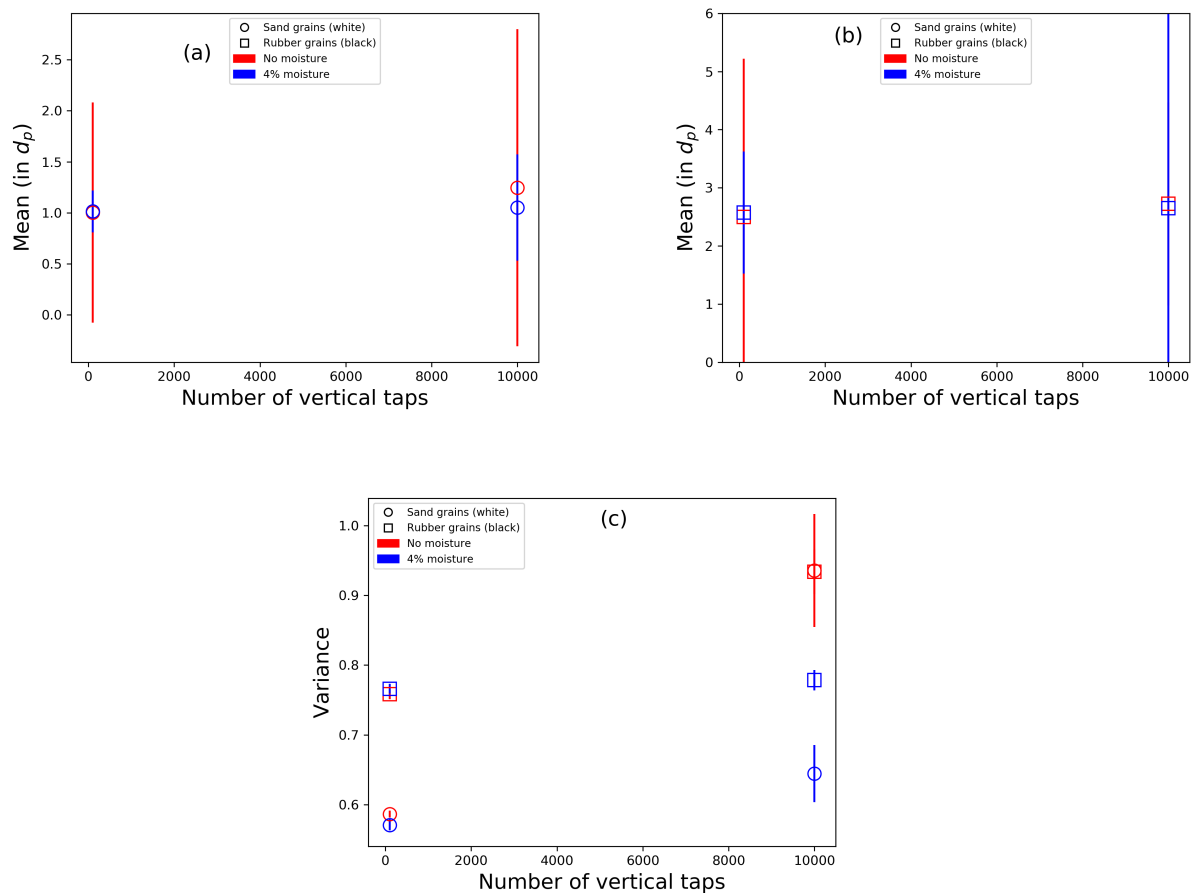
FIGURE 2.21. The statistical data over all the slices of sand-rubber mixture samples with and without moisture after mixing and after 10000 vertical taps: (a) Mean of the lengths for white pixel series, (b) Mean of the lengths for black pixel series and (c) Variance of the lengths for white and black pixel series.

Fig. 2.20 shows the images of sample slices for both the cases of mixing and vertical taps for the two conditions, *i.e.* without water and with water. From the images, a noteworthy difference can be observed between the two conditions. In the absence of water, the mixture can be seen to segregate due to being subjected to the vertical taps. However, if the slices for the samples with the water content are observed, no visible segregation can be observed even after 10000 vertical taps. Of course, due to the water addition, the formation of liquid bridges can be seen

to encourage the formation of clusters, but there are no visible sand grain segregated or rubber grain segregated zones.

A better understanding can be obtained by analyzing the statistical descriptors of the lengths of white and black pixels, *i.e.* mean and variance (see Fig. 2.21). Again, the two conditions shown are with and without water and for mixing and vertical tap processes. Clearly, if the difference in the mean value for mixing and vertical tap processes are observed (see Fig. 2.21(a) and (b)), then the samples with 4% water show nearly a negligible difference in the mean value for sand and rubber grains over the entire sample as compared to the samples without the water content. However, this difference observed in the case of non-water samples is still not significant. It can be better understood if the plot for the variance is observed (see Fig. 2.21(c)). The difference between the variance values for mixing and vertical tap processes is very low (negligible for rubber) in the case of samples with water than in the case of samples without water.

The results thus suggest that the introduction of wetting liquid such as water can reduce the segregation in sand-rubber mixtures under the conditions mentioned in this study.

2.7   Discussion and Perspectives

The segregation for sand-rubber mixtures was verified under two conditions, *viz.* mixing and vertical taps. The different varying parameters whose effect was studied were sand/rubber size ratio (S/R), rubber fraction (by volume) and moisture content. The segregation analysis was carried out using Digital Image Analysis techniques.

In general for all the varying parameters, segregation was observed during the mixing as well as after the vertical taps. For the cases of mixing, rubber particles were observed to be more sensitive to segregation than sand particles and consequently clusters of rubber grains were observed even after mixing. The segregation increases with the increasing number of vertical taps and this was clearly pointed out in all the cases by the plot for the variance of the histogram of average length of contiguous black and white pixels. For the lower S/R, *i.e.* 0.63, sand showed more sensitivity towards segregation by forming bigger clusters than the rubber particles and exactly opposite was observed in the case of S/R= 1.98. In case of lower rubber fraction, *i.e.* 25%, the rubber still showed a tendency to form clusters and segregate with the increasing number of vertical taps, however the segregation observed was lower than in the case of 50% rubber fraction. With the addition of moisture, the segregation was observed to be minimized for both mixing as well as vertical taps. This suggested that addition of water suppressed the segregation phenomena in sand-rubber mixtures for this study.

The phenomena of segregation studied here was under complex and constrained conditions. Vertical tap experiments using a vibrating shaker with a counter-mass placed on the top of the mixture container were performed. An effort was made to realize a real-time condition of transport of sand-rubber mixtures using lorries. Although these tests performed in this study

cannot be directly linked with such an application, they can serve as the preliminary results in order to understand such a complex condition. At this point of time, the exact mechanism due to which segregation is observed is difficult to explain. However certain important conclusions can be drawn from the results presented in this study.

There was no vertical segregation observed for any of the tests. The effect of the size and shape of the container used was thus clearly minimized by using the counter-mass. Thus, the segregation observed cannot be attributed due to the convective effect (remixing). Further, the segregation was observed to be more concentrated near the walls of the container. This might be a shear induced segregation due to the shearing near the walls, which causes the particles to settle and form clusters near the walls. There is no specific phenomena observed such as percolation of fine particles, rise of coarse particles, etc. which further makes it difficult to conclude concerning a particular segregation mechanism.

In totality, these results are not sufficient to describe the mechanism for the segregation observed. Similar experiments using a larger/ smaller container can be helpful to further validate this phenomena. Moreover, the phenomena of vertical taps studied here can be simulated using the Discrete Element Method (DEM) which would help to better quantify the mechanism of segregation under such conditions.

Nevertheless, an important result here is the presence of segregation in sand-rubber mixtures even after they have been mixed thoroughly, which thus highlights that studying the effect of mixing quality is indeed important for such mixtures. The subsequent chapters will present the study concerning the effect of the mixing quality on the mechanical response of sand-rubber mixtures.

EXPERIMENTAL ANALYSIS USING OEDOMETER TESTS

Summary

This chapter presents the results of the conventional oedometer tests performed on sand-rubber mixtures. The results will be discussed on the basis of 4 main parameters *viz.* initial packing void ratio characterized as dense and loose packing, size ratio between the sand and rubber grains, sample size of sand and rubber grains and particle arrangement. This chapter helps to understand the effect of these important parameters on the mechanical behavior of sand-rubber mixtures. Moreover, the last Section of this Chapter includes the results for the tests performed to study the effect of mixing quality.

Contents

3.1   Introduction

The oedometer test has been performed on sand-rubber mixtures with an aim to characterize their mechanical response under compression. These oedometer tests were performed at the Geotechnical Testing Laboratory of University of Bristol, UK. The methodology for the oedometer test has already been explained in Chapter 1. However, there is another type of oedometer test called the continuous loading test wherein the data logging for stress and displacement during compression is automatic. This test has several advantages over the conventional consolidation tests, one of the most important being the removal of human errors due to manual loading of the sample. The difference between these two tests has been pointed out previously [Davison and Atkinson, 1990, Skuodis et al., 2017]. It has been noted that one of the major difference in these two tests is the magnitude of displacement of the sample due to compression. In case of conventional loading test, due to the intervals for which the load is applied is high, the test sample has a higher displacement magnitude as compared to a continuous loading test [Skuodis et al., 2017]. Davison and Atkinson [1990] aptly point out the advantages of continuous loading tests over the conventional stage loading tests. Due to automatic measurement in terms of data logging, much more data is obtained as compared to a conventional test. Thus, there is a better control in terms of definition of the properties such as compression and swelling indices, incremental confined modulus, identification of yield point, etc.

The oedometer tests have been performed using the continuous loading test. The experimental procedure began with the sand-rubber sample preparation. The method of fabrication of sand-rubber samples will be explained briefly in the next section 3.2.

3.2   Methodology

3.2.1   Fabrication of sand-rubber mixtures

The sand and rubber used for the experiments were Leighton Buzzard sand and powdered recycled tire rubber respectively. The different methods of fabrication of sand-rubber mixtures for laboratory testing have already been discussed in Chapter 1. Moist tamping method was used for the sand-rubber mixture fabrication. It is one of the most widely used methods for the preparation of sand-rubber mixtures [Rouhanifar, 2017]. The process started with the measurement of the sand and rubber in terms of mass (calculated as per the volume for the required void ratio) in a mixing bowl. The target fabrication height of the sand-rubber samples was fixed to be 40mm. The oedometer metal cylindrical ring used for the test had a diameter of 74mm. Hence, the entire sample was prepared in two equal layers. The measured quantities of sand and rubber were mixed by adding 10% of water (by volume of sand) in a mixing bowl. They were then thoroughly mixed using a spoon to ensure a good distribution of the

FIGURE 3.1. Preparation of sand-rubber mixtures using moist tamping method

rubber particles throughout the mixture. After mixing, the mixture was then deposited in the oedometer cell from a zero drop height in two successive layers as mentioned before. Each layer was compacted using a steel rod till the required sample height and void ratio was achieved. The fabrication process has been shown in Fig. 3.1. The mass of the sand and rubber used for mixing varied according to the rubber fraction (0-50% by volume). After mixing and deposition, the homogeneity of the mixtures was ensured by visual inspection.

The variation of the different parameters *viz.* initial void ratio, sand/rubber size ratio, rubber volume fraction, etc. will be discussed in the sections where the results for the respective parameters will be explained. The experimental setup for the oedometer test performed is discussed in the next subsection 3.2.2.

3.2.2 Oedometer test procedure

The sand-rubber samples prepared were tested using a uniaxial load cell apparatus or the continuous oedometer loading test apparatus. The test setup consists of a load cell, a Linear Variable Displacement Transducer (LVDT), oedometer cell with the test sample, water tank and acquisition system (see Fig. 3.2). Since water has been added during the mixing of sand and rubber, it was necessary to ensure that the bridges formed between the particles were broken and thus minimize the effect of water addition. Hence, the tests were performed under saturated condition. For this purpose, water from the water tank was let in through the inlets of the oedometer cell until the sample was completely saturated. The platform was adjusted using the test control apparatus in order to bring the load cell in contact with the top cap of the oedometer cell. Once ensured that the load cell was properly seated on the top cap, the values for the LVDT and the load cell in the program for the data acquisition were set to zero. Being a displacement controlled apparatus, the velocity in the test control apparatus was set
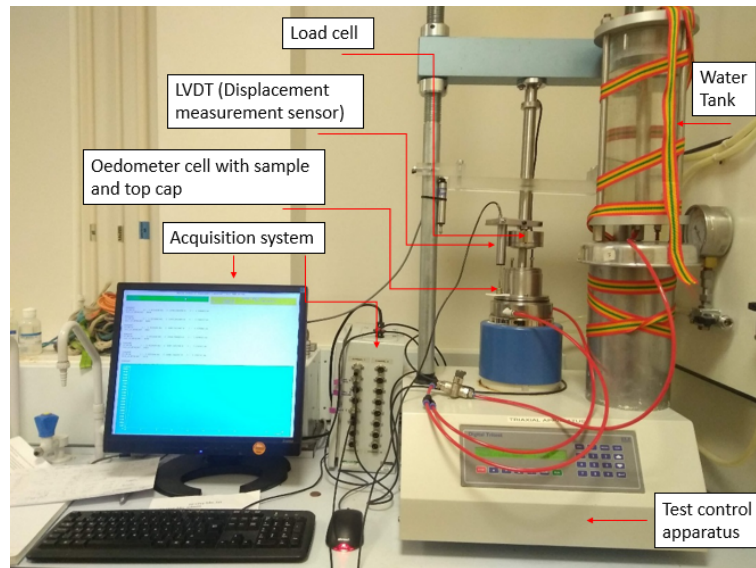
Figure 3.2: Experimental setup for the oedometric compression tests.

as 0.5mm/min for all the tests. The direction of loading in the test apparatus was reversed once the force reached the load cell limiting value (10kN). Further, it was ensured that the unloading phase was completed by verifying the final force and displacement values. The oedometer cell was then removed, the height with the top cap was measured and then the top cap was removed and the sand-rubber sample was allowed to relax. A final measurement of height was also done after the relaxation.

A generalized fabrication process used for the sand-rubber sample preparation was discussed in this section. Moreover, the experimental setup and the test procedure used has also been presented. The results obtained from the oedometer tests performed will be discussed in the further sections. As mentioned before, a number of parameters were varied during the test in order to analyze the effect of different parameters on the mechanical response of the sand-rubber mixtures. Each parameter varied has been discussed in each of the following sections.

3.2.3   Initial void ratio

The initial void ratio of the sand-rubber mixtures was varied in order to study its effect on the mechanical response of the mixtures under compression. The void ratio is given by,

$$e = \frac{V_{voids}}{V_{solids}},$$
(3.1)

where, V_{voids} is the volume of voids and V_{solids} is the volume of solids. Hence,

$$e = \frac{V_T - V_{solids}}{V_{solids}},$$
(3.2)

where, V_T is the total volume. The relative density, D_R is given by,

$$D_R = \frac{e_{max} - e}{e_{max} - e_{min}},$$
(3.3)

where, e, e_{max} and e_{min} are the in situ void ratio, maximum void ratio corresponding to very loose state and minimum void ratio corresponding to very dense state respectively. For the Leighton Buzzard sand used, the maximum and minimum limit fabrication void ratios were fixed to be $e_{max} = 0.83$ and $e_{min} = 0.55$ due to technical limitations in determining the maximum and minimum void ratios in the laboratory. Irrespective of the target initial void ratio of the packing, these limits were considered to be the same.

Consequently, for a given sand and sand-rubber mixture type and for the ease of comparison, the target sample fabrication void ratio was fixed for all samples. Thus, in this case, it was fixed as $e = 0.65$ for dense packings and $e = 0.75$ for loose packings. Hence, the corresponding initial relative densities were, $D_{Rdense} = 64.3\%$ and $D_{Rloose} = 28.6\%$ for dense and loose packings respectively.

The corresponding volume of the solids was calculated for dense and loose packings. Further, depending on the required rubber fraction (percentage by volume), the corresponding volume of rubber sand sand was calculated. On the basis of these volumes, using the densities of sand and rubber ($\rho_{sand} = 2.65 g/cm^3$ and $\rho_{rubber} = 1.04 g/cm^3$), the corresponding masses of sand and rubber were calculated to be used for the sample fabrication. The sand and rubber used for dense and loose packings had a particle sample size range of 1.6-2mm.

Initial void ratio for dense packings		Initial void ratio for loose packings	
x_R (%)	Void Ratio	x_R (%)	Void Ratio
0	0.647	0	0.748
10	0.646	10	0.746
20	0.644	20	0.744
25	0.643	25	0.7437
30	0.642	30	0.742
40	0.641	40	0.7415
50	0.64	50	0.74

Table 3.1: Void ratios for dense and loose packings for different rubber volume fractions under an initial stress of 1.6 KPa.

Although the fabrication void ratios for dense and loose sand and sand-rubber mixtures were fixed, due to the compressible nature of rubber, the actual void ratios varied slightly for the different rubber volume fractions. The values of the initial void ratios for dense and loose packings have been reported in Table 3.1. These void ratios correspond to an initial stress of 1.6 KPa acting on the test samples on account of the weight of the top cap placed on them.

3.2.4 Control and data acquisition

The oedometer test setup used was displacement controlled with velocity fixed as 0.5mm/min for all the tests. Hence, the strain rate can explain the control of the test apparatus used. Given

that the test is a uniaxial compression, the vertical strain is given by,

$$\Delta epsilon_v = \frac{\Delta H}{H_0},$$ (3.4)

where, H_0 is the initial height of the sample, ΔH is the change in the height of the sample due to incremental displacement. Hence, $\Delta H = H_0 - H$.

The data acquisition system automatically logged and saved the data from the displacement and load sensors in the form of displacement (mm) and force (kN) respectively. With the help of calibration factors for the respective sensors, the corresponding force and displacement values were calculated and consequently the stress was also calculated. As mentioned before, the diameter of the oedometer ring was 74mm and the target sample height was fixed to be 40mm. Hence, the total volume,

$$V_T = \frac{\pi D^2 H}{4},$$ (3.5)

where, D is the diameter of the oedometer ring and H is the target sample height. Hence, $V_T = 172 cm^3$.

Fig. 3.3 shows the plot for strain vs time for all the rubber fractions of dense and loose packings. It shows the evolution of the strain for the entire duration of the test *i.e.* loading as well as unloading phase and hence acts as the basis to understand the progress of the test in both these phases of the test. Consequently, it can be observed that the strain level increases with
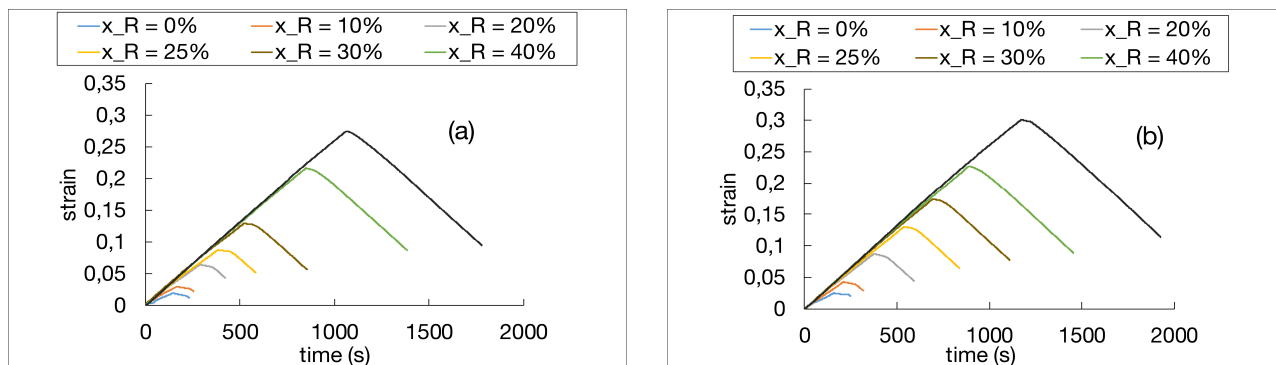
FIGURE 3.3. Strain vs time plot for (a) dense packings and (b) loose packings.

the increasing rubber fraction in both dense and loose packings indicating the increase in the deformable characteristics of the packing due to the rubber inclusion.

It should be taken into account that although the data logging was automatic for the test, the reversal of the direction of loading *i.e.* the change from loading to the unloading phase was done manually. Hence, the magnitude of the maximum stress level is slightly different for each rubber fraction. The maximum stress values for both dense and loose packings for each rubber fraction are presented in Table 3.2. The strain vs time plot helps to understand the basic working control of the test. The results will be discussed further in terms of different individual parameters.

Maximum stress level for dense packings		Maximum stress level for loose packings	
x_R (%)	Stress (kPa)	x_R (%)	Stress (kPa)
0	2290	0	2312
10	2308	10	2280
20	2297	20	2268
25	2276	25	2263
30	2285	30	2300
40	2280	40	2283
50	2273	50	2296

Table 3.2: Maximum stress level values for different rubber fractions of dense and loose packings.

3.3 Loading-unloading behavior

In oedometric conditions the lateral strain is null under the loading conditions. With the knowledge of the vertical strain, it is then possible to calculate volumetric strain and so, the current void ratio, which is given by equation 3.6, *i.e.*,

$$e = e_0 - \Delta\epsilon_v(1 + e_0),\tag{3.6}$$

where, e is the current void ratio, ϵ_v is the vertical strain (positive cf. soil mechanics convention) and e_0 is the initial void ratio. Thus, the void ratio and stress can be represented in a conventional plot with stress plotted on a logarithmic scale. Fig. 3.4 shows the plot for dense and loose packing for all the rubber fractions. From the plot, it is clear that with the increasing rubber fraction, the magnitude of packing deformation increases which is obvious due to rubber being deformable in nature.
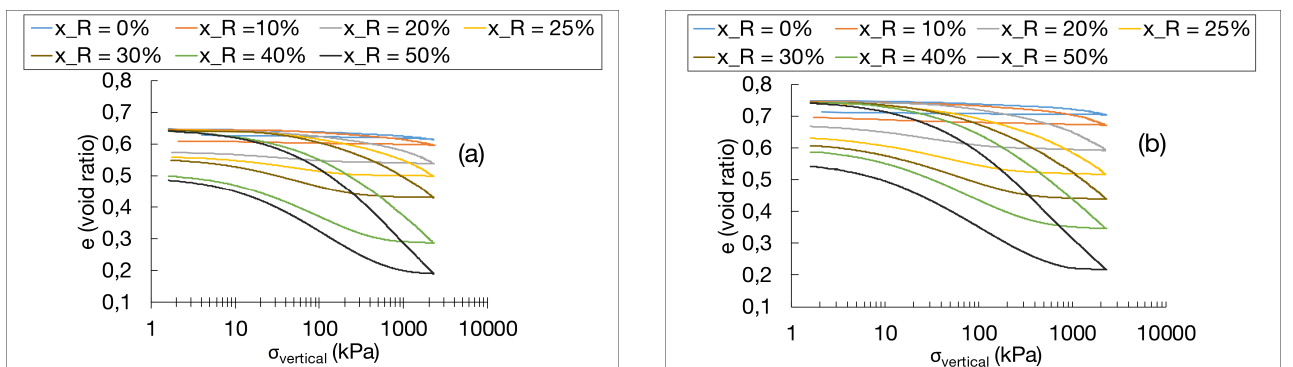
FIGURE 3.4. Void ratio vs log (vertical stress) plot for (a)dense packings and (b)loose packings.

3.3.1 Compressibility

1. **Sand-like and rubber-like responses**
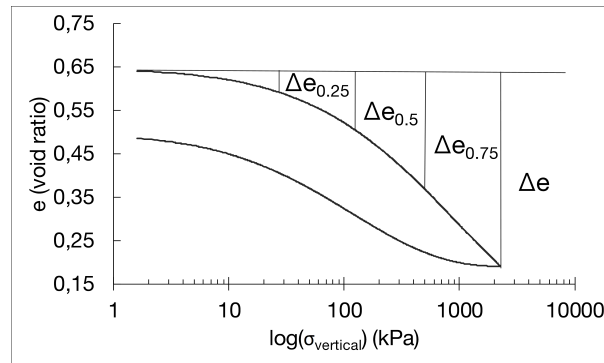
FIGURE 3.5. Schematic used to calculate the change in void ratio for different rubber fractions at the same stress level.

The change in void ratio under loading, Δe as function of the rubber fractions was analyzed at 4 given stress levels: 25%, 50%, 75% and 100% of the maximum stress value tested. The maximum stress values were fixed here to 2273 kPa in case of dense packings and 2263 kPa in case of loose packings. This can be well understood from the schematic presented in Fig. 3.5. Consequently, the Δe vs rubber fraction plot has been presented for the different stress values (see Fig. 3.6).

As expected, the compressibility of the loose packings is higher than for the dense packings at any rubber fraction and stress level.
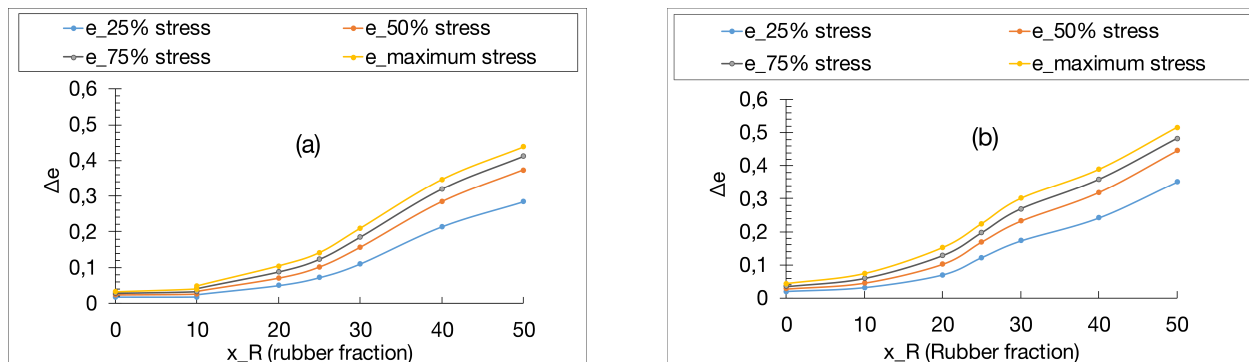
FIGURE 3.6. Differential void ratio for different rubber fractions at the same stress values for (a) dense packings and (b) loose packings.

It is important to take into account the accuracy of the experimental test control for lower rubber fractions *i.e.* up to 20% rubber fraction dense and loose packings. The discussion concerning the confidence level for all the rubber fractions has been included in the discussion on confined modulus (M) which is obtained from the stress and strain values for each packing.

When comparing the evolution of the void ratio with the vertical strain, for different couples of loose and dense packings, at similar rubber content (refer Fig. 3.7(a)), an asymptotic logarithmic evolution can be observed, most clearly with the increasing rubber fraction. The linearity in the void ratio, $e - $ log of vertical stress, $log(\sigma_v)$ plane

was tested at higher vertical stresses by analyzing the ratio of the slope of the secant line between 75% and 100% of the maximum stress to the slope of the secant line between 50% and 100% of the maximum stress on one hand, and on the other hand, slope of the secant line between 75% and 100% of the maximum stress to the slope of the secant line between 25% and 100% of the maximum stress.(see Fig. 3.7(b)). Of course, the slope ratio
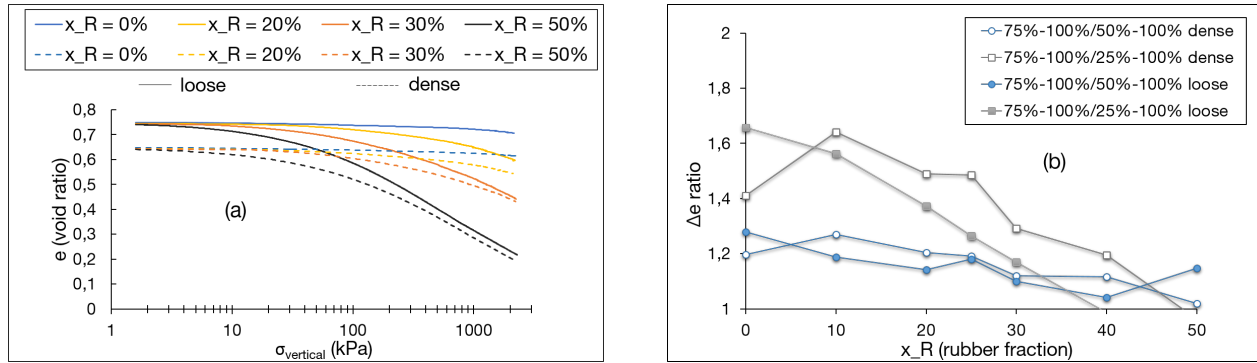
FIGURE 3.7. (a) Evolution of void ratio with the vertical stress and (b) Ratio of slope of the $e - log(\sigma_v)$ curve evolution with the rubber fraction; the ratio is between the slope among 75% and 100% of the maximum vertical stress and 50% (or 25%) and 100% of the maximum vertical stress.

of 1 strongly presumes a linear behavior. It can be observed that generally the e-$log(\sigma_v)$ curve is convex (slope ratio higher than unity). The convexity decreases with the rubber fraction and the behavior becomes mostly linear for x_R of 40% and 50%. The convexity is higher between 25% and 50% of the maximum vertical stress than for 50% to 100%. It should also be considered that the initial void ratio seems to have only a marginal or no influence on the convexity of the curve at high vertical stress. More accurate description of the e-$log(\sigma_v)$ behavior has been presented in the subsequent section by using the confined modulus.

2. **Confined Modulus**

As mentioned before in Chapter 1, the confined modulus or the confined stiffness is the measure of stiffness of the test sample under confinement. The value of confined modulus (M) is not constant since with compression, the test sample becomes denser and its stiffness increases. A typical relation for the confined modulus has been mentioned before in Chapter 1, given as,

$$M = m\sigma_{ref}\left(\frac{\sigma_v}{\sigma_{ref}}\right)^{\alpha},$$

(3.7)

where: σ_v is the effective vertical stress, σ_{ref} is the reference pressure of 100 kPa, m and α are material parameters. This relation was first suggested by Janbu [1963]. The value of the exponent, α controls the change in the incremental stiffness with the vertical stress. In other words, if $\alpha = 0$, then stiffness is constant, and hence, $M = m\sigma_{ref}$. Hence, stiffness does not change with the vertical stress in this case and linear elasticity is observed.

Particle crushing data for dense packings		Particle crushing data for loose packings	
x_R (%)	Crushed material (%)	x_R (%)	Crushed material (%)
0	26.98	0	29.54
10	27.98	10	29.98
20	25.68	20	29.67
25	25.69	25	28.72
30	26.83	30	26.39
40	25.83	40	27.86
50	23.43	50	27.81

Table 3.3: Particle crushing data for the dense and loose packings.

Such a value can be observed for rocks. If $\alpha = 1$, then stiffness is directly proportional to the vertical stress. The second material parameter, m is called the modulus number. It indicates the magnitude of the stiffness at the reference stress level.

In the following, the confined modulus (M) is analyzed at low level of vertical stress, i.e. 100 kPa to 500 kPa. This level of stress was chosen avoid the influence of the particle crushing at high level of compression [McDowell et al., 1996]. Indeed, when the oedometer tests were performed, a considerable amount of crushing of the grains was observed. To quantify this particle crushing observed during the tests, the tests samples were carefully dried after the completion of test and then sieved. The data for crushing can be seen in Table 3.3. The crushed amount has been presented as a percentage of the total dry weight noted before sieving these samples. The parameters in Eq. 3.7 have been determined after calculating the confined modulus from the ratio of incremental stress and incremental strain in the loading phase. A triple mean filtering technique (low-pass filter) was applied in order to diminish the noise in the determination of confined modulus. Further, the parameters m and α were obtained by power law fit where, y = (confined modulus (M)/reference stress (σ_{ref})), x = (vertical stress (σ_v)/reference stress (σ_{ref})). The error in the measurement has been quantified by the standard error of the power regression for a confidence level fixed to 95%. The individual fits for each rubber fraction of dense and loose packings have been shown in Fig. 3.8 and Fig. 3.9, on a log-log scale.

The margin of error has been represented in the plots for the individual parameters, m and α vs rubber fraction (see Fig. 3.10). It can be observed that the margin of error is higher for lower rubber fractions, *i.e.* up to 20% rubber fraction (inclusive). One of the reasons for this is the sensitivity of the sensors used in the oedometer test. It can be imagined that for lower rubber fractions, the displacement of the packing at the same stress level is quite small, and hence it could affect the accuracy of the data recording in turn depending on the sensitivity of the sensors. The evolution of the fitting parameters with the rubber fraction is given in Fig. 3.10. The variation of exponent, α is moderate and, in a first approximation, the power index is considered constant and independent

FIGURE 3.8. Individual fits for confined modulus vs vertical stress for all rubber fractions of dense packings.
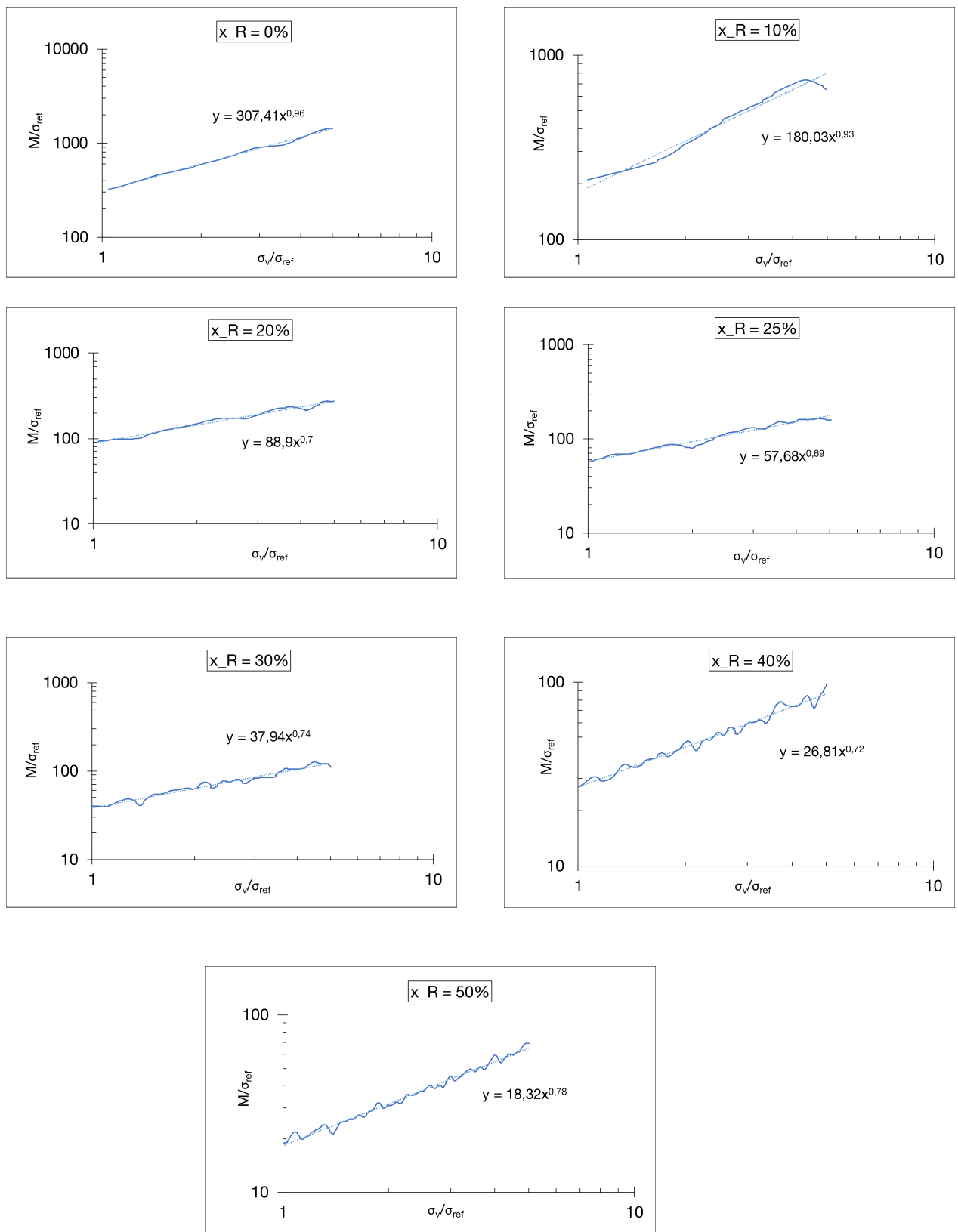
FIGURE 3.9. Individual fits for confined modulus vs vertical stress for all rubber fractions of loose packings.
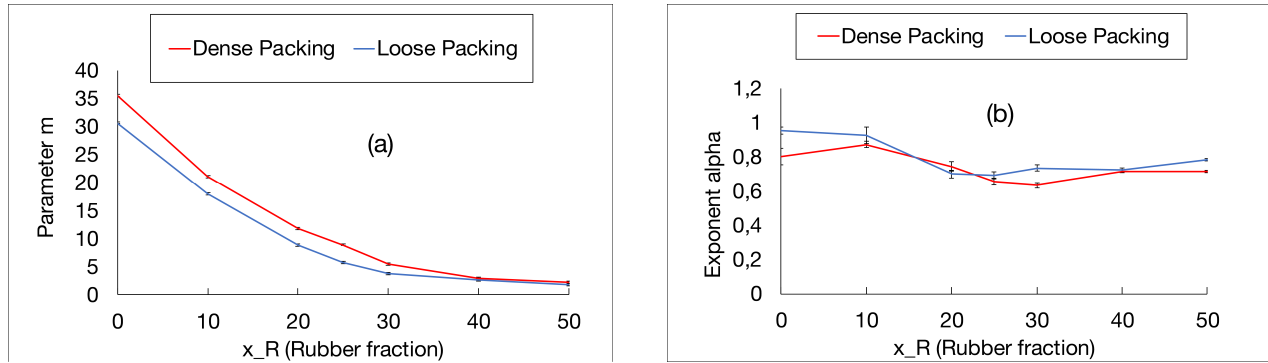
FIGURE 3.10. Fit parameters (a) m and (b) α for different rubber fractions of dense and loose packings.

of the initial void ratio (in the present case, approximately 0.70 for $x_R \geq 20\%$). The parameter m decreases exponentially with the rubber fraction and the decay coefficient of this exponential decrease, β is independent of the void ratio (in the present case, 0.059). This exponential decay is given by the equation,

$$m = e^{-\frac{x_R}{\beta}}.$$

(3.8)

where, m= fit parameter, x_R= rubber fraction and β= decay coefficient. At a given rubber fraction m is higher for denser packing (in the present case 26% higher). The parameter m signifies the magnitude of the incremental stiffness at the given stress level and it follows a logical behavior, since the stiffness of the packing will decrease with the increase in the rubber fraction. Also, denser packings are stiffer. These results are in well accordance with the literature available [Lee et al., 2009].

3.3.2 Unloading expansion

A typical 'S' shape of the plots can be observed for both dense and loose packings in the unloading phase. The curvature and the prominence of this 'S' shape increases with the increasing rubber fraction. Such 'S' shape in the unloading phase of the plots can also be observed in the literature [Lee et al., 2009, 2007, Kim and Santamarina, 2008, Fu et al., 2014]. However, in the literature data, the non-linearity is not so prominent.

The significant difference between the tests performed here and in the previously cited researches is the use of a continuous oedometer loading test apparatus. In the previous literature, conventional stage loading consolidation tests were used. In the conventional stage loading consolidation test, the test sample has higher displacement magnitude and it can be imagined that the time effect on the strain is drastically reduced at the beginning of the unloading. Hence, an important parameter for the presence of this 'S' shape is supposed to be the test duration or the test time. In order to understand the significance of this particular behavior, several hypotheses are presented in the next sections.

3.3.3 Quantifying the loading-unloading behavior

1. **Swelling Index**

   The sample is unloaded at the end of an oedometric compression loading (maximum stress) to any point on the "swelling line". For classical soils, it is generally admitted that the unloading deformation is recovered during a new loading stage. It is also generally admitted that the swelling curve is linear in a void ratio – log (vertical stress) space. As mentioned in Chapter 1, the swelling index for a sample is given by,

   $$C_s = -\frac{\Delta e}{\Delta(log\sigma_v)}, \tag{3.9}$$

   and it supposed here, that it permits the assessment of the swelling deformation of a pure sand packing. It is important to clarify that the swelling deformation of the packings consisting of rigid particles is recovered during re-loading but it is not reversible in a thermodynamic sense. The swelling deformation concerns the plasticity in both the contact network and at the level of individual contacts. The difference developed in the plasticity during the initial loading is recovered in the form of swelling plasticity, i.e. the packing retrieves its compacity during reloading; at the beginning of the unloading. The contribution of the elastic behavior is very small, as it depends on the deformation of the grains. In the context of the sand-rubber mixtures, given the contrast of the elasticity of the particles, it has been considered that the sand particles are perfectly rigid and the elasticity of pure sand mixtures has thus been neglected.

2. **Particles' elasticity**

   Rubber particles induce a new phenomenon in the packing deformability. The particles are elastically deformed under compression and generate geometrical evolution of the whole packing. This deformation produced directly (geometrically) by the grains' elasticity is addressed in the following as the elastic deformation, Δe_g. The elastic deformation under loading (compressibility) is assumed to be recovered during an unloading stage [Fonseca et al., 2019]. It is proposed here to dissociate the elastic deformation and the deformation produced by the evolution of the contact network, Δe_p . This second component of the total deformation is termed as the plastic deformation. It is then postulated that the deformation of the packing between two states is composed of a plastic deformation and an elastic deformation,

   $$\Delta e = \Delta e_p + \Delta e_g, \tag{3.10}$$

   At a first glance, Eq. 3.10 suggests that there is no interaction between Δe_p and Δe_g. In fact, this is not the case and a detailed explanation has been proposed below.

   The plastic behavior of a packing consisting of rigid particles is not as high as suggested by an intrinsic compression line as proposed by Burland [1990] for clays. Jamming phenomena are supposed to block the movement of the particles and drastically diminish the number of contact rearrangements in isotropic or oedometric compression. The rubber

(deformable) particles participate to unjam the packing. Indeed, the rubber particles deform under oedometric compression and liberate the movement of the rigid particles, thus increasing the plastic phenomena. Similarly, during the unloading phase, the rubber particles progressively recover their initial shape and induce perturbations in the packing, liberating the recovery of some plastic behavior developed under loading. So, the plastic deformation is not the deformation which should be developed by a packing of rigid particles, but the deformation of this packing by including the liberation of plastic deformation, equivalent to what happens in the rubber-sand mixture. In other words, the plastic deformation includes both, *viz.* the rigid particles' packing plasticity and the plasticity induced by the interaction with the deformation of rubber particles. On the contrary, elastic deformation includes only the geometrical evolution induced by the deformation of the rubber particles and directly depends on the stress state.

3. **Swelling line for sand-rubber packings**

It is considered that the classically defined swelling behavior is not concerned by the elastic deformability. In this context, the swelling behavior should not take into account the elastic deformation for the sand-rubber mixtures. Then, it could not be defined at high vertical stress levels where the rubber deformation is significant. On the other hand, the tangent behavior of the unloading when the vertical stress converges to zero, could be associated with a theoretical swelling index of an ideal equivalent packing of rigid particles. Indeed, when the mean pressure in the sample becomes low, the grain elasticity deformation is supposed to asymptotically vanish.

By considering the so defined swelling index, C_s and the final unloading void ratio, e_{uo}, it can be deduced from the Eq. 3.9, that the theoretical void ratio corresponding to the plastic deformation at the maximum vertical stress of the loading-unloading cycle,

$$e_p(\sigma_{max}) = e_{uo} - C_s log\left(\frac{\sigma_{max}}{\sigma_o}\right), \tag{3.11}$$

and the corresponding equivalent rigid particles' deformation during loading is,

$$\Delta e_p(\sigma_{max}) = e_p(\sigma_{max}) - e_{lo}. \tag{3.12}$$

where, $e(\sigma_{max})$ is the measured void ratio at the inversion of the vertical stress σ_{max} and e_{lo}, the initial void ratio (at σ_o).

4. **Elastic deformation**

From the previous inferences, the plastic deformation during loading can be determined using Eq.3.12 and the corresponding grain elasticity deformation level is obtained using,

$$\Delta e_g(\sigma_{max}) = e_p(\sigma_{max}) - e(\sigma_{max}). \tag{3.13}$$

The new assumption here is that the ratio of grain elasticity deformation to the total

deformation is independent of the vertical stress level during the loading. Through this hypothesis, it is possible to determine now the grain elasticity deformation, $\Delta e_g(\sigma_v)$ at any level of vertical stress, σ_v, under the loading condition.

5. **Plastic expansion**

Similar to the loading behavior, the deformation of the packing during the unloading is composed of an elastic and a plastic deformation. The elastic deformation only depends on the stress level. During the unloading, the elastic deformation which is still to be recovered up to the end of the unloading is equal to the elastic deformation produced during the loading up to the same stress level.

The plastic deformation is then determined by the difference between the total measured deformation and the elastic one; at a given vertical stress level. It could be expected, that the plastic expansion during unloading follows the swelling line. In practice, this is not the case and one can observe that the plastic expansion could be divided in two components: one which corresponds to the expected linear swelling, Δe_r, and a second remaining component, Δe_c. This last plastic component is linked to the 'S' shape of the unloading behavior in the void ratio - log (vertical stress) space.

6. **Time effect**

As previously suggested, it is supposed here that the origin of Δe_c evolution lies in the time effect of the sand-rubber mixture. In conventional consolidation tests, the tests are vertical stress-controlled. Time effect is thus consumed by creep stages during the time for which the load is applied during each incremental loading stage. In the oedometer tests performed in this study, the control has been imposed in the form of strain rate. Also, the loading is continuous and faster than in conventional consolidation tests. So, time effects are supposed to be still significant when the reversal of strain loading is suddenly imposed to the sample. There are a few studies available quantifying the creep behavior of sand-rubber mixtures. Ngo and Valdes [2007] have shown that the classical creep model used for fine-grained soils can be easily applied for sand-rubber mixtures as well. They conducted one-dimensional consolidation tests on sand-rubber mixtures (Ottawa sand and granulated tire rubber chips) and pointed out that the sand-rubber creep is significant. Further, AbdelRazek et al. [2018] conducted one-dimensional loading tests on sand-rubber mixtures and observed that with the increasing rubber fraction, the mixtures exhibited higher deformation rate under constant loading. In both the papers, an increasing time effect was observed with the increasing rubber content in sand-rubber mixtures.

3.3.4 Discussion on the loading-unloading behavior

1. **Swelling Index**

For practical reasons, the tangent of the unloading curve at low vertical compression is

approximated here by the secant line passing through two small vertical stresses (1.6 and 4 kPa)- see Fig. 3.11(a). The swelling index was estimated using this method for
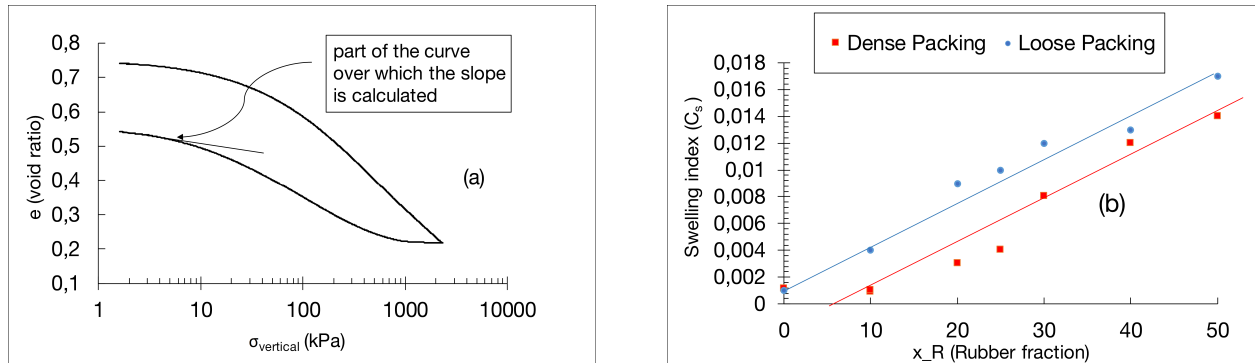
FIGURE 3.11. (a) Schematic for calculating the swelling index and (b) Swelling index values for all rubber fractions of dense and loose packings.

all the rubber fractions and Fig. 3.11(b) shows the corresponding swelling index values for different rubber fractions of dense and loose packings. The swelling index increases with the increasing rubber fraction for both dense and loose packings. In terms of dense and loose packings, the loose packings having a higher initial void ratio, exhibit a higher swelling index as compared to the same rubber fraction of dense packing. In a first approximation, it seems that the difference in the swelling index between loose and dense packing does not depend on the rubber fraction. These observations are in accordance with the data presented in the literature [Benessalah et al., 2019], which is however for much lower rubber fraction levels.

2. **Grain elasticity to total loading deformation ratio**
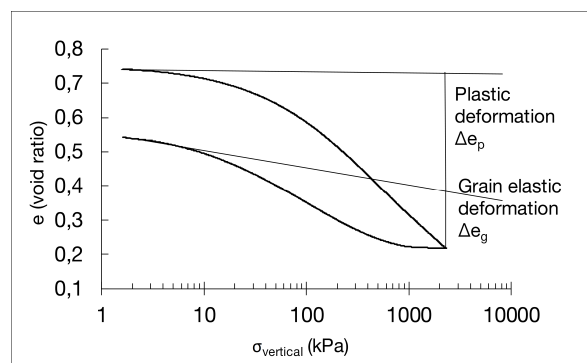
FIGURE 3.12. Schematic used for differentiating the strain into 2 components to characterize the 'S' shape of the unloading curve.

The ratio of (grain) elastic deformation (Δe_g) to the total deformation (Δe), determined using the estimated swelling indices (as shown in Fig. 3.12), is shown in Fig. 3.13 as an evolution with the rubber fraction. As per the aforementioned hypothesis, the ratio of grain elasticity component to the total differential void ratio should vary linearly with

71

the increasing rubber fraction. This is confirmed experimentally by the results presented in Fig 3.13. Moreover, it is observed that in proportion, the amount of grain elasticity
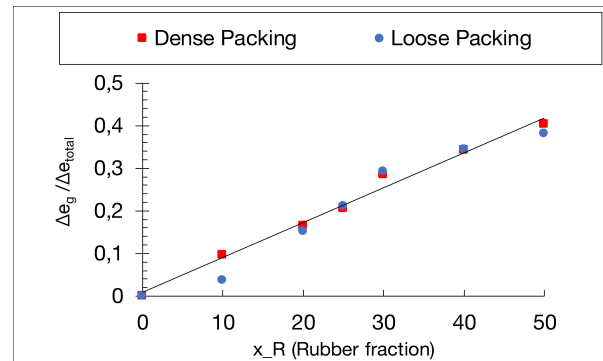
FIGURE 3.13. Change in the ratio of grain elastic deformation (Δe_g) to the total deformation (Δe_{total}) against rubber fraction.

deformation does not depend on the void ratio. By analyzing conjointly the evolutions in Fig. 3.13 and Fig. 3.11b, it can be concluded that the effect of the rubber fraction on the liberation of the plasticity potential of the packing under oedometric loading/ unloading also depends linearly on the rubber fraction. For the loose packing, the potential of plasticity is liberated from the first rubber particles introduced in the packing. For the dense packing, the first few rubber particles do not liberate the plasticity potential and a minimum rubber content is needed to achieve this phenomenon. Once the phenomenon is achieved, it evolves similarly with the rubber fraction for the loose and dense packings.

3. **Plastic behavior**

   As the ratio of elastic deformation to the total deformation is considered constant during the loading phase, the elastic deformation is determined at each level of vertical stress. Subsequently, the plastic response of the mixture is determined from the total deformation by subtracting the elastic deformation at each stress level. Eq. 3.13 is valid not only for the stress value corresponding to the inversion of vertical stress, σ_{max}, but also for any stress value. Hence, using this equation, elastic deformation is calculated and subsequently the plastic response of the mixture is determined. A typical plastic response of the packing is shown in Fig. 3.14.

4. **Time effect**

   The part of the unloading plastic deformation attributed to the time effect is determined by subtracting the plastic deformation (given by the swelling index and considering the linearity in the semi-log scale postulated above) from the unloading plastic deformation. Thus, from the hypothetical plot for plastic behavior obtained in Fig. 3.14, the time dependent behavior can be easily distinguished. Hence, the remainder 'S' shape in the plastic deformation plot represents the time-dependent mechanical response of the sand-rubber mixtures (see Fig. 3.15). This analysis was applied for all the rubber fractions of
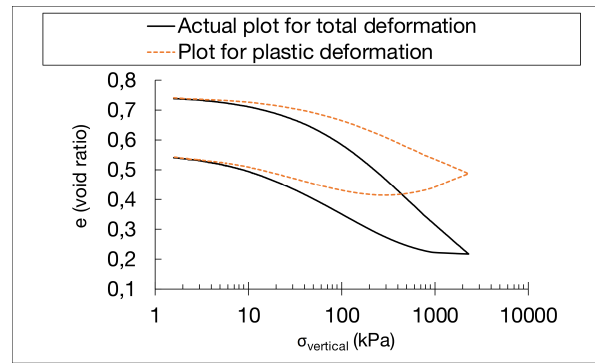
FIGURE 3.14. Schematic for plot obtained after subtracting the grain elastic deformation (Δe_g) from the total deformation (Δe_{total}) at every level of incremental stress.
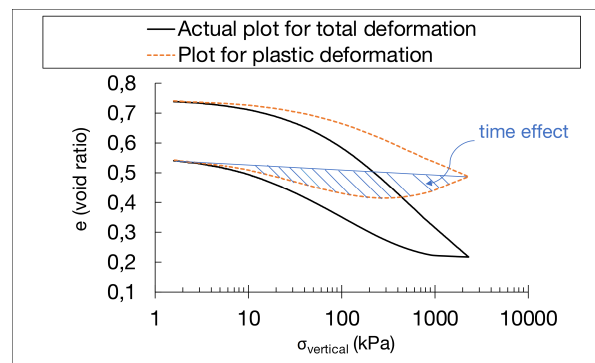
FIGURE 3.15. Schematic for understanding the time-dependent mechanical response of sand-rubber mixtures.

dense and loose packings and the respective plots can be seen in Fig. 3.16 and Fig. 3.17.

The time-dependent behavior can be characterized by studying the rate of change of displacement or the change in the void ratio with time. Fig. 3.18 and Fig. 3.19 show the rate of change of Δe_c with time. These plots shown here are in accordance with the literature available [AbdelRazek et al., 2018, Ngo and Valdes, 2007], showing that the deformation rate increases with the increasing rubber fraction. The strain evolution during the unloading is also represented. It can be observed that in all cases, for some tens of seconds, the stress level is maintained almost constant. The duration of this period, imposed by the experimental control system, is similar for all rubber fractions and initial densities. During this period of time, the mixture experiences a relaxation stage and the vertical stress level drastically decreases. As a consequence, an elastic expansion is developed. This explains that a plastic deformation, in the direction of the compressibility, should compensate, in order to maintain the total deformation constant. After this transitory stage of relaxation, the strain evolution is imposed at a fixed unloading rate. Given the still effective time effect, the decrease in vertical stress is higher than the evolution expected by a classical swelling behavior. A plastic compatibility is still needed

73
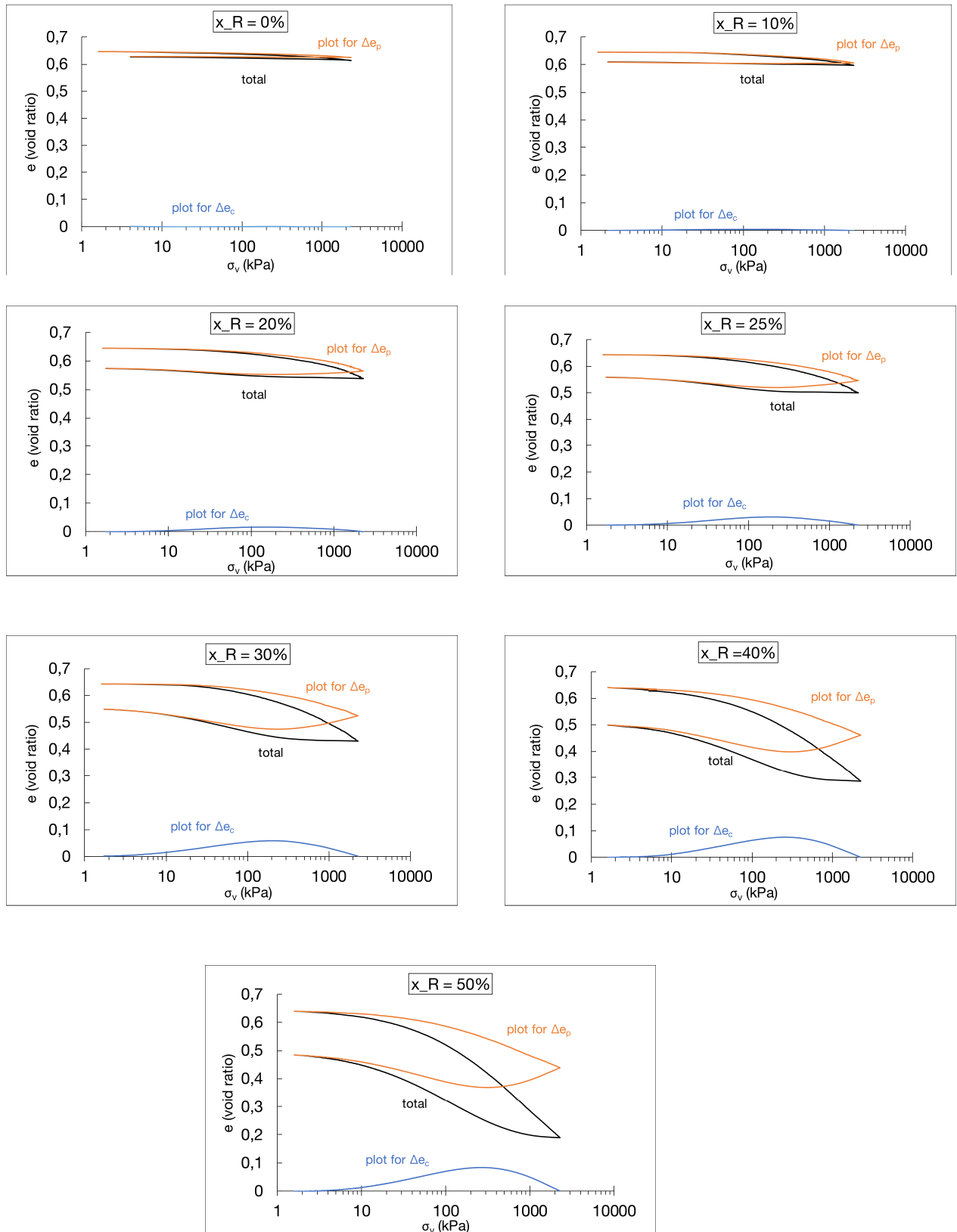
FIGURE 3.16. Void ratio vs log (vertical stress) plots for all rubber fractions of dense packing characterizing the 'S' shape of unloading and showing the time dependent behavior.
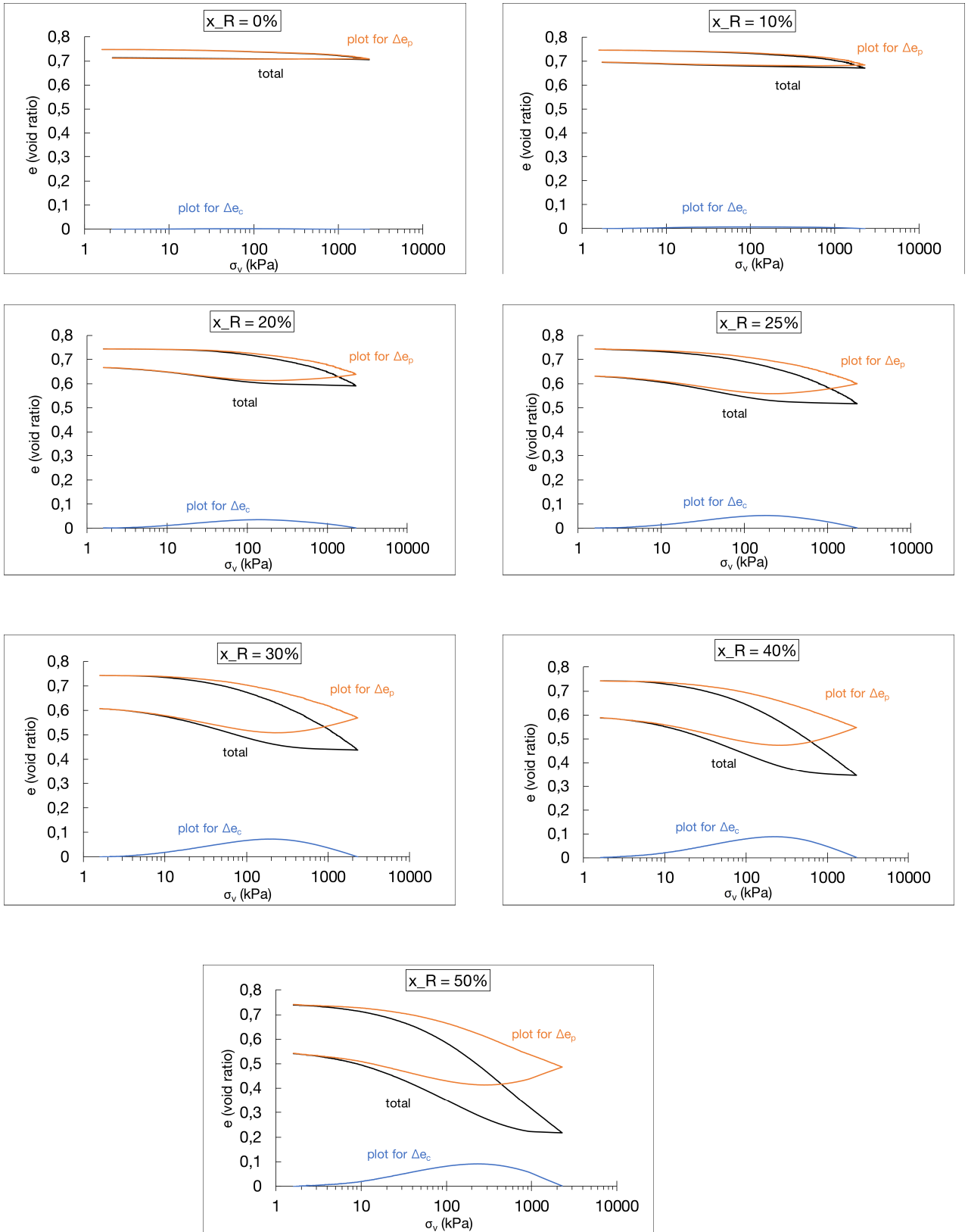
FIGURE 3.17. Void ratio vs log (vertical stress) plots for all rubber fractions of loose packing characterizing the 'S' shape of unloading and showing the time dependent behavior.
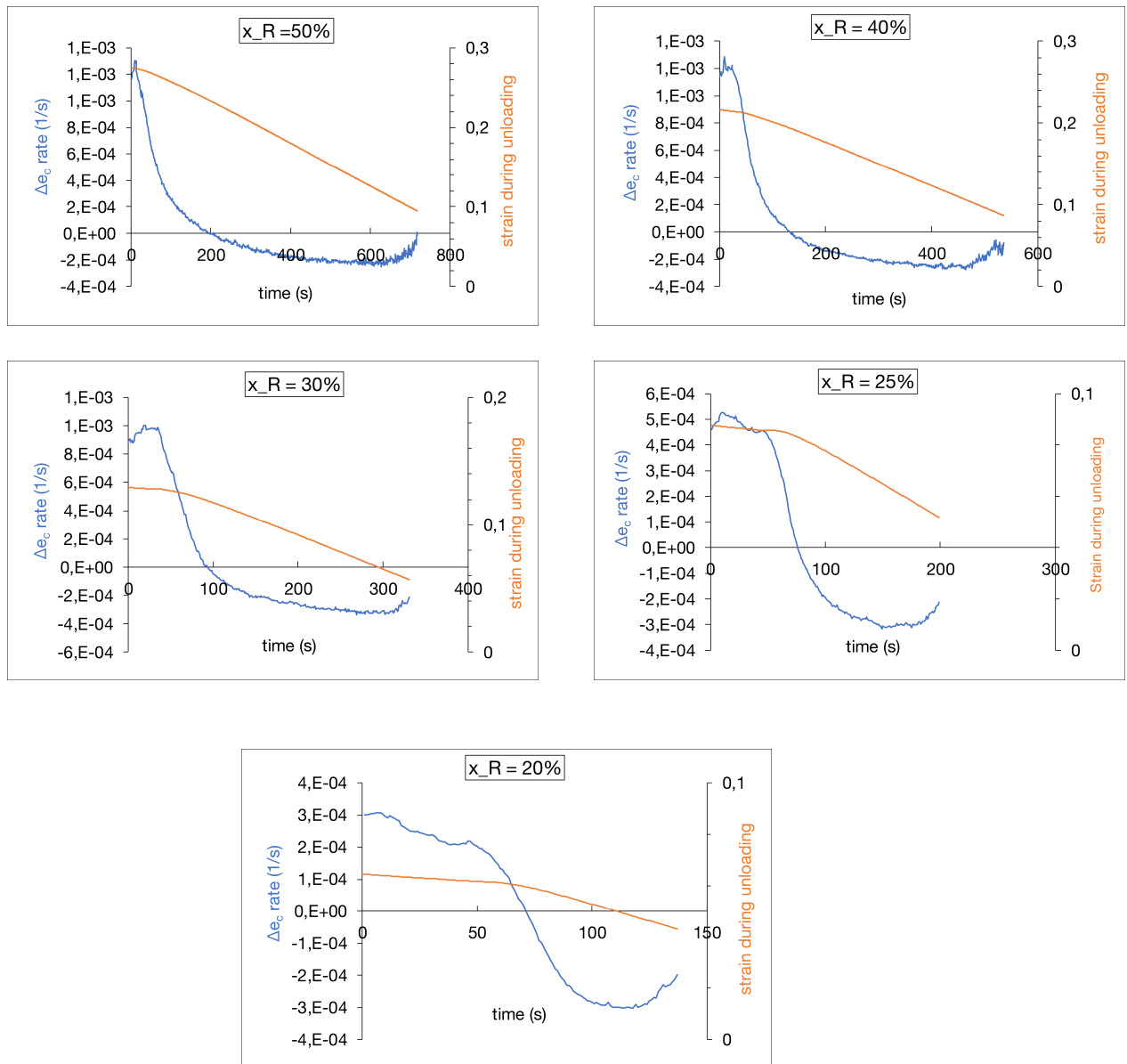
FIGURE 3.18. Rate of change of Δe_c and the unloading strain rate for dense packings (20% -50% rubber fractions).

to compensate the larger than expected elastic expansion. With the increasing test duration and decreasing vertical stress, the time effect progressively vanishes and the total strain evolution recovers the classical swelling behavior. For rubber contents lower
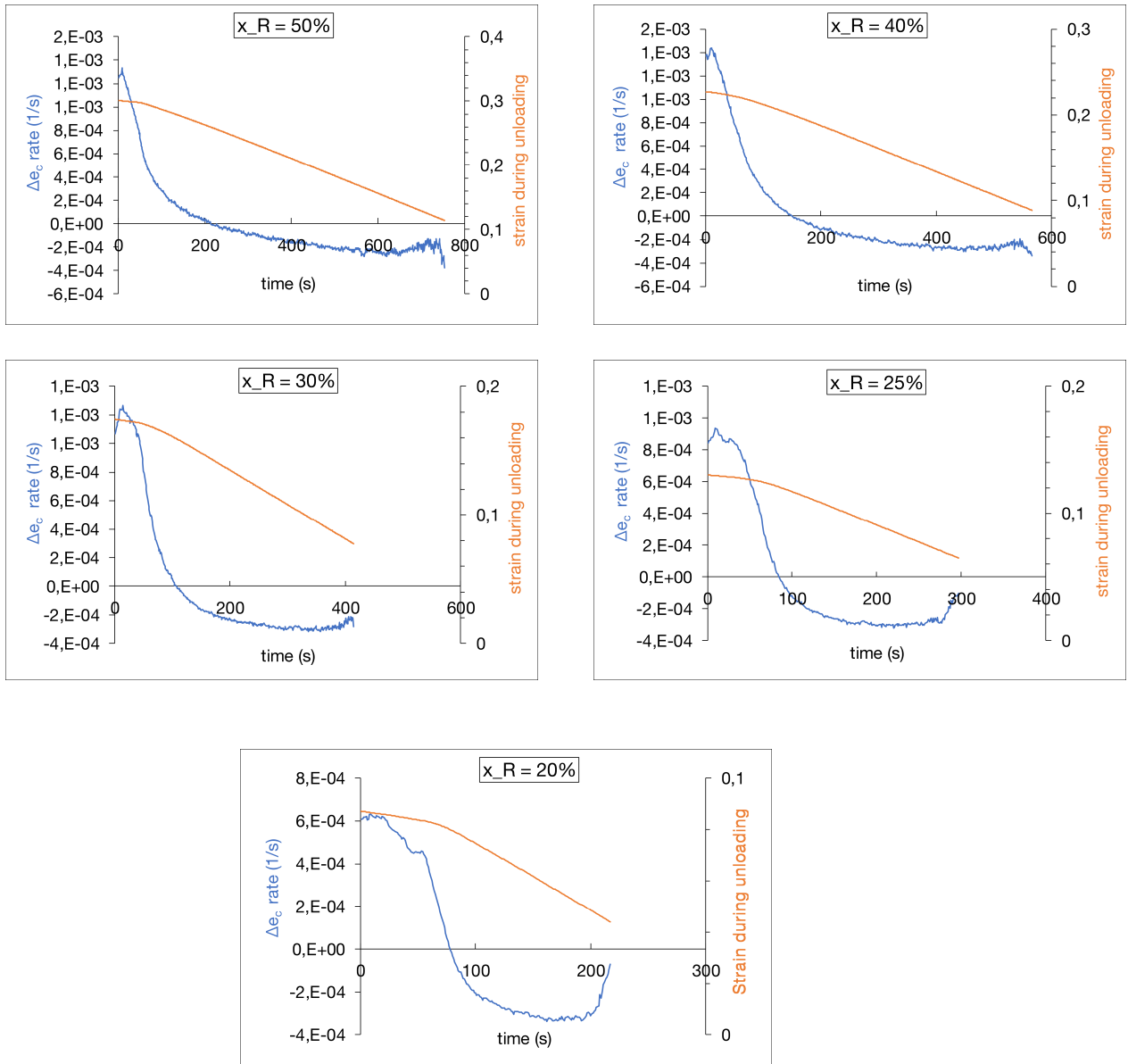
FIGURE 3.19. Rate of change of Δe_c and the unloading strain rate for loose packings (20% -50% rubber fractions).

than 20%, the time effect is not much observed. But as suggested previously the time effect (relaxation) is increasing with the rubber fraction. This explains the increasing plastic compressibility with the rubber fraction during the beginning of the unloading stage. With an aim to characterize the influence of the time effect with the changing initial void ratio, the ratio of time for dense and loose packings at which the maximum time effect plastic deformation is observed was studied for all the rubber fractions. The evolution of this ratio with the rubber content (see Fig. 3.20) is almost constant. It can

77

be suggested that the influence of the void ratio on the time effect plastic deformation is independent of the rubber content.
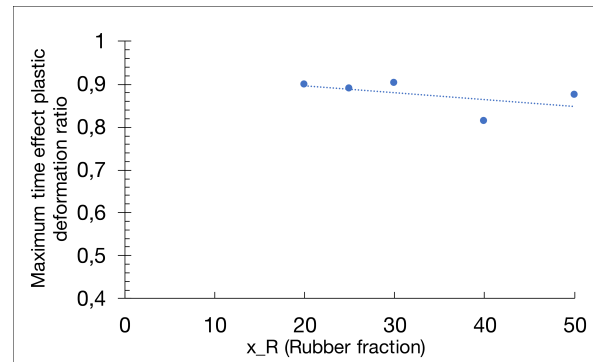
FIGURE 3.20. Ratio of maximum time effect plastic deformation between dense and loose packings of same rubber fraction.

5. **Confined modulus using the plastic behavior**

In the previous section, the strains have been differentiated into plastic and elastic components. As mentioned before, the plastic strain takes into account the effect of overall packing rearrangements but does not consider the strain related to the elastic grain deformation under loading. Moreover, confined modulus is the measure of stiffness of the packing under confinement. The increasing confining pressure encourages the granular rearrangements. Hence, it is interesting to isolate the plastic strain and study the confined stiffness using this strain.

The individual fits for dense and loose packings for all the rubber fractions have been shown in Fig. 3.21 and Fig. 3.22. The plots for the parameter m and exponent α have been presented in Fig. 3.23. It can be observed from the plots, that the magnitudes of parameters m and α are quite similar to the magnitudes of m and α for the confined modulus using the total strain (see Fig. 3.10).

Of course, this is expected, given i) the hypothesis of a constant grain elasticity to total loading deformation ratio and ii) the affine relation between this ratio and the rubber content, observed experimentally. As a result, the exponent α is the same when determined from the total strain or from the plastic strain. The parameter m decreases exponentially in the two cases but slower when determined from the plastic strain: the decay coefficient, β, independent of the void ratio is 0.049 in place of 0.059. In both the cases, at a given rubber fraction, m is higher for denser packing (in the present case 26% higher).

All the results presented in this section point out the effect of the initial void ratio on the mechanical response of sand-rubber mixtures. Although important, the initial void ratio is not the only parameter which affects the behavior of sand-rubber mixtures. The size ratio between
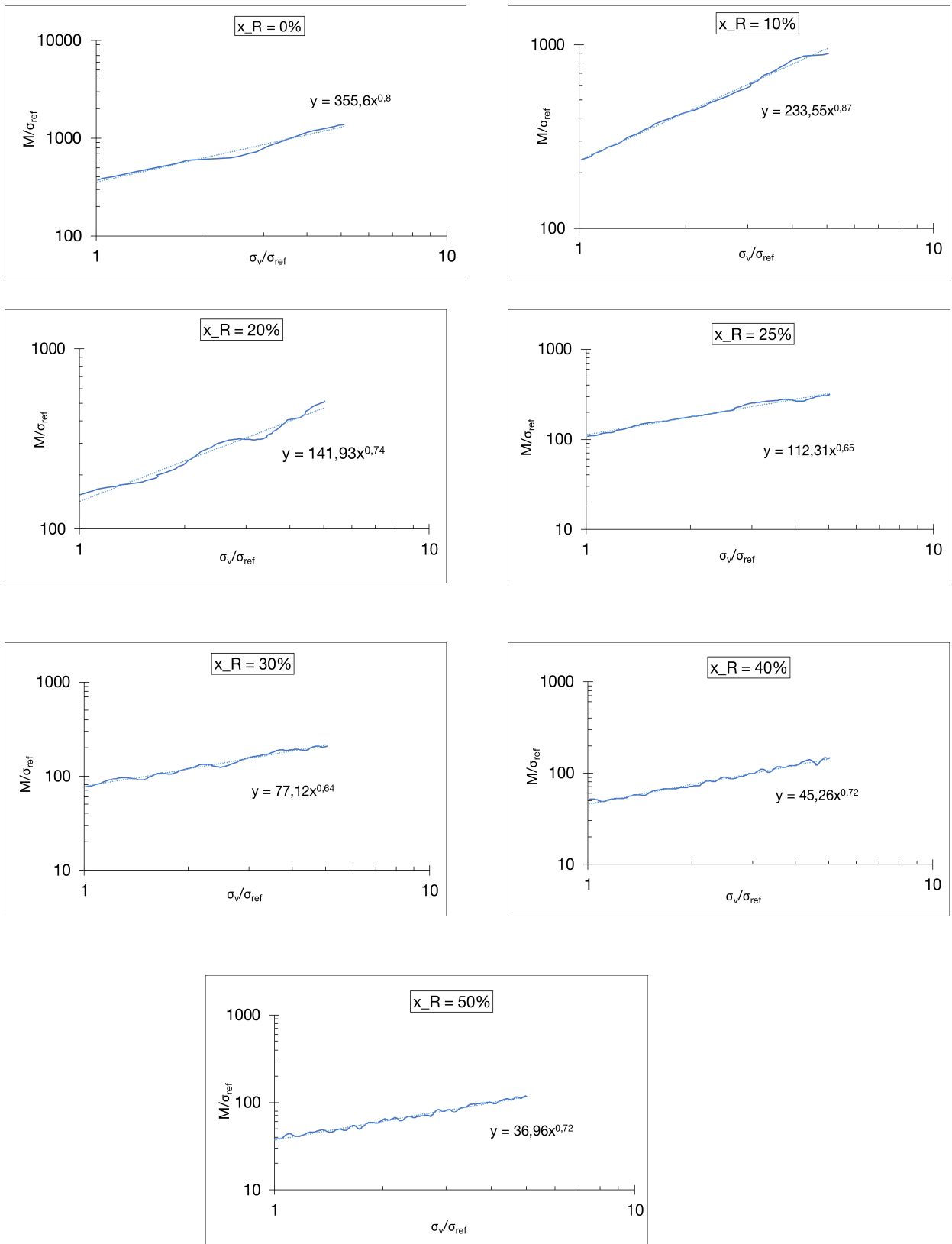
FIGURE 3.21. Individual fits for confined modulus vs vertical stress for all rubber fractions of dense packings using plastic strain.
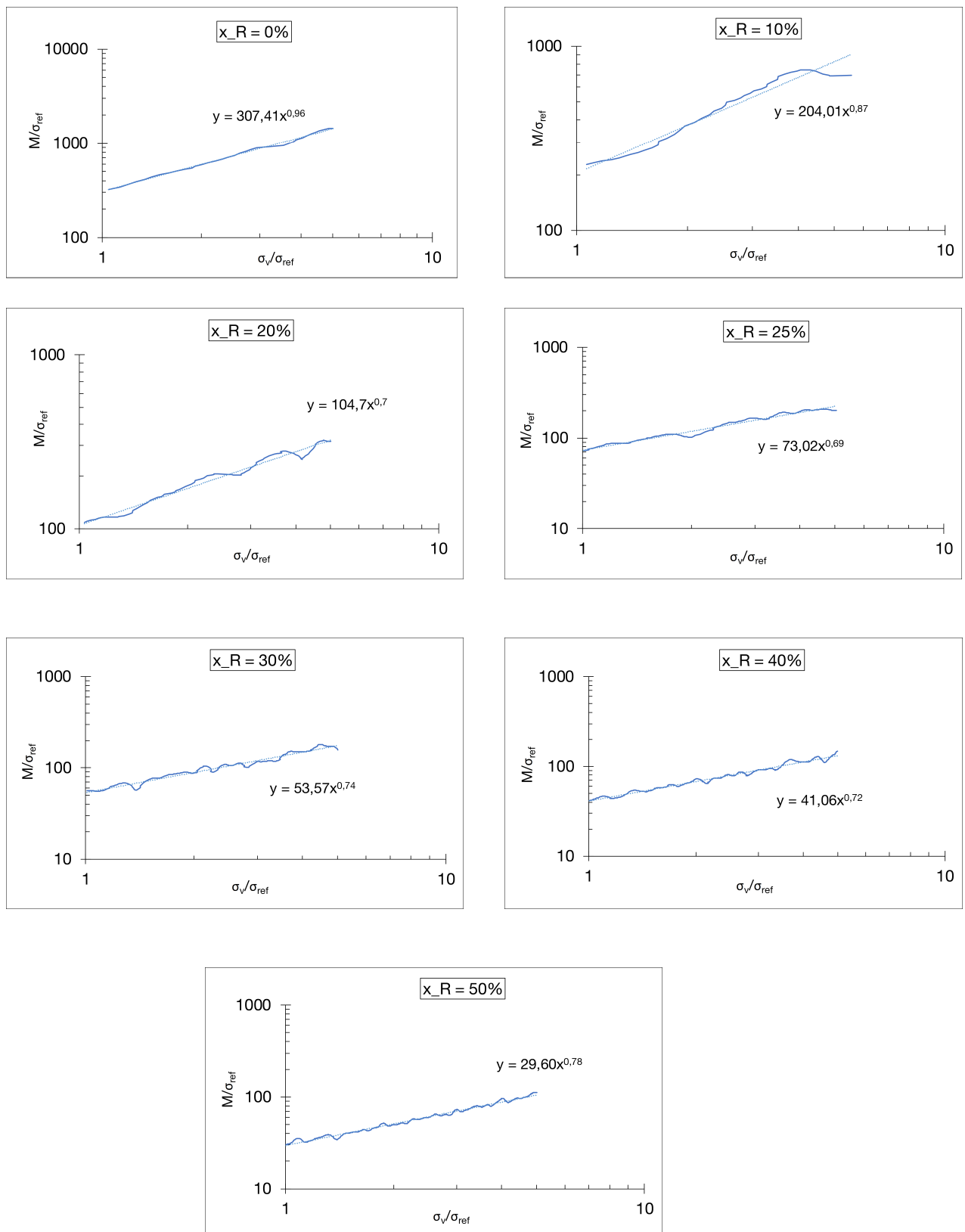
FIGURE 3.22. Individual fits for confined modulus vs vertical stress for all rubber fractions of loose packings using plastic strain.
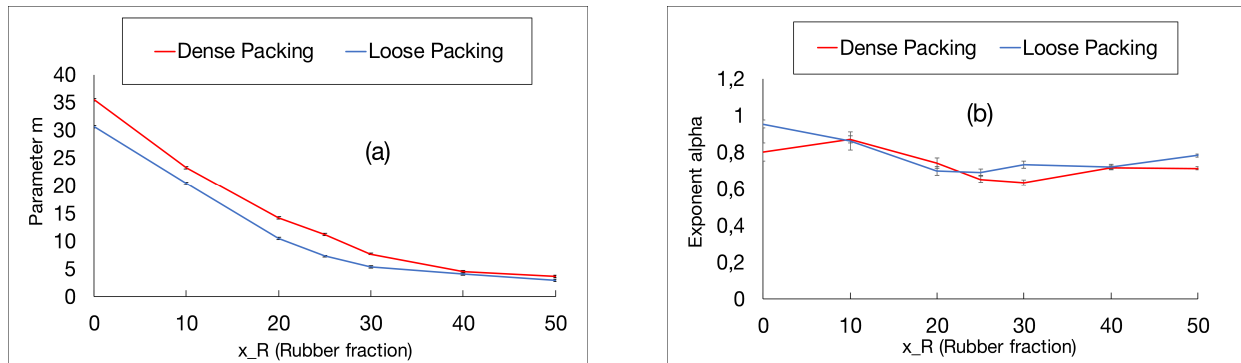
FIGURE 3.23. Fit parameters (a) m and (b) α for different rubber fractions of dense and loose packings using the plastic strain.

the sand and rubber particles in the mixtures as well as the variation in the particle size also affects the mechanical response of these mixtures. These parameters will be discussed in the subsequent sections.

3.4 Effect of particle size

The size of the sand and rubber grains used for the oedometer tests described before was 1.6-2mm. Tests were also performed on size distribution of 1.25-1.6mm. For the Leighton Buzzard sand used, as discussed before (see Section 3.2.3), the maximum and minimum limit fabrication void ratios were fixed to be e_{max} = 0.83 and e_{min} = 0.55. Irrespective of the target initial void ratio of the packing or size distribution, these limits were considered to be the same. The sand-rubber packings were fabricated for all the rubber fractions (0-50% by volume) and a similar initial target fabrication void ratio as that of dense packings, *i.e.* 0.65. However, like mentioned before as well, the actual initial void ratios were different and have been mentioned in Table 3.4. Fig. 3.24 compares the deformation evolution with the vertical stress for the two

Initial void ratio for sample size 1.6-2mm		Initial void ratio for sample size 1.25-1.6mm	
x_R (%)	Void Ratio	x_R (%)	Void Ratio
0	0.647	0	0.647
10	0.646	10	0.645
20	0.644	20	0.645
25	0.643	25	0.644
30	0.642	30	0.643
40	0.641	40	0.642
50	0.64	50	0.642

Table 3.4: Actual fabrication void ratios for the two sample size distributions under an initial stress of 1.6kPa (void ratio values for 1.6-2mm packings are the values for dense packings mentioned before).

particle sizes. Statistically, no difference in the measured void ratio at the inversion vertical

stress σ_{max} was observed between the two packings, at the same rubber content (non-zero difference has a probability less than 5%). The differences at each rubber fraction could be generally explained by experimental errors. For instance, the packing with sample size 1.25-1.6mm is slightly looser than the other packing for lower rubber fractions. For 20%, 25% and 30% rubber fractions, the packing with the sample size 1.6-2mm is slightly looser than the other packing.

Globally, a higher difference is observed for the packings with 25% and 30% of rubber. At this intermediate rubber content, there is a higher probability of different rubber arrangements throughout the packing. Hence, with each repetition of the test, the observation will be slightly different. As it will be discussed later, this distribution can change the deformation behavior. The difference between each pair of tests for a given rubber fraction could be considered an estimation of the repeatability of the tests. The standard deviation of the repeatability is estimated to be 0.008 in terms of void ratio at the maximum vertical stress. This effect of particle size is important to consider before understanding the effect of sand/rubber particle size ratio on the mechanical response of the packings. The next section will present the results of the effect of size ratio on the packing behavior.

3.5   Effect of sand/rubber particle size ratio

Oedometer tests were also performed on sand-rubber mixtures by varying the sand/rubber particle size ratio (S/R). The tests were conducted on three different sand/rubber size ratios (S/R), *i.e.* S/R=0.5, S/R=1 and S/R=1.5. The rubber used for all these tests was of the size 1.25-1.6mm (D_{50} = 1.4mm). Whereas, for S/R=0.5, sand used was 0.6-0.8mm (D_{50} = 0.7mm), for the tests on S/R=1, it was 1.25-1.6mm (D_{50} = 1.4mm) and for the tests of S/R=1.5, the sand used was 2-2.24mm (D_{50} = 2.1mm). The tests were performed only on 2 rubber fractions, *i.e.*

x_R=10% packings		x_R=50% packings	
S/R	Initial void ratio	S/R	Initial void ratio
0.5	0.646	0.5	0.642
1	0.645	1	0.642
1.5	0.645	1.5	0.642

Table 3.5: Actual fabrication void ratios for the packings of different size ratios for 10% and 50% rubber fraction under an initial stress of 1.6kPa.

10% and 50%. The target fabrication void ratio for all these packings was 0.65. The actual fabrication void ratios for each packing have been given in Table 3.5. Similar parameters were studied for these packings as were studied in case of the packings discussed in Section 3.3. The results have been presented here in terms of these different parameters.
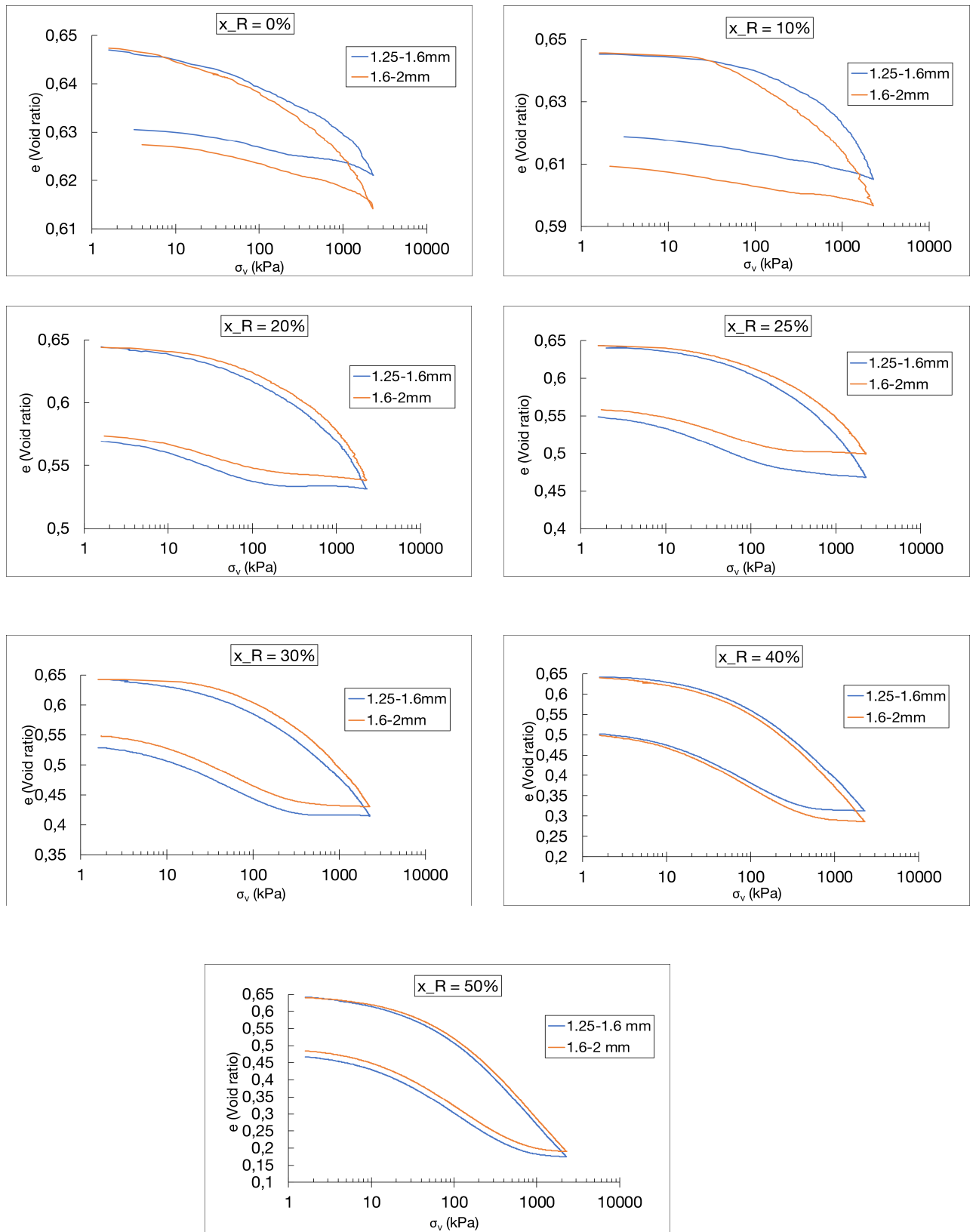
FIGURE 3.24. Comparison between the two sample size distributions for all rubber fractions of sand-rubber packings.

3.5.1 Compressibility
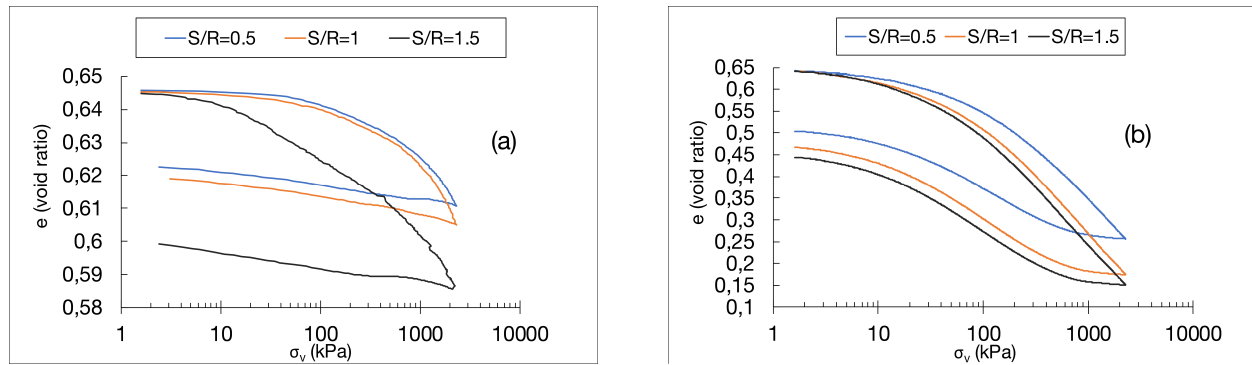
FIGURE 3.25. Void ratio vs log (vertical stress) plot for all sand/rubber size ratios (S/R) of (a) 10% rubber fraction packings and (b) 50% rubber fraction packings.

As explained in Section 3.4, for a given packing of similar rubber fraction, with the varying particle size, the packing actually fabricated may be slightly looser or denser. Hence, for a given rubber fraction, the packings show a slight variation in the void ratio, with S/R=0.5 packing being the loosest and S/R=1.5 packing being the densest of the three. One of the explanations can be the size of the local voids inside the packings varying with the sample size of the sand used. For S/R=0.5, with a sand of D_{50}= 0.7mm, voids are smaller than in the case of S/R= 1.5 with a sand of D_{50}= 2.1mm. Therefore, for the same rubber fraction, less rubber particles will be accommodated in the voids in case of S/R=0.5 than in the case of S/R=1.5. Thus, the rubber particles which according to the literature mostly help in stabilizing the primary force chains, will be more inclusive in the case of S/R=1.5 than in the case of S/R=0.5, and consequently, the difference is observed. However, it is noteworthy that this difference is not very high and decreases with the increasing rubber fraction.

Fig. 3.25 shows the plot for void ratio vs log (vertical stress) for the different S/R of 10% and 50% rubber fraction packings. The trend of the plots shown in Fig. 3.25(a) and (b) is the same. The difference between each S/R packing is minimized when the rubber fraction increases from 10% to 50%.

3.5.2 Confined modulus

The 1-D confined stiffness or confined modulus was studied for the different size ratio (S/R) packings as well, as was studied in the case of dense and loose packings discussed before. The individual fits for all the packings has been shown in Fig. 3.26. A similar technique was used to linearize the plots of confined modulus vs stress as was described in Section 2. Further, power law was used to fit these plots according to Eq. 3.7. The fit for the plots was done in the stress range of 100kPa (reference stress) and 500kPa in order to avoid the excess non-linearity in the curves and uncertainty due to the effect of crushing of sand particles at higher stresses.

The equations shown on the individual plots are the fit equations, where, y = (confined modulus

(M)/reference stress (σ_{ref})), x = (vertical stress (σ_v)/reference stress (σ_{ref})), coefficient of x = parameter m and the exponent = α.
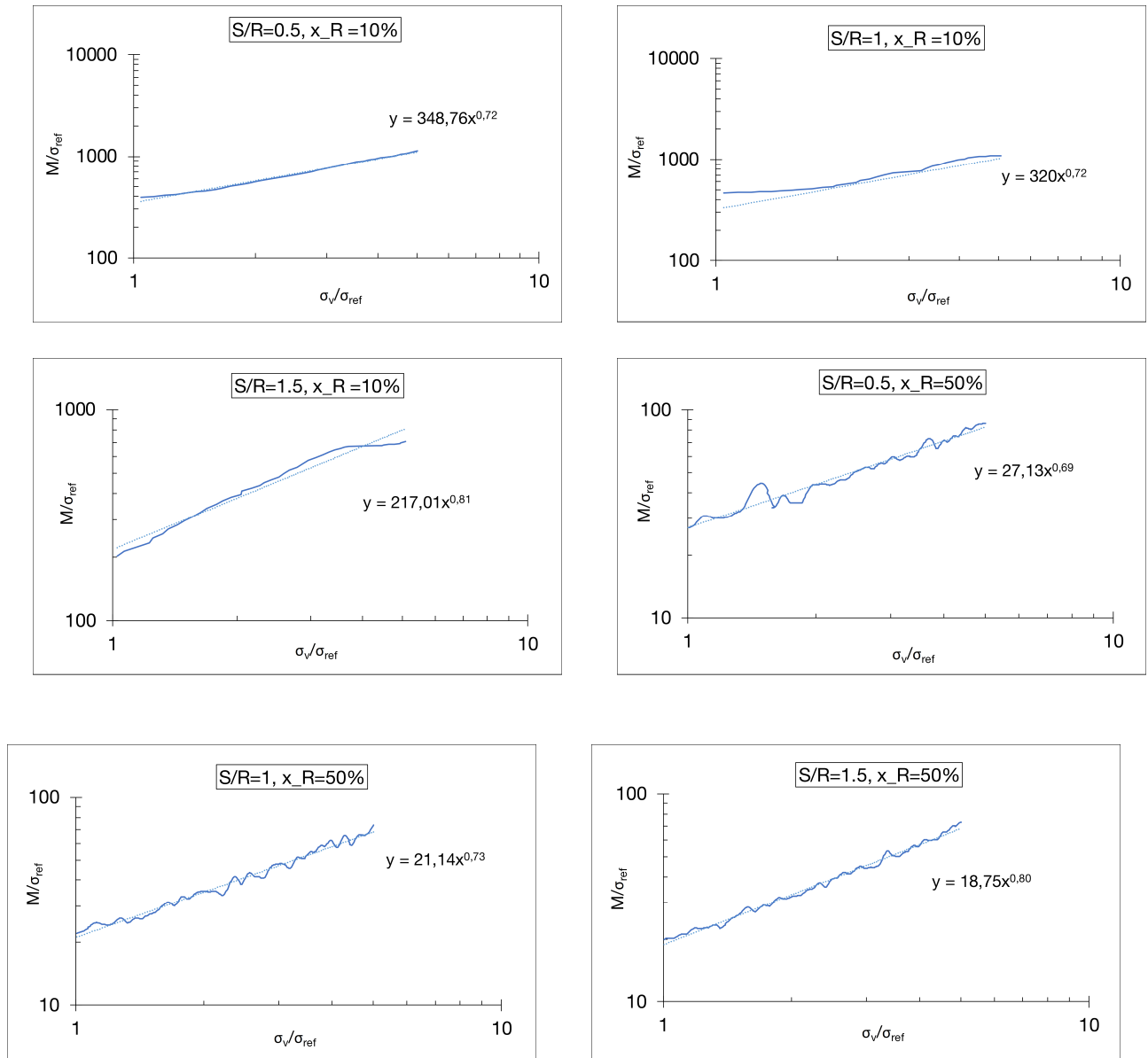
FIGURE 3.26. Individual fits for confined modulus vs vertical stress for all size ratios (S/R) for 10% and 50% rubber fraction packings.

The parameter m signifies the magnitude of the confined modulus whereas the exponent α denotes the range of the change in the confined modulus with the vertical stress. The results for parameters m and α have been shown in Fig. 3.27(a) for 10% rubber fraction packings for all three S/R values and Fig. 3.27(b) for 50% rubber fraction packings of all three S/R values. The parameter m shows a decreasing trend for both 10% as well as 50% rubber fractions with the size ratio (S/R), thus indicating that the magnitude of confined modulus decreases with the increasing size ratio (S/R). With the increasing size ratio (S/R), sand grains in the
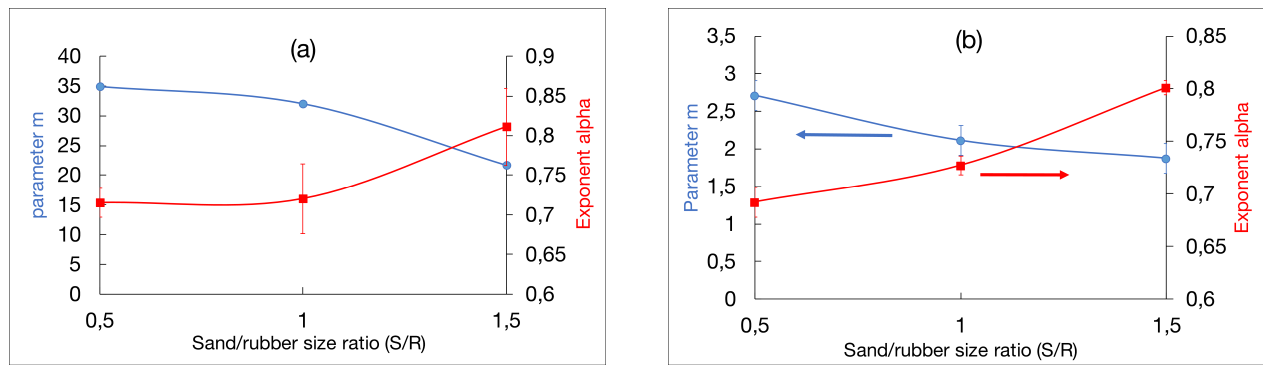
FIGURE 3.27. Parameters m and α for all size ratios (S/R) of (a) 10% rubber fraction packings and (b) 50% rubber fraction packings.

packing are bigger, hence the voids are bigger and more rubber is accommodated in the voids for a similar rubber fraction and a similar packing volume fraction. Hence, the modulus of the confined stiffness reduces with the increasing size ratio. On the other hand, α value increases, which shows that with the increasing size ratio, the stiffness becomes closer to being directly proportional to the applied vertical stress. The trend observed for the sand-rubber packings with the changing size ratio is in well accordance with the literature available as well [Lee et al., 2009]. It should be noted however that the increase of the power exponent α is in the range of variation observed in the Fig. 3.10.

3.5.3 Swelling Index

Swelling index was calculated for the sand-rubber packings with different size ratios by using the same method as explained in Section 3.3.4. The swelling index has been observed to increase with the increasing rubber fraction which was already explained in the same section. Fig. 3.28 shows the swelling index for the different size ratio sand-rubber packings of 10% and 50% rubber fractions. The swelling index values for 50% rubber fraction packings are evidently higher than for 10% rubber fraction packings. Moreover, the swelling index value can be observed to increase with the increasing sand/rubber size ratio (S/R). With the increase in the size ratio, as explained before, the rubber grains are smaller as compared to the sand grains. Hence, for bigger sand grains, the voids are bigger and hence, more rubber is accommodated in the voids and thus, due to a local increase in the rubber content, the unconfined expansion characteristics of the packing increases. Moreover, it has been reported in the literature as well, that the rubber particles play a major role of stabilizing the force chain networks. Hence, mostly, very less rubber particles are involved in the major force carrier networks and thus the rubber acts like a lubricant. An analogical case can be imagined of oil in sand, wherein with larger voids, the oil is well distributed throughout the sand. Hence, with larger voids, rubber gets well distributed throughout the voids in the packings and hence, the swelling observed is higher than for a packing of lower size ratio and similar rubber fraction. The swelling index calculation helps to gain a deeper insight into the behavior of these mixtures in terms of their
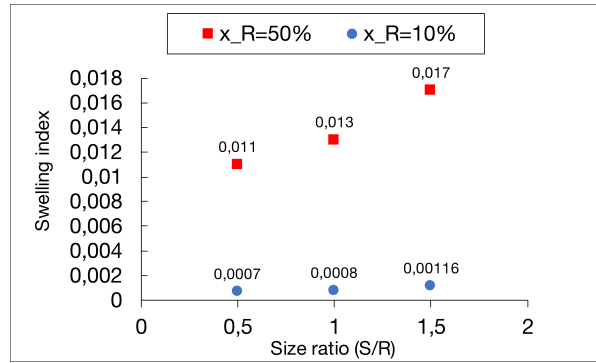
FIGURE 3.28. Swelling index for all the size ratios of 10% and 50% rubber fraction packings.

size ratio. Thus, a similar analysis has been performed on these packings, as was done in the case of dense and loose packings. The swelling index characterization, hence helped to characterize the packing behavior in terms of plastic deformation and elastic deformation. The same will be explained in the next section.

3.5.4 Elastic and plastic deformation

As per the hypothesis explained in section 3.3.3, it is interesting to verify the behavior of the ratio of elastic to the total deformation with the varying sand/rubber size ratio (S/R). Fig. 3.29 shows the variation of this ratio with the sand/rubber size ratio for 10% and 50% rubber fraction mixtures. The ratio has a linear decrease with the increasing size ratio. Further, for
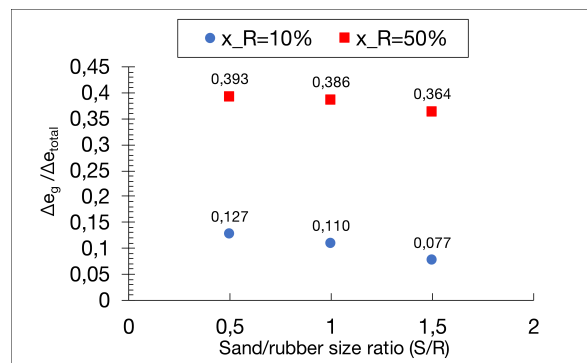
FIGURE 3.29. Change in the ratio of grain elastic deformation (Δe_g) to the total deformation (Δe_{total}) against size ratio (S/R) for 10% and 50% rubber fraction mixtures.

higher rubber fraction, this level of decrease is lower. For a lower size ratio packing, the rubber grains being larger than the sand grains, there are more localized rubber-rubber contacts as compared to higher size ratio packings. In case of higher size ratio packings, due to bigger voids, the rubber is much well distributed throughout the packing. Hence, for similar rubber fraction, the contribution of the grain elastic component, i.e. the change in the void ratio due to the

elastic properties of the grains is higher in case of lower size ratio packings than in the case of higher size ratio packings. Evidently, this effect goes on decreasing with the increasing rubber fraction and hence, a lower magnitude of decrease is observed in the case of 50% mixtures than in the case of 10% mixtures.

As can be seen from the plots in Fig. 3.30 presented in the next section, with the increasing size ratio, the sand-rubber packing undergoes an increased plastic deformation. It means that for higher size ratio, since rubber is much well distributed, the effect of rubber is much more pronounced.

The hypothesis established in Section 3.3.3, thus was found to be valid for the mixtures with varying size ratios as well due to an expected observation of linearized behavior of the ratio of elastic to the total deformation over the size ratio. Hence, evidently, it can be interesting to study the time-dependent behavior of the sand-rubber mixtures for varying size ratios.

3.5.5 Time effect
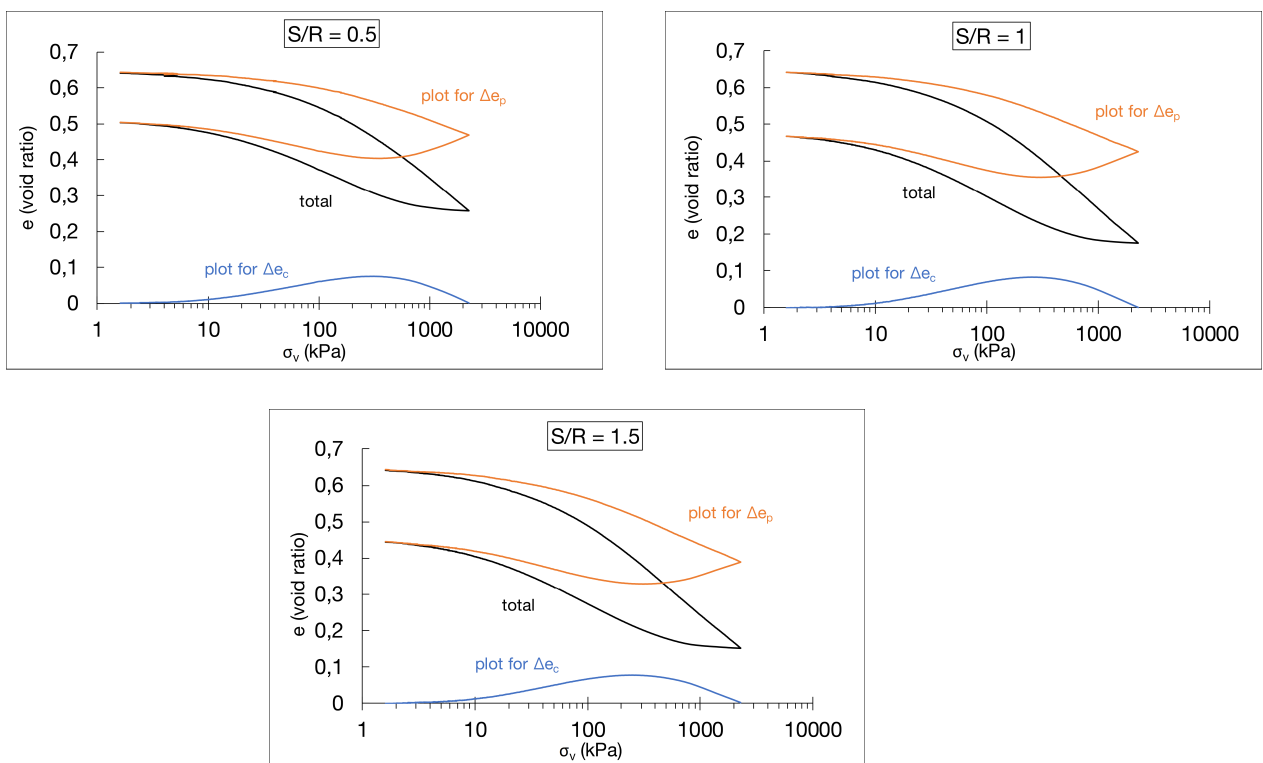
FIGURE 3.30. Plots for all size ratios of 50% rubber fraction mixtures characterizing the 'S' shape of unloading and showing the time-dependent mechanical behavior.

The time effect behavior of sand-rubber mixtures has been clearly established in Section 3.3.4. However, in the aforementioned section, only the effect of rubber fraction and the packing volume fraction was considered. This section presents the effect of size ratio on the time effect behavior of sand-rubber packing. The time effect for the different packings was calculated as

per the procedure mentioned in Section 3.3.3. Since time effect has shown an increasing trend with the increasing rubber fraction; for 10% rubber fraction packings, the effect is quite low. Hence, the results presented in Fig. 3.30 show the time effect for different size ratios for 50% rubber fraction mixtures. The plastic deformation during unloading related to the time effect is the same for the three size ratios. This can be clearly observed in the plots shown in Fig. 3.31. These plots show the rate of change of time effect void ratio and the unloading strain with
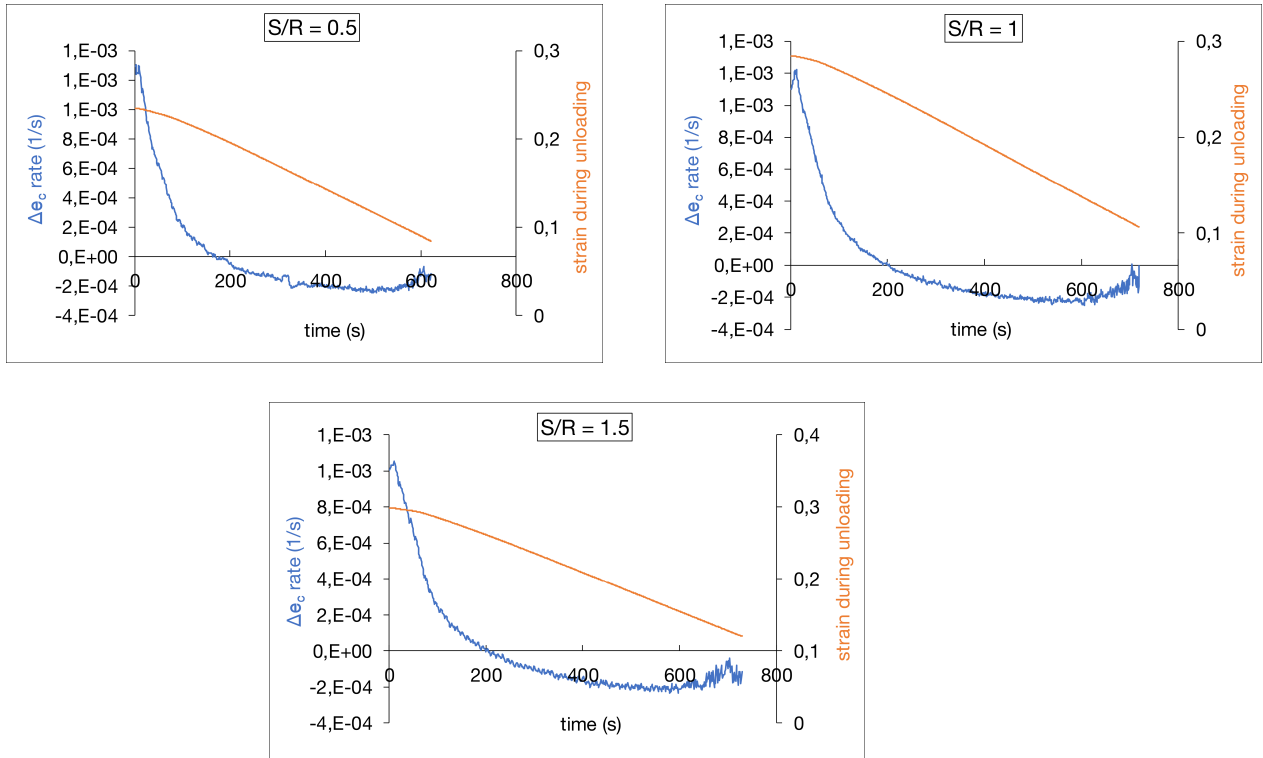
FIGURE 3.31. Plots for the time effect void ratio rate and the unloading strain rate for all size ratios of 50% rubber fraction mixtures.

time. The strain is shown along with the time effect void ratio Since the time effect behavior also depends on the test equipment control used and hence, the strain rate in turn verifies this behavior observed. These observations are also valid for 10% of rubber content.

The time effect behavior characterization using the hypothesis of elastic and plastic components helps to study the plastic confined modulus, which has been presented in the next section.

3.5.6 Confined modulus using the plastic strain

In order to characterize the time-dependent behavior of the sand-rubber mixtures with the varying size ratio, the strains were differentiated into elastic and plastic strain. As pointed out previously, with the increasing confining pressure, the granular rearrangements increase and hence, it is interesting to study the confined stiffness due to the plastic strain. Fig. 3.32 show the individual fits for all the size ratios of 10% and 50% rubber fraction packings by calculating the confined modulus using only the plastic strain component during the loading
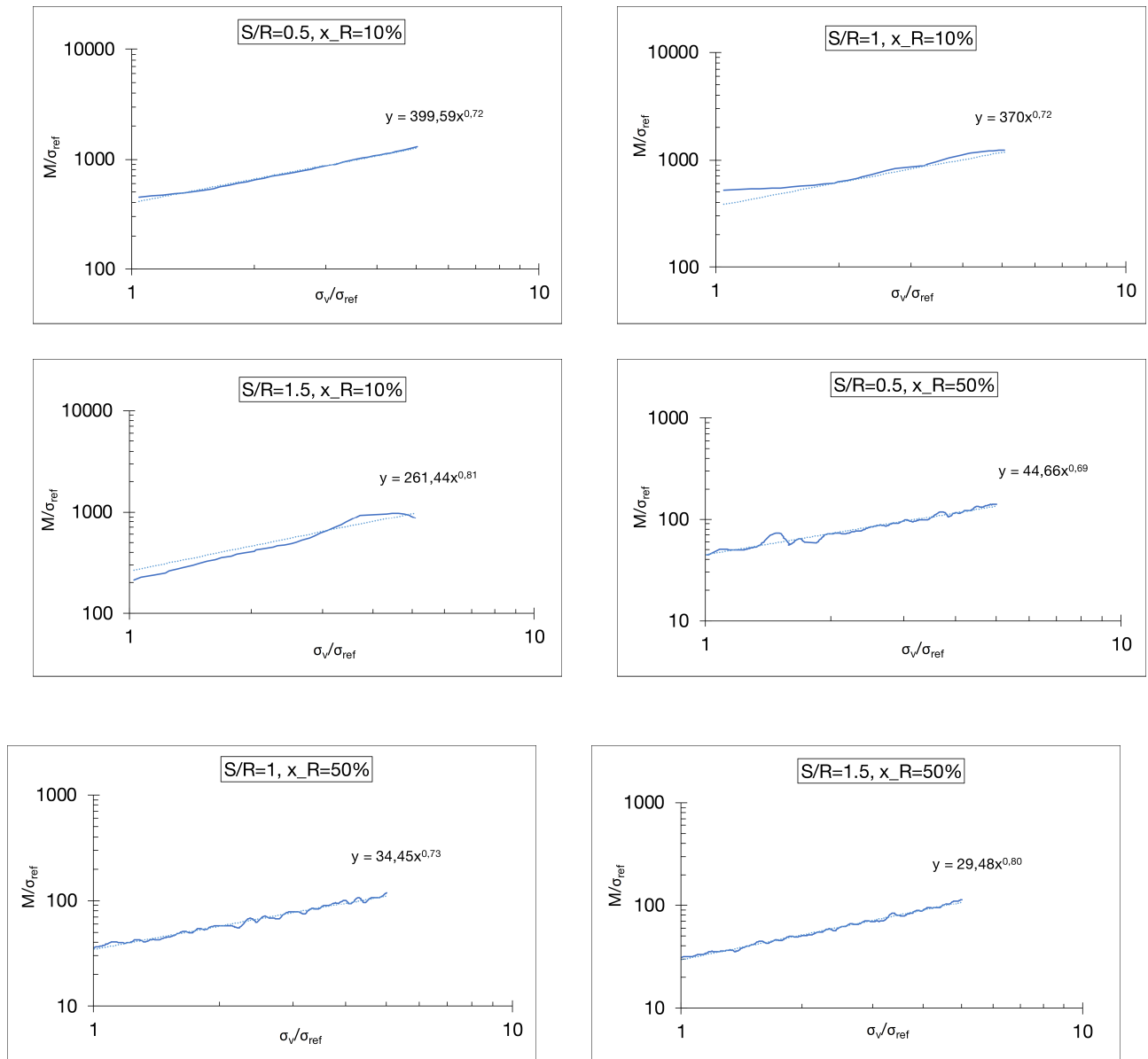
FIGURE 3.32. Individual fits for confined modulus vs vertical stress for all size ratios of 10% and 50% rubber fraction packings using plastic strain.

phase. From the plots for individual fits, it can be seen that the exponent, α value is the same for all the packings as the α value reported in Section 3.5.2. This indicates that the confined modulus varies in a similar way with the vertical stress in case of both, total strain as well as the plastic strain. However, the parameter m values can be observed to be slightly higher than in the previous case. This signifies the effect of packing rearrangements on the confined modulus magnitude for the different sand-rubber size ratios. Fig. 3.33 shows the variance of parameters m and α with the size ratio for 10% and 50% rubber fraction packings. The trend
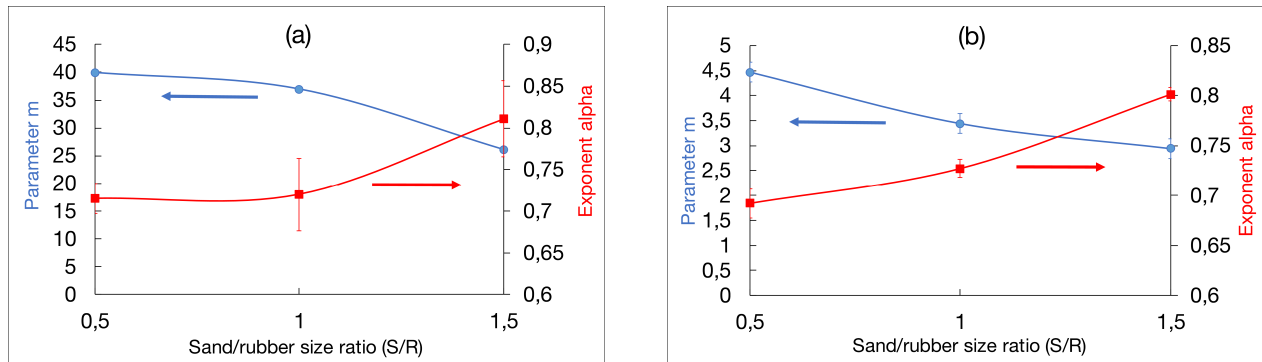
FIGURE 3.33. Fit parameters m and α for different size ratios of (a) 10% rubber fraction and (b) 50% rubber fraction packings using the packing elasticity strain.

of these parameters is similar as in the previous case mentioned in Section 3.5.2, however the magnitude is slightly higher for m, thus indicating a greater effect of plastic strain on the magnitude of confined modulus.

The effect of sand/rubber size ratio (S/R) on the mechanical response of sand-rubber mixtures was studied in this section. The section pointed out the significance of the size ratio variation by means of different mechanical characterization parameters. This section concludes the conventional study of the effect of different parameters on the behavior of sand-rubber mixtures. The next section will present the idea concerning the uniformity of mixing and its importance for sand-rubber mixtures with the help of certain oedometer test results performed on different mixture arrangements.

3.6 Effect of mixing quality on sand-rubber mixtures

A brief account of the importance of mixing quality for sand-rubber mixtures was given in Section 1.6. Moreover, the results presented in the preceding sections concerning the effect of initial void ratio, rubber fraction, particle size ratio, etc. point out clearly that, the better the distribution of rubber throughout the packing, the better can be seen the effect of rubber on the mechanical response of the mixtures. However, till date there has been no particular study concentrating on the effect of mixing quality. For these reasons, the study of mixing quality was interesting to be done. For this purpose, it was important to implement certain specific particle arrangements which could be observed in real-time conditions. The sections further detail

out the fabrication and mechanical testing performed on different granular arrangements of sand-rubber packings in order to quantify the effect of quality of mixing.

3.6.1 Fabrication of packing arrangements

The particular granular arrangements which were implemented have been briefly explained below. The target initial void ratio for these packings was set to 0.65 and the sample size of the sand and rubber grains used was 1.6-2mm.

1. **Random packing arrangement**

   In any mixing process, the most uniform or homogeneous mixture quality can be said to be random packing, wherein the particle or grain arrangement is random in nature and this randomness is equal throughout the packing. Random arrangement mixtures tend to be homogeneous. During the oedometer experiments, all the packings explained in the previous sections, *i.e.* dense and loose packings, different size ratio packings, different sample size packings were random packings. Of course, the degree of randomness controlled in the experiments was only by visual inspection. A typical random mixture used for the experiments has been shown in Fig. 3.1.

2. **Cluster packing arrangement**

   The most common form of heterogeneity observed during any mixing process is the localized clustering of particles. In case of sand-rubber mixtures, localized clusters of rubber grains can cause a difference in the mechanical response of these mixtures. However, in laboratory testing, it is difficult to realize a controlled clustering of particles

FIGURE 3.34. Snapshots of some steps in the preparation of cluster packing arrangements of sand-rubber mixtures (10% rubber fraction arrangement is shown here).

for all the rubber fractions of mixtures. Hence, in this case cluster packings were prepared and tested only for 10% and 25% rubber fractions, since with the increasing rubber fraction, the clustering was difficult to achieve. To obtain the clusters, first the entire target fabrication height was divided into 4 layers. The volume and consequently mass of sand and rubber required for each layer was calculated which depended on the volume of the oedometer cell. For each layer, the mass of rubber was divided in such a way as to

have 5 approximately equal localized clusters. These rubber clusters were then arranged in the oedometer cell. Then, the sand grains were poured in the oedometer cell for the specific layer. The layer was then tamped in order to ensure to have sand and rubber at a similar height. Similar moisture content (10% of sand mass) in total was used, however it was divided as per the mass of sand for each layer. With each layer, the position of the clusters was varied, in order to ensure a nearly homogeneous distribution of clusters. Fig. 3.34 shows some layers in the preparation of the cluster packings.

3. **Single grain and double grain layer packing arrangement**

Since the objective is to study the effect of mixing quality on sand-rubber mixtures, certain arrangements employing forced segregation between sand and rubber grains can be interesting to analyze. With this aim, a layers packing arrangement was prepared. In real-time conditions, it can be imagined to have a layers packing if alternately sand and rubber are poured over each other. In laboratory conditions, the layers packing was prepared for 10% and 50% rubber fractions, in order to have the two limits of packing behavior, *i.e.* sand-dominated and rubber dominated respectively. Moreover, two types of
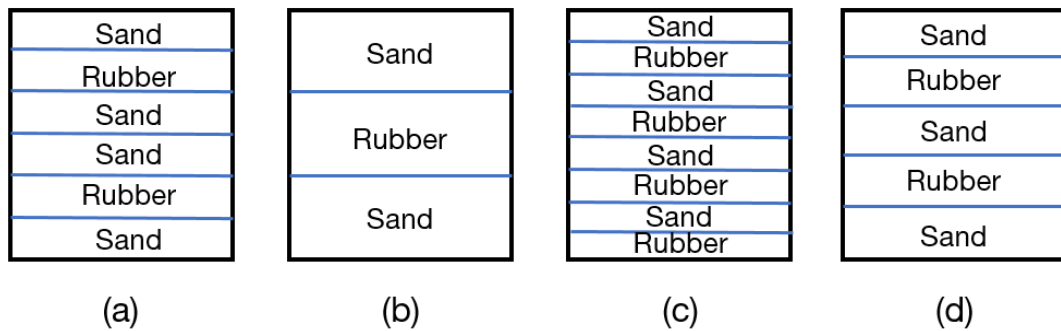
FIGURE 3.35. Schematic to obtain equally distributed layers arrangement in sand-rubber mixtures: (a) 10% single layers arrangement, (b) 10% double layers arrangement, (c) 50% single layers arrangement and (a) 50% double layers arrangement (schematic is only to show the number of layers in the arrangement and the width of each layer should not be related to the rubber fraction).

layer arrangements were prepared. A single layers arrangement in which the layer had the height equivalent to the diameter of one grain. A double layers packing ensured a double grain height of these layers prepared. In order to have an equal distribution of layers of rubber and sand throughout the packing, the layers were prepared and arranged as shown in Fig. 3.35. Similar to the clusters packing arrangements, the total mass of sand and rubber was equally divided in order to have the same mass of sand and rubber respectively in each layer. The volume of the solids (sand and rubber) for each layer was calculated by using the volume of the oedometer cell, and in turn the mass of the material for each layer was calculated. So each layer of sand and rubber was deposited in the oedometer cell and with every layer deposition, it was lightly tamped in order to

achieve the final target void ratio of the initial packings. Similar to clusters packings, the moisture content was used only in case of sand layer deposition. Fig. 3.36 shows the actual photos of some steps in achieving the layers packings experimentally.

FIGURE 3.36. Snapshots for some steps in the experimental preparation of layers packing in the oedometer cell.

A thought experiment was done in order to have a hypothetical granular arrangement. In any granular packing subjected to 1-D compression, the force chains will be in a nearly vertical direction. In a granular packing such as sand-rubber mixture, the main force carrying network involves a maximum number of stiff particles, and thus softer grains are less involved in the main force carrying network [Lee et al., 2007]. Hence, an analogy similar to parallel springs network can be imagined, wherein the spring denotes the force chains, and hence the sand and rubber grain force chains will be nearly parallel to each other. Such a kind of packing, will hence force even some of the strong forces to pass through the rubber chains. Such a packing was prepared experimentally, called as vertical stripes packing.

4. **Vertical stripes packing arrangement**

   In laboratory, the vertical stripes packing was prepared only for 10% rubber fraction. The process started with depositing the measured mass of only the sand in the oedometer cell and lightly tamping it. Then, a plastic straw was gently pushed into this sand packing at several locations til the bottom-most depth of the packing. The measured mass of rubber was then deposited into this column hole created by the straw and the packing was again slightly tamped once the hole was filled with rubber particles. The mass of rubber for each column hole was calculated by using the height of the packing, volume of the oedometer cell, rubber fraction and the total number of columns which could be fit inside the circular area of the oedometer cell. The preparation of this packing arrangement has been shown in Fig. 3.37. Thus, at laboratory scale, the only possible way to realize this packing was to prepare it as described before, in the form of vertical columns of rubber grains.

Thus, different granular arrangements were prepared in order to study their mechanical response under 1-D compression in an oedometer cell. The test results for the random packing

FIGURE 3.37. Snapshots for the experimental preparation of vertical stripes packing in the oedometer cell.

arrangements have already been presented during the discussion on dense packings. However, these results will be again shown in the further sections for the purpose of comparison. the mechanical response of these packing arrangements has been quantified in terms of the similar important parameters, *viz.* macroscopic mechanical response (void ratio vs vertical stress), swelling index, creep behavior, etc. These have been discussed in the subsequent sections.

3.6.2 Compressibility

As mentioned before, it was not feasible and straightforward to prepare the different mixture arrangements for all the rubber fractions. Hence, the packing arrangements were prepared only for selective rubber fractions. In case of 10% rubber fraction, all the packing arrangements were prepared and tested. For 25% rubber fraction, only the clusters and random packing arrangements were prepared, whereas for 50% rubber fraction, random, single grain layers and double grain layers packings were prepared and tested. Again, as mentioned before the target fabrication void ratio for all these packings was 0.65. However, due to the initial stress of the top cap (1.6 kPa) and the compressible nature of rubber, the actual initial void ratios were observed to be different. The corrected values of void ratios have been mentioned in Table 3.6. Fig. 3.38 shows the macroscopic mechanical response of the different packings in terms of void ratio vs vertical stress. From Fig. 3.38(a), the mechanical response for 10% rubber fraction mixing arrangements can be compared. For 10% rubber fraction, all the mixture arrangements have been tested. It is clear from the plots that mixing quality or granular arrangement does have a significant effect on the mechanical response of the sand-rubber mixtures. Two distinctive packing behavior families can be observed, *viz.* family 1 of random, clusters and vertical stripes packing and family 2 of single and double layers packing arrangements. A

Sand-rubber packing arrangement	x_R (%)	Void Ratio
Random packing	10	0.646
Clusters packing	10	0.646
Vertical Stripes packing	10	0.645
Single layers packing	10	0.646
Double layers packing	10	0.645
Random packing	25	0.643
Clusters packing	25	0.644
Random packing	50	0.64
Single layers packing	50	0.641
Double layers packing	50	0.642

Table 3.6: Actual fabrication void ratios for the different packing arrangements for 10%, 25% and 50% rubber fraction under an initial stress of 1.6kPa.

logical explanation for this type of behavior can be given in terms of the number of sand-sand, sand-rubber, rubber-rubber contacts overall in the packing as well as their varying number in the force carrying chains.

In the family 1 at 10% of rubber fraction, the stiffest packing as expected was the vertical stripes packing. The reason for this being a higher number of sand-only contacts in the major force carrying networks. Even though, the rubber chains are in parallel to the sand chains, these rubber chains act as stabilizers and prevent the buckling of the sand force chains (in accordance with the findings reported by Lee et al. [2007]).

However, at high vertical stress, the difference between the vertical stripes and the cluster and random packings becomes small, in the limit of the repeatability of the test. The response of clusters and random packing arrangements is mostly identical for 10% rubber fraction. With the increasing rubber fraction to 25%, this difference increases as can be seen from Fig. 3.38(b), where the random packing is stiffer. Nevertheless, the difference in void ratio at the maximum vertical stress is about 0.035 and the response of the cluster packing is very close to the response of the packing with smaller particles, at the same rubber fraction. It is suggested here that the results of the cluster and random packings are not as different as expected. A possible explanation is that the fabrication of the random packing does not succeed in avoiding the clustering of the rubber particles. This can be easily seen when the fabric of rubber/sand mixtures is analyzed by tomography like it was done by [Rouhanifar, 2017]. Also, the vertical strips of rubber evolves during the loading. At the end of their loading, the internal structure could be imagined to be not so different from the random or cluster packings.

The most deformable packing arrangements for 10% rubber fraction are single layers and double layers packings. In case of these arrangements, it is evident that a higher number of rubber particles will be included in the major force chain networks as compared to the packings of family 1. Moreover, a continuous layer of rubber grains in between sand grains equally distributed throughout the packing height causes a rubber-dominated type of mechanical response and hence a higher deformability of the packings. In terms of single and double
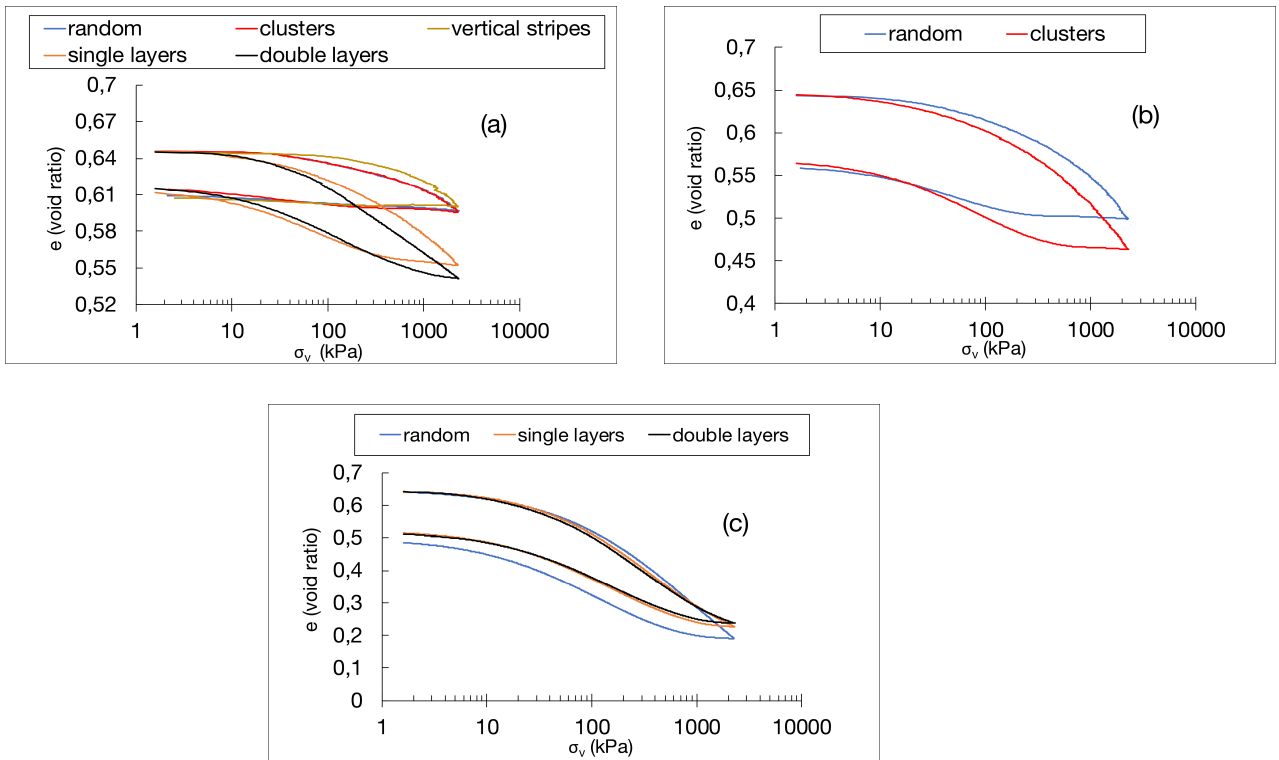
FIGURE 3.38. Void ratio vs log (vertical stress) plot for different packing arrangements of (a) 10% rubber fraction, (b) 25% rubber fraction and (c) 50% rubber fraction.

layers packings, the double layers packings show a higher deformability than the single layers packings. However, with the increasing rubber fraction, the effect of mixing arrangements is reduced and thus for 50% rubber fraction packing arrangements, the response trend of all the packings can be found to converge and thus close to each other. Nevertheless, at high vertical stress level, the behavior of the single and double layers packings change and become closer to a rubber type behavior as described by [Fonseca et al., 2019], *i.e.* concavity in the void ratio – log of vertical stress plane.

3.6.3 Swelling Index

The swelling index was calculated for sand-rubber mixtures having different packing arrangements of different rubber fractions by using the similar method adopted during the analysis of other packings discussed before. Fig. 3.39 shows the swelling index values for the different arrangements. Evidently, the swelling index values show an increasing trend with the increasing rubber fraction, irrespective of the packing arrangement as discussed in the previous section (refer Section 3.3.4). In case of 10% rubber fraction, the swelling index values are higher for the single and double layers packing arrangements and the least for the stripes packing arrangement. However, all values are fairly close, as it is also the case for the cluster and random packings at 25% rubber fraction. Indeed, it was previously discussed that at the end of the loading, all packings have similar internal structures. As a consequence, the

97

unloading behavior should be rather similar, at the same rubber fraction. For 50% rubber
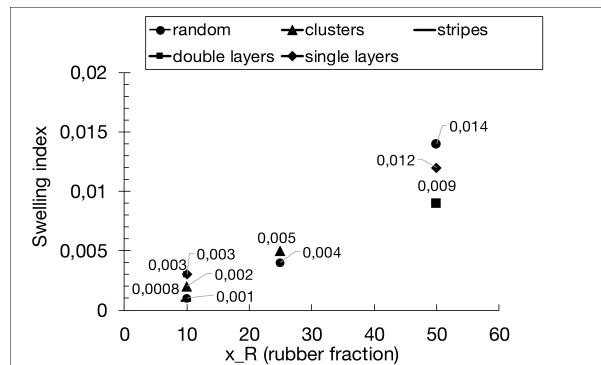
FIGURE 3.39. Swelling index for all the packing arrangements of 10%, 25% and 50% rubber fraction mixtures.

fraction packings, the single and double layers packings present similar swelling index, which is significantly higher than for the random packing. It has been discussed previously that the behavior of single and double layers packings at the end of the loading becomes closer to a rubber-dominated mixture. It is normal then, that the unloading behavior is different from the sand-type behavior, as it is the case for the random packing at 50% rubber fraction.

3.6.4 Elastic and plastic behavior

According to the hypothesis explained before, it is interesting to verify the behavior of the ratio of elastic to total deformation for the different packing arrangements of sand-rubber mixtures. Fig. 3.40 shows the variation of this ratio for the different packing arrangements with the increasing rubber fraction, i.e. 10%, 25% and 50%. A linearly increasing trend was observed
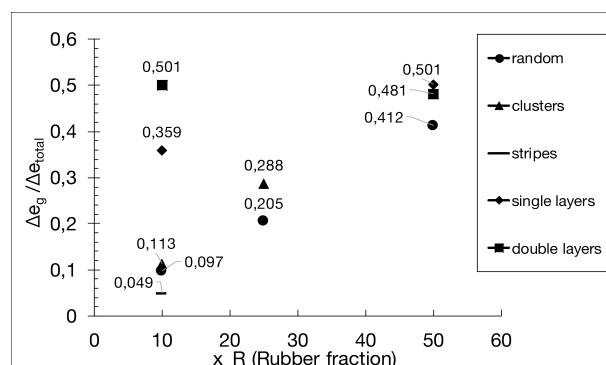
FIGURE 3.40. Change in the ratio of grain elastic deformation (Δe_g) to the total deformation (Δe_{total}) for different packing arrangements of 10%, 25% and 50% rubber fraction mixtures.

with the increasing rubber fraction. Further, for a given rubber fraction, higher the proportion of rubber-rubber contacts, higher will be the contribution due to the elastic properties of the grains. Hence, in Fig. 3.40, for 10% rubber fraction, higher values are observed for the layers

packing arrangements as compared to the random, clusters and vertical stripes arrangements. These results further reiterate the observation of 2 distinct families of packing behavior which converge with the increasing rubber fraction. Consequently, for 50% rubber fraction packings, the values can be observed to be quite close to each other, indicating a less effect of mixing quality on the mechanical response of the packings. In case of 25% rubber fraction, the clusters and random packings seem to have values quite close to each other, however, the clusters packings having more localized rubber-rubber contacts, and thus tend to have the effect of the grain elasticity slightly higher.

Thus, the hypothesis reported in Section 3.3.3 seems to be logical Since it was observed to be valid for all the varying parameters for the sand-rubber mixtures, viz. rubber fraction, packing volume fraction (initial void ratio), sand/rubber size ratio and mixing arrangements. Hence, similar to the previous parameters, the hypothesis will be extended to report the time effect behavior of sand-rubber mixtures to quantify the effect of mixing on the time-dependent mechanical response.

3.6.5 Time effect

The time effect, *i.e.* the phenomena signifying the deformation capacity of the material has been explained in the previous sections. Hence, to further strengthen the observation concerning the effect of mixing quality on the mechanical response of sand-rubber mixtures, it is interesting to quantify the time effect behavior of these packings. Hence, a similar procedure was adopted as for the previous packings and the time effect was quantified for the mixing arrangements. The same has been presented in Fig. 3.41.

Since the significance of time effect increases with the increasing rubber fractions, hence the results have been presented in a decreasing rubber fraction sense. Further, due to the less sensitivity of the testing equipment used and less significance of time effect for lower rubber fractions (already discussed in Section 3.3.4), the results for 10% rubber fraction packing arrangements have not been presented. Even for the packings of different mixing arrangements, the prominence of 'S' shape of the unloading phase of the curve can be seen to increase with the increasing rubber fraction. A noteworthy point is the difference in this 'S' form for different packing arrangements.

As can be observed in Fig. 3.41, for 50% rubber fraction packings, the 'S' form for both the layers packing arrangements is quite different from that of the random packing arrangement. Consequently, a significant difference can be observed in the time effect characteristics of these packing arrangements. Hence, the time effect is lower in case of layers packings whereas higher for random packing arrangements. In case of 25% rubber fraction, the time effect observed seems to be higher in the case of clusters packing than in the case of random packing arrangement (see Fig. 3.41) but the evolutions are mostly similar.

Thus, an initial observation indicates that the better is the distribution of the proportion of rubber-rubber contacts throughout the packings, higher is the significance of the time effect,
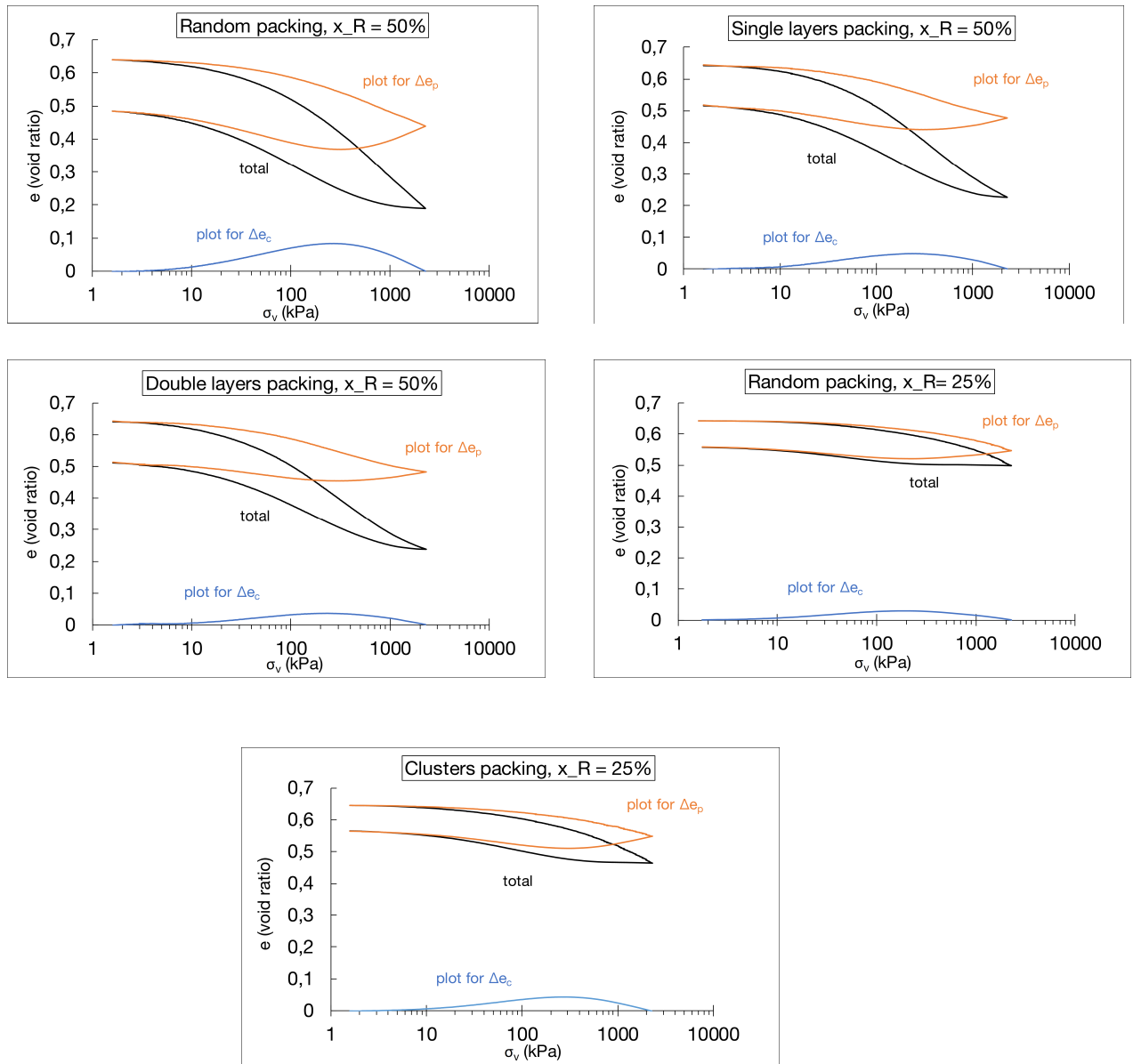
FIGURE 3.41. Plots for different packing arrangements of 25% and 50% rubber fraction mixtures characterizing the 'S' shape of unloading and showing the creep behavior.
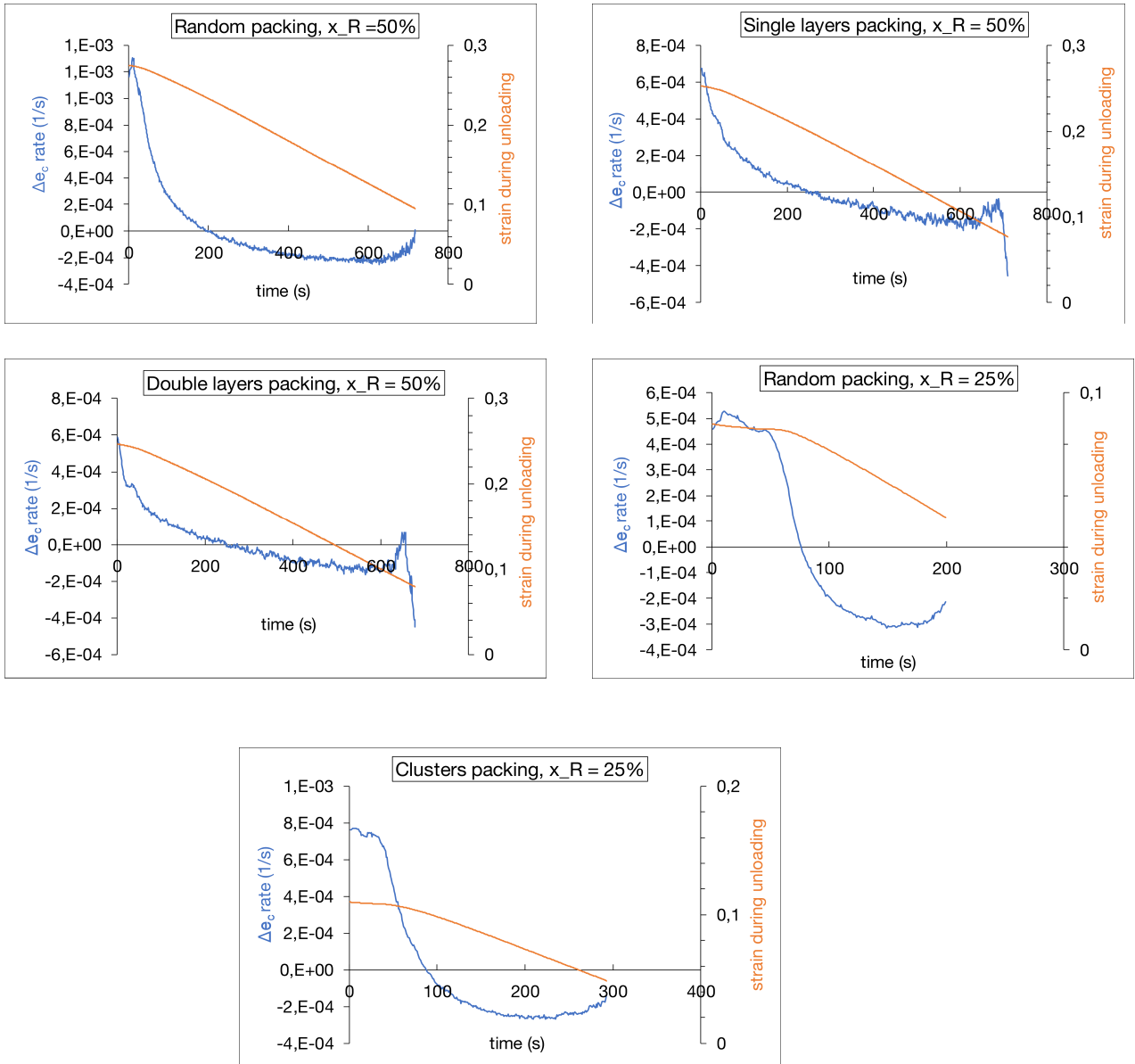
FIGURE 3.42. Plots for the time effect void ratio rate and the strain rate for different packing arrangements of 25% and 50% rubber fraction mixtures.

thus suggesting the effect of mixing quality on the time effect behavior. This can be further understood well by analyzing the time effect rate for all these packing arrangements, which has been shown in Fig. 3.42. Again, to better visualize the effect of rubber fraction, the results have been presented in a decreasing order of rubber fraction. Along with the time effect rate, the strain evolution during unloading has also been shown since it signifies the control of the test equipment which clearly affects the time effect behavior observed. The trend in the plots for the time effect rate clearly indicates the macroscopic response of the packing arrangements observed (Fig. 3.38).

Thus, it is evident that time effect is quite significant in case of sand-rubber mixtures for all the varying parameters. Further, time effect seems to be more sensitive to the overall distribution of rubber-rubber contacts throughout the packing.

3.7 Partial conclusion

Different sand-rubber mixtures were tested in the laboratory under 1-D oedometer compression with an aim to study the mechanical response of these mixtures under compression. For this purpose, different parameters were varied, *viz.* rubber fraction, initial packing volume fraction (initial void ratio), particle size and sand/rubber size ratio. Further, a campaign of experiments was also conducted on different packing arrangements prepared in the laboratory with an aim to analyze the effect of mixing quality on these mixtures.

The effect of these parameters was quantified with the help of conventional parameters such as macroscopic void ratio vs stress, confined modulus and swelling index. Further, a hypothesis was used to point out the effect of these parameters on the mechanical response of the packings in terms of plasticity, grain elasticity, time effect behavior as well as the rate of change of the latter.

With the increasing rubber fraction, the deformability of the packings was observed to increase as well as the swelling characteristics. The time effect response was observed to be significant in sand-rubber mixtures and its prominence increased with the increasing rubber fraction. Time effect is an important parameter to consider before using such sand-rubber mixtures for real-time applications, since it signifies the deformation rate of the mixtures. The results for different mixing arrangements clearly pointed out the importance of mixing quality, especially for lower rubber fraction packings. In general, it was observed that the better is the distribution of the proportion of rubber-rubber contacts throughout the packings, the better is the involvement of rubber particles played in the mixtures, specifically in terms of stabilizing the major force carrying networks and an overall packing deformability characteristics.

It is clear that the mechanical response of the sand-rubber packings significantly depends on certain microscopic properties such as sand-sand, sand-rubber and rubber-rubber contact distributions, distribution of force carrying networks throughout the packing, etc. Hence, it is important to perform a numerical analysis on the sand-rubber mixtures using the Discrete

Element Method (DEM) in order to quantify the microscopic behavior and relate it to the macroscopic mechanical response observed.

The next chapter will discuss the numerical analysis performed on sand-rubber mixtures using DEM to study their mechanical response under 1-D oedometer compression. This chapter, in turn will thus help to better quantify the macroscopic behavior of the sand-rubber packings observed in the laboratory experiments.

DISCRETE ELEMENT METHOD ANALYSIS UNDER OEDOMETER COMPRESSION

Summary

The previous chapter dealt with the oedometer experimental analysis performed on sand-rubber mixtures. In order to better understand the behavior of sand-rubber mixtures and to quantify their micro-mechanical response, a numerical analysis using Discrete Element Method (DEM) was done. This chapter explains this analysis in detail. The chapter begins with the description of the model and the methodology used for the DEM numerical simulations on sand-rubber mixtures. Further, results have been presented which detail out the micro-mechanical properties of the sand-rubber mixtures, *viz.* contact distribution, contact forces, strong and weak contact forces. Since the previous Chapter introduced the investigation of importance of mixing quality in sand-rubber mixtures, it has been explored in complete detail in this Chapter.

Contents

4.1   Introduction

The principle of Discrete Element Method (DEM) has been elaborated in Chapter 1. DEM is useful for analyzing the behavior of granular materials since it helps to study the statistics at the micro scale, *i.e.* at the contacts of the particles. In the previous chapter, the mechanical response of sand-rubber mixtures was studied using conventional oedometer tests. The numerical simulations using DEM help to further analyze the mechanical response of these mixtures by linking the micro-scale properties, *viz.* contacts forces, contact orientations, contact force distributions, etc. with their macro-mechanical response. As observed in the previous chapter, this is quite important to study since the mechanical response of the sand-rubber mixtures has been observed to evolve significantly with the particle size as well as particle arrangements. Molecular Dynamics soft sphere model, as first developed by Cundall and Strack [1979] was used in order to calculate the contact particle forces, which further allowed to solve the Newton's equations of motion and thus calculate the accelerations, velocities and positions of the particles for consecutive time-steps. The soft sphere approach allowed to account for the particle elasticity to a certain extent and thus helped in studying the effect of inclusion of softer particles, *i.e.* rubber. The next section will detail out the methodology of the DEM simulations carried out to study the mechanical response of sand-rubber mixtures.

4.2   Methodology

The DEM calculation cycle consisted of two important steps, *viz.* preparation of initial packings and oedometric compression to study the mechanical response of the packings under compression. The initial packing consisted of 9000 sand grains. The important parameters used for initializing the formation of the packing are stated in the table (see Table 4.1). For the sake of

Parameter	Value
Number of grains	9000
Young's modulus of elasticity (sand)	0.7 GPa
Young's modulus of elasticity (rubber)	0.001 GPa
Mean radius of grains	0.25 mm
Coefficient of friction between the grains (μ)	0 (dense packing) 0.5 (loose packing)
Coefficient of friction between the grains and wall (μ_W)	0 (dense packing) 0.5 (loose packing)
Cylinder radius (Rcyl)	4.95 mm
Cylinder height	12.78 mm (dense packing) 13.31 mm (loose packing)
Velocity of imposition (v_{imp})	$1\text{mm}s^{-1}$

Table 4.1: Different important parameters to define the initial packing.

simplicity, the grains were considered to have the same size distribution and spherically shaped,

thus neglecting the shape and size effects. Subsequently, the positions and velocities of each grain were calculated at every time step and updated to solve the Newton's equations of motion. The Velocity Verlet algorithm was implemented for the same. The Discrete Element Method considers the grains to be non-deformable. However, the constituent grains being studied were sand and rubber. Sand grains being stiffer than the rubber grains, they tend to deform less than the rubber grains. Hence, in order to account for the inclusion of rubber grains, the soft sphere model was used, *i.e.* in other words, a small overlap between the contacting sand and rubber grains was considered which in turn facilitated the calculation of the contact forces as shown in Fig. 4.1. An appropriate model has to be used to calculate the normal and tangential components of the contact force. Here, the Hertz model was used to calculate the normal forces while the tangential forces were calculated using a regularized Coulomb friction model. Hence,
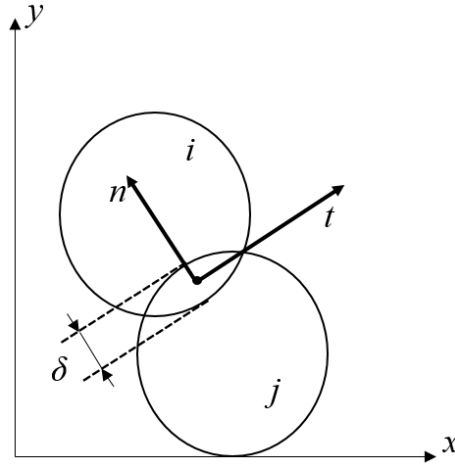
Figure 4.1: A schematic for the interaction between two contacting grains, i and j wherein δ is the overlap between the two grains, n and t are the normal and tangential vectors of the contact forces respectively.

$$F_n = K_n \delta^{3/2}, \tag{4.1}$$

where, F_n is the normal contact force, K_n is the stiffness and δ is an exaggerated overlap between the contacting grains. The normal stiffness is given by:

$$K_n = \frac{4}{3} E_{eff} \sqrt{R_{eff}}, \tag{4.2}$$

where, E_{eff} is the effective Young's modulus of elasticity for the contacting i and j particle given by, $E_{eff} = \frac{E_i E_j}{E_i + E_j}$ and similarly R_{eff} is the effective radius of the contacting grains i and j given by, $R_{eff} = \frac{R_i R_j}{R_i + R_j}$. If the values of the Young's modulus of elasticity for sand and rubber are observed carefully in Table 4.1, then it can be seen that they are very small as compared to the real values of Young's modulus for sand and rubber. The primary reason for this is to reduce the computational time. Hence, it is important to note here that the numerical analysis results should not directly be compared quantitatively with the experimental results. To account for

dissipation, a viscous-like force is chosen to ensure a velocity-independent normal coefficient of restitution, e_n [Antypov and Elliott, 2011]:

$$F_{diss,n} = \frac{-\sqrt{5}\ln e_n}{\ln^2 e_n + \pi^2}\sqrt{m_{eff}K_n}\,\delta^{1/4}\dot{\delta}. \tag{4.3}$$

The tangential force is given by,

$$F_t = K_t\Delta, \tag{4.4}$$

where, K_t is the tangential stiffness and Δ is the incremental tangential displacement. Since it is based on the Coulomb's law, the criterion for sliding between the grains is $F_t > \mu_t F_n$. Consequently the tangential displacement Δ is truncated to satisfy the latter inequality.

4.2.1 Assembly of initial packings

After defining all the necessary parameters mentioned before, the process started with the deposition of the grains within the cylinder of predefined dimensions (see Table 4.1). Due to the presence of the gravity, the grains started settling at the bottom of the cylinder. Consequently, the cylinder started filling up with the new grains occupying the positions above the previously stabilized grains in the cylinder. The process continued till the packing had achieved a state of equilibrium. To confirm this, the kinetic energy of the system and the mean position of the packing height were verified over a sufficiently large time period. It was verified from the values of the ratio of kinetic to potential energy over the period of time. Initially these values were observed to be in the range of 10^{-3}; slowly over time, they were in the range of 10^{-1}, the increase being explained by the acceleration of grains due to gravity. Finally, the values approached more towards zero in the range of 10^{-10}, thus indicating the stabilization of the packing. After obtaining the initial packings by this method, the sand rubber mixtures were prepared by defining the properties of some sand grains with that of the rubber grains. The number of grains chosen to change the property definition from sand to rubber depended on the rubber volume fraction desired. Similar rubber fractions were used as in the case of experiments (10%-50%). The sample initial sand-rubber packings for different rubber volume fractions have been shown in Fig. 4.2.

Further, in order to analyze the effect of change in the initial void ratio of the packings, two initial packings with different initial void ratios were prepared. This was achieved by defining different inter-granular and grain-wall friction coefficients for both the packings, as mentioned in Table 4.1. Fig. 4.3 gives a better idea of the difference in the initial void ratios. The void ratio was calculated over the entire height of the initial packing by dividing the height into layers of small thickness in order to have a precise value. Henceforth, the initial packing with an average void ratio of 0.632 will be referred to as dense packing and the other with the average void ratio of 0.69 will be referred to as loose packing. The average void ratio mentioned is the value measured for the bulk of the packing (indicated as black vertical lines in Fig. 4.3). This was done in order to minimize the effect of the sidewalls which may cause a difference in the
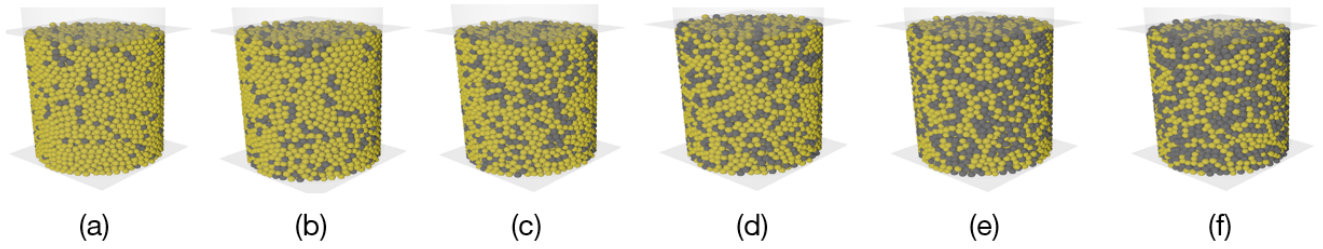
Figure 4.2: Snapshots of the initial packings of sand-rubber mixtures for (a) 10% rubber fraction, (b) 20% rubber fraction, (c) 25% rubber fraction, (d) 30% rubber fraction, (e) 40% rubber fraction and (f) 50% rubber fraction.
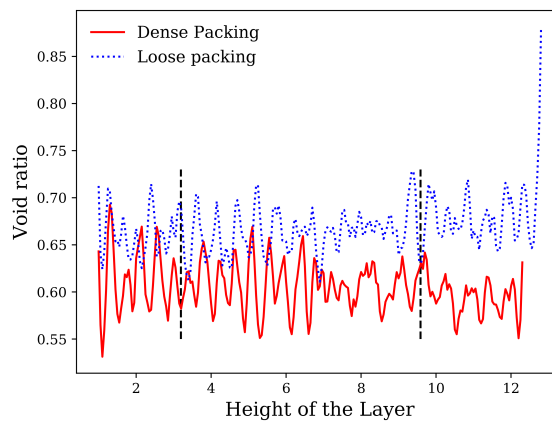
Figure 4.3: The void ratio for dense and loose initial packing over the entire height of the packing.

local voids between the grains. The initial void ratio of the packings was measured using the formula,

$$e = \frac{1-\phi}{\phi}, \tag{4.5}$$

where, e is the void ratio and ϕ is the packing volume fraction.

Consequently, the corresponding packing volume fractions were 0.61 for dense initial packing and 0.59 for loose initial packing. It is quite difficult to obtain a dense packing close to Random Close Packing (RCP), *i.e.* the one having packing volume fraction of 0.64, due to a strong effect of the confinement. Hence, the dense packing obtained here has the packing volume fraction of 0.61. Even if this difference between the initial void ratios/ packing volume fractions is weak, its effect on the mechanical response of the mixtures is quite large.

4.2.2 Assembly of sand-rubber mixture arrangements

In the oedometric experiments performed on the sand-rubber mixtures (discussed in Chapter 3), an effort has been made to prepare typical mixing arrangements of sand and rubber in order to verify the effect of the mixing quality on the mechanical response of these mixtures.

However, it was not possible to fabricate all the packing arrangements for all the values of rubber fractions. On the other hand, since numerically it is possible to simulate such mixing arrangement, the initial packings were prepared for all the rubber fractions and for both dense as well as loose mixtures. This section entails the process of achieving the different mixing arrangements.

After the preparation of the initial packings by the deposition of sand grains under gravity, different sand rubber mixtures were prepared by defining the properties of some sand grains with that of the rubber grains. The objective of preparing these initial packings with different mixture arrangements was to analyze the effect of quality of mixing on the sand-rubber mixtures. Consequently, different packing arrangements were made as named in the case of experiments, *viz.* : cluster packing, random packing, single grain size layers packing, double grain size layers packing and vertical stripes packing. Some of these mixture arrangements can be considered to be cases of perfect (random packing) and imperfect (clusters and layers packing) mixing.
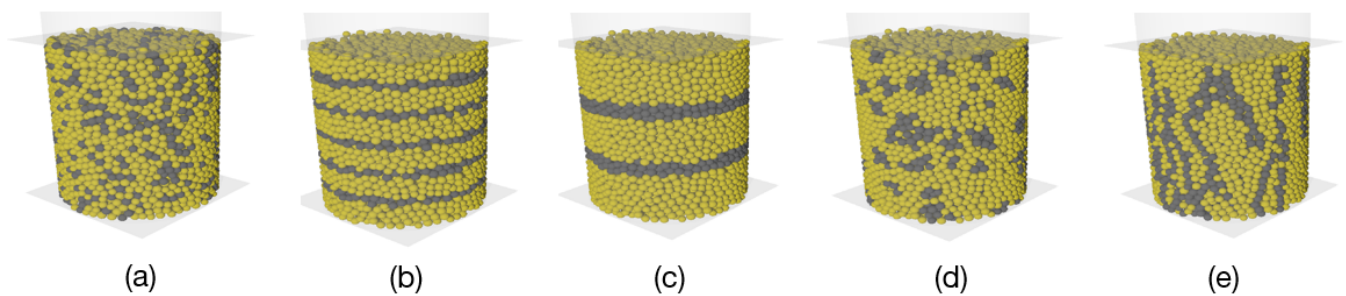
Figure 4.4: Snapshots of the different sand-rubber mixture arrangements (same rubber fraction of 25%): (a) Random packing, (b) Single layers packing, (c) Double layers packing, (d) Clusters packing and (e) Vertical stripes packing.

The same arrangements have been shown in Fig.4.4 for visual reference.

- **Random Packing**

  The random packing prepared can be said to be the most practically possible case as can be seen from Fig.4.4(a). The sand grains in the initial packing were randomly replaced with the rubber grains. The procedure began with a random selection of grains by specifying a probability for the selection to be done. This probability is a function of the rubber volume fraction intended. It was also checked that the vertical distribution of rubber grains was uniform.

- **Cluster Packing**

  In the case of clusters packing, it was not defined to distribute the rubber grains randomly but to obtain a clustered organization. Thus, it was evident to check for the contact between the two adjoining grains and select the contacting grains to form clusters. Thus,

the probability based selection of the grains was done when selecting a single grain to search for the neighboring contacting grains. The selection of these grains was done based upon the intended rubber fraction. Further when defining the total number of the neighbors for cluster formation, a cluster of approximately 30 grains was formed. The type of these cluster grains was then changed from sand to rubber. Here as well, it was verified that the vertical distribution of rubber grains was uniform. The cluster packing can also be considered to be a case of an imperfect mixture.

- **Single-grain size layer packing**

  Another practical case of an imperfect sand-rubber mixture is the layers packing. The layers packing can be obtained by successive pouring of sand and rubber. Consequently, from the point of view of studying the effect of mixing quality, it was interesting to study the two cases of layers packing of which single layers packing has been discussed here and double layers packing will be discussed further. The preparation of this packing began by specifying the size of the layer. So, the entire packing could be imagined to be made of horizontal layers of grains over the packing height (see Fig.4.4(b)). One important consideration here, was to achieve symmetrical layers over the entire height of the packing to truly visualize the effect of such kind of packing. This was achieved by considering the number of rubber layers intended as a function of the required rubber fraction. These selected layers were then converted into rubber layers by redefining the type of grains.

- **Double-grain size layer packing**

  The process of assembly for this packing was similar to that of the single-grain size layers. The only difference was the specification of layer height. Here, the layer height was defined as twice the size of the grain. So, for the same rubber volume fraction, the number of layers for the single-grain size and double-grain size layers is definitely different. But, like in the case of single grain size layers, the layers are spread uniformly over the height of the packing.

  Another mixing arrangement, fabricated only for 10% rubber fraction in the case of experiments, was prepared for all the rubber fractions to simulate it numerically. This is the vertical stripes packing.

- **Vertical stripes packing**

  The vertical stripes packing consists of each type of grain arranged in the form of vertical stripes or vertical chains. It is obvious, due to the disordered character of the granular packings used here, strict vertical stripes were impossible to obtain. To obtain the vertical stripes (see Fig. 4.4(e)), initially all the grains of the bottom-most horizontal layer were selected. Depending on the intended rubber fraction, a fraction of these selected grains were changed from sand to rubber. Further, it was imposed to find and select the grains which are nearly in a vertical direction with respect to the bottom-most selected grain.

The grains which met this criteria were selected and replaced with rubber in order to obtain a vertical stripe. Thus, vertical chains of sand and rubber grains can be observed in the packing.

In this way, different initial packing arrangements have been obtained by varying the particle arrangements as well as the rubber fraction (10%, 20%, 25%, 30 %, 40%, 50% by volume). It is important to take into account that since most of the grain replacement was a probability based procedure, the rubber fraction does not exactly correspond to the intended value *esp.* for the layers packing (a relative fluctuation of 20% from the intended value was noted in the lower rubber fractions in case of layers packings).

4.2.3 Oedometer Compression of sand-rubber mixtures

The sand-rubber packings prepared were simulated using the Discrete Element Method (DEM) with a velocity imposed oedometric compression model (see Fig. 4.5). Since the replacement of
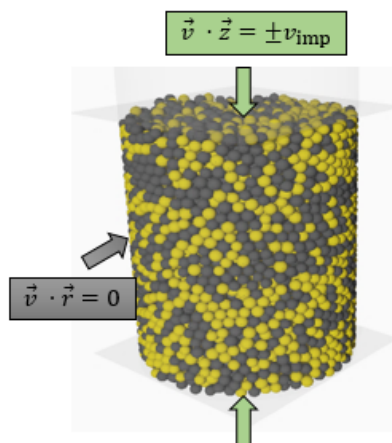
Figure 4.5: Schematic of the setup for the oedometer compression of sand-rubber mixtures using DEM simulations, where v_{imp} is the imposed velocity.

sand grains by rubber grains changed the equilibrium of the packing due to the difference in the sand and rubber properties, the packing was allowed to relax and stabilize before the actual compression was imposed. Further, the relaxation time was fixed by verifying whether the mean position of the packing height was stable for a sufficient time period. The process began by defining the initial positions and velocities of the grains. The grains in the top-most and the bottom-most layers of the packing were imposed with velocity. Since the aim is to simulate the oedometer compression, there was no lateral velocity imposition on the packings. However, the sidewall friction is taken into account during the calculation of the forces similar to the real-time conditions. Moreover, a limiting condition for average grain deformation was imposed in order to ensure that the calculations are still in the valid DEM regime and also include a small measure of the elasticity of rubber. The simulations were stopped once the average

grain overlap (see δ in Fig. 4.1) (for rubber-rubber type of contact) due to the compression exceeded the order of 10^{-2}. Above this value, it is assumed that the grain overlap is not negligible anymore and consequently DEM stands invalid. This condition was imposed for the simulations consisting of only loading phase.

In order to simulate the unloading phase, a negative velocity was imposed on the packings. This sign change of the velocity helped to mimic the experimental oedometric condition wherein the direction of the displacement was varied. It was necessary to unload the packings at the same stress rather than at the same strain in order to compare them. Rubber being the softer particle, the stress at the highest rubber fraction, *i.e.* 50% was noted for all the packings and the other rubber fraction packings were unloaded at the same stress value. This process was done for all the mixing arrangements of sand-rubber packings.

4.3 Loading-unloading behavior

As mentioned before for the experiments as well, the lateral strain is null under loading for the oedometric conditions. In the numerical simulations, during the calculation process, the vertical strain, axial force, lateral stress, etc. are some of the quantities recorded for the subsequent time-steps. As a result, due to the knowledge of the vertical strain and the initial void ratio, it is possible to calculate the current void ratio at every time-step, given by Eq. 3.6, *i.e.*,

$$e = e_0 - \Delta\epsilon_v(1 + e_0), \tag{4.6}$$

where, e is the current void ratio, $\Delta epsilon_v$ is the incremental vertical strain (positive cf. soil mechanics convention) and e_0 is the initial void ratio. Consequently, with the knowledge of the axial force, it is possible to calculate the vertical stress value, σ_v, given by,

$$\sigma_v = \frac{F}{A}, \tag{4.7}$$

where, F is the force and A is the surface area on which the force is imposed, in this case a circle due to a cylindrical packing. The surface area, A is given by,

$$A = \pi R_{cyl}^2. \tag{4.8}$$

where, R_{cyl} is the radius of the cylinder given in Table 4.1. Thus, the void ratio and vertical stress can be plotted as per convention on a logarithmic scale. Fig. 4.6 which shows the plot for the void ratio vs the vertical stress for sand-only packings has been presented in order to have an idea about the difference in the initial void ratios of the sand-rubber mixtures. Moreover, as mentioned before, for the simulations to be valid in the DEM regime, the calculations were stopped when the average rubber-rubber grain overlap reached the value of 10^{-2} times the grain size. However, in the case of sand-only packings, it was possible to simulate higher order of strains due to a higher value of Young's modulus of elasticity. Consequently, the loading-unloading response has been shown in Fig. 4.6.
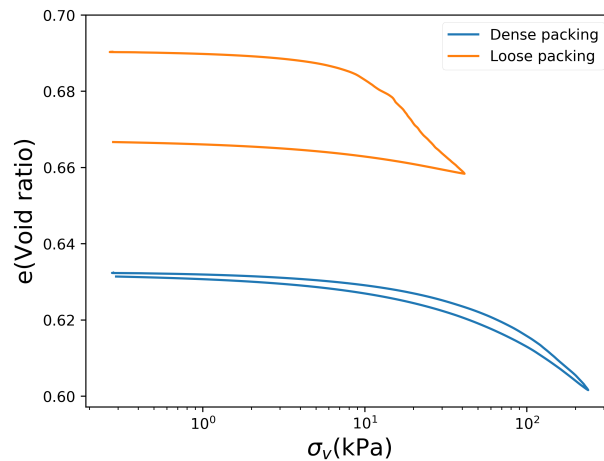
Figure 4.6: Void ratio vs log(vertical stress) for both dense and loose packings of 0% rubber fraction.

A striking difference between the dense and loose packing shown in Fig. 4.6 is the amount of stress recovery. In the case of dense packing, since the voids are less, there will be lesser particle rearrangements and hence there will be lesser plastic events. Consequently, the final void ratio can be observed to be very close to the initial value. On the other hand, for loose packing, higher number of voids causes more plastic events and hence a higher residual strain can be observed.

Arrangement	Rubber fraction, x_R (%)					
	10	20	25	30	40	50
Random packing	0.629	0.627	0.627	0.626	0.625	0.622
Clusters packing	0.629	0.627	0.626	0.625	0.624	0.623
Vertical stripes packing	0.63	0.628	0.627	0.625	0.623	0.622
Single layers packing	0.629	0.628	0.627	0.625	0.624	0.623
Double layers packing	0.629	0.628	0.628	0.626	0.625	0.623

Table 4.2: Initial void ratios for all rubber fractions and all mixture arrangements of dense packing (precision of ±0.001).

The initial void ratios of 0.632 for dense packing and 0.69 for loose packing are the values for sand-only packings, *i.e.* 0% rubber fraction packings. As mentioned before, after the replacement of certain sand grains with the rubber grains (depending on the rubber fraction), before the compression, the packings were allowed to relax for a sufficiently long time. It is obvious that due to the replacement of sand by rubber grains and this relaxation time, the packings do not achieve the same initial void ratios as that of the target void ratio, *i.e.* 0.632 for dense packing and 0.69 for loose packing.

Hence, each packing has a slightly different initial void ratio similar to the case of experiments. The initial void ratios for both dense and loose packings for all the mixture arrangements have
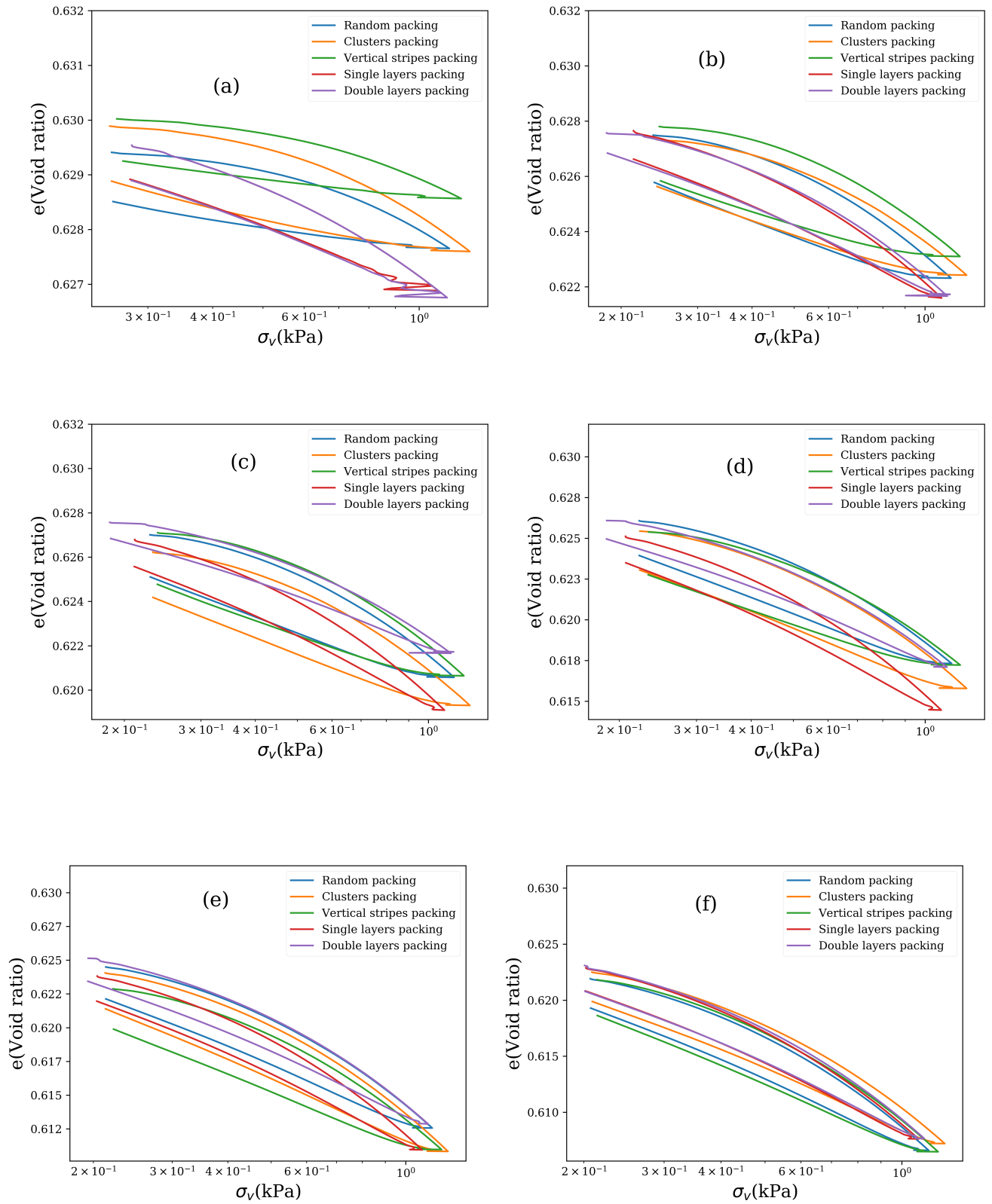
FIGURE 4.7. Void ratio vs log(vertical stress) plot for all mixing arrangements of dense packing: from (a) to (f): 10%, 20%, 25%, 30%, 40% and 50% rubber fraction.
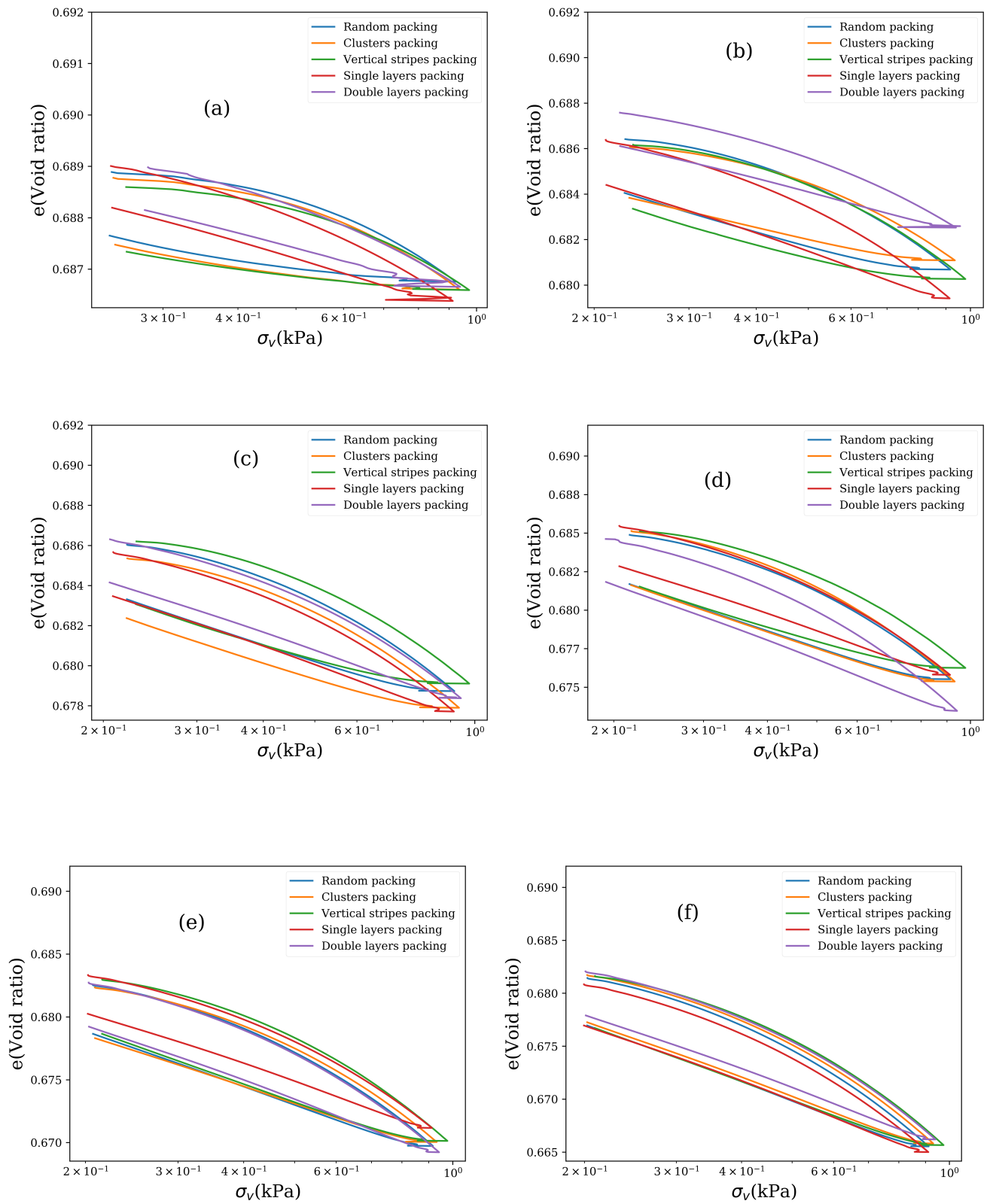
FIGURE 4.8. Void ratio vs log(vertical stress) plot for all mixing arrangements of loose packing: from (a) to (f): 10%, 20%, 25%, 30%, 40% and 50% rubber fraction.

Arrangement	Rubber fraction, x_R (%)					
	10	20	25	30	40	50
Random packing	0.689	0.686	0.686	0.685	0.683	0.681
Clusters packing	0.689	0.686	0.685	0.685	0.682	0.682
Vertical stripes packing	0.689	0.686	0.686	0.685	0.683	0.682
Single layers packing	0.689	0.686	0.686	0.685	0.683	0.68
Double layers packing	0.689	0.688	0.686	0.685	0.683	0.682

Table 4.3: Initial void ratios for all rubber fractions and all mixture arrangements of loose packing (precision of ±0.001).

been mentioned in Table 4.2 and Table 4.3. Consequently, the void ratio vs log(vertical stress) plots for all the arrangements of dense and loose packings have been shown in Figures 4.7 and 4.8. The difference between the different mixture arrangements observed in case of the
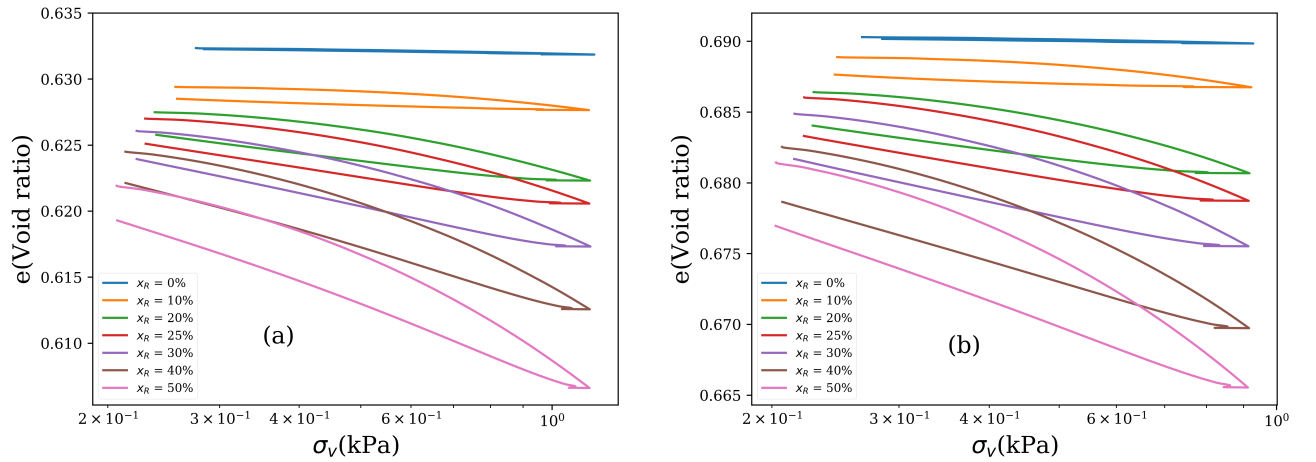
FIGURE 4.9. Void ratio vs log(vertical stress) plot for all rubber fractions of random mixtures of (a) dense packing and (b) loose packing.

experiments can also be seen in case of the numerical simulations from the plots shown above. It seems to reduce with the increasing rubber fraction. Moreover, these macroscopic results suggest that the effect of mixing is less in the case of loose packings than the dense packings. For lower rubber fractions, *i.e.* up to 20%, a noise can be observed at the start of the unloading curve. As mentioned before, for unloading, the sign of the velocity imposition is changed. Thus, a sudden change in the imposed velocity acts like a shock for these packings. For sand-rubber mixtures, especially for lower rubber fractions, the localized effect of the elasticity difference between the sand and rubber grains is higher. Hence, this effect is more pronounced in the case of lower rubber fractions. Further, this noise is more visible in the case of layered packings, suggesting the higher susceptibility of these packings to the change in the imposed velocity. The increasing rubber fraction causes an increase in the deformability of the sand-rubber mixture. This is evident from the plots for dense and loose packings shown in Fig. 4.9. For

simplicity, the plots have been shown only for random mixture arrangement.

Since the packings were unloaded at the same stress, it is easier to observe the effect of the rubber addition on the mixture response. With the increasing rubber fraction, the amount of initial state recovery goes on decreasing. This is obvious, since increasing rubber fraction leads to increased plastic events due to the particle rearrangements and hence results in a reduced initial state recovery. This can be well understood by studying the residual strain for each packing which will be discussed in the subsequent sections.

4.4 Discussion on loading-unloading behavior

In order to well characterize the effect of mixing quality on the sand-rubber mixtures, it is important that the loading-unloading response presented in the results above be modeled. This section will present the results showing the different parameters explaining the loading-unloading behavior and consequently, the effect of mixing quality on this behavior.

4.4.1 Stress-strain response under loading

Numerical simulations were performed wherein the same initial packings for the different mixing arrangements were used, however the loading was performed upto the limit of the DEM regime, in other words, upto 1% of rubber grain deformation. To start with, the plots have been shown for sand-only packings of dense and loose mixtures in Fig. 4.10. The first
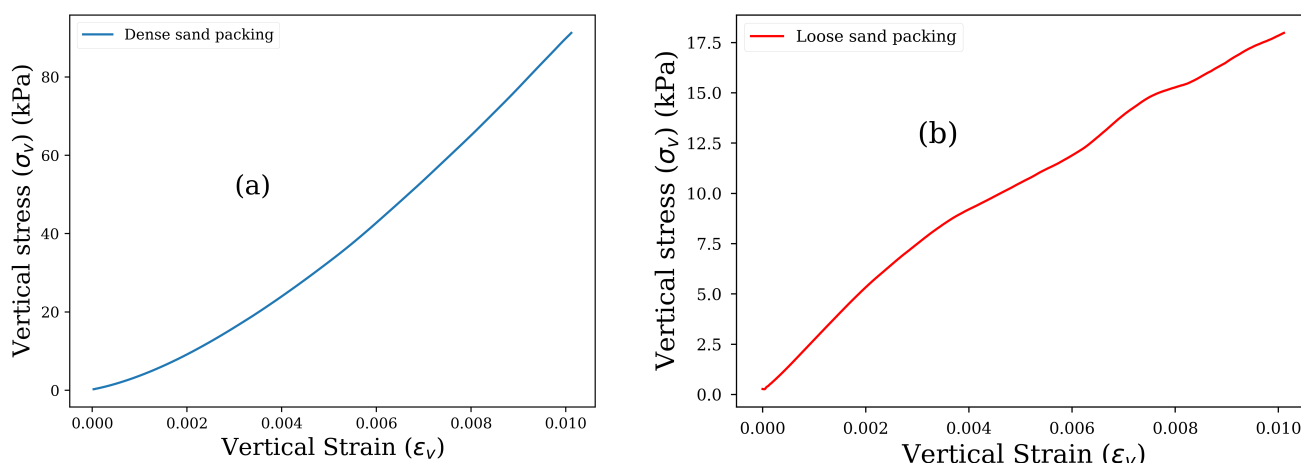
FIGURE 4.10. Figure showing the vertical stress vs vertical strain plot for (a) dense packing and (b) loose packing of 0% rubber fraction (sand-only packing).

noteworthy observation is the nature of the curve. In the case of dense packing, the curve is concave similar to experimental observation. However, in case of loose packing, it can be seen that the curve starts with a convex shape and then near strain of 0.01, it begins to become

concave in shape. In other words, the relative variation of stress is slower than that of the strain. So, an initial conclusion was to check whether the packing is well stabilized before the start of compression. Thus, a test was performed in order to check if increasing the relaxation time would affect it in any way. For this purpose, the relaxation time before the compression was doubled as compared to the previous value. However, as can be seen from the plot in Fig.
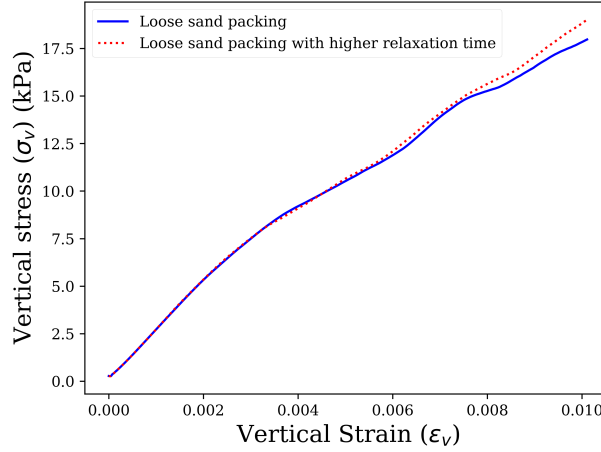
Figure 4.11: Stress vs strain plot for loose packing of 0% rubber fraction with different relaxation times.

4.11, the relaxation time has negligible effect on the response of the packing. This in fact can be associated to the behavior of an extremely loose packing (close to Random Loose Packing). When such a packing close to Random Loose Packing (RLP) is compressed, at the start of the compression, there will be a lot of plastic events involving particle rearrangements. This causes the strain to vary relatively faster than the stress, thus leading to the trend of the curve observed. Note that however, such very loose packings are not easy to obtain experimentally [Farrell et al., 2010] and hence a similar curvature is not observed experimentally.

Figures 4.12 and 4.13 present the stress vs strain plot for the different mixture arrangements and rubber fractions. Since the loose packing is close to the Random Loose Packing (RLP) state, a small amount of rubber addition cannot affect the characteristics observed in the sand-only packing. Hence, we can observe similar trend for the loose packings upto 20% rubber fraction (inclusive), especially for packings of random, clusters and vertical stripes arrangements.

Of course, the stress-strain response shows a similar trend between the packing arrangements as observed initially in the load-unload plots. A clear distinction cannot be observed between the packing arrangements. This is valid for both dense and loose packings (neglecting the effect of RLP). For higher rubber fractions of 40% and 50%, the response of the arrangements seems to be very close to each other than in the cases of other rubber fractions.

The above stated fact suggests the effect of the grain arrangement on the macroscopic response of the packings. In other words, at a first instance, it seems that mixing quality affects the mechanical response of the packings. To quantify this and better understand the response of

FIGURE 4.12. Vertical stress vs vertical strain response for all the mixing arrangements of dense packing: from (a) to (f): 10%, 20%, 25%, 30%, 40% and 50% rubber fraction.

FIGURE 4.13. Vertical stress vs vertical strain response for all the mixing arrangements of loose packing: from (a) to (f): 10%, 20%, 25%, 30%, 40% and 50% rubber fraction.

the packings under loading, they were modeled using a power law fit, *i.e.* $y = ax^b$, where, $y =$ vertical stress (σ_v), x = vertical strain (ϵ_v), and a,b are the fit parameters.

The power law fit was found to capture the response of the packings in an effective way. This model equation can be treated to be analogous with the Hertz equation for the force between the contacting elastic bodies. Hertz equation is given by,

$$F = \frac{4}{3} E R^{1/2} d^{3/2} \tag{4.9}$$

where, F is the applied force, E is the effective Young's modulus of elasticity, R is the effective radius and d is the displacement. Hence, applying the equation in this case, takes the form of

$$\sigma_v = a\epsilon_v^b \tag{4.10}$$

where, σ_v is the vertical stress, ϵ_v is the vertical strain, a is a constant stress and exponent, b is the fit parameter. Fig. 4.14 shows the fit parameter b for all the mixture arrangements of dense and loose packings. The plots shown here clearly indicate that the difference between the
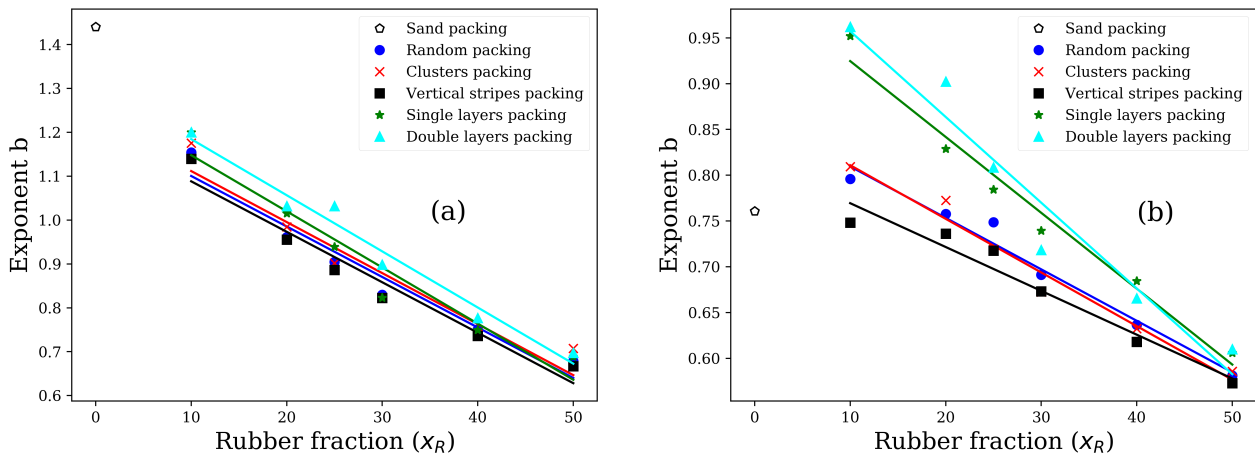
FIGURE 4.14. Variation of the fit parameter, b for all rubber fractions of mixture arrangements of (a)dense packing and (b)loose packing.

different mixture arrangements is higher at lower rubber fractions upto nearly 25%. Whereas, the points collapse together at rubber fraction of 50% indicating a negligible effect of the mixing quality. Moreover, the value of the exponent b for dense sand packing can be observed to be quite close to 1.5 (close to the exponent of 'd' in the case of Hertz equation), thus indicating an elastic behavior and hence explaining the macroscopic response observed in Fig. 4.6. On the other hand, it is lower for loose packing, indicating higher number of plastic events due to particle rearrangements.

For the arrangements of random, clusters and vertical stripes, the proportion of sand-sand contacts and thus the force networks formed by these sand grains is higher than in the case of layers packings. In other words, stiffer contacts are higher, thus leading to stronger force

networks and hence a stiffer packing. This will be discussed in detail in the further sections. Since the mixing quality is clearly associated with the granular arrangement, it is evident that a different initial packing will lead to different granular positions and different mixture arrangements, thus leading to a difference in the behavior observed. In order to further investigate this, 3 more initial packings were created (in total 4 initial packings) and simulations were performed on all the rubber fractions of one mixture arrangement, *viz.* random packing for both dense and loose mixtures. The plots for the fit parameter, b incorporating the repeatability effect has been shown in Fig. 4.15.
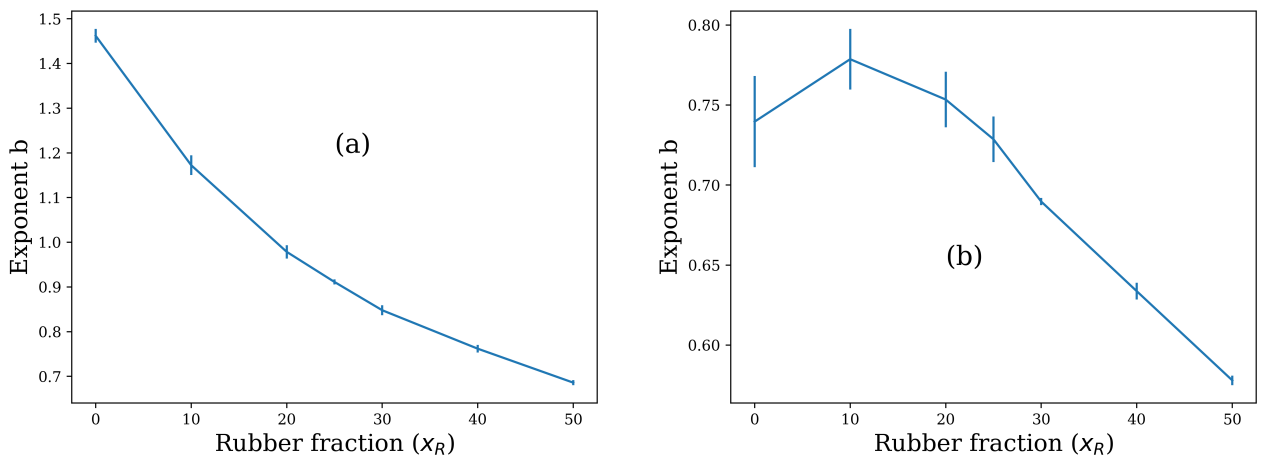
FIGURE 4.15. Variation of the fit parameter, b for 4 different initial packings of all rubber fractions of random mixture arrangement for (a)dense packing and (b)loose packing.

From the plots shown here, it is clear that the effect of the initial grain arrangement is higher upto 25% rubber fraction with the standard deviation being the highest for the packing of 10% rubber fraction, nearly equal to 0.02 in case of dense packing. Similarly, for loose packings, a higher effect of the initial packing arrangement can be observed, however, again upto 25% rubber fraction. In case of loose packings, the standard deviation observed was the highest for sand-only packing, approximately equal to 0.03 and for 10% rubber fraction, it was again nearly 0.02. This clearly suggests the effect of the initial packing arrangement on the macroscopic response. Moreover, since the selection of grains for replacement with rubber was totally random, this increases the deviation in the observed response much more (although not as high as the effect of the initial packing arrangement).

The high value of standard deviation upto 25% rubber fraction is obvious, since for lower rubber fractions, there is a higher probability of achieving different mixture arrangement, hence higher probability of different granular arrangements, thus affecting the packing response.

4.4.2 Residual strain

Residual strain, or in other words remnant strain is the difference between the strains corresponding to the start of the loading stress and the end of the unloading stress. In actual compression experiments involving coarse-grained soils, residual strains occur due to the densification and crushing phenomena of these grains [Valdes and Evans, 2008]. However, the numerical simulations fail to capture such phenomena and hence, the residual strains here indicate more the effect of the plastic events occurring due to the particle rearrangements. Since the packings studied here are not perfectly elastic, the strain at the end of unloading will not be the same as at the start of the loading phase (as in the case of dense sand-only packing). Thus, there will always be an unrecoverable deformation that the packing would undergo which would be indicated by the residual strain. However, since the different sand-rubber mixtures were not unloaded at the same strain, but at the same stress, it is important that the residual strains be divided by the maximum strain (ϵ_{max}) which is the value of strain at which the unloading starts, in order to have a better comparison between the different mixtures arrangements. Fig. 4.16 shows the plot for the ratio of residual strain (ϵ_{rem}) to the maximum
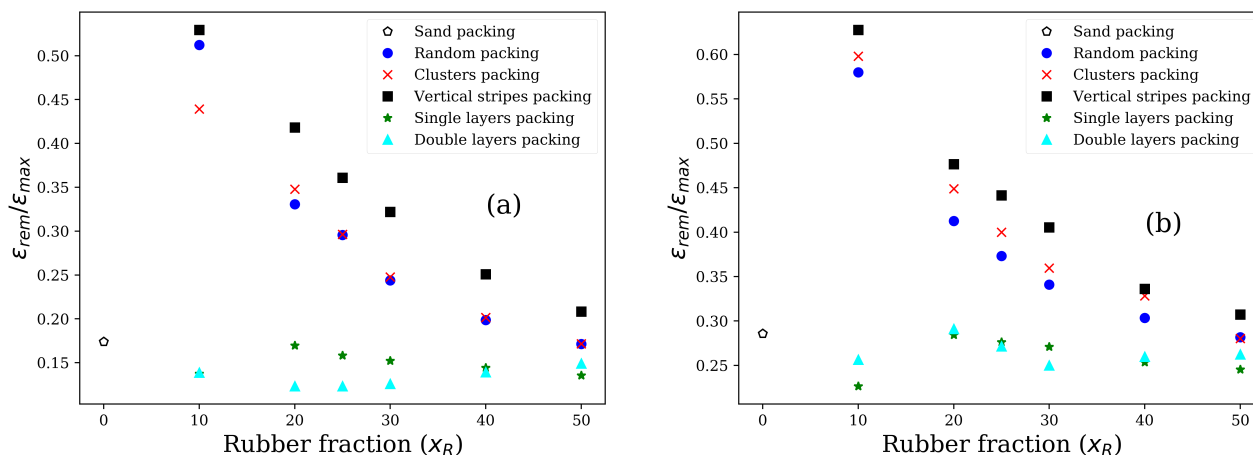
FIGURE 4.16. $\epsilon_{rem}/\epsilon_{max}$ vs rubber fraction (x_R) plot for all mixtures arrangements of (a)dense packing and (b)loose packing.

strain (ϵ_{max}) vs rubber fraction (x_R) for all the mixture arrangements.

The magnitude of the strain ratio is slightly higher for a similar rubber fraction mixture arrangement of loose packing than its corresponding dense packing. It is obvious, since with higher void ratio, there will be more plastic events due to particle rearrangements, thus leading to an irrecoverable part of the initial packing state. The ratio is the lowest in the case of sand-only packings indicating a lower number of plastic events since there is no rubber addition. The initial hypothesis of the effect of mixing quality can be observed to be true from these results. It an be said that there exist two families of packings, *i.e.* random, clusters, vertical stripes packings and single, double layers packings. A noteworthy point here is a huge distinction

between these two families of packings for rubber fractions nearly upto 30% (inclusive) for both dense and loose state. For the packings of the first family, there is a higher number of localized particle rearrangements due to random location of the rubber particles, leading to a higher number of plastic events. However, for higher rubber fractions, this can be seen to be close to the other family of packings, thus indicating that for high rubber fraction such as 50%, there is not much difference between the particle arrangements.

The residual strain ratio analysis allows to say that the unloading behavior of sand-rubber mixtures depends on both rubber fraction as well as the mixture quality.

4.4.3 Horizontal stress ratio

Horizontal stress ratio is given by a coefficient (K),

$$K = \frac{\sigma_h}{\sigma_v}, \tag{4.11}$$

where, σ_h is the horizontal or the lateral stress and σ_v is the vertical stress. In the case of oedometer experiments, it is possible to measure using a special K_0 oedometer apparatus. However, in the experiments performed in this study, such a device was not used. But, the horizontal stress value is captured in the numerical simulations, thus helping to better understand its significance on the packing response. It is clear that in case of mixtures such as sand-rubber,
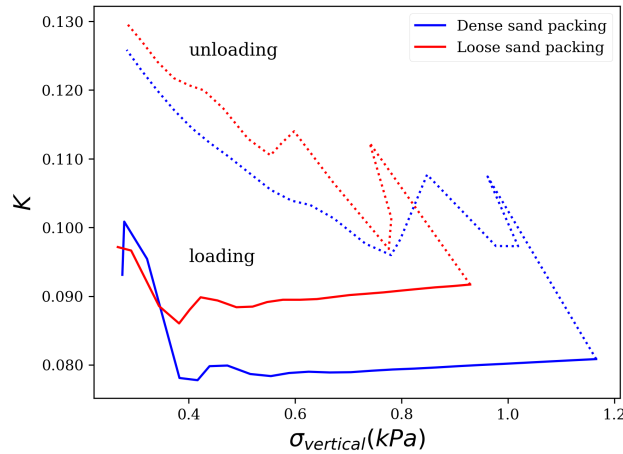
Figure 4.17: Horizontal stress ratio vs vertical stress (σ_v) for loading and unloading phases of both dense and loose packings of 0% rubber fraction.

the contact behavior is evidently responsible for the macroscopic response observed and hence an effect of mixing quality is observed. The contact force distribution has a significant effect on the horizontal stress ratio. The horizontal stress ratio signifies the effect of the sidewall stresses on the packing behavior. Consequently, the interparticle slips and deformations affect the horizontal stress ratio [Lee et al., 2014].
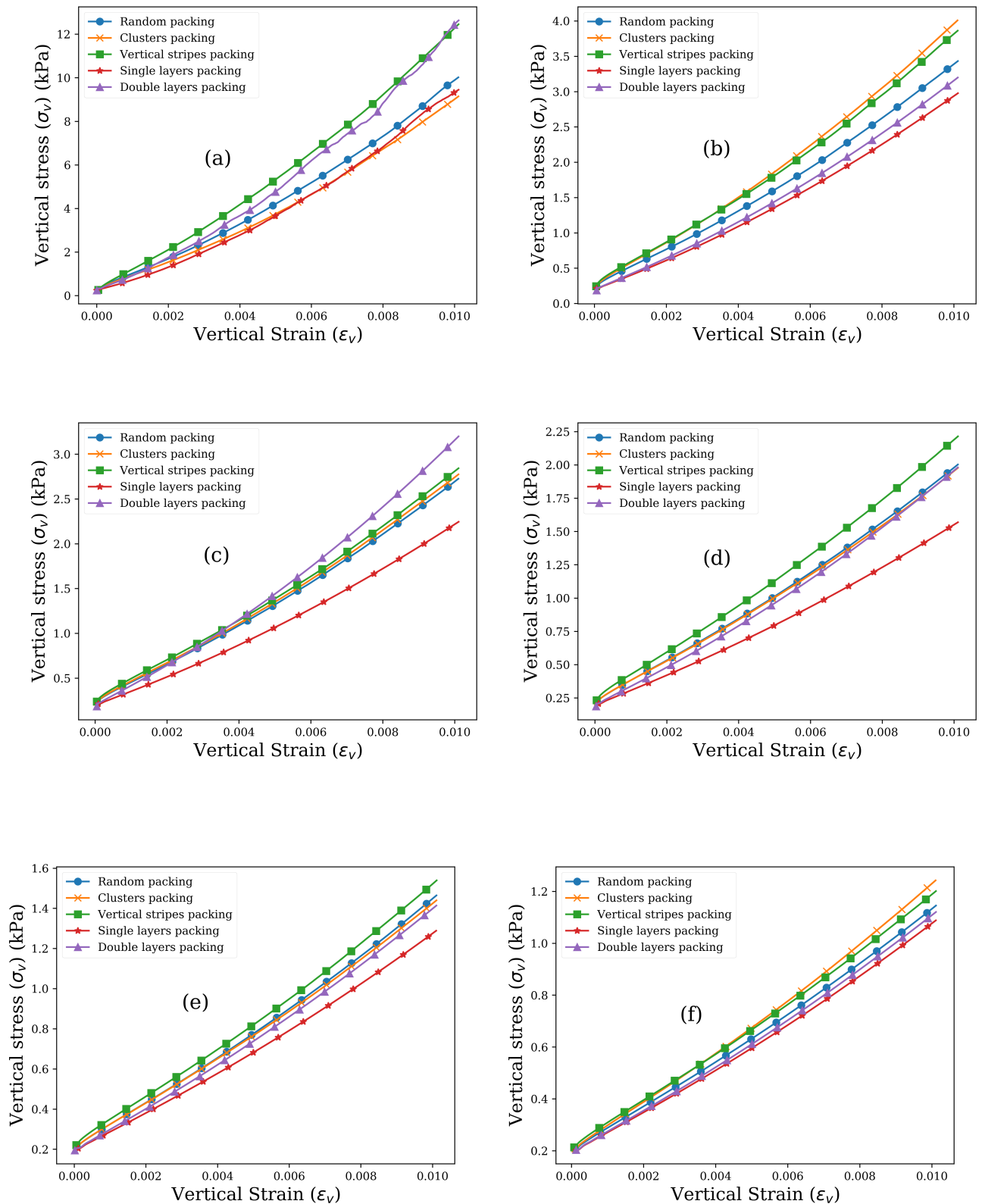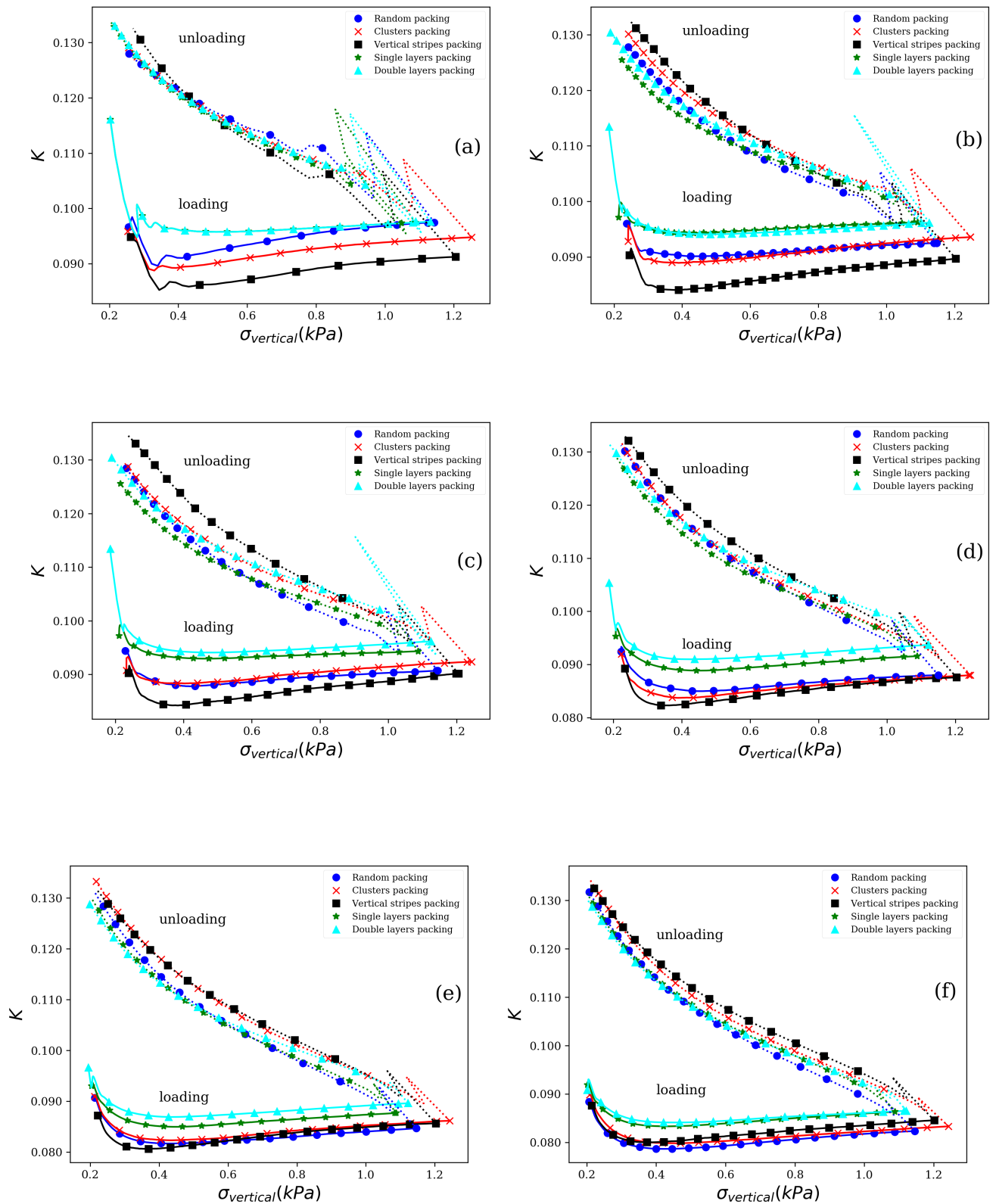
FIGURE 4.18. Horizontal stress ratio vs vertical stress plot for all the mixing arrangements of dense packing: from (a) to (f): 10%, 20%, 25%, 30%, 40% and 50% rubber fraction.

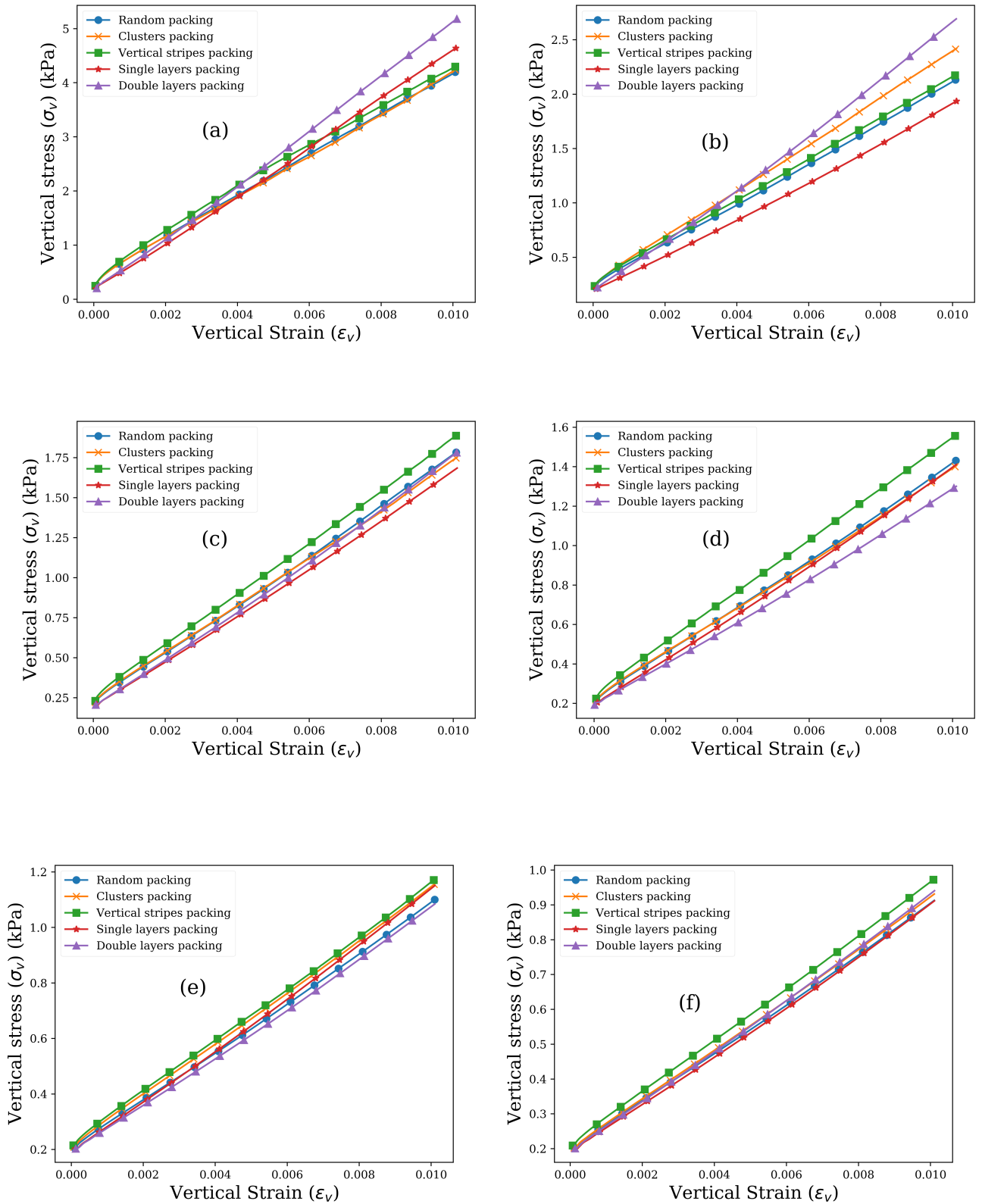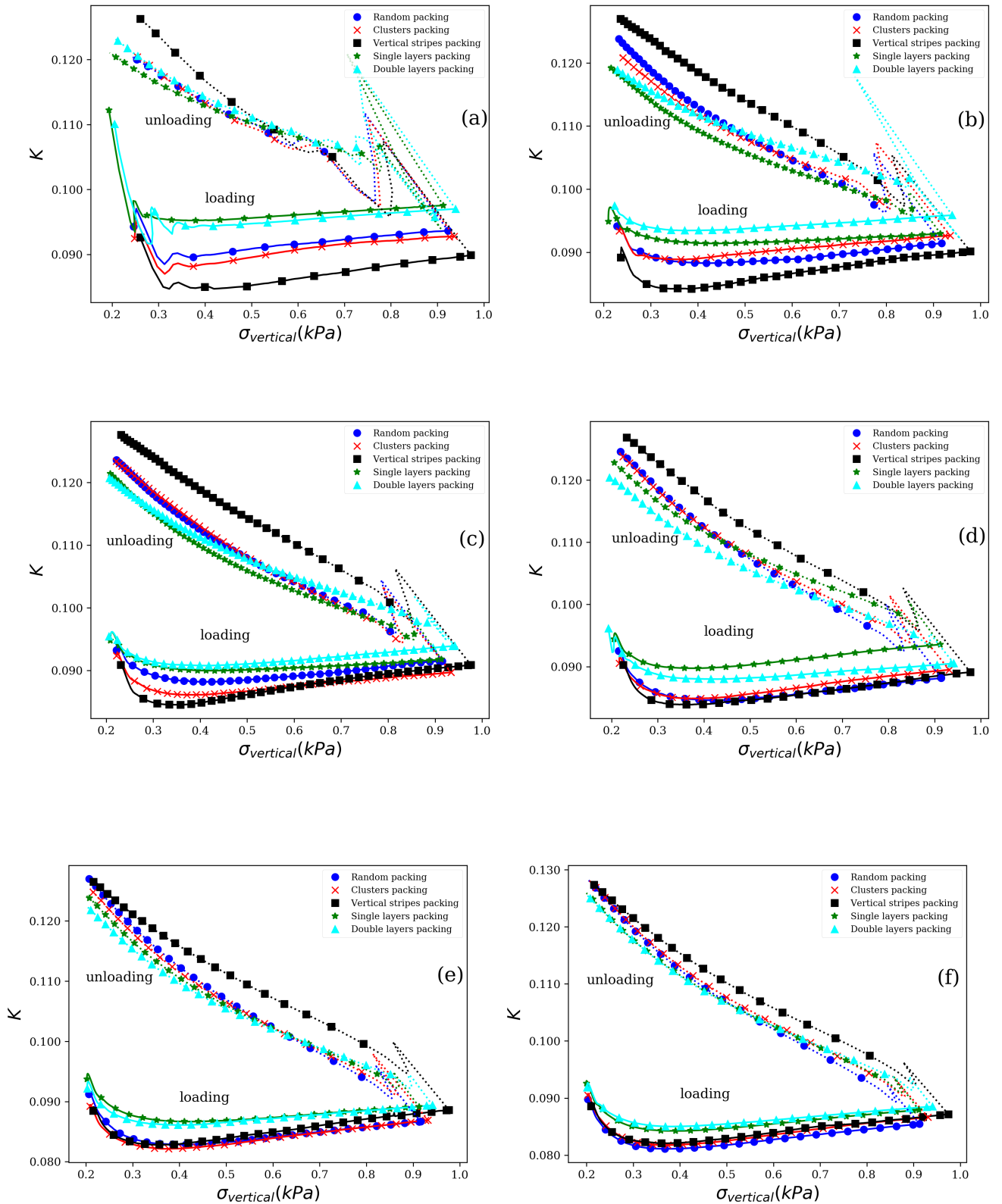FIGURE 4.19. Horizontal stress ratio vs vertical stress plot for all the mixing arrangements of loose packing: from (a) to (f): 10%, 20%, 25%, 30%, 40% and 50% rubber fraction.

Fig. 4.17 presents the horizontal stress ratio vs vertical stress for sand-only packings of both dense and loose state. Since the packings consist of only sand particles, the interparticle contact slips will be lesser and hence, a constant variation of stress ratio can be observed with the vertical stress in case of loading phase for both dense and loose packings. During the unloading phase, the stress ratio can be seen to increase with the decreasing vertical stress (unloading plots have to be seen in the reverse direction, *i.e* from right to left). With the increase in the confined pressure, the particles are highly compressed. Hence, when the packing is unloaded at such a state, there is an interparticle lock-in which causes an increase in the sidewall stresses. Further, Fig. 4.18 and 4.19 show the horizontal stress ratio for loading and unloading of dense and loose packings for all the mixture arrangements. An interesting observation here is that for lower rubber fractions, during loading, the stress ratio is quite constant, whereas for higher rubber fractions, it shows a higher dependence on the vertical stress. These plots as well justify the effect of the mixing quality. For same rubber fraction, the layers packing family shows a higher stress ratio. It can be explained by the fact that the layers packings have more sand-rubber and rubber-rubber grain contacts for same rubber fraction as compared to the other packings. Consequently, an irrecoverable plastic sliding at the contacts occurs which leads to the observed behavior. Obviously, with the increasing rubber fraction, the difference between the mixture arrangements again decreases. The trend of the results shown here is in well accordance with the literature [Lee et al., 2014].

4.5 Micromechanical parameters

An advantage of Discrete Element Method (DEM) is the possibility of studying different parameters at the contact scale, *e.g.* contact forces, contact force orientations, contact force distribution, etc. to name a few and correlating them with the macroscopic response. This is not possible to achieve in the case of experiments. The discussion in this section will involve the micromechanical parameters which will help to further understand the results studied till now.

4.5.1 Average contact forces

The average contact force is the total average force at the contacts of the particles in the packings. Since the packings under study are binary mixtures of sand and rubber particles, and the primary interest was to verify the effect of the mixing quality on the sand-rubber mixtures, the contacts were divided into two types, *i.e.* sand and rubber. Consequently, the contact force was represented into two parts, the one for the sand type particle and the other for the rubber type particle. Hence, the average contact force consists of two components, average contact force for sand particles ($F_{S_{avg}}$) and average contact force for rubber particles ($F_{R_{avg}}$).
For simplicity and better understanding of the effect of the average contact force on the macroscopic behavior of the mixtures, the average force for sand and rubber particles has been represented for an intermediate stage of compression (ϵ_v=0.005) in Fig. 4.20. Moreover, since
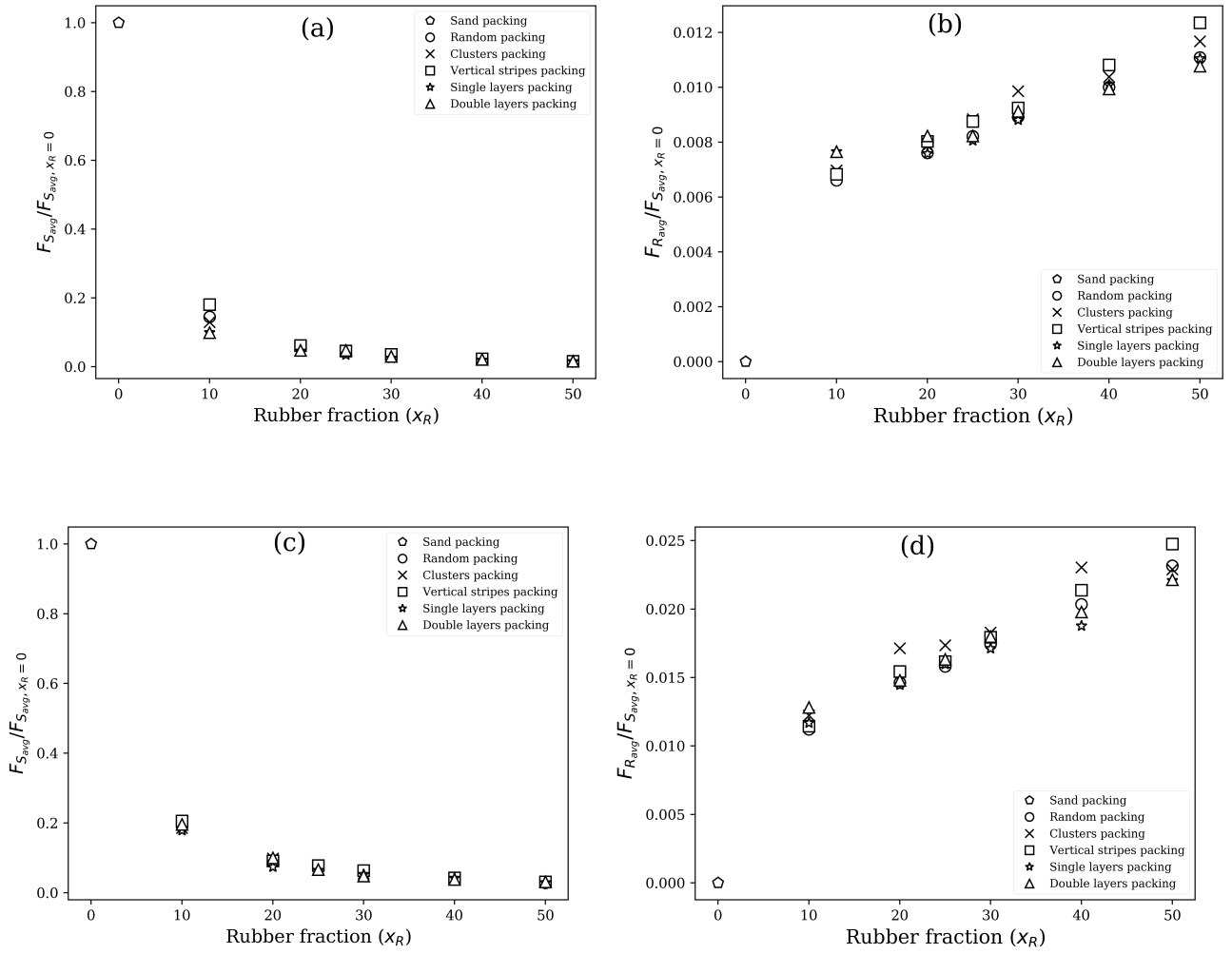
FIGURE 4.20. Average contact force vs rubber fraction plot for all the mixing arrangements:(a) $F_{avg(sand)}$ for dense packing, (b) $F_{avg(rubber)}$ for dense packing, (c) $F_{avg(sand)}$ for loose packing, (d) $F_{avg(rubber)}$ for loose packing.

the average sand force for 0% rubber fraction packings was quite high, hence all the values of average sand force ($F_{S_{avg}}$) have been divided by the average sand force value for 0% rubber fraction packing. Clearly, the magnitude of the sand component of the average force is quite higher than the rubber component at a given strain. However, with the increasing rubber fraction, the ($F_{R_{avg}}$) shows an increasing trend. This observation is valid for both dense as well as loose packings irrespective of the type of mixture arrangement. It is quite obvious that for lower rubber fractions, the amount of contacts involving the sand grains in the force chains will be higher than those involving the rubber grains.

These plots only show the individual average contact forces for sand and rubber particles at a given strain. However, to obtain a better insight and well characterize the average contact forces, the proportion of the average contact force for rubber particles over the total average

129

force ($F_{R_{avg}}/F_{avg}$) was plotted for both dense and loose packings with the increasing rubber fraction.
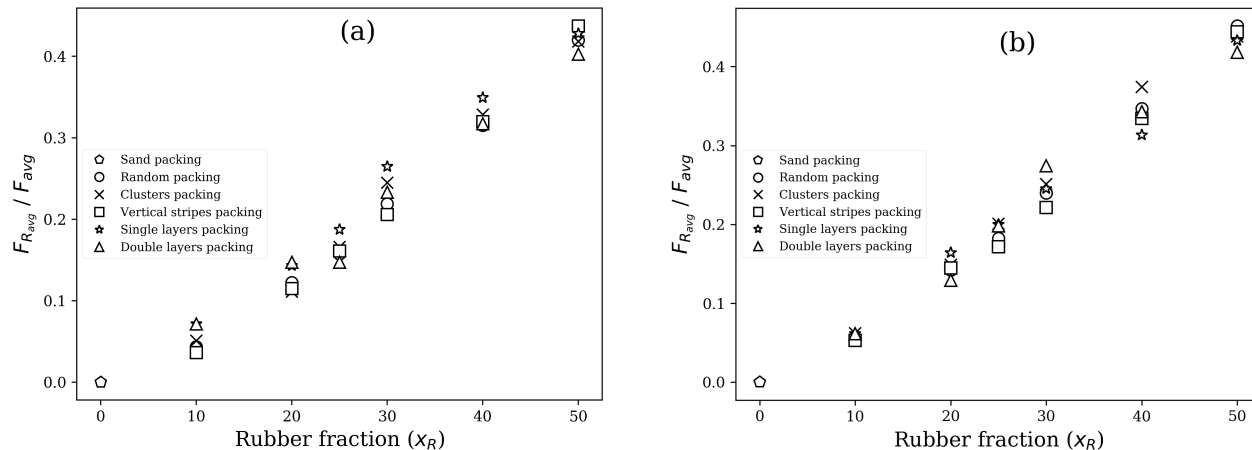
FIGURE 4.21. Rubber/sand ratio of average contact force vs rubber fraction plot for all the mixing arrangements:(a) ($F_{R_{avg}}/F_{avg}$) for dense packing and (b) ($F_{R_{avg}}/F_{avg}$) for loose packing.

Fig. 4.21 shows the ratio of $F_{R_{avg}}$ and F_{avg} with the increasing rubber fraction for different mixture arrangements. As per the mean field approach, the contribution of the rubber particles should be equivalent to the rubber fraction. In other words, for 10% rubber fraction the ratio plotted in Fig. 4.21 should be 0.1. It can be seen that the evolution is not linear and the values less than expected, thus showing that the rubber grains are also included in the major force carrying chains and this proportion goes on increasing with the rubber fraction. This increase in the proportion is equivalent to the corresponding rubber fraction. Hence, for 50% rubber fraction, the value can be observed to be close to 0.45. However, even for 50% rubber fraction, sand grains still remain the major force carriers. For 10% rubber fraction, the ratio is nearly the same for all the mixture arrangements. This clearly indicates that the macroscopic response observed for 10% rubber fraction is highly affected by the proportion of sand particles in the force chains. Whereas, the ratio is quite high for higher rubber fractions of 40% and 50% indicating a higher involvement of rubber particles as well in the major force carrying chains. In case of clusters, vertical stripes and random packings, even for higher rubber fractions, there will always be a good proportion of sand contacts in the force networks. Hence, even for higher rubber fraction, although the rubber particles contribute nearly 50% towards the total average force, it is the proportion of sand particles which impacts the macroscopic response to a greater extent. Nevertheless, it is extremely important to note that for increasing rubber fractions, rubber particles participate more in the force carrying networks, thus causing the mixing phenomena to lose its importance.

4.5.2 Normalized force distribution

The force distribution plots have been shown in Fig. 4.22. The plots have been normalized with respect to the average normal forces. Hence, if $F_{n,i}$ is the normal force for each contact, i, then

$$\langle F_n \rangle = \frac{1}{N_c} \sum_{n=i}^{N_c} F_{n,i},$$

where, N_c is the total number of contacts and $\langle F_n \rangle$ is the total average normal force. The plot
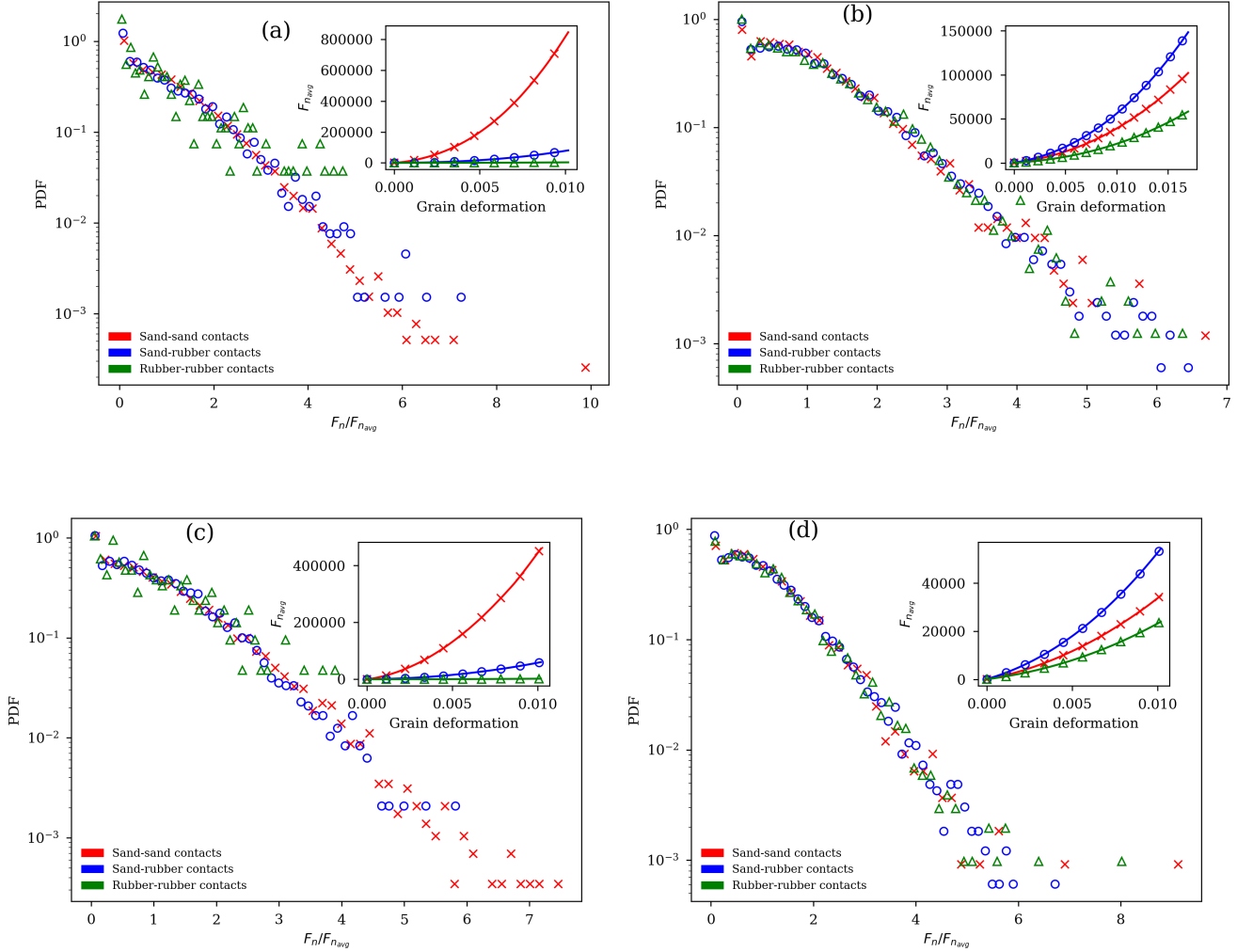
FIGURE 4.22. PDF for the normalized average contact forces for sand-sand, sand-rubber and rubber-rubber contacts of (a)10% RF random dense packing, (b)50% RF random dense packing, (c)10% RF random loose packing, (d)50% RF random loose packing. In the inset plot: Average sand-sand, sand-rubber and rubber-rubber contact forces vs grain deformation.

for the average normal force ($F_{n_{avg}}$) vs grain deformation is shown in the inset of the force distribution plots. The grain deformation is the overlap between the contacting grains, *i.e.* δ.

For simplicity and better analysis, the plots have been shown here for an intermediate stage of compression (ϵ_v=0.005), similar to the average contact forces. To begin with, the plots have been shown here for 10% and 50% rubber fraction dense and loose packings for random mixture arrangement only. However, instead of just dividing the type of contacts as sand type and rubber type, for a better idea, they have been divided here into three types, *viz.* sand-sand, sand-rubber and rubber-rubber depending on the type of the contacting grains. It can be observed from the plots that the normalized force distribution follows almost a similar trend for the three types of contacts and it is exponential in nature for large forces. Although, for 10% rubber fraction, the tail of the plots is clearly different. It is evident that sand-sand contacts are much well distributed throughout the packing in case of lower rubber fractions, thus leading to a sand-dominated behavior. However, it is normalized with respect to the average normal force for each type of contact. As a result, the force distribution is a function of the average normal force. In short, the subplot of average normal force vs grain deformation (see inset plot in Fig. 4.22) can be studied to analyze and differentiate between the different types of contacts for a specific packing arrangement. Since it is evident that the sand-sand contacts are higher in number in the major force carrying networks, and not much a difference was observed between each type of contact in terms of distribution, the sand-sand contact forces have been plotted for 10%, 25% and 50% rubber fractions of all the mixture arrangements of dense and loose packings in Fig. 4.23.

The plots shown here in Fig. 4.23 can be studied to compare the different mixture arrangements. In this case, a distinction between the two families of packing arrangements (*i.e.* cluster, random packings and single and double layers packings) can be observed and it becomes much more significant at the tail of the force distribution curve. However, for 50% rubber fraction, there is no visible difference in the distribution plot and the average normal forces are very close to each other, thus explaining the macroscopic response of no visible effect of mixing quality. This clearly indicates that the large forces are favored in the case of the cluster and random packings. The subplot of the average normal force for the packing arrangements further strengthens this fact. The sand-sand contacts are the strongest contacts among the three types of contacts. Hence, the main distinguishing factor responsible for the presence of two families is the fact that the sand-sand contacts are the major carriers of forces. The force distribution curve was also plotted for the 100% sand grain packing along with 10% rubber fraction packings to better understand the effect of rubber addition. As mentioned before, the addition of rubber leads to heterogeneity. But, in fact if the plot in Fig. 4.23(a) and (d) is observed, then we can find quite similar behavior with a prominent difference at the tail of the force distribution plot. The difference between the packings is due to the fact that the sand packing is less heterogeneous than the other packings, since it has less number of plastic events concerning the particle rearrangements. Again, the subplot of the average forces provides a better insight to distinguish between the different packings. Hence, it can be observed that even a small rubber fraction has a huge effect on the mechanical response of the packing. In terms of dense and loose packings,
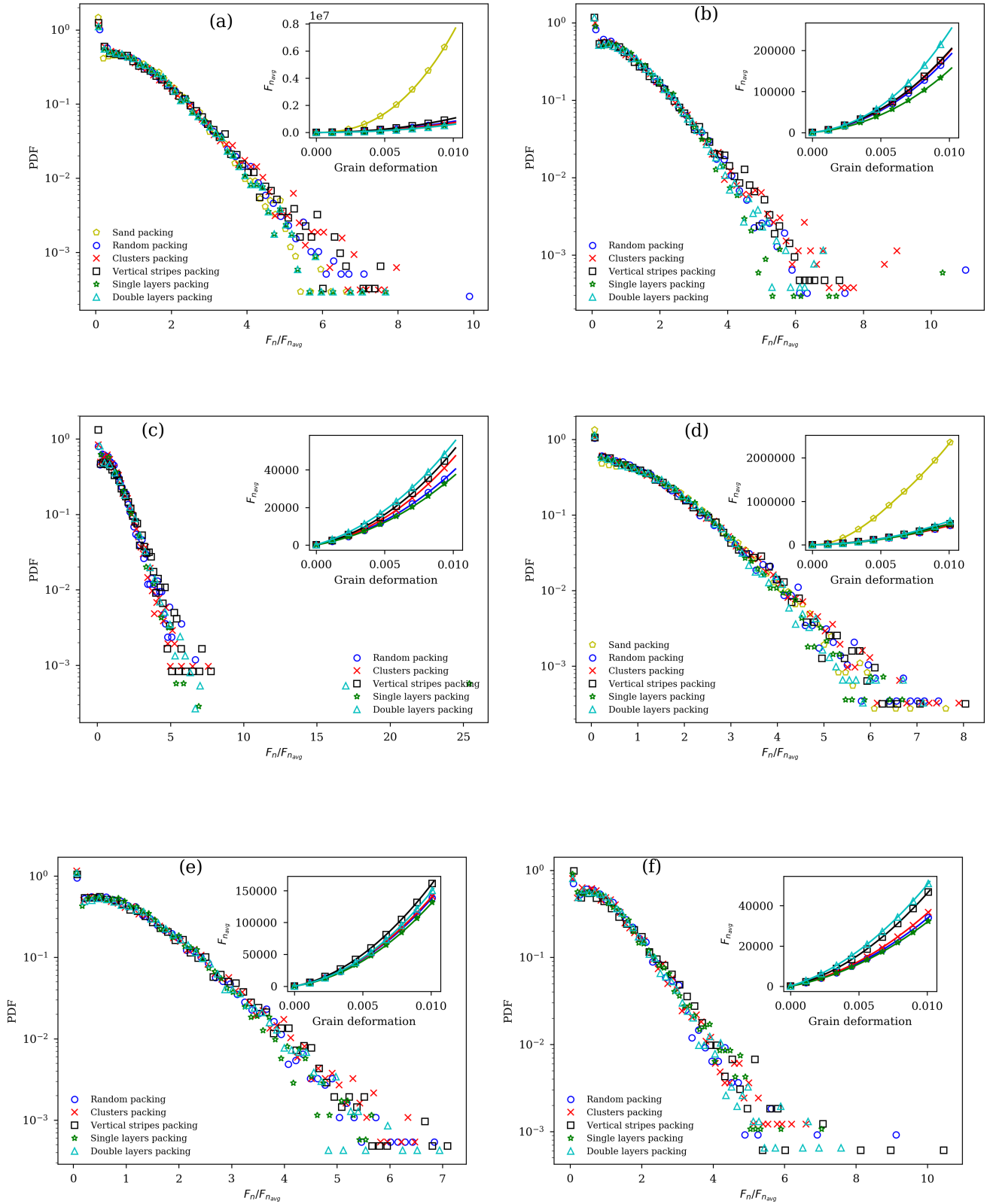
FIGURE 4.23. PDF for the normalized average contact forces for sand-sand contacts of all mixture arrangements for: (a)10% RF dense packing, (b)25% RF dense packing, (c)50% RF dense packing, (d)10% RF loose packing, (e)25% RF loose packing, (f)50% RF loose packing. In the inset plot: Average sand-sand contact force vs grain deformation.

nearly similar trend of force distribution is observed for both the cases.

4.5.3 Contact force orientation

The main objective of this study is to analyze the effect of the different packing arrangements on the mechanical response of the sand-rubber mixtures. Thus, studying the orientation of the contact forces can act as a supporting factor in proving the influence of these geometrical arrangements. The angle calculated to plot the force orientation curves here is the polar angle *i.e.* the angle made by the branch vector linking the two contacting grains with the vertical axis (or in other words, the direction of deformation of the packing), which corresponds to θ in Fig. 4.24(a). Figures 4.24(b) and (c) show the contact force orientation for all three types of contacts, *i.e.* sand-sand, sand-rubber and rubber-rubber for 10% and 50% rubber fraction random packings for dense state and the same is shown for loose random packings in Fig. 4.24(d) and (e). For 10% rubber fraction of both dense and loose packings, there is not much difference between sand-sand and sand-rubber types of contact forces where more forces are inclined towards 90°. On the other hand, some deviations can be observed for rubber-rubber contacts and higher number of forces are inclined between 45°and 135°. Whereas, for 50% rubber fraction, there is negligible difference observed between the three types of contact forces and more forces are inclined towards 90°. Again, all the plots shown here for contact force orientations have been plotted for an intermediate stage of compression (ϵ_v=0.005).

As discussed before in the case of normalized force distribution, since sand-sand type of contacts are the important force-carrying contacts out of the three and no visible difference is observed for the three types of contact force orientations, hence for the comparison between different mixture arrangements, only sand-sand contact force orientation curves have been plotted in Fig. 4.25. Further, for simplicity purposes, plots have been shown here for 10%, 25% and 50% rubber fractions only for both dense and loose state packings. Clearly, a difference can be seen between the different mixture arrangements starting from 10% rubber fraction. The layers packing family has more forces aligned near 90°, which can be related with the macroscopic results (stress vs strain), since a similar difference between the families is observed. Further, it can be seen that for 25% rubber fraction, the number of these contact forces aligned towards 90°increases for the layers packing family as compared with the other mixture arrangements, and for 50% rubber fraction, this difference increases further. On the other hand, with the increasing rubber fraction the macroscopic curves (stress vs strain) have been seen to collapse. Thus, with the increasing rubber fraction, the force orientation seems to lose its importance.

4.5.4 Hypothesis on strong contact forces

All the results presented above suggest that the mechanical response of the sand-rubber packing is affected by the grain arrangements as well as the rubber fraction. However, the force network of a granular system is highly heterogeneous and forms a non-homogeneous
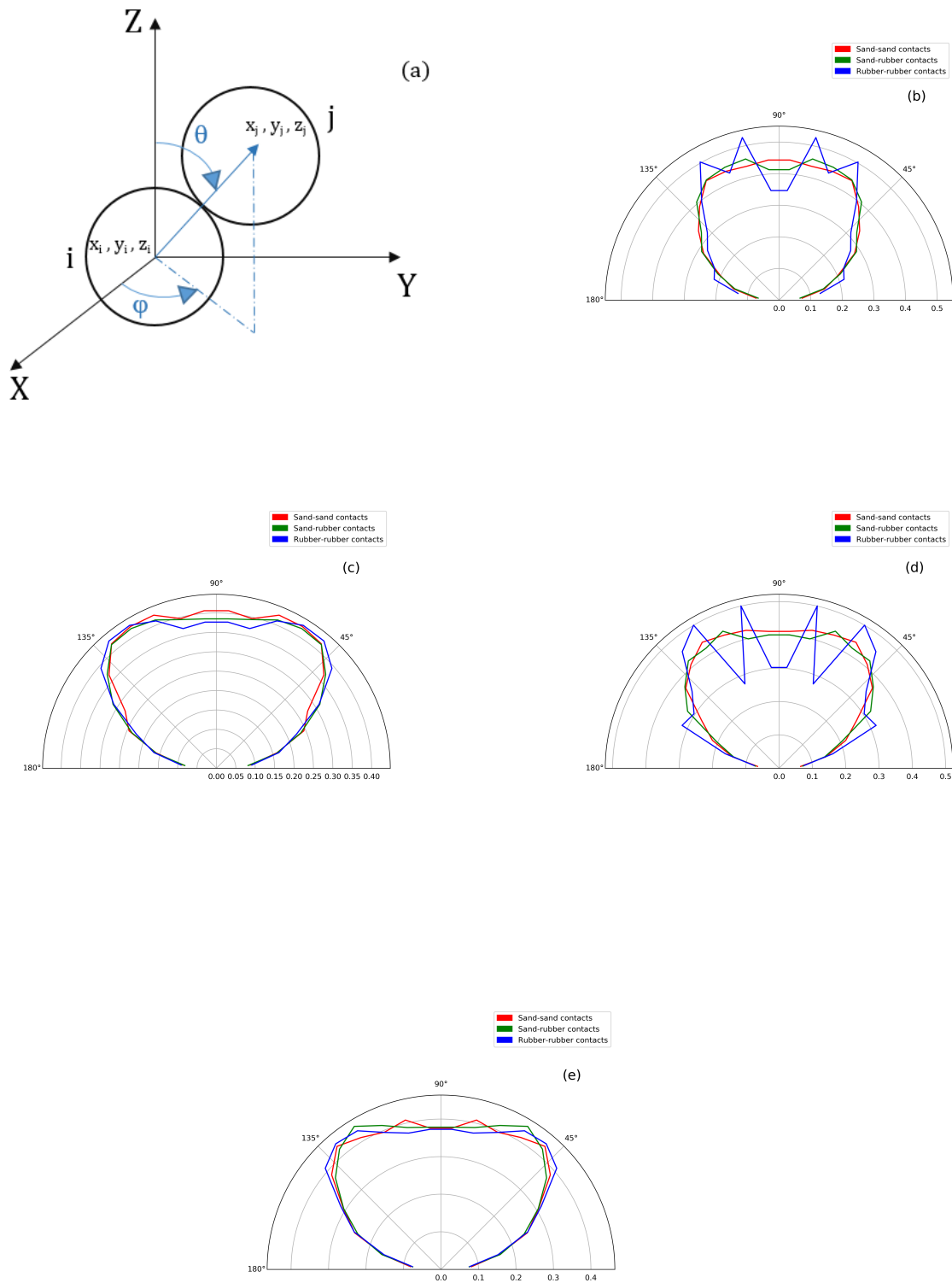
FIGURE 4.24. (a) Angle used to calculate the orientation of contact forces, and the force orientation plots for sand-sand, sand-rubber and rubber-rubber contacts for the random mixture arrangement of (b) 10% rubber fraction dense packing, (c) 50% rubber fraction dense packing, (d) 10% rubber fraction loose packing, (e) 50% rubber fraction loose packing.
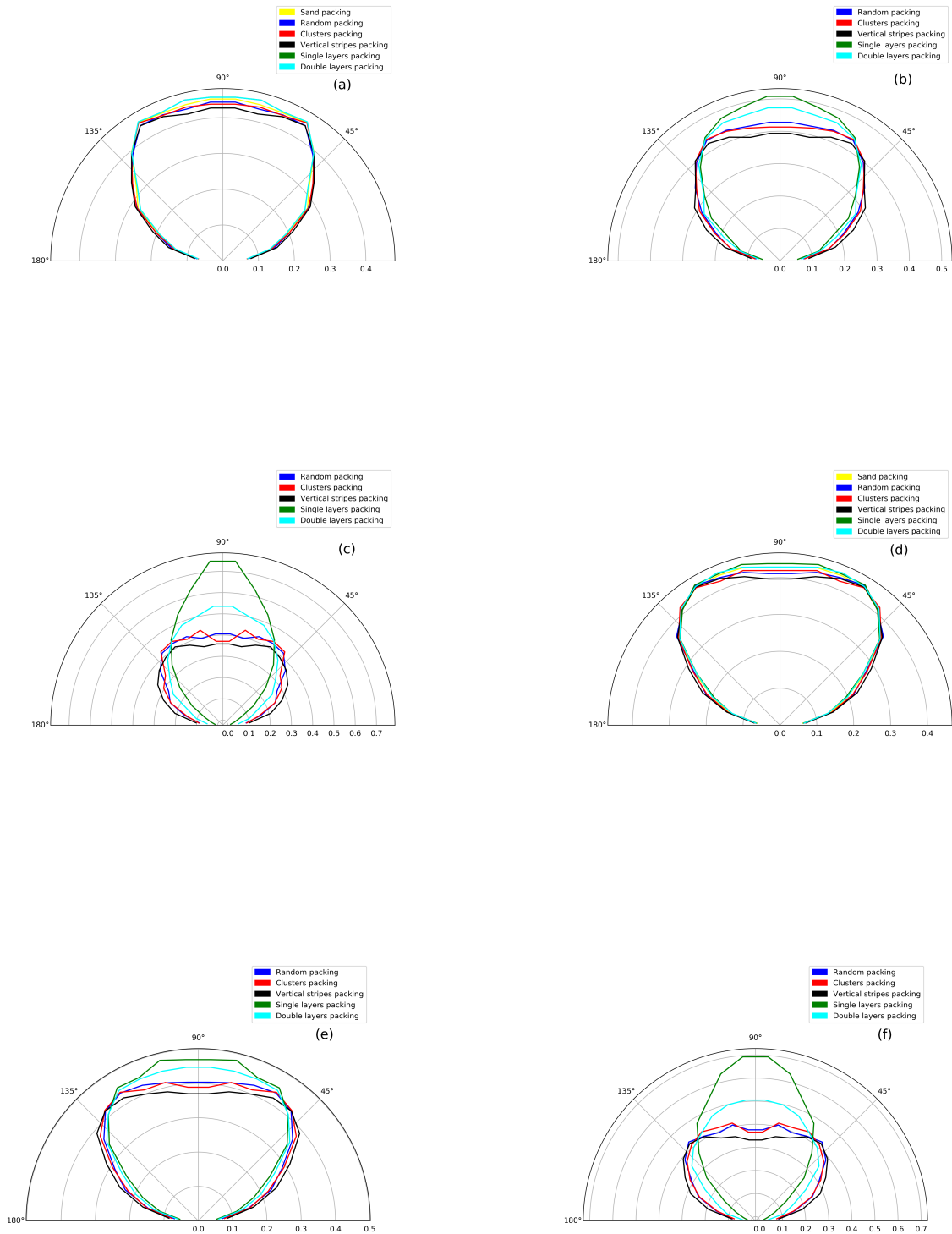
FIGURE 4.25. Sand-sand force orientation plots for all the mixture arrangements: (a) 10% RF dense packing, (b) 25% RF dense packing, (c) 50% RF dense packing, (d) 10% RF loose packing, (e) 25% RF loose packing, (f) 50% RF loose packing.

distribution of force chains. In other words, some contacts bear strong loads (strong contacts) and others bearing almost no load (weak contacts). Thus, a better insight can be obtained by studying the evolution of the strong contacts as can be found in some previous works [Radjai et al., 1999, Peters et al., 2005]. This will help in elaborating the effect of the mixing quality on the mechanical response of the sand-rubber mixtures.

The contacts having the intergranular force greater than the total average force can be categorized as the contacts carrying the strong forces or in other words; strong contacts. Thus, for each type of contact, if $F_{n,i} > \langle F_n \rangle$, then it can be categorized as a strong contact ($\langle F_n \rangle$ is defined in Section 4.5.2).

For simplicity purposes, the plots shown here in fig. 4.26 and 4.27 represent one mixture arrangement from each of the two families of packing responses observed. In other words, the plots in the figures are for random and double layers mixture arrangements. For comparison purposes, the plots for random and double layers packings have been shown side to side. Moreover, the plots have been shown for 10%, 25% and 50% rubber fractions.

It can be said that the strong contacts are the major contributors to the total forces or in other words, the maximum load (the force chains) is carried by the strong contacts. It is also true if the response of the packing is observed with the increasing rubber fraction. For 10% rubber fraction, there are more sand-sand contacts as compared to 50% rubber fraction in the case of any packing arrangement. If the two types of mixture arrangements are closely observed, then it can be visualized that for low rubber fraction, the force chains can primarily involve strong sand-sand contacts for both the packings. However, the magnitude of these contacts is larger in the case of random packings. In contrast, since the force chains percolate vertically throughout the packing, those within the double grain size layer packings have to involve the rubber grains as well. Consequently, their mechanical response is potentially different. As the rubber fraction increases, the differences between the two families weakens (refer fig. 4.26e and f and 4.27e and f). This can be easily explained, Since larger the rubber fraction, higher is the probability for the force chains to involve rubber grains. Consequently, even in the cases of random packings, the mechanical response is influenced by rubber grains like the double layers packings.

The plots in Fig. 4.26 and 4.27 clearly justify the influence of the different packing arrangements on the mechanical behavior of the sand-rubber packing. It can also be inferred from the results that the macroscopic response of the packings can be characterized as sand dependent or rubber dependent depending on the rubber fraction for all the types of mixture arrangements. This is found to be well in agreement with the available literature as well.[Perez et al., 2017]. The rubber-rubber type of contacts are the weakest among the three, still there is convergence of the two families of packing arrangements (*i.e.* on one hand cluster and random packings and, on the other hand, single and double layers packings) with the increasing rubber fraction. This suggests that the fraction of the rubber-rubber contacts participating in the strong force chains actually helps to stabilize the contact networks which is in agreement with the literature[Lee
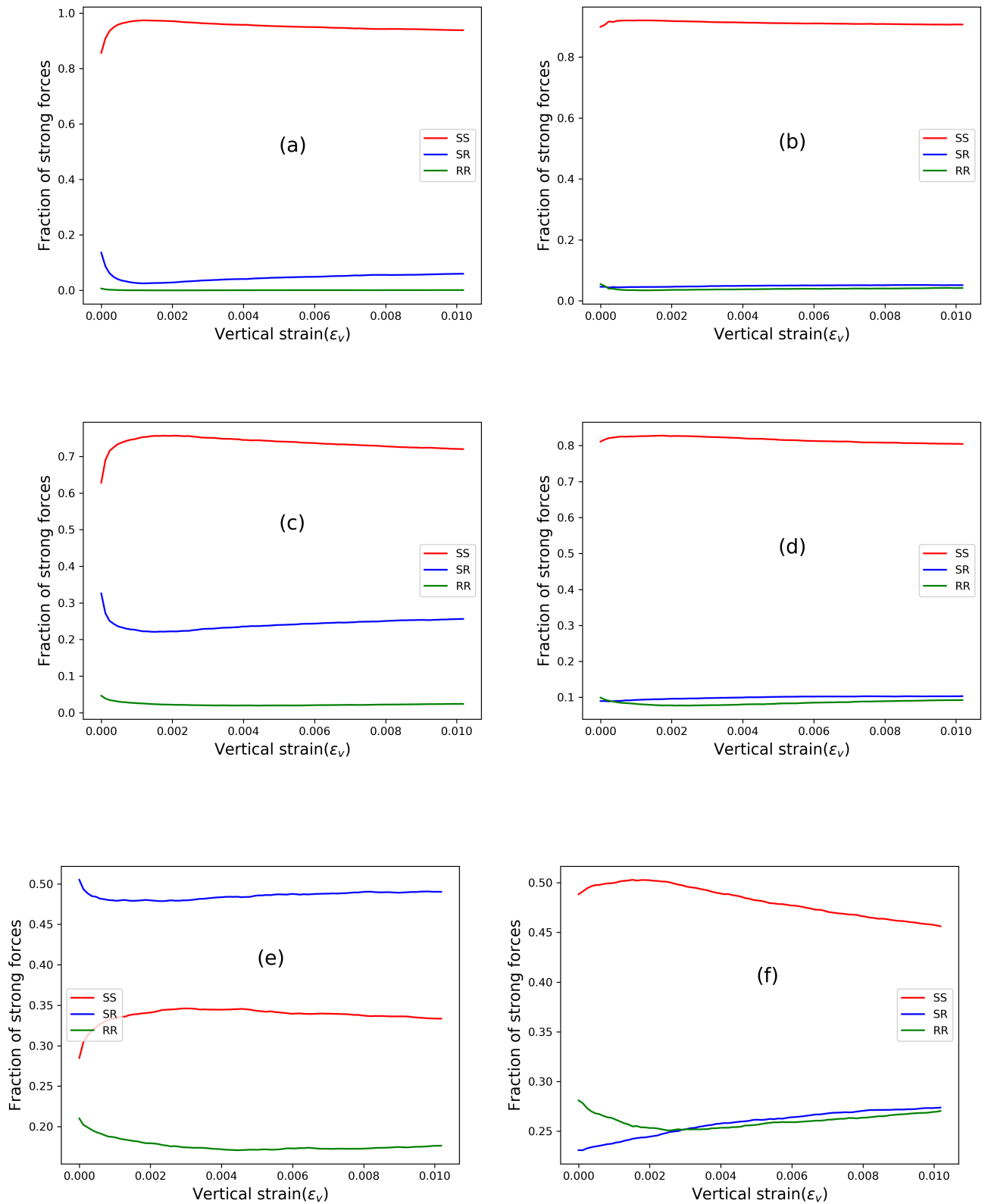
FIGURE 4.26. The proportion of strong contacts vs vertical strain for dense packings of: (a) 10% random arrangement, (b) 10% double layers arrangement, (c) 25% random arrangement, (d) 25% double layers arrangement, (e) 50% random arrangement and (f) 50% double layers arrangement.
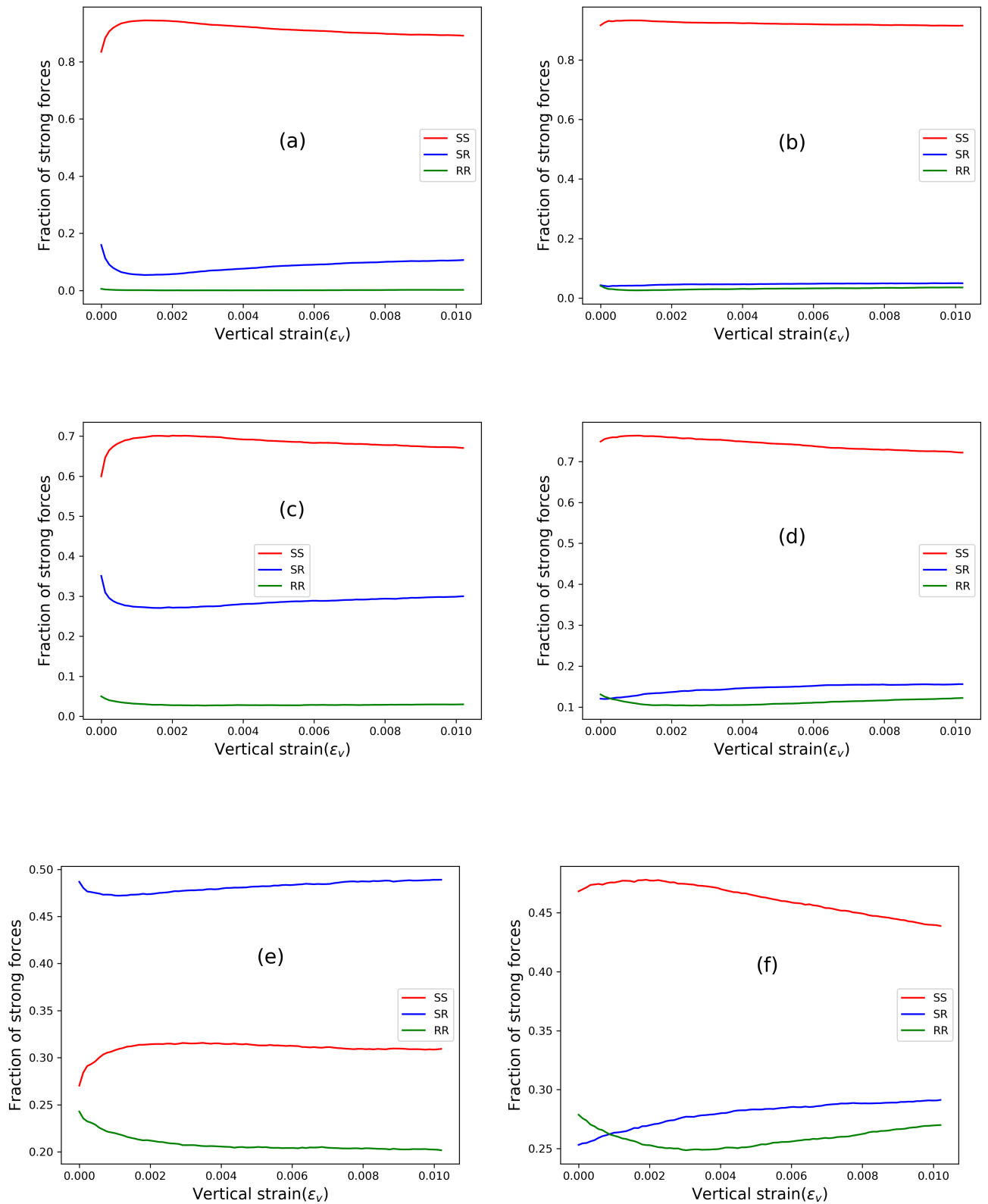
FIGURE 4.27. The proportion of strong contacts vs vertical strain for loose packings of: (a) 10% random arrangement, (b) 10% double layers arrangement, (c) 25% random arrangement, (d) 25% double layers arrangement, (e) 50% random arrangement and (f) 50% double layers arrangement.

et al., 2009].

4.6   Partial conclusion

Numerical simulations using DEM involving oedometric compression were performed on different sand-rubber mixtures. The primary objective was to analyze the effect of mixing quality on the mechanical response of the sand-rubber mixtures. Hence, different mixture arrangements were prepared with the varying rubber fraction and packing volume fraction and were tested using the DEM simulations. The macroscopic results put forward the mechanical response of the mixtures in loading and unloading phases. The macroscopic results point out the difference in the mixture arrangements for lower rubber fractions, thus suggesting the effect of the mixing quality. In order to support the macroscopic results, the grain contact parameters such as average contact force, force distribution, etc. were studied.

The quality of mixing does affect the mechanical response of the sand-rubber mixtures. However, with the increasing rubber fraction, this effect was observed to minimize. Moreover, for loose packings as well, the effect was observed to decrease with the increasing rubber fractions. Apart from the mixing quality, the initial granular arrangement is also an important factor, especially for lower rubber fractions as pointed out in Section 4.4.1.

The micromechanical parameters support this observation. It was observed, as expected that with the increasing rubber fraction, more rubber grains were involved in the force carrying networks. These increasing rubber grains liberate more sand contacts and act as stabilizers for the force carrying chains. This can be deduced from the strong contact force analysis performed.

An important point to be considered is that the experimental and the numerical results show a similar trend of the mechanical response. However, there are several parameters which the numerical model cannot take into account such as contact damages at higher stresses, imperfect spherical shape of the grains in the case of experiments, and deformability of rubber particles. Further, to reduce the computational time, the Young's modulus of elasticity values for sand and rubber used in the case of numerical simulations were very low as compared to the real values. Also, the value of the Young's modulus of elasticity for rubber was not measured experimentally and its characteristic range is rather large. Due to all these reasons, the magnitude of the stress and strain in case of numerical simulations is quite low as compared to that in the experiments. For this purpose, these results should be studied from a qualitative point of view and a direct quantitative comparison is not possible to be done. Nevertheless, the results show a good qualitative agreement and point out the importance of the mixing quality in sand-rubber mixtures. The effect of sand/rubber (S/R) size ratio was also studied. However, the initial void ratios of the packings obtained in DEM cannot be controlled precisely and this effect is more pronounced in the different size ratio packings. Thus, these results need improvement. But, the preliminary results have been presented in Appendix A.

INCORPORATE DEFORMATION IN DEM SIMULATIONS: A FIRST APPROACH

Summary

This Chapter introduces to a new numerical model wherein an effort has been made to include the effect of rubber grain deformation in the DEM simulations, thus enabling to study the mechanical response of sand-rubber mixtures at moderate strains. The model has been compared with the previous model, *i.e.* soft sphere approach in order to visualize the exact difference between the mechanical responses observed. This model is a part of a perspective for this study and is under continuous improvement.However, the first results observed were interesting and hence have been presented in this Chapter.

Contents

5.1   Introduction

Soft Contact Discrete Element Methods are a powerful tool to study statics and dynamics of granular materials [Richard and Taberlet, 2008]. In such methods, macroscopic material properties originate from a collective behavior of an assembly of grains (discrete elements) interacting with one another via forces. Although grains of different shapes can be treated, most of the studies deal with spherical-shaped grains.

In the soft contact DEM formulation, the grains are rigid bodies with deformation concentrated at the contact points. Yet, these methods are limited to non-deformable grains. One of the principle of this method is indeed that the forces applied on a grain are independent and that the properties of one of them do not influence the properties of the other forces. In other words, the contact model is purely local and pairwise. This assumption is very reasonable in the case of rigid particles but no more true for deformable particles (like rubber chips). In soft contact DEM approaches, two contacting grains overlap even if they are rigid. The overlaps, used to determine the normal forces, are assumed to be small enough to be neglected. In the case of deformable particles, the overlap might be important and thus non-negligible. The use of such a method and the corresponding results have already been presented in the previous Chapter.

Recently, there have been several successful attempts to use DEM in case of deformable particles. Brodu et al. [2015] have implemented a new non-local contact model in DEM by calculating the grain shape deformation according to analytical linear elasticity and correcting the grain overlap accordingly which potentially leads to the formation of new contacts. Rojek et al. [2018] propose a similar model in which, instead of calculating the deformation according to linear elasticity, they assume that the particles are deformed globally under the uniform internal stress. This new approach, called the deformable discrete element method (DDEM), has been described in detail numerically by Madan et al. [2019].

Another approach consists in discretizing the discrete elements with finite elements (e.g. [Onate and Rojek, 2004]). Grain deformability can also be taken into account by using other discretization methods for grains like the continuum-based Material Point Method (MPM) [Nezamabadi et al., 2017, Vu, Thi Lo et al., 2017] or the discrete-based Bonded Particle Method (BPM) [Dosta, Maksym et al., 2017, Nezamabadi et al., 2017]. The methods based on the discretization of grains are very powerful [Vu et al., 2019]. They can be used to simulate grains of arbitrary shapes and different deformation mechanisms assuming the elastic or plastic behavior of deformable grains. It is also possible to model the breakage of grains. These methods are interesting for studying significant deformation, but their computation cost is high which questions their use, in particular for (i) small to intermediate deformation, (ii) 3D systems and (iii) systems with a large number of grains.

In this study, the focus has been on the mixture of rigid grains with deformable (but incompressible grains) and a simple model has been presented that takes into account the deformable

nature of the incompressible grains up to intermediate deformation. It can be seen as an adaptation to rigid-deformable mixtures of the model proposed by Haustein et al. [2017] for a system of deformable grains. It is based on the expansion of the radii of the deformable spherical grains, depending on their overlap with their neighbors, so that the volumes of the grains are kept constant. Here, the final aim is to simulate sand-rubber mixtures under moderate strain. In the following sections, first the principle of the method will be presented and it will be explained how deformable - deformable and rigid - deformable interactions are taken into account. Then, a way to solve numerically the equations leading to the evolution of the radii of the deformable grains will be demonstrated. Further, some preliminary results obtained by implementing this model will also be presented.

It is important to note that this Chapter is a perspective of this thesis study. The results presented here are primitive and are under continuous improvement. For the same reason, quite a limited number of results have been presented here since the numerical simulations are still under improvement.

5.2 Principle

Although the method presented here is valid for any type of rigid- deformable mixtures of spherical grains, as long as the deformable spheres are incompressible, the interest of this study is sand-rubber mixtures. Consequently, 'sand grains' and 'rubber grains' have been defined in the model as rigid and non-compressible deformable grains, respectively.

Consider two rigid grains i (position $\overrightarrow{r}_i = (x_i, y_i, z_i)$, volume V_i and radius R_i) and j (position $\overrightarrow{r}_j = (x_j, y_j, z_j)$, volume V_j and radius R_j). In DEM, they can overlap slightly and the overlap is used to determine the normal force between them. Classically, a normal repulsive force, proportional to the overlap to a given power is applied. It has to be noted as well, that a tangential force is also applied to the contacting spheres, similar to as explained in Chapter 4. For rigid grains, the volume of the overlap, ϖ_{ij} is small enough to be neglected. Thus, the non-overlapping volumes of the grains i and j (respectively $\mathcal{V}_i = V_i - \varpi_{ij}$ and $\mathcal{V}_j = V_j - \varpi_{ij}$) are considered to be close to the volume of the grains: $\mathcal{V}_i \approx V_i$ and $\mathcal{V}_j \approx V_j$.

Consider a grain i which can be either a sand grain $\chi_i = s$ or a rubber grain $\chi_i = r$. As mentioned above, sand grains are non-deformable, their volume is assumed to be constant whatever the stress load. In contrast, the rubber grains are deformable (but incompressible).

Let us assume that if a rubber grain interacts with another grain, the volume of the overlap (which is not physical) has to be redistributed to modify the grain shape. The way the overlap is redistributed depends on the type of the grain involved in the interaction. Consequently, two types of interactions involving rubber grains that can be encountered in sand-rubber packings have been considered: sand-rubber and rubber-rubber interactions.

5.2.1 Sand - rubber interactions
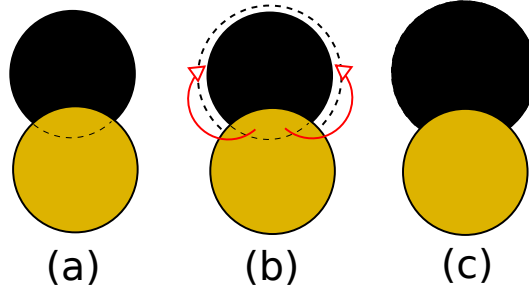
Figure 5.1: Schematic illustration of a deformable and incompressible grain (black) in contact with a rigid grain (yellow). In (a) the usual DEM-formulation is shown with an overlap between the two grains. In (b) the volume of the overlap is redistributed at the surface of the deformable grain resulting in an increased radius and overlapping-distance, and in (c) the changed shape of the spheres after redistribution has been shown.

Let us first consider a contact between a rubber particle (labelled i, position $\vec{r_i} = (x_i, yi, z_i)$ and radius R_i) and a sand particle (labelled j, position $\vec{r_j} = (x_j, y_j, z_j)$ and radius R_j). Due to low stiffness of the rubber, the overlap is potentially not negligible. Since rubber is not compressible, its volume is constant, so the volume of the overlap has to be redistributed. As mentioned above, it is assumed that the shape of the rubber grain is that of a 'virtual' sphere to which the shape of the overlap has been readjusted (see Fig. 5.1). Since the volume is constant, the diameter of the latter 'virtual' sphere evolves with the applied stress. Its virtual volume is given by,

$$\tilde{V}_i = \frac{4}{3}\pi\tilde{R}_i^3 = \frac{4}{3}\pi R_i^3 + \omega(\tilde{R}_i, R_j, \Delta_{ij}),$$

where $\Delta_{ij} = \sqrt{(x_i - x_j)^2 + (y_i - y_j)^2 + (z_i - z_j)^2}$ is the distance between the centers of the grains. Thus, its 'virtual' radius is,

$$\tilde{R}_i = R_i \left(1 + \frac{3}{4\pi}\frac{\omega(\tilde{R}_i, R_j, \Delta_{ij})}{R_i^3}\right)^{1/3}.$$

The overlapping volume of the two contacting spheres separated by the distance Δ_{ij} can be obtained straightforwardly by determining the contact plane and by adding the volumes of the caps:

$$\omega_{ij}(\tilde{R}_i, \tilde{R}_j, \Delta_{ij}) = \frac{\pi}{12}\frac{(\tilde{R}_i + R_j - \Delta_{ij})^2\left(\Delta_{ij}^2 + 2\Delta_{ij}(\tilde{R}_i + R_j) - 3(\tilde{R}_i^2 + R_j^2) + 6\tilde{R}_i R_j\right)}{\Delta_{ij}}. \tag{5.1}$$

5.2.2 Rubber - rubber interactions

As shown in the preceding section, in case of a sand-rubber interaction, the volume of the overlap is redistributed to the rubber grain. In the case of a rubber-rubber interaction, it has to be redistributed to the two interacting rubber grains. Let us consider two interacting
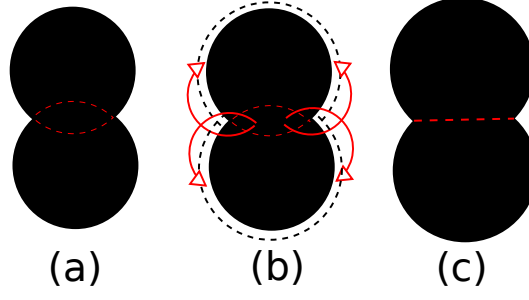
Figure 5.2: Schematic illustration of two incompressible, deformable grains in contact. In (a) the usual DEM-formulation is shown with an overlap between the two grains. In (b) the volume of the overlap is redistributed at the surface of the two grains resulting in an increased radius and overlapping-distance and in (c) the augmented shape of the grains after volume redistribution has been shown.

rubber grains. The equations of the two spheres are, $(x - x_i)^2 + (y - y_i)^2 + (z - z_i)^2 = R_i^2$ and $(x - x_j)^2 + (y - y_j)^2 + (z - z_j)^2 = R_j^2$ which, by combination, lead to the equation of the intersection plane given by,

$$\delta^2 - R_i^2 + R_j^2 - 2\left[(x_j - x_i)x + (y_j - y_i)y + (z_j - z_i)z\right] = 0,$$

with $\delta^2 = \left|\vec{r_j}\right|^2 - \left|\vec{r_i}\right|^2 = x_j^2 + y_j^2 + z_j^2 - x_i^2 - y_i^2 - z_i^2$. The distance between the center of the sphere i and the intersection plane is given by,

$$d_{M_i,\Delta} = \frac{\left|\delta^2 + R_i^2 - R_j^2 - 2\left[(x_j - x_i)x_i + (y_j - y_i)y_i + (z_j - z_i)z_i\right]\right|}{2\Delta_{ij}}.$$

The volume of the virtual deformed sphere should be the sum of the volume of the undeformed sphere and the volume of the spherical cap. With the height $h = \tilde{R}_i - d_{M_i/\Delta}$ of the cap, the radius of the undeformed sphere R_i, and the radius of the virtual sphere after deformation $\tilde{R}_i$, the volume of the spherical cap is then given by,

$$\psi_i(R_i, R_j, \tilde{R}_i, \vec{r}_i, \vec{r}_j) = \frac{\pi \left(\tilde{R}_i - d_{M_i/\Delta}\right)^2}{3}\left[3\tilde{R}_i - \tilde{R}_i + d_{M_i/\Delta}\right],$$

i.e.

$$\psi_i(R_i, R_j, \tilde{R}_i, \vec{r}_i, \vec{r}_j) = \frac{\pi \left(\tilde{R}_i - d_{M_i/\Delta}\right)^2}{3}\left[2\tilde{R}_i + d_{M_i/\Delta}\right],$$

A schematic for the rubber - rubber grain interaction has been shown in Fig. 5.2.

5.2.3 Generalization

To generalize the approach explained above, it can be considered that a grain, i, interacting with several neighbors is defined by their ensemble $\mathscr{C}_i$. In the following, the Kronecker symbol δ_{χ_i,χ_j} defined as $\delta_{ij} = 1$ if $\chi_i = \chi_j$ and $\delta_{ij} = 0$ if $\chi_i \neq \chi_j$ has been used.

The virtual volume of the rubber grain i is defined as,

$$\tilde{V}_i = \frac{4\pi}{3}\tilde{R}_i^3 \tag{5.2}$$

$$= \frac{4\pi}{3}R_i^3 + \sum_{j\in\mathscr{C}_i}\delta_{\chi_j,s}\varpi_{ij}(\tilde{R}_i,R_j,\Delta_{ij}) \tag{5.3}$$

$$+ \sum_{j\in\mathscr{C}_i}\delta_{\chi_j,r}\psi_i(\tilde{R}_i,\tilde{R}_j,\Delta_{ij}). \tag{5.4}$$

The virtual radius $\tilde{R}_i$ is given by,

$$\tilde{R}_i(t) = R_i\left[1 + \frac{3}{4\pi}\left(\delta_{\chi_i,r}\sum_{j\in\mathscr{C}_i}\frac{\varpi_{ij}(\tilde{R}_i,\tilde{R}_j,\Delta_{ij})}{R_i^3} + \sum_{j\in\mathscr{C}_i}\delta_{\chi_j,r}\psi_i(\tilde{R}_i,R_j,\Delta_{ij})\right)\right]^{1/3}. \tag{5.5}$$

Note that, the latter equation can also be written as following, in a more compact way:

$$\tilde{R}_i(t) = R_i\left(\frac{\tilde{V}_i}{V_i}\right)^{1/3}. \tag{5.6}$$

Consequently, if i is a sand grain, its size remains constant whatever the nature of its contacts. In case of the sand-rubber contact, the volume of the overlap is used to modify the shape of the rubber grains and in the case of a rubber-rubber contact, the volume of the overlap is divided by two as expected. It should be pointed out here that the volume of the overlap corresponding to an interaction between the two grains is the sum of the volume of grain i overlapped by grains j and the volume of grain j overlapped by the grain i.

5.3 Newton-Raphson Method

The Newton-Raphson method is an iterative method which allows to find roots of real-valued function, *e.g.* solutions of an equation $f(x) = 0$. It starts with an initial guess x_0 for a root of the function f. If f can be derived, the $x_1 = x_0 - f(x_0)/f'(x_0)$ is a better approximation of the root. Note that, geometrically $(x_1, 0)$ is the intersection of the $x-$axis and the tangent of the graph of f at $(x_0, f(x_0))$. The process is iteratively repeated, *i.e.* $x_{n+1} = x_n - f(x_n)/f'(x_n)$ until a sufficient accurate value is reached.

In this study, the equation to solve is,

$$0 = f(\tilde{R}_i) = -\frac{4\pi}{3}\tilde{R}_i^3 + \frac{4\pi}{3}R_i^3 + \delta_{\chi_i,s}\sum_{j\in\mathscr{C}_i}\varpi_{ij}(\tilde{R}_i,R_j,\Delta_{ij}) + \delta_{\chi_i,r}\sum_{j\in\mathscr{C}_i}\psi_{ij}(\tilde{R}_i,R_j,\Delta_{ij}). \tag{5.7}$$

We have,

$$f'(\tilde{R}_i) = -4\pi\tilde{R}_i^2 + \delta_{\chi_i,s}\sum_{j\in\mathscr{C}_i}\varpi'_{ij}(\tilde{R}_i,R_j,\Delta_{ij}) + \delta_{\chi_i,r}\sum_{j\in\mathscr{C}_i}\psi'_{ij}(\tilde{R}_i,R_j,\Delta_{ij}).$$

with

$$\psi'_{ij}(\tilde{R}_i,R_j,\Delta_{ij}) = 2\pi\tilde{R}_i\left(\tilde{R}_i - d_{M_i/\Delta}\right),$$

and

$$\varpi'_{ij}(\tilde{R}_i,R_j,\Delta_{ij}) = \frac{\pi}{\Delta_{ij}}\left(-\tilde{R}_i^3 + 2\Delta_{ij}\tilde{R}_i^2 + \tilde{R}_i\left(R_j^2 - \Delta_{ij}^2\right)\right).$$

146

The initial guess for $\tilde{R}_i$ is the radius at the previous time step. The convergence is found to be very fast (a few interactions) which is expected, since the time step used in DEM simulations is very small and, consequently, so is the modification of the radii of the incompressible and deformable grains.

5.4 Methodology

5.4.1 Preparation of initial packings

Particle size distribution (PSD) of the simulated sand is a Gaussian with a mean equal to 1.8mm and a variance equal to 0.0333 mm^2. The rubber particles have the same particle size distribution. The vessel used is a frictional cylinder with the friction coefficient of 0.5. Initially, the sand grains are poured in the cylinder until a stable state is reached. Then some of the sand grains are randomly replaced by rubber grains of the same size at the same position. Then the system is relaxed to erase the perturbations due to the aforementioned replacements and reach a new steady state. Obviously the number of sand particles replaced by the rubber ones depend on the chosen rubber fraction.

The procedure adopted for the assembly of the initial packing was similar to that mentioned in Section 4.2.1. However, the dimensions of the cylinder used in this study are larger than the previous one in Chapter 4. The radius of the cylinder used is 20mm and the height is nearly 38mm. Moreover, the grains used were larger and have a mean diameter in the range of 1.6mm - 2mm. The number of grains used in this study are 12000. In terms of mixture arrangements, only random packing arrangements were prepared and have been studied.

5.4.2 Oedometric compression: effect of the grain deformation

In order to be coherent with the ongoing study, the mechanical response of the these prepared packings under oedometer compression was studied. The methodology adopted is similar to the one described in Section 4.2.3. However, in case of the numerical simulations including the effect of the rubber grain deformation, the new radius calculated as per the aforementioned model was updated and considered in the calculations. The results will thus be discussed as a comparison of the two models, *i.e.* the new model including the effect of rubber grain deformation and the previous model wherein no deformation is considered. It can be imagined that higher the rubber fraction, higher can the effect of rubber grain deformation be observed. Hence, the results further will be discussed for 20% and 50% rubber fraction.

Since this model has been presented as a perspective, the simulations were performed starting with the study of the mechanical response of the packings only under loading conditions. However, numerical simulations are currently in progress in order to investigate the behavior of the packings under both loading and unloading conditions. The results will be discussed in the form of macroscopic and microscopic scale responses.

5.5 Macroscopic behavior: Stress-strain response under loading

The stress-strain response of the packings under loading has been studied. Since in the case of packings involving the effect of grain deformation, it is possible to study the response at higher strains, hence, the results here have been studied up to a vertical strain of 0.12. For
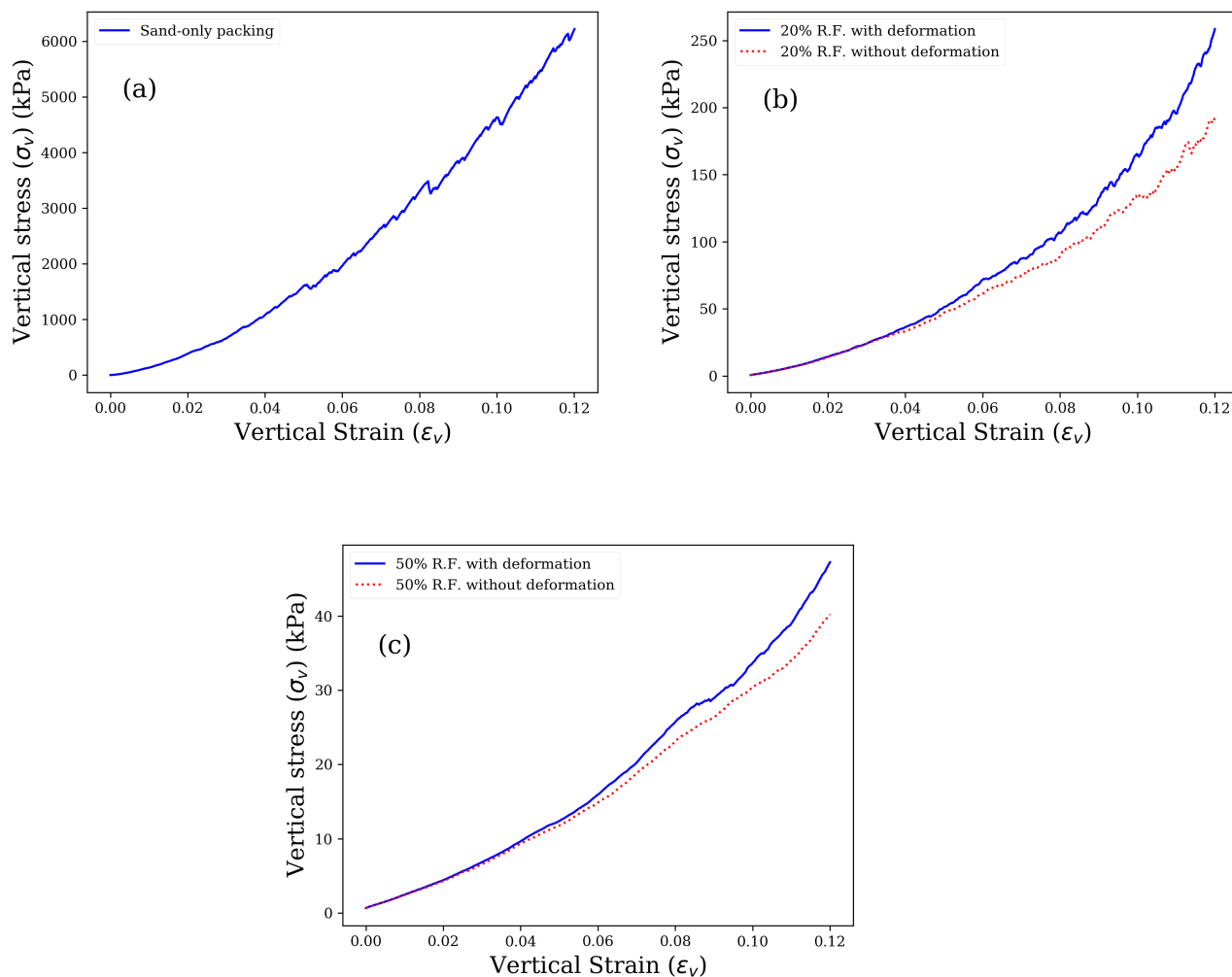
FIGURE 5.3. Vertical stress vs vertical strain plots for (a) Sand-only packing, (b) 20% rubber fraction packing for both models and (c) 50% rubber fraction packing for both models.

a comparison with the non-deformation model, the results have been studied till the same level of strain. However, it is important to note that the response of the packings which do not consider the effect of deformation is an artifact above the strain level of 0.01. And hence, the difference observed in the mechanical response between these two packings (one involving deformation effect and other with non-deformation effect) can be considered as an error in the calculation due to the non-consideration of the deformation of the rubber grains. The difference

between the two models can be observed in Fig. 5.3. It is interesting to note that for small level of strain, there is no visible difference between the two cases for both 20% as well as 50% rubber fraction packings. The two curves start separating nearly at the strain level of 0.06. This in turn signifies the inclusion of the deformation effect of the rubber grains.

The magnitude of the stress can be observed to be higher than in the previous case discussed in Chapter 4. This is obvious, since the size of the system being studied itself is larger than the previous case. Also, one can observe that for a given strain above 0.06 the stress obtained in the deformable case is larger than that obtained in the non-deformable case. This is expected as in the former case, the radius of an overlapped rubber grain increases and so does the force applied on it. For a given strain, if the magnitude of the difference between the stress obtained for the deformable and non-deformable cases is compared, then this difference is observed to be higher for $x_R = 20\%$ than for $x_R = 50\%$. This point will be explained in the next section by comparing the grain deformation in both the cases. Thus, it can be interesting to verify the grain-scale behavior of the packings which will in turn help to better understand the global mechanical response.

5.6 Grain-scale properties

Since the new model incorporates the rubber grain deformation, it is interesting to study the variation of this grain deformation with the global strain level. Moreover, the average contact forces and the normalized force distribution plots can help to quantify the macroscopic response. These quantities have been further discussed in the following.

5.6.1 Grain scale deformation

Since the new model explained in this Chapter considers the effect of the rubber grain deformation, it was interesting to quantify this deformation with respect to the global vertical strain (ϵ_v). Consequently, the rubber grain deformation was calculated for all the rubber particles for a given strain value using,

$$\delta_r = \frac{R - R_0}{R_0}, \tag{5.8}$$

where, δ_r is the rubber grain deformation, R is the new calculated radius of the rubber grain due to the volume redistribution and R_0 is the initial radius of the grain. Thus, the mean of the rubber grain deformation over all the rubber grains at a given strain value has been plotted against the global vertical strain in Fig. 5.4. Moreover, a line for 0% deformation has also been shown in Fig. 5.4 representing the non-deformable model.

A first observation from the plot shown in Fig. 5.4(a) is the striking difference between the deformation magnitudes for 20% and 50% rubber fraction packings. For a given strain value, the rubber grain deformation is higher for 20% rubber fraction packing than 50% packing. This can be explained with the help of a spring network analogy. Consider a network of springs
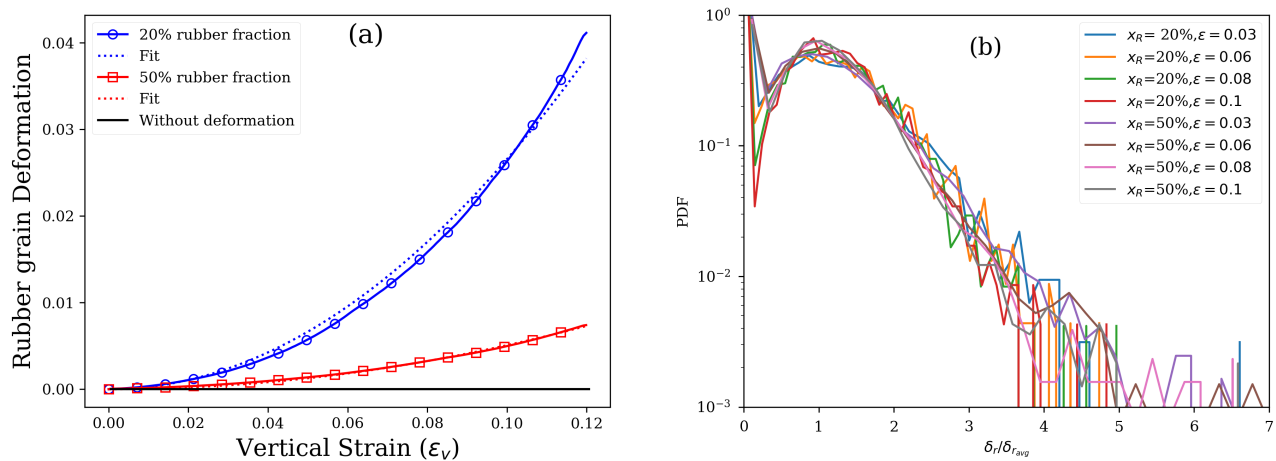
FIGURE 5.4. Plot for (a) rubber grain deformation vs global vertical strain (ϵ_v) for the packings of 20% and 50% rubber fraction which include the effect of rubber grain deformation, (b) Normalized distribution of the rubber grain deformation at different strain levels for both 20% and 50% rubber fractions.

Rubber fraction (%)	Fit parameter a
20	2.657
50	0.508

Table 5.1: Fit parameters for the rubber grain deformation plot of 20% and 50% rubber fraction packings.

and undeformable rods, with the springs placed randomly in the network. For a given level of strain, the lower the number of springs in the network, the higher will they deform due to an externally applied load. In case of the network with higher number of springs, the same load will be distributed over a larger number of springs and thus the deformation level will be smaller than in the previous case. Similarly, the rubber grains in the case of 20% rubber fraction being lower in number will deform more than in the case of 50% rubber fraction and hence a higher rubber grain deformation value is observed in the case of 20% rubber fraction. Obviously, this has to be true for any given level of strain and rubber fraction value.

A parabolic fit was used in order to fit these curves and the fits have been shown in Fig. 5.4(a). The fit parameters have been reported in Table 5.1. A good fitting in turn suggests an existence of the same relation with the varying rubber fraction and strain level as explained above.

However, as stated before as well, the results being discussed here are primitive and are under continuous improvement. Hence, more numerical simulations need to be run for different rubber fractions in order to quantify the fit parameters in a better way. For the same reason, the fit parameters have not been presented in a relation with the rubber fraction. Nevertheless, the first results show the significance of the rubber grain deformation and its inclusion using the model.

The distribution of $\delta_r/\delta_{r,avg}$ (see Fig. 5.4(b)) was also studied. It is surprising to observe that this distribution is independent of both the rubber fraction and the strain level. The shape of the distribution is also similar to that of the normal force between grains (refer section 5.6.3), *i.e.* an exponential tail for $\delta_r/\delta_{r,avg} \gtrsim 1$. This can be explained by the fact that normal forces have been calculated using the overlap which depends on the effective radius of the rubber particles.

5.6.2 Average contact forces
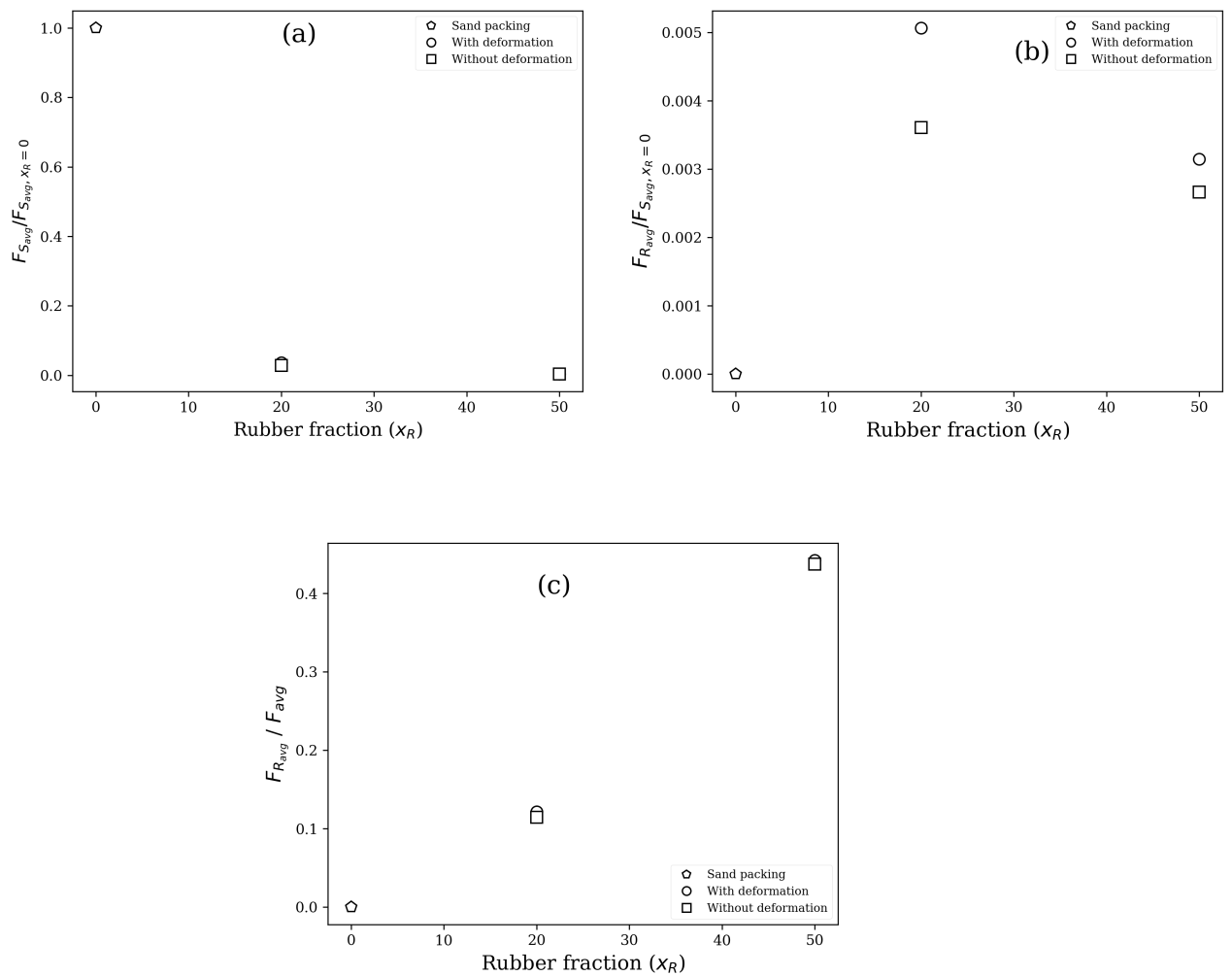
FIGURE 5.5. Average normal contact force for 0%, 20% and 50% rubber fraction packings: (a) ($F_{S_{avg}}$) and (b) ($F_{R_{avg}}$), (c) ($F_{R_{avg}}/F_{avg}$) vs rubber fraction for all the packings.

As in the previous Chapter (Chapter 4), the average contact forces for the rubber and sand grains were calculated and have been presented here. For better quantification of the model used, the results shown in Fig. 5.5 have been shown for both the model including the effect of

deformation and the one not including the deformation effect along with the sand-only packing. For simplicity and better understanding, all these results have been shown for only one step of compression (ϵ_v= 0.1). It is obvious from Fig. 5.5(a), that the average sand forces for the packings using the two models is almost the same. However, a difference can be seen in the value of the average rubber contact force ($F_{R_{avg}}$) for the two different models. It is higher for the case considering the effect of rubber grain deformation for both 20% and 50% rubber fraction packings. This is interesting to observe since it signifies that the contribution of the rubber contact force towards the total force is higher in the case of the packings which consider the effect of rubber grain deformation. This, in turn suggests that the rubber grains are involved in the major force carrying networks.

Fig. 5.5(c) shows the proportion of the average rubber contact force to the total average force ($F_{R_{avg}}/F_{avg}$). This plot is not linear, so the average rubber force is not proportional to x_R indicating the presence of correlations. For 20% and 50% rubber fraction packings, the proportion of average rubber forces are below the respective expected values as shown in Fig. 5.5(c). Also even for x_R = 50%, the sand particles remain the major force carriers. It should be pointed out that a slight difference in the proportion can be observed for the two different packings of same rubber fraction considering and not considering the rubber grain deformation. The average contact force gives an idea of the contribution of the sand and the rubber grains individually irrespective of the type of the contacting particles. However, to better analyze, the contacts were further divided into sand-sand, sand-rubber and rubber-rubber depending on the type of the interacting grains. The following section presents the normalized force distribution with a consideration of the average contact forces for these different types of contacts.

5.6.3 Normalized force distribution

The force distribution plots have been shown in Fig. 5.6. The plots have been normalized with respect to the average normal forces. Hence, if $F_{n,i}$ is the normal force for each contact, i, then

$$\langle F_n \rangle = \frac{1}{N_c} \sum_{n=i}^{N_c} F_{n,i},$$

where, N_c is the total number of contacts and $\langle F_n \rangle$ is the total average normal force.

The plot for the average normal force ($F_{n_{avg}}$) vs grain deformation is shown in the inset of the force distribution plots. The grain deformation is the overlap between the contacting grains, *i.e.* δ. Again, for simplicity and better analysis, the plots have been shown here for one stage of compression (ϵ_v=0.1), similar to the average contact forces. The plots here have been shown for the two cases of inclusion and non-inclusion of rubber grain deformation for both 20% and 50% rubber fractions. Fig. 5.6(a) and (b) compare the two models for 20% rubber fraction packings. A significant change cannot be observed for 20% rubber fraction packings between the two cases. However, a difference in the magnitude of the average normal force ($F_{n_{avg}}$) can be observed. This is true in the case of 50% rubber fraction packing as well. However, as explained
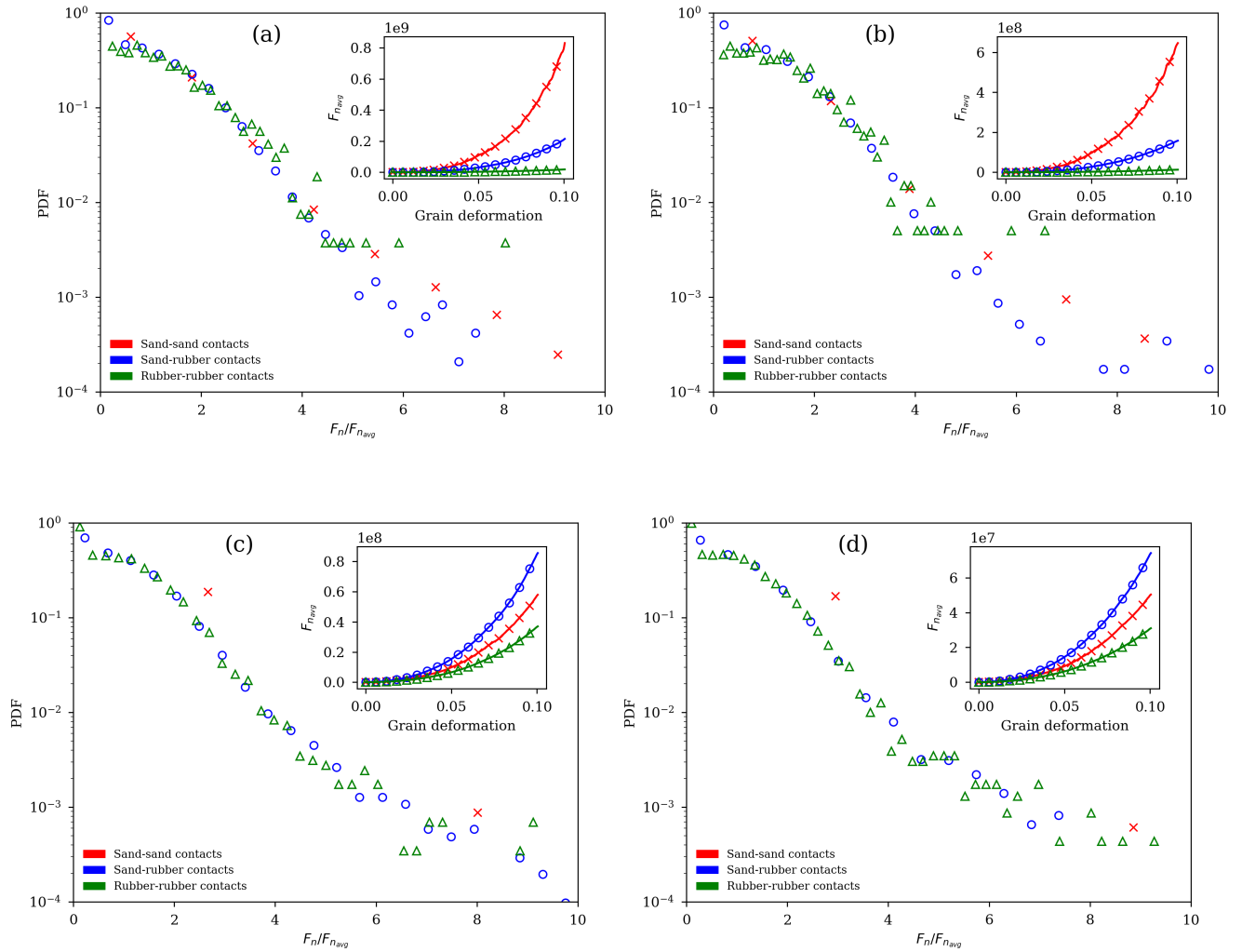
FIGURE 5.6. PDF for the normalized average contact forces for sand-sand, sand-rubber and rubber-rubber contacts of (a) 20% rubber fraction with deformation packing, (b) 20% rubber fraction without deformation packing, (c) 50% rubber fraction with deformation packing and (d) 50% rubber fraction without deformation packing. In the inset plot: Average sand-sand, sand-rubber and rubber-rubber contact forces vs grain deformation.

in Chapter 4, the inset, *i.e.* ($F_{n_{avg}}$) plot can help in the comparison of these packings. It is evident, like explained also in the previous Section, that the magnitude of the average contact forces is higher in the case of packings which include the effect of rubber grain deformation than the packings which do not consider the effect of rubber grain deformation.

5.7   Partial perspectives

As stated at the beginning of this Chapter, the numerical simulations using the model which considers the effect of the rubber grain deformation are still in the primitive phase. Although the model is well implemented, the simulations itself need an improvement for better quantification of the results obtained. Nevertheless, the preliminary results presented above are interesting and signify to an extent the capability of the model to include the effect of the rubber grain deformation and its effect on the global mechanical response of sand-rubber mixtures.

To better quantify the results presented, it is important that rigorous simulations be carried out for all the rubber fractions in the range of 10% - 50% as done in the case of Chapter 4. Moreover, the effect of the geometrical arrangements can be an important parameter to be quantified since the inclusion of rubber grain deformation may significantly vary the magnitude of the difference between the mixture arrangements such as random, clusters and layers packings. The characterization of the response of the packings under unloading conditions needs to be studied. The simulations for the unloading conditions of the sand-rubber mixtures are currently in progress and will be analyzed in the near future.

CONCLUSION AND PERSPECTIVES

The amount of waste tires at the landfill sites is increasing with the day and it is extremely important to implement multiple sustainable solutions to reduce this waste. There are already good solutions available to recycle this waste rubber and reuse it. One such solution is to convert the recycled rubber into powdered/ shredded form and mix it with soil for different geotechnical applications such as backfill of the retaining structures, highway embankments and reinforced soil structures. Such sand-rubber mixtures have already been under research for the last decade and their use seems to be promising. On the other hand, there are many problems which still need to be answered. One of the unanswered issues has been the segregation between sand and rubber in case of such mixtures and its effect on their mechanical response. In this study, an effort has been done in order to investigate the segregation of sand and rubber and in turn analyze the effect of the mixing quality on the mechanical response of such sand-rubber mixtures.

The segregation analysis between sand and rubber was done mainly for two conditions, *viz.* during the mixing phase and under vertical taps using a vibrating shaker. The process was followed by solidifying the final mixture at the end of the aforementioned conditions with the help of a gel. Further, it was cut into slices and images were captured. An image analysis framework was used to analyze the segregation between sand and rubber. It was observed that the segregation existed even after the mixing phase (without being subjected to the vertical taps). The rubber grains exhibited a tendency to form clusters and segregate during the mixing phase. After being subjected to the vertical taps, the mixtures segregated further. However, no vertical profile for segregation was observed. The pattern of segregation was more in the form of clusters of rubber and sand. Moreover, the segregation was observed close to the walls of the mixture container. With the addition of water during the mixing phase, the tendency of segregation reduced. Even when the mixtures were submitted to vertical taps, they did not segregate as in the previous cases. Although segregation was clearly visible, the type of study undertaken was quite complex and it was difficult to define the mechanism for segregation. In the future, it can be interesting to simulate the same experiments performed with the help of numerical simulations using Discrete Element Method (DEM). Further, it can also be interesting to conduct the experiments for smaller as well as larger system sizes. However, an important conclusion concerning the presence of segregation in such mixtures still serves as an interesting result.

Further, it was important to analyze the mechanical response of such mixtures and for this purpose, oedometer compression experiments were performed. The response of the sand-rubber mixtures was studied as a function of the varying initial void ratio, rubber volume fraction, sand/rubber size ratio and finally the mixture arrangements. An interesting phenomena of the combination of elastic and plastic behaviors was observed and characterized in these experiments. Further, the mechanical response of the mixtures was observed to be lying in the regimens of sand-dependent or rubber-dependent depending upon the rubber volume fraction. For rubber volume fractions up to 20%, the effect of rubber was observed to be minimal. However, with the increasing rubber fraction, the behavior of the mixtures was found to deviate from sand-dependent to rubber-dependent. It was also noted that a uniform distribution of the rubber grains throughout the mixture sample caused the rubber grains to better stabilize the major force-carrying chains consisting of sand grains. Some mixture arrangements were prepared and tested in order to verify the effect of the mixture quality on their mechanical response. It was noteworthy that the effect of the mixing quality was very high for rubber fractions up to 25%, whereas, further it decreased and for 50% rubber fraction, it was noted to be the lowest. This, in turn confirmed the presence of the effect of mixture quality on their mechanical response and hence, it was decided to better understand it with the help of numerical tools.

The mechanical response of sand-rubber mixtures under oedometer compression was studied using Discrete Element Method (DEM). A similar analysis as in the case of experiments was conducted in these simulations. Since DEM was used for this study, it is important to note that the Young's modulus of elasticity for sand and rubber defined was very low as compared to their real values and hence, the results obtained in the experiments have been compared qualitatively with the numerical results. Nevertheless, the results of the DEM simulations were in good qualitative agreement with the experimental results and they pointed out as well, the effect of mixing quality on the mechanical response of sand-rubber mixtures. The mixtures with lower rubber fraction (nearly upto 25%) were found to be more sensitive to the mixing quality whereas, mixing had no effect for higher rubber volume fractions. In general, the effect of mixing quality was observed to be less on the loose sand-rubber mixtures (packings with higher initial void ratio) than the corresponding dense packings. With the DEM simulations, it was possible to analyze certain data at the grain-scale such as contact forces, force distribution, strong and weak contact forces, etc. which enabled to better characterize the effect of mixing observed at the macroscopic scale.

Since the DEM simulations were found to be effective in characterizing the mechanical response of sand-rubber mixtures, a model was developed in order to include the rubber deformation using DEM and thus study a real response of such mixtures. The idea behind this model was that the volume of the overlap between the contacting sand and rubber grains during their interaction, was redistributed to the corresponding rubber grain. The preliminary results obtained by implementing this model were found to show a notable difference in the

inclusion of the response of the rubber grains than in the previous case. These preliminary results seem to be promising and further development of this model can help in the better understanding of the mechanical response of such soft-rigid grain mixtures.
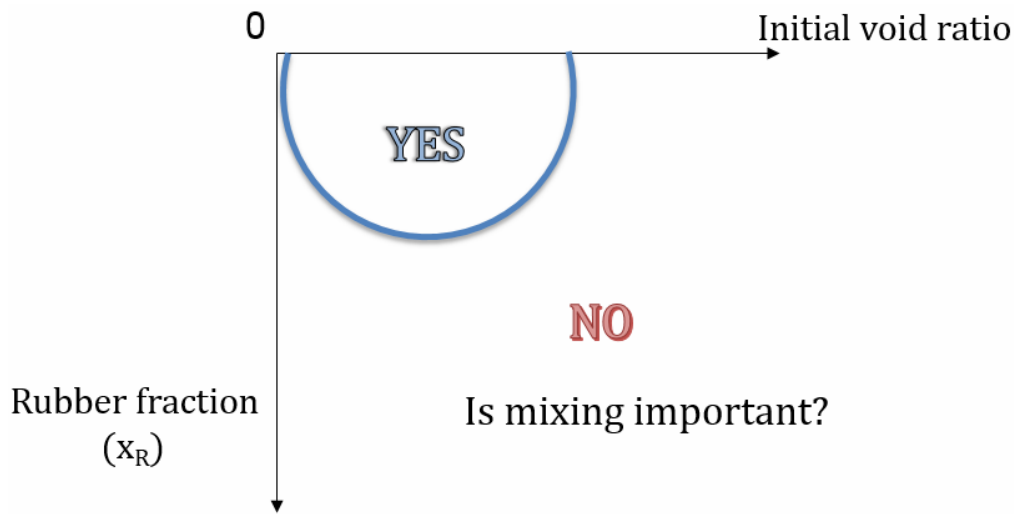
FIGURE C. Phase diagram showing the importance of mixing with respect to rubber fraction and initial void ratio.

The importance of mixing is the question which still remains to be answered in the case of sand rubber mixtures. It is quite difficult to obtain a perfect mixture if we consider the factors involved in the process such as time, operating costs, energy expenditure, etc. So, a further question arises whether it is worth to obtain a perfect mixture. The importance of mixing is dependent on the specific application for which the sand-rubber mixtures are to be used. From the results discussed before, it is evident that mixing is important for dense packing, especially for lower rubber fractions. With the increasing rubber fractions, mixing loses its importance. In real conditions, the maximum pressure at the point of application of the sand-rubber mixtures will be known. Consequently, if the application pressure is low, then mixing might not be important and hence,

1. higher rubber fraction will be used in order to help recycle more number of waste used tires (which is the main objective) and

2. preferably a loose packing will be used since the geometrical arrangements lose their importance.

Thus, the simplest way to obtain the resulting sand-rubber mixtures would be layers of sand and rubber. On the other hand, if the application pressure is high, then mixing will be important but it will not be necessary to achieve an extremely perfect mixture (clearly suggested by imperfect packing like clusters). Thus,

1. lower rubber fraction will be used in such cases and

2. preferably a dense packing.

A phase diagram shown in Fig. C can be considered as a preliminary basis for deciding the importance of mixing in case of sand-rubber mixtures.

As a future work, an effort can be made to prepare the sand-rubber mixtures as done in this study and analyze their mechanical response using other conventional experiments such as triaxial tests, direct shear tests or even by using a K_0 oedometer test in order to measure their mechanical response under shear. In this study, an effort was made to hypothesize the time-dependent behavior of such mixtures. Rubber is a material sensitive to time. Hence, the cyclic loading and unloading tests of such mixtures can help to shed light on their liquefaction properties and thus help in investigating their time-dependent behavior in a much better way. In terms of numerical simulations, the model developed at the end of this study, presented in Chapter 5 can be used to analyze the mechanical response of the different mixing arrangements. A detailed and rigorous study is ongoing using this model in order to better quantify the performance of the model in terms of the mechanical response of the mixtures.

An effort was made to quantify the effect of sand/ rubber (S/R) size ratio using the DEM simulations. However, in case of DEM, it is not easy to control the initial void ratio and it was found that for different size ratios, the initial void ratios were different and thus the results obtained were not found to be coherent with the experimental results. This can also be improved and thus the difference in the size be quantified using DEM.

As explained in the manuscript classical DEM is limited to very small grain deformation. In Chapter 5, a new method allowing to reach larger strains was introduced. To obtain even larger strains, combined FEM-DEM studies have to be implemented.

A real-time application of such mixtures, *e.g.* retaining wall can be investigated and it is important to develop methodologies towards the constitutive law in order to better analyze such a case.

As mentioned before as well, a better analysis of segregation between sand and rubber can be done by simulating similar experiments using DEM and also by performing experiments for larger and smaller system sizes.

From an environmental point of view, it can be imagined that the addition of rubber to soil for real-time applications may cause leaching problems. This is another perspective aspect which will require new skills.

In a gist, the domain of sand-rubber mixtures is so wide that there are still a lot of interesting aspects to be unearthed.

APPENDIX A

Effect of sand/rubber size ratio using Discrete Element Method (DEM)

The effect of sand/rubber size ratio on the mechanical response of sand-rubber mixtures was tested along with the other parameters already presented in Chapter 4. The sand/rubber (S/R) size ratios studied were 0.5, 1, 1.5 and 2. Since the packings to be studied were polydisperse, it was important to modify certain initial parameters for the DEM simulations. The most important parameter varied was the cell size. The cell size for defining the positions of the grains had to be modified with respect to the biggest size of the particle. Consequently, it changed with the size ratio. If it had been unchanged, it would have caused a greater overlap during the interaction of the particles and thus the simulations would not have worked.

The second important parameter varied was the rubber volume fraction. Since the effect of rubber volume fraction was already justified, the rubber volume fractions chosen to analyze the effect of sand/rubber size ratio were 10%, 25% and 50%. There was an option to define this percentage either on the basis of number fraction of the rubber grains or the volume fraction. Since all the previous results have been studied in the form of volume fraction of the rubber grains, it was decided to study the same. This was an important parameter since it would decide the total number of grains inside the cylinder. However, for this purpose, two parameters had to be fixed, *viz.* height of the packing and the packing volume fraction (packing compacity). A simple relation for the packing volume fraction can be given by,

$$\phi = \frac{V_{grains}}{V_{cyl}}, \tag{A.1}$$

where, ϕ is the packing volume fraction, V_{grains} is the volume occupied by the grains and V_{cyl} is the volume of the cylinder. Hence,

$$\phi = \frac{\Sigma(4/3\pi R_i^3)}{\pi R_{cyl}^2 h}, \tag{A.2}$$

where, R_i is the radius of the grains, R_{cyl} is the radius of the cylinder and h is the height of the cylinder. Since there are two types of grains, *i.e.* sand and rubber, the equation hence becomes,

$$\phi = \frac{4/3(R_s^3 N_s + R_r^3 N_r)}{R_{cyl}^2 h}, \tag{A.3}$$

So, as mentioned before, the two parameters important to be fixed were ϕ and h. Consequently, ϕ was fixed to be 0.6 and h was fixed as 20mm and thus the number of sand and rubber grains were defined. Fig. A.1 shows the snapshots of the initial packings of 50% rubber volume fraction for different sand/rubber (S/R) size ratios. However, in the DEM simulations, it was difficult to

(a)   (b)   (c)   (d)
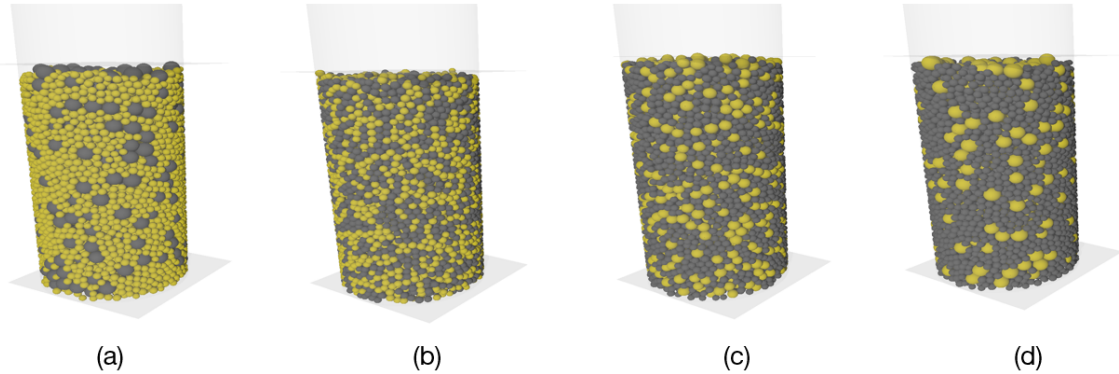
Figure A.1: Snapshots of the initial packings of sand-rubber mixtures for 50% rubber volume fraction of (a) S/R= 0.5, (b) S/R= 1, (c) S/R= 1.5 and (d) S/R= 2.

precisely control the void ratio/ packing volume fraction for these initial packings. Hence, the corresponding initial packings obtained were found to have varying initial void ratios. Just as an example, for 10% rubber fraction, the initial void ratios for the packings were 0.664, 0.721, 0.7007 and 0.6474 for S/R size ratio of 0.5, 1, 1.5 and 2 respectively. Thus, it was not possible to have a direct comparison for the mechanical response of these packings. Nevertheless, a direct comparison has been shown for all the size ratios in Fig. A.2.

It can further be seen in the plots, especially for 10% rubber fraction, the packings appear to be very loose and thus the curves start with a convex shape and then near the strain of 0.01, they begin to become concave in shape. In other words, the relative variation of stress is slower than that of the strain. This is similar to the phenomena observed in the case of lower rubber fractions of loose packings in Chapter 4.

A definite trend of the curves with the varying size ratios is difficult to be described here due to the different problems mentioned before. Moreover, the results at the grain-scale level were not analyzed for the same reason. Thus, as a perspective of this work, in order to check for the effect of size ratio on the mechanical response of the packings using DEM, a precise control method for the initial void ratios of these packings needs to be established and only then can the results be analyzed.
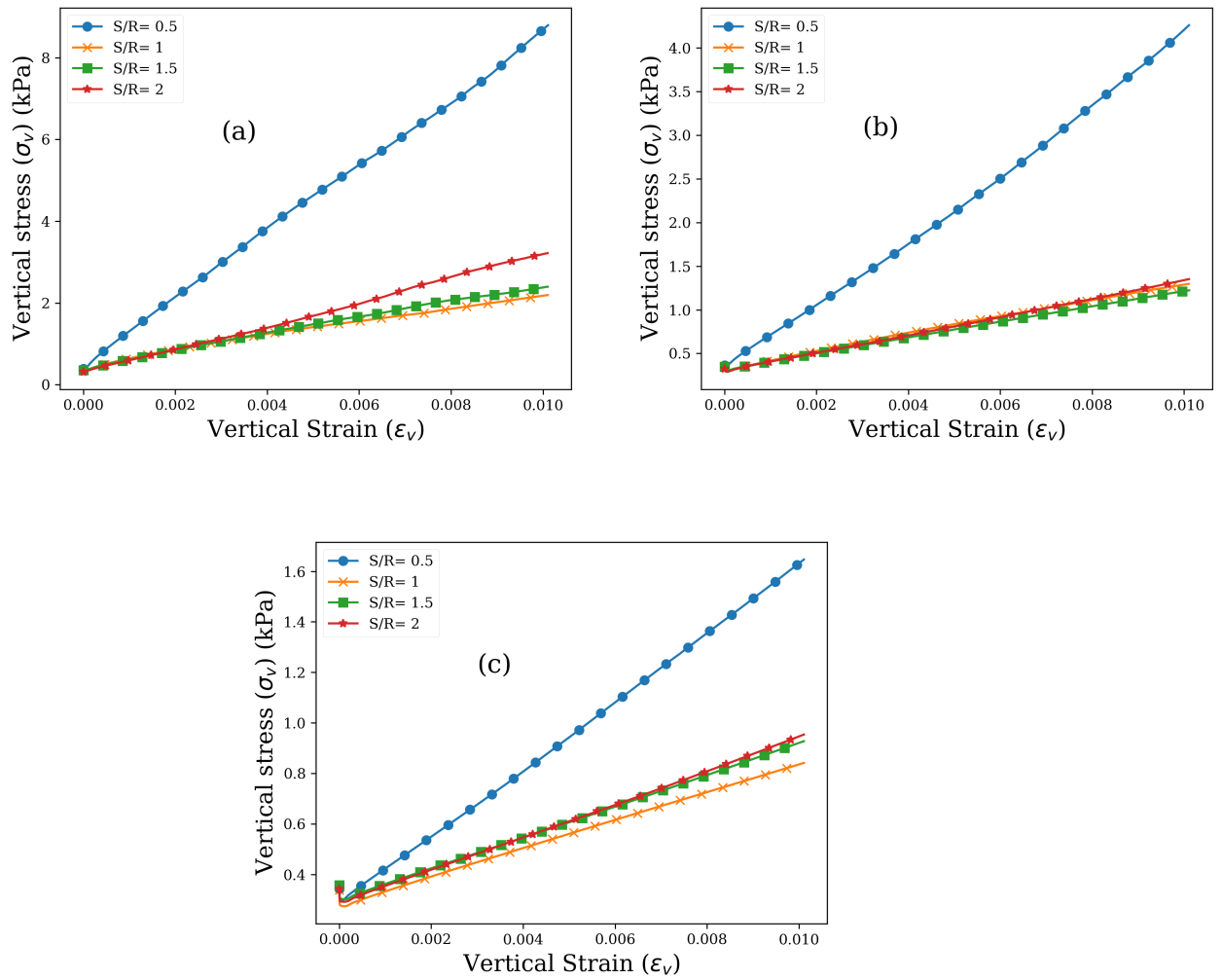
FIGURE A.2. Vertical stress vs vertical strain plots comparing the different S/R size ratios for (a) 10% rubber fraction, (b) 25% rubber fraction and (c) 50% rubber fraction.

BIBLIOGRAPHY

AbdelRazek, A., El-Sherbiny, R. M., and Lotfi, H. A. (2018). Mechanical properties and time-dependent behaviour of sand-granulated rubber mixtures. *Geomechanics and Geoengineering*, 13(4):288–300.

Ahmed, I. (1993). Laboratory study on properties of rubber-soils.

Antypov, D. and Elliott, J. A. (2011). On an analytical solution for the damped hertzian spring. *EPL (Europhysics Letters)*, 94(5):50004.

Artoni, R., Loro, G., Richard, P., Gabrieli, F., and C. Santomaso, A. (2019). Drag in wet granular materials. *Powder Technology*.

Asadi, M., Mahboubi, A., and Thoeni, K. (2018). Discrete modeling of sand–tire mixture considering grain-scale deformability. *Granular Matter*, 20(2):18.

Atkinson, J. (2000). Non-linear soil stiffness in routine design. *Géotechnique*, 50(5):487–508.

Balaha, M., Badawy, A., and Hashish, M. (2007). Effect of using ground waste tire rubber as fine aggregate on the behaviour of concrete mixes.

Benessalah, I., Arab, A., Sadek, M., and Bouferra, R. (2019). Laboratory study on the compressibility of sand–rubber mixtures under one dimensional consolidation loading conditions. *Granular Matter*, 21(1):7.

Bosscher, P. J., Edil, T. B., and Kuraoka, S. (1997). Design of highway embankments using tire chips. *Journal of Geotechnical and Geoenvironmental Engineering*, 123(4):295–304.

Brodu, N., Dijksman, J. A., and Behringer, R. P. (2015). Multiple-contact discrete-element model for simulating dense granular media. *Physical Review E*, 91(3):032201.

Brunet, S., de la Llera, J. C., and Kausel, E. (2016). Non-linear modeling of seismic isolation systems made of recycled tire-rubber. *Soil Dynamics and Earthquake Engineering*, 85:134–145.

Burland, J. (1990). On the compressibility and shear strength of natural clays. *Géotechnique*, 40(3):329–378.

Cao, W. (2007). Study on properties of recycled tire rubber modified asphalt mixtures using dry process. *Construction and Building Materials*, 21(5):1011–1015.

Choi, G.-G., Jung, S.-H., Oh, S.-J., and Kim, J.-S. (2014). Total utilization of waste tire rubber through pyrolysis to obtain oils and co2 activation of pyrolysis char. *Fuel Processing Technology*, 123:57–64.

Cundall, P. A. and Strack, O. D. (1979). A discrete numerical model for granular assemblies. *geotechnique*, 29(1):47–65.

Dal Grande, F., Santomaso, A., and Canu, P. (2008). Improving local composition measurements of binary mixtures by image analysis. *Powder Technology*, 187(3):205–213.

Davison, L. and Atkinson, J. (1990). Continuous loading oedometer testing of soils. *Quarterly Journal of Engineering Geology and Hydrogeology*, 23(4):347–355.

di Prisco, C. and Nova, R. (1993). A constitutive model for soil reinforced by continuous threads. *Geotextiles and Geomembranes*, 12(2):161–178.

Diambra, A., Ibraim, E., Russell, A., and Wood, D. M. (2011). Modelling the undrained response of fibre reinforced sands. *Soils and foundations*, 51(4):625–636.

Diambra, A., Ibraim, E., Wood, D. M., and Russell, A. (2010). Fibre reinforced sands: experiments and modelling. *Geotextiles and geomembranes*, 28(3):238–250.

Donald, M. and Roseman, B. (1962). Mixing and de-mixing of solid particles. *Br. Chem. Eng*, 7:749–752.

Dosta, Maksym, Costa, Clara, and Al-Qureshi, Hazim (2017). Numerical investigation of compaction of deformable particles with bonded-particle model. *EPJ Web Conf.*, 140:15021.

Dubois, F., Acary, V., and Jean, M. (2018). The contact dynamics method: A nonsmooth story. *Comptes Rendus Mécanique*, 346(3):247–262.

Edil, T. B. and Bosscher, P. J. (1994). Engineering properties of tire chips and soil mixtures. *Geotechnical testing journal*, 17(4):453–464.

Eidgahee, D. R. and Hosseininia, E. S. (2013). Mechanical behavior modeling of sand-rubber chips mixtures using discrete element method (dem). In *AIP Conference Proceedings*, volume 1542, pages 269–272. AIP.

Eiras, J., Segovia, F., Borrachero, M., Monzó, J., Bonilla, M., and Payá, J. (2014). Physical and mechanical properties of foamed portland cement composite containing crumb rubber from worn tires. *Materials & Design*, 59:550–557.

Elchalakani, M., Aly, T., and Abu-Aisheh, E. (2016). Mechanical properties of rubberised concrete for road side barriers. *Australian Journal of Civil Engineering*, 14(1):1–12.

Evans, T. M. and Valdes, J. R. (2011). The microstructure of particulate mixtures in one-dimensional compression: numerical studies. *Granular Matter*, 13(5):657–669.

Fang, Y., Zhan, M., and Wang, Y. (2001). The status of recycling of waste rubber. *Materials & Design*, 22(2):123–128.

Farhan, A. H., Dawson, A. R., and Thom, N. H. (2016). Effect of cementation level on performance of rubberized cement-stabilized aggregate mixtures. *Materials and Design*, 97:98 – 107.

Farrell, G. R., Martini, K. M., and Menon, N. (2010). Loose packings of frictional spheres. *Soft Matter*, 6(13):2925–2930.

Feng, Z.-Y. and Sutter, K. G. (2000). Dynamic properties of granulated rubber/sand mixtures. *Geotechnical Testing Journal*, 23(3):338–344.

Fonseca, J., Riaz, A., Bernal-Sanchez, J., Barreto, D., McDougall, J., Miranda-Manzanares, M., Marinelli, A., and Dimitriadi, V. (2019). Particle–scale interactions and energy dissipation mechanisms in sand–rubber mixtures. *Géotechnique Letters*.

Foose, G. J., Benson, C. H., and Bosscher, P. J. (1996). Sand reinforced with shredded waste tires. *Journal of Geotechnical Engineering*, 122(9):760–767.

Fu, R., Coop, M., and Li, X. (2014). The mechanics of a compressive sand mixed with tyre rubber. *Géotechnique Letters*, 4(3):238–243.

Fu, R., Coop, M., and Li, X. (2017). Influence of particle type on the mechanics of sand–rubber mixtures. *Journal of Geotechnical and Geoenvironmental Engineering*, 143(9):04017059.

Garga, V. K. and O'shaughnessy, V. (2000). Tire-reinforced earthfill. part 1: Construction of a test fill, performance, and retaining wall design. *Canadian Geotechnical Journal*, 37(1):75–96.

Ghazavi, M. and Sakhi, M. A. (2005). Influence of optimized tire shreds on shear strength parameters of sand. *International Journal of Geomechanics*, 5(1):58–65.

Haustein, M., Gladkyy, A., and Schwarze, R. (2017). Discrete element modeling of deformable particles in yade. *SoftwareX*, 6:118–123.

Hazarika, H., Otani, J., and Kikuchi, Y. (2012). Evaluation of tyre products as ground improving geomaterials. *Proceedings of the Institution of Civil Engineers-Ground Improvement*, 165(4):267–282.

Heitzman, M. A. (1992). State of the practice-design and construction of asphalt paving materials with crumb rubber modifier.

Huang, H. and Tang, L. (2009). Pyrolysis treatment of waste tire powder in a capacitively coupled rf plasma reactor. *Energy Conversion and Management*, 50(3):611–617.

Ibraim, E., Diambra, A., Wood, D. M., and Russell, A. (2010). Static liquefaction of fibre reinforced sand under monotonic loading. *Geotextiles and Geomembranes*, 28(4):374–385.

Indraratna, B., Qi, Y., Ngo, T. N., Rujikiatkamjorn, C., Neville, T., Ferreira, F. B., and Shahkolahi, A. (2019). Use of geogrids and recycled rubber in railroad infrastructure for enhanced performance. *Geosciences*, 9(1):30.

Irfan, M., Ali, Y., Ahmed, S., and Hafeez, I. (2018). Performance evaluation of crumb rubber-modified asphalt mixtures based on laboratory and field investigations. *Arabian Journal for Science and Engineering*, 43(4):1795–1806.

Janbu, N. (1963). Soil compressibility as determined by odometer and triaxial tests. In *Proc. Europ. Conf. SMFE*, volume 1, pages 19–25.

Kaneko, T., Orense, R. P., Hyodo, M., and Yoshimoto, N. (2012). Seismic response characteristics of saturated sand deposits mixed with tire chips. *Journal of Geotechnical and Geoenvironmental Engineering*, 139(4):633–643.

Kawata, S., Hyodo, M., Orense, P., Yamada, S., and Hazarika, H. (2007). Undrained and drained shear behavior of sand and tire chips composite material. In *Proceedings of the international workshop on scrap tire derived geomaterials—opportunities and challenges, Yokosuka, Japan*, pages 277–283.

Kim, H.-K. and Santamarina, J. (2008). Sand–rubber mixtures (large rubber chips). *Canadian Geotechnical Journal*, 45(10):1457–1466.

Kudrolli, A. (2004). Size separation in vibrated granular matter. *Reports on progress in physics*, 67(3):209.

Kuerbis, R. and Vaid, Y. (1988). Sand sample preparation-the slurry deposition method. *Soils and Foundations*, 28(4):107–118.

Ladd, R. (1978). Preparing test specimens using undercompaction. *Geotechnical Testing Journal*, 1(1):16–23.

Lee, C., Shin, H., and Lee, J.-S. (2014). Behavior of sand–rubber particle mixtures: experimental observations and numerical simulations. *International Journal for Numerical and Analytical Methods in Geomechanics*, 38(16):1651–1663.

Lee, C., Truong, Q. H., and Lee, J.-S. (2010). Cementation and bond degradation of rubber–sand mixtures. *Canadian Geotechnical Journal*, 47(7):763–774.

Lee, C., Truong, Q. H., Lee, W., and Lee, J.-S. (2009). Characteristics of rubber-sand particle mixtures according to size ratio. *Journal of materials in civil engineering*, 22(4):323–331.

Lee, J., Salgado, R., Bernal, A., and Lovell, C. (1999). Shredded tires and rubber-sand as lightweight backfill. *Journal of geotechnical and geoenvironmental engineering*, 125(2):132–141.

Lee, J.-S., Dodds, J., and Santamarina, J. C. (2007). Behavior of rigid-soft particle mixtures. *Journal of materials in civil engineering*, 19(2):179–184.

Liang, R. Y. and Lee, S. (1996). Short-term and long-term aging behavior of rubber modified asphalt paving mixture. *Transportation Research Record*, 1530(1):11–17.

Lopera Perez, J. and Kwok, C. (2016). Influence of rubber content on static liquefaction of sand-rubber mixtures. In *The 2016 World Congress on Advances in Civil, Environmental, and Materials Research (ACEM16), 28 August–1 September 2016, Jeju Island, Korea*.

Lopera Perez, J., Kwok, C., and Senetakis, K. (2017a). Effect of rubber content on the unstable behaviour of sand–rubber mixtures under static loading: a micro-mechanical study. *Géotechnique*, 68(7):561–574.

Lopera Perez, J., Kwok, C., and Senetakis, K. (2017b). Investigation of the micro-mechanics of sand–rubber mixtures at very small strains. *Geosynthetics International*.

Lőrincz, J., Imre, E., Gálos, M., Trang, Q., Rajkai, K., Fityus, S., and Telekes, G. (2005). Grading entropy variation due to soil crushing. *International Journal of Geomechanics*, 5(4):311–319.

Madan, N., Rojek, J., and Nosewicz, S. (2019). Convergence and stability analysis of the deformable discrete element method. *International Journal for Numerical Methods in Engineering*, 118(6):320–344.

Mashiri, M., Vinod, J., Sheikh, M. N., and Tsang, H.-H. (2015). Shear strength and dilatancy behaviour of sand–tyre chip mixtures. *Soils and Foundations*, 55(3):517–528.

McDowell, G., Bolton, M., and Robertson, D. (1996). The fractal crushing of granular materials. *Journal of the Mechanics and Physics of Solids*, 44(12):2079–2101.

Mindlin, R. (1949). Compliance of elastic bodies in contact. *J. Appl. Mech., ASME*, 16:259–268.

Mosby, J., de Silva, S. R., and Enstad, G. G. (1996). Segregation of particulate materials–mechanisms and testers. *KONA Powder and Particle Journal*, 14:31–43.

Najim, K. B. and Hall, M. R. (2012). Mechanical and dynamic properties of self-compacting crumb rubber modified concrete. *Construction and building materials*, 27(1):521–530.

Neaz Sheikh, M., Mashiri, M., Vinod, J., and Tsang, H.-H. (2012). Shear and compressibility behavior of sand–tire crumb mixtures. *Journal of Materials in Civil Engineering*, 25(10):1366–1374.

Nezamabadi, S., Nguyen, T. H., Delenne, J.-Y., and Radjai, F. (2017). Modeling soft granular materials. *Granular Matter*, 19(1):8.

Ngo, A. T. and Valdes, J. R. (2007). Creep of sand–rubber mixtures. *Journal of materials in civil engineering*, 19(12):1101–1105.

Onate, E. and Rojek, J. (2004). Combination of discrete element and finite element methods for dynamic analysis of geomechanics problems. *Computer methods in applied mechanics and engineering*, 193(27-29):3087–3128.

Ottino, J. M. and Khakhar, D. (2000). Mixing and segregation of granular materials. *Annual review of fluid mechanics*, 32(1):55–91.

Pamukcu, S. and Akbulut, S. (2006). Thermoelastic enhancement of damping of sand using synthetic ground rubber. *Journal of Geotechnical and Geoenvironmental Engineering*, 132(4):501–510.

Perez, J. L., Kwok, C., and Senetakis, K. (2016). Effect of rubber size on the behaviour of sand-rubber mixtures: A numerical investigation. *Computers and Geotechnics*, 80:199 – 214.

Perez, J. L., Kwok, C., and Senetakis, K. (2017). Micromechanical analyses of the effect of rubber size and content on sand-rubber mixtures at the critical state. *Geotextiles and Geomembranes*, 45(2):81–97.

Peters, J. F., Muthuswamy, M., Wibowo, J., and Tordesillas, A. (2005). Characterization of force chains in granular material. *Phys. Rev. E*, 72:041307.

Philippe, P. (2002). *Etude théorique et expérimentale de la densification des milieux granulaires*. PhD thesis.

Pindera, M.-J., Khatam, H., Drago, A. S., and Bansal, Y. (2009). Micromechanics of spatially uniform heterogeneous media: a critical review and emerging approaches. *Composites Part B: Engineering*, 40(5):349–378.

Platzer, A., Rouhanifar, S., Richard, P., Cazacliu, B., and Ibraim, E. (2018). Sand–rubber mixtures undergoing isotropic loading: derivation and experimental probing of a physical model. *Granular Matter*, 20(4):81.

Poh, P. S. and Broms, B. B. (1995). Slope stabilization using old rubber tires and geotextiles. *Journal of performance of constructed facilities*, 9(1):76–79.

Promputthangkoon, P. (2009). *Liquefaction of sand-tyre chip mixtures*. PhD thesis, The University of Sheffield.

Promputthangkoon, P. and Hyde, A. (2007). Compressibility and liquefaction potential of rubber composite soils. In *Proceedings of the international workshop on scrap tire derived geomaterials—opportunities and challenges, Yokosuka, Japan*, pages 161–170.

Radjai, F., Roux, S., and Moreau, J. J. (1999). Contact forces in a granular packing. *Chaos: An Interdisciplinary Journal of Nonlinear Science*, 9(3):544–550.

Rajalingam, P., Sharpe, J., and Baker, W. (1993). Ground rubber tire/thermoplastic composites: effect of different ground rubber tires. *Rubber Chemistry and Technology*, 66(4):664–677.

Rao, G. V. and Dutta, R. (2006). Compressibility and strength behaviour of sand–tyre chip mixtures. *Geotechnical & Geological Engineering*, 24(3):711–724.

Reuss, A. (1929). Berechnung der fliessgrenze von mishkristallen auf grund der plastizitatsbeding fur einkristalle math.

Ribiere, P., Richard, P., Bideau, D., and Delannay, R. (2005). Experimental compaction of anisotropic granular media. *The European Physical Journal E*, 16(4):415–420.

Richard, P. and Taberlet, N. (2008). Recent advances in dem simulations of grains in a rotating drum. *Soft Matter*, 4(7):1345–1348.

Rojek, J., Zubelewicz, A., Madan, N., and Nosewicz, S. (2018). The discrete element method with deformable particles. *International Journal for Numerical Methods in Engineering*, 114(8):828–860.

Rouhanifar, S. (2017). *Mechanics of soft-rigid soil mixtures*. PhD thesis, University of Bristol.

Rouhanifar, S. and Ibraim, E. (2015). Laboratory investigation on the mechanics of soft-rigid soil mixtures.

Sandbækken, G., Berre, T., and Lacasse, S. (1986). Oedometer testing at the norwegian geotechnical institute.

Shu, X. and Huang, B. (2014). Recycling of waste tire rubber in asphalt and portland cement concrete: An overview. *Construction and Building Materials*, 67:217–224.

Skuodis, Š., Karaman, A. H., and Dirgėlienė, N. (2017). Comparison of one-step and step-wise compression tests. *Geologija. Geografija*, 3(1).

Tang, P. and Puri, V. (2004). Methods for minimizing segregation: a review. *Particulate Science and Technology*, 22(4):321–337.

Trouzine, H., Bekhiti, M., and Asroun, A. (2012). Effects of scrap tyre rubber fibre on swelling behaviour of two clayey soils in algeria. *Geosynthetics International*, 19(2):124–132.

Valdes, J. R. and Evans, T. M. (2008). Sand–rubber mixtures: Experiments and numerical simulations. *Canadian Geotechnical Journal*, 45(4):588–595.

Villard, P., Jouve, P., and Riou, Y. (1990). Modélisation du comportement mécanique du texsol. *Bulletin de liaison des laboratoires des ponts et chaussees*, (168).

Voigt, W. (1889). Ueber die beziehung zwischen den beiden elasticitätsconstanten isotroper körper. *Annalen der physik*, 274(12):573–587.

Vu, T.-L., Barés, J., Mora, S., and Nezamabadi, S. (2019). Numerical simulations of the compaction of assemblies of rubberlike particles: A quantitative comparison with experiments. *Physical Review E*, 99(6):062903.

Vu, Thi Lo, Nezamabadi, Saeid, Barés, Jonathan, and Mora, Serge (2017). Analysis of dense packing of highly deformed grains. *EPJ Web Conf.*, 140:15031.

Vucetic, M. (1994). Cyclic threshold shear strains in soils. *Journal of Geotechnical engineering*, 120(12):2208–2228.

Wang, C., Deng, A., and Taheri, A. (2018). Digital image processing on segregation of rubber sand mixture. *International Journal of Geomechanics*, 18(10):04018138.

Watabe, Y., Shinsha, H., Yoneya, H., and Ko, C. (2014). Description of partial sandy layers of dredged clay deposit using penetration resistance in installation of prefabricated vertical drains. *Soils and Foundations*, 54(5):1006–1017.

Williams, J. C. (1976). The segregation of particulate materials. a review. *Powder technology*, 15(2):245–251.

Williams, P. and Brindle, A. (2003). Fluidised bed pyrolysis and catalytic pyrolysis of scrap tyres. *Environmental technology*, 24(7):921–929.

Xiong, W., Yan, M. R., and Li, Y. Z. (2014). Geotechnical seismic isolation system-further experimental study. In *Applied Mechanics and Materials*, volume 580, pages 1490–1493. Trans Tech Publ.

Yang, S., Lohnes, R. A., and Kjartanson, B. H. (2002). Mechanical properties of shredded tires. *Geotechnical Testing Journal*, 25(1):44–52.

Yoshimine, M. and Koike, R. (2005). Liquefaction of clean sand with stratified structure due to segregation of particle size. *Soils and foundations*, 45(4):89–98.

Youwai, S. and Bergado, D. T. (2003). Strength and deformation characteristics of shredded rubber tire sand mixtures. *Canadian Geotechnical Journal*, 40(2):254–264.

Youwai, S. and Bergado, D. T. (2004). Numerical analysis of reinforced wall using rubber tire chips–sand mixtures as backfill material. *Computers and Geotechnics*, 31(2):103–114.

Zaharia, M., Sahajwalla, V., Kim, B.-C., Khanna, R., Saha-Chaudhury, N., O'Kane, P., Dicker, J., Skidmore, C., and Knights, D. (2009). Recycling of rubber tires in electric arc furnace steelmaking: simultaneous combustion of metallurgical coke and rubber tyres blends. *Energy & Fuels*, 23(5):2467–2474.

Zhu, H., Zhou, Z., Yang, R., and Yu, A. (2007). Discrete particle simulation of particulate systems: theoretical developments. *Chemical Engineering Science*, 62(13):3378–3396.

Zornberg, J. G., Cabral, A. R., and Viratjandr, C. (2004). Behaviour of tire shred sand mixtures. *Canadian geotechnical journal*, 41(2):227–241.

Titre : Matériaux composites sable et rebut de caoutchouc : Une analyse micromécanique

Mots clés : ségrégation, mélange, œdomètre, éléments discrets, caoutchouc.

Résumé : Les déchets issus de caoutchouc (pneus usagés) sont produits en grand nombre par nos industries et par notre mode de vie. Afin de réduire leur impact sur l'environnement et de s'inscrire dans une logique d'économie circulaire, il est envisageable de recycler ces déchets dans des matériaux granulaires dans le but d'obtenir des composites aux propriétés notables. L'objectif de ce projet est d'étudier si l'ajout de grains de caoutchouc dans les sols à base de sable améliore les propriétés des matériaux ainsi obtenus. Ce projet porte ainsi sur l'étude des composites caoutchouc-sable et en particulier sur la relation entre la qualité du mélange obtenu et les propriétés mécaniques. Les expériences caractérisant le mélange du sable et du caoutchouc ont été effectuées. La caractérisation de nos mélanges sable/caoutchouc a montré la présence de ségrégation. Dans le but de quantifier l'effet de cette dernière sur les propriétés mécaniques de nos mélanges, des tests mécaniques classiques à l'œdomètre ont été réalisés et en plus des simulations de type éléments discrets (DEM) ont été réalisées. L'importance de cette ségrégation sur les propriétés mécaniques n'est pas forcément cruciale, notamment à forte fraction volumique de caoutchouc. Nous avons également montré que des outils numériques pouvaient être utilisés à bon escient pour comprendre les mécanismes à l'échelle du grain.

Title : Sand/ waste rubber mixtures : A micromechanical analysis

Keywords : segregation, mixture, oedometer, Discrete Element Method, rubber.

Abstract : A huge amount of waste tires is dumped at the landfill sites. Such a waste is posing an environmental hazard. It is high time to reduce their impact on the environment in a sustainable way and hence recycle them. One of the options is to recycle these waste tires, convert them into powdered form and use this granular rubber with other granular materials, e.g. soil to improve their properties. This study is based on the analysis of such sand-rubber mixtures. In particular, the focus of this study is to investigate the effect of quality of mixing on the mechanical response of such sand-rubber mixtures. The study began with characterizing the segregation of sand and rubber for specific conditions, i.e. mixing and under vertical taps. The experiments pointed out segregation in such mixtures. Hence, it was interesting to study its effect on the mechanical response of these mixtures by performing classic oedometer experiments and also with the help of Discrete Element Method (DEM) simulations. It was concluded that the segregation did not have a crucial effect on the mixtures, especially for important rubber volume fractions. For rubber volume fractions up to 25% however, it showed a considerable effect on the mechanical response of these mixtures. The use of DEM simulations helped to better understand the effect of mixing quality by relating the properties observed at the grain-scale level such as contact forces, force distribution, etc. with the macroscopic response of these mixtures.